Spectroscopy of selected metal-containing diatomic molecules

by

Iouli E. Gordon

A thesis
presented to the University of Waterloo
in fulfilment of the
thesis requirement for the degree of
Doctor of Philosophy
in
Physics

Waterloo, Ontario, Canada, 2005

I hereby declare that I am the sole author of this thesis. This is a true copy of the thesis, including any required final revisions, as accepted by my examiners.

I understand that my thesis may be made electronically available to the public.

Abstract

Fourier transform infrared emission spectra of MnH and MnD were observed in the ground $X^7\Sigma^+$ electronic state. The vibration-rotation bands from $\upsilon = 1 \rightarrow 0$ to $\upsilon = 3 \rightarrow 2$ for MnH, and from $\upsilon = 1 \rightarrow 0$ to $\upsilon = 4 \rightarrow 3$ for MnD were recorded at an instrumental resolution of 0.0085 cm^{-1}. Spectroscopic constants were determined for each vibrational level and equilibrium constants were found from a Dunham-type fit. The equilibrium vibrational constant ω_e for MnH was found to be 1546.84518(65) cm^{-1}, the equilibrium rotational constant B_e was found to be 5.6856789(103) cm^{-1} and the equilibrium bond distance r_e was determined to be 1.7308601(47) Å.

New high resolution emission spectra of CoH and CoD molecules have been recorded in the 640 nm to 3.5 μm region using a Fourier transform spectrometer. Many bands were observed for the $A'^3\Phi - X^3\Phi$ electronic transition of CoH and CoD. In addition, a new [13.3]4 electronic state was found by observing the $[13.3]4 - X^3\Phi_3$ and $[13.3]4 - X^3\Phi_4$ transitions in the spectrum of CoD. Analysis of the transitions with $\Delta\Omega = 0, \pm1$ provided more accurate values of spin-orbit splittings between $\Omega = 4$ and $\Omega = 3$ components. The ground state for both molecules was fitted both to band and Dunham-type constants. The estimated band constants of the perturbed upper states were also obtained.

The emission spectrum of gas-phase YbO has been investigated using a Fourier transform spectrometer. A total of 8 red-degraded bands in the range 9 800 – 11 300 cm^{-1} were recorded at a resolution of 0.04 cm^{-1}. Because of the multiple isotopomers present in the spectra, only 3 bands were rotationally analyzed. Perturbations were identified in two of these bands and all 3 transitions were found to terminate at the $X^1\Sigma^+$ ground electronic state. The electronic configurations that give rise to the observed states are discussed and molecular parameters for all of the analyzed bands are reported.

Electronic spectra of the previously unobserved EuH and EuD molecules were studied by means of Fourier transform spectroscopy and laser-induced fluorescence. The extreme complexity of these transitions made rotational assignments of EuH bands impossible. However, the spin-spin interaction constant, λ, and Fermi contact parameter, b_F, in the ground $X^9\Sigma^-$ electronic state were estimated for the ^{151}EuH and ^{153}EuH isotopologues.

Electronic spectra of SmH, SmCl, TmH and ErF molecules were recorded for the first time using Fourier transform spectrometer. The poor signal to noise ratio of the observed bands coupled with their complexity prevented a rotational analysis. The electronic states that may be involved in the observed transitions are discussed.

Acknowledgments

First of all I would like to thank Prof. Peter Bernath for being, in my opinion, a model graduate supervisor. His abilitiy to motivate his students and to provide detailed answers to any questions are most admirable. I was fortunate to have learned from such a distinguished scientist.

I would like to express a deep gratitude to Prof. Robert J. Le Roy whose advice and help have benefited me in research and beyond. I wish to thank Prof. T. C. Steimle, at the Arizona State University for inviting Mike Dick and myself into his laboratory to conduct experiments on EuH and EuF. We learned a lot in those two weeks. It was an honor to be able to conduct experiments with world-caliber spectroscopists during their visits to our laboratory. While not all of these experiments worked, I am very thankful to Dr. Colan Linton, Dr. Bernard Pinchemel and Dr. Ram Ram for sharing their experience with me.

Academic research is usually conducted on a tight budget and I am thankful to Daniel An at Hefa Rare Earth for providing us with the lanthanide metals used in our experiments at affordable prices.

I am grateful to Dr. Todd Melville for igniting our laboratory interest in lanthanide-containing molecules, which started after his visit to our lab. I am also thankful to Keith Tereszchuk for showing me everything during my first days in the lab and for being a good friend. Together Dr. Dominique Appadoo, Alireza Shayesteh and I have undertaken a number of successful (and sometimes not very successful) experiments involving the tube furnace and DC discharge and I have enjoyed this fruitful collaboration.

I wish to thank Mike Dick for being a great friend, colleague and roommate. For all these years I have enjoyed sharing an office with Ray Nassar and I thank him for his friendship, support, and introducing me to different parts of Waterloo. I am grateful to other current and former members of the Bernath laboratory, Dr. Jin-Guo Wang, Dr. Phillip Sheridan, Dr. Tsuyoshi Hirao, Dr. Kaley Walker, Dr. Jian Tang, Dr. Gang Li, Andrew Janca, Shanshan Yu, and Dejian Fu, for their help and friendship.

I would also like to thank all of my friends at the University and in the Russian community, without them the graduate school would have seemed less enjoyable. My deep gratitude goes to Helia Jalili for her support during the writing of this thesis.

Finally, I am indebted to my parents for their encouragement and support during my academic career. It is to them I wish to dedicate this thesis.

Dedication

To my parents

Contents

1 Introduction and motivation **1**

1.1 Transition metal hydrides 1

1.2 Lanthanide-containing molecules 4

2 General theory **9**

2.1 Born–Oppenheimer approximation 9

2.2 Rotational structure 10

2.3 Vibrational structure 10

2.4 Electronic spectroscopy of diatomic molecules 12

2.4.1 Angular momenta in diatomic molecules 12

2.4.2 Hund's coupling cases 12

2.4.3 Parity 16

2.4.4 Transitions between electronic states 17

3 Experimental **20**

3.1 Fourier transform emission spectroscopy 20

3.1.1 Emission spectroscopy vs absorption spectroscopy 20

3.1.2 Fourier transform spectroscopy 21

3.2 Emission sources 24

3.2.1 Broida oven 24

3.2.2 The high temperature furnace/electrical discharge emission source 27

3.2.3 The King furnace 28
3.3 Laser ablation/molecular beam apparatus 30

4 Infrared emission spectra of MnH and MnD 33
4.1 Introduction 33
4.2 Experimental 35
4.3 Results and discussion 35
4.4 Conclusions 47

5 Electronic emission spectra of CoH and CoD 51
5.1 Introduction 51
5.2 Experimental details 53
5.3 Observations and analysis 54
5.4 Discussion 63
5.5 Conclusions 65

6 Fourier transform spectroscopy of ytterbium monoxide 69
6.1 Introduction 69
6.2 Experimental Arrangement 70
6.3 Results and Discussion 71

7 Electronic spectra of europium monohydride 79
7.1 Introduction 79
7.2 Experimental 80
7.2.1 Fourier transform spectra of EuH and EuD 80
7.2.2 Laser ablation/molecular beam experiment 81
7.3 Results and Discussion 84
7.3.1 Electronic states of EuH 84
7.3.2 FT spectra of EuH/D 87
7.3.3 The “cold” spectrum of EuH 88
7.4 Conclusions and future work 101

8 First observations of the gas-phase spectra of SmH, SmCl, TmH and ErF 105

8.1 Samarium monohydride 105
8.2 Samarium monochloride 107
8.3 Thulium monohydride 108
8.4 Erbium monofluoride 109
8.5 Conclusions 111

APPENDIX 113

A Line lists for MnH and MnD 114

A.1 Line list for MnH 114
A.2 Line list for MnD 141

B Line lists for CoH and CoD 178

B.1 Line list for CoH 178
B.2 Line list for CoD 196

C Line list for YbO 235

C.1 Line list for YbO. System 1 235
C.2 Line list for YbO. System 2 239
C.3 Line list for YbO. System 3 242

List of Figures

1.1 Molecular orbital diagram for the $3d$-transition metal monohydrides. 3

2.1 Hund's coupling cases. 13

3.1 The schematic diagram of a Michelson interferometer. 21

3.2 Selected metal vapor pressures as a function of temperature. 25

3.3 Broida oven at the University of Waterloo. 26

3.4 DC discharge/high temperature furnace source. 27

3.5 A schematic of the King furnace 29

4.1 An overview of the infrared emission spectrum of MnH. 36

4.2 An overview of the infrared emission spectrum of MnD after baseline correction. 37

4.3 Fine structure of the low rotational levels of the $X^7\Sigma^+$state of MnH. 38

4.4 Example of spin-splitting in MnH lines. 39

5.1 An overview spectrum of CoD after baseline correction. 54

5.2 Unassigned bands of CoH at 8000 cm^{-1}. 56

5.3 The dependence of DRMSD on the Ω-doubling constant used to fit (0,0) band of $A'^3\Phi_4 \rightarrow X^3\Phi_4$ transition of CoH. 57

5.4 An energy level diagram showing the electronic states found in previous experiments and this work. 65

6.1 An overview of the emission spectrum of YbO. 72

6.2 The observed YbO chemiluminescence spectrum of the strongest band (System 2). 74

7.1 An overview of the FT spectrum of EuD and EuH. 82

7.2 A survey laser excitation scan of the 16 975-17 125 cm^{-1} region. . . . 84

7.3 An example of "raw" high resolution LIF scan. 85

7.4 The 14 500 cm^{-1} transition of EuH observed by FT emission spectroscopy. 87

7.5 Distribution of population for the rotational temperature of 10 K and 70 K. 89

7.6 An example of the transitions between hyperfine levels in excited and ground electronic states. 91

7.7 An example of the graphical method for making the J'' assignments in the observed transitions. 95

8.1 SmH electronic transitions. 106

8.2 Observed bands of SmCl. 108

8.3 TmH electronic transition. 109

8.4 ErF electronic transitions. 110

List of Tables

2.1 Angular momenta in diatomic molecules. 12

2.2 Coupling of angular momenta. 14

4.1 $^7\Sigma^+$ Hamiltonian matrix. 41

4.2 Equilibrium constants for MnH. 42

4.3 Equilibrium constants for MnD and estimated Born–Oppenheimer breakdown parameters. 43

4.4 Spectroscopic constants for the $X^7\Sigma^+$ ground state of MnH. 44

4.5 Spectroscopic constants for the $X^7\Sigma^+$ ground state of MnD. 45

5.1 Spectroscopic constants (in cm^{-1}) for the $X^3\Phi_4$ and $X^3\Phi_3$ states of CoH and CoD. 59

5.2 Spectroscopic constants for the excited states of CoH. 60

5.3 Spectroscopic constants for the excited states of CoD. 61

5.4 Dunham-type parameters and Born–Oppenheimer breakdown parameters (in cm^{-1}) for the $X^3\Phi_4$ state of CoH determined from the combined-isotopologue analysis. 62

5.5 Dunham-type parameters for the $X^3\Phi_4$ state of CoH and CoD. . . . 63

6.1 Observed YbO bandhead positions (cm^{-1}). 71

6.2 Molecular parameters (cm^{-1}) for the observed ^{174}YbO bands. 75

7.1 The regions covered by high-resolution LIF scans. 86

7.2 The Eu nuclear data. 90

7.3 The assigned lines, and some parameters associated with them. . . . 94
7.4 Overall widths of magnetic hyperfine energy multiplets of $^9\Sigma^-$ state. 96
7.5 Assignment of some of the transitions observed in the high-resolution LIF scans. 98
7.5 Assignment of some of the transitions observed in the high-resolution LIF scans. 99
7.5 Assignment of some of the transitions observed in the high-resolution LIF scans. 100

A.1 Line list for MnH. 114
A.2 Line list for MnD. 141

B.1 Line list for CoH. 178
B.2 Line list for CoD. 196

C.1 Line list for System 1. 235
C.2 Line list for the System 2. 239
C.3 Line list for the System 3. 242

Chapter 1

Introduction and motivation

High resolution spectroscopy is one of the fundamental experimental tools of chemical physics. From the analysis of molecular spectra one can obtain detailed information about the bonding, structure, and interactions in the molecules as well as properties of their physical environment. This thesis concentrates on the spectroscopic studies of metal-containing diatomic molecules in the gas phase in order to gain a better understanding of their structural, electronic and bonding properties.

Metal-containing molecules are important in a variety of scientific areas such as chemical catalysis (including hydrogenation), metallurgy, astrophysics, high-density fuel research and even protein biology [1]. The study of the electronic structure of small molecules containing a metal atom is an interesting area of chemical physics, because these species can serve as models for more complicated systems.

1.1 Transition metal hydrides

The first two molecules described in this thesis are first row transition metal hydrides: MnH and CoH and their isotopologues. Diatomic molecules containing transition metal atoms have important applications. For example first row transition metal oxides such as TiO and VO are important in astrophysics because their spectra are used to classify cool stars [2]. Transition metal hydrides are also expected to be present in various stars and nebulae, and in the interstellar medium. Some of these hydrides have already been detected in the spectra of extraterrestrial objects. Lambert and Mallia [3] tentatively observed the NiH molecule in the spectra of sunspots. CrH was also observed in the spectra of sunspots [4], while spectra of FeH [5, 6] and perhaps TiH [7] were identified in M-type stars. The spectrum of CoH is also expected to be found in sunspots, since the solar abundance of cobalt is just one order of magnitude less than that of chromium [8]. Transition metal monohydrides are also important because they represent the simplest metal-hydrogen bond, and their studies provide a starting point for research on gas-surface interactions and catalytic processes.

Although the electronic spectra of many first row transition metal hydrides have been known for decades not all of them have been fully interpreted. The reason is that the open d-shells of these metals give rise to a large number of low-lying excited electronic states with large spin and orbital angular momenta. These states lie close to each other, which results in perturbations of the rotational levels, making the spectra hard to assign. The complex symmetry of the electronic states (due to the metals' unpaired d electrons) also complicates the spectra. For example, the ground states of the molecules studied in this thesis are $^7\Sigma^+$ for MnH, arising from the $3d^54s$ configuration of Mn^+ ion, and $^3\Phi_i$ for CoH (see further discussion below). The most recent review of experimental data for the ground states of transition metal monohydrides was completed by Bernath in 2000 [9].

The electronic structure of the first row transition metal monohydrides can be explained using a simple qualitative valence molecular orbital diagram (Figure 1.1) [9]. The 1σ orbital is always bonding and formed by the interaction of the $(s+p)$-metal hybrid orbital with the hydrogen $1s$ orbital [10]. The 2σ orbital is predominantly an $(s-p)$–metal non-bonding orbital which is located on the side of metal atom away from the partially negatively-charged hydrogen. The 1δ, 1π and 3σ orbitals are nearly pure metal $3d$ non-bonding orbitals. The ionicity of the ground states of metal hydrides is generally $M^{\delta+}$–$H^{\delta-}$. The ground states are derived by adding to the molecular orbitals of MH the valence electrons of the metal and hydrogen.

The MnH molecule has 8 valence electrons; they are distributed among the molecular orbitals to maximize the total spin, except for the bonding 1σ orbital that has two electrons. The ground electron configuration of MnH is therefore $1\sigma^2 2\sigma^1 3\sigma^1 1\delta^2 1\pi^2$ [11]. The 1σ bonding orbital is a Mn $4s$–H $1s$ combination, the 2σ non-bonding orbital is a Mn $4s$-$4p$ hybrid orbital, while the 1δ, 1π and 3σ orbitals are metal $3d$ non-bonding orbitals. CoH molecule has two additional electrons (10 valence electrons) as compared to MnH; they are added to the low-lying 2σ and 1δ orbitals, and the 3σ electron shifts to the 1π orbital. The ground $^3\Phi_i$ electronic state of CoH is derived from the $1\sigma^2 2\sigma^2 1\delta^3 1\pi^3$ configuration.

Ab initio calculations are in many ways ahead of the experiments, and large basis sets are available for transition metal atoms for performing such calculations.

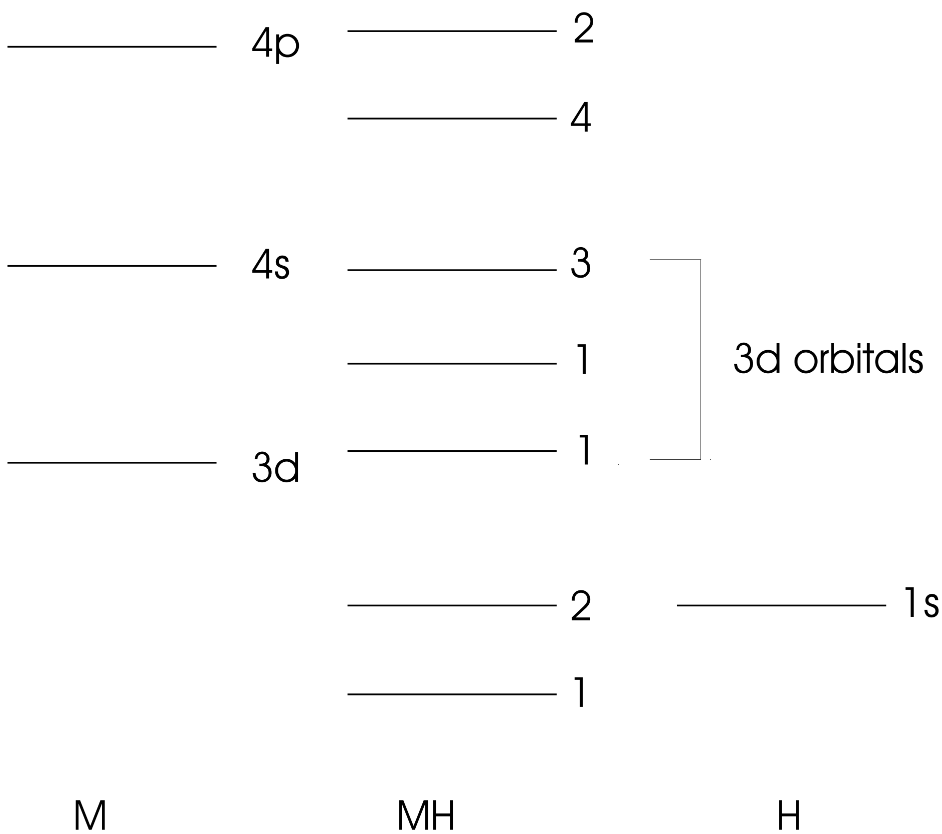

Figure 1.1: Molecular orbital diagram for the 3*d*-transition metal monohydrides.

The pioneering work to predict the properties of the low-lying electronic states of the transition metals are those of Chong *et al*. [12], for the first row (ScH to ZnH), and Langhoff *et al*. [13] and Balasubramanian [14], for the second row (YH to CdH). *Ab initio* calculations for the third row transition metal hydrides are more difficult because of the necessity to include the effects of spin-orbit coupling, but Balasubramanian has also completed calculations for 5*d* metal hydrides [14].

The literature overview of the spectroscopic work on MnH and CoH is given in Chapters 4 and 5.

1.2 Lanthanide-containing molecules

Studies of molecules that contain lanthanide metal atoms are motivated by their use in semiconductors [15, 16], magnetic [16, 17] and laser materials [16], hydrogen storage materials [18] and many other applications [16]. Astrophysical interest in these molecules has not developed yet, as the only lanthanide-containing molecule found in the spectra of astronomical objects is CeO, which was observed in the spectra of S stars by Wyckoff and Weninger [19]. However, the laboratory spectra of rare-earth metal-containing molecules, against which astrophysicists can compare their spectra, are limited, and some of the unidentified bands in the spectra of stars could be due to these molecules.

The experimental information for the lanthanide-containing molecules is limited for many reasons. The first obstacle is the price of the rare-earth metals (for instance the price of the Tm metal is about $65 (US) per gram, depending on the supplier). Fortunately for the experiments in this thesis, we have been able to take advantage of the moderate prices provided to us by the HEFA Rare Earth Canada Company. Secondly, the high reactivity of the rare earth metals, together with their low vapor pressures at the temperatures that can be achieved by conventional methods, make the creation of these molecules in the gas phase a major challenge.

The difficulty in interpretation of the observed spectra is similar to that of spectra of molecules containing $3d$ transition metal atoms. The lanthanide metal atoms and ions possess a large number of unpaired electrons in $4f$ orbitals, which results in many low-lying electronic states with complex structure. The high density of states produces perturbations and band overlaps in the observed spectra. Additional obstacles that complicate the spectra are the relatively small rotational constants (due to heavy atoms of lanthanide elements), the large numbers of isotopes for many rare earth metals, and the hyperfine structure due to large nuclear spins of some of these isotopes.

The majority of the available spectroscopic studies of lanthanide-containing molecules in the gas phase concentrate on lanthanide oxides such as CeO [20], PrO [21], NdO [22, 23], SmO [24], EuO [25], GdO [26, 27], TbO [28], DyO [28], HoO [28, 29], ErO [30], YbO (see Chapter 6 and references therein) and LuO [31]. A new electronic emission spectrum of YbO is discussed in Chapter 6 of this thesis.

The lanthanide metal halides were studied less extensively, but experimental data on YbCl [32], YbF [33], DyF [34], HoF [35], HoCl [36] and CeF [37] are available. This thesis reports the first observations of the electronic spectra of ErF and SmCl (Chapter 8).

The lanthanide metal hydrides are studied the least and so far only experiments on YbH and LuH have been reported. The literature survey of the experimental and theoretical work on rare earth metal hydrides is given in Chapter 7. The spectra of EuH, SmH and TmH were observed in this work for the first time and these observations are reported in Chapters 7 and 8.

Ab initio calculations for lanthanide-containing molecules are very difficult because one has to account for relativistic and correlation effects. Nevertheless, pseudopotential or effective core potential approaches have recently been developed (see Ref. [38] and references therein). Density functional calculations had also been tried for the lanthanide oxides [39]. Semiempirical approaches and particulary ligand field theory (LFT) have proved to be useful in predicting the spectral properties of lanthanide oxides [40, 41] and halides [42]. This theory predicts the energy and ordering of molecular electronic states that arise from perturbation of the lanthanide ionic states by a negatively charged ligand.

One of the main goals of our experiments on lanthanide-containing molecules is to aid the development of the theoretical calculations for such molecules, and in particular to provide theoreticians with reference data for comparison with their calculations.

Bibliography

[1] L. Moran, K. Scrimgeour, H. Horton, R. Ochs, and J. Rawn, *Biochemistry*, Prentice–Hall, Engelwood Cliffs, NJ, 2nd edition, 1994.

[2] N. M. White and R. F. Wing, Astrophys. J. **222**, 209 (1978).

[3] D. L. Lambert and E. A. Mallia, Mon. Not. R. Astron. Soc. London **151**, 437 (1971).

[4] O. Engvold, H. Wöhl, and J. W. Brault, Astron. Astrophys. Supp. Series **42**, 209 (1980).

[5] B. Lindgren and G. Olofsson, Astron. Astrophys. **84**, 300 (1980).

[6] P. K. Carroll, P. McCormack, and S. O'Connor, Astrophys. J. **208**, 903 (1976).

[7] R. Yerle, Astron. Astrophys. **73**, 346 (1979).

[8] S. P. Beaton, K. Evenson, and J. M. Brown, J. Mol. Spectrosc. **164**, 395 (1994).

[9] P. Bernath, Transition metal monohydrides, in *Advances in Metal and Semiconductor Clusters, vol. 5*, edited by M. Duncan, Elsevier, 2000.

[10] S. Walch and C. Bauschlicher Jr., J. Chem. Phys. **78**, 4597 (1983).

[11] S. Langhoff, C. Bauschlicher Jr, and A. Rendell, J. Mol. Spectrosc. **138**, 108 (1989).

[12] D. Chong, S. Langhoff, C. Bauschlicher Jr, S. Walch, and H. Partridge, J. Chem. Phys. **85**, 2850 (1986).

[13] S. Langhoff, L. G. M. Pettersson, C. Bauschlicher, and H. Partridge, J. Chem. Phys. **86**, 268 (1987).

[14] K. Balasubramanian, J. Chem. Phys. **93**, 8061 (1990).

[15] P. Vaida and J. N. Daou, Phys. Rev. B **49**, 3275 (1994).

[16] http://www.americanelements.com.

[17] W. Bauhofer, W. Joss, R. K. Kremer, H. J. Mattausch, and A. Simon, J. Magn. Mater. **104**, 1243 (1992).

[18] C. Rao and J. Gopalkrishnan, *New Directions in Solid State Chemistry*, CUP, London, 3rd edition, 1986.

[19] S. Wyckoff and P. A. Wehinger, Astrophys. J. **212**, L139 (1977).

[20] C. Linton et al., J. Mol. Spectrosc. **102**, 441 (1983).

[21] M. Dulick and R. W. Field, J. Mol. Spectrosc. **113**, 105 (1985).

[22] C. Linton et al., J. Mol. Spectrosc. **225**, 132 (2004).

[23] C. Effantin, A. Bernard, P. Crozet, A. J. Ross, and J. D'Incan, J. Mol. Spectrosc. **231**, 154 (2005).

[24] B. Guo and C. Linton, J. Mol. Spectrosc. **137**, 114 (1989).

[25] S. McDonald, PhD thesis, MIT, Cambridge, MA, 1985.

[26] P. Carrette, A. Hocquet, M. Douay, and B. Pinchemel, J. Mol. Spectrosc. **124**, 243 (1987).

[27] L. A. Kaledin, M. Erickson, and M. C. Heaven, J. Mol. Spectrosc. **165**, 323 (1994).

[28] L. A. Kaledin and E. A. Shenyavskaya, J. Mol. Spectrosc. **90**, 590 (1981).

[29] Y. Liu, H. Schall, R. Field, and C. Linton, J. Mol. Spectrosc. **104**, 72 (1984).

[30] L. A. Kaledin and E. A. Shenyavskaya, J. Mol. Spectrosc. **133**, 469 (1989).

[31] A. Bernard and C. Effantin, Can. J. Phys. **64**, 246 (1986).

[32] C. Linton and A. Adam, J. Mol. Spectrosc. **206**, 161 (2001).

[33] K. Dunfield, C. Linton, T. E. Clarke, J. McBride, and A. G. Adam, J. Mol. Spectrosc. **174**, 433 (1995).

[34] M. McCarthy, J. C. Bloch, R. W. Field, and L. A. Kaledin, J. Mol. Spectrosc. **179**, 253 (1996).

[35] M. McCarthy, J. C. Bloch, R. W. Field, and L. A. Kaledin, J. Mol. Spectrosc. **154**, 417 (1996).

[36] M. J. Dick and C. Linton, J. Mol. Spectrosc. **217**, 26 (2003).

[37] M. McCarthy, J. C. Bloch, R. W. Field, and L. A. Kaledin, J. Mol. Spectrosc. **107**, 119 (1984).

[38] M. Dolg and H. Stoll, *Electronic Structure Calculations for Molecules Containing Lanthanide Atoms*, volume 22, Elsevier, Amsterdam.

[39] S. G. Wang, D. K. Pan, and W. Schwarz, J. Chem. Phys. **102**, 9296 (1995).

[40] S. A. McDonald, S. Rice, R. Field, and C. Linton, J. Chem. Phys. **93**, 7676 (1990).

[41] P. Carette and A. Hocquet, J. Mol. Spectrosc. **131**, 301 (1988).

[42] A. L. Kaledin, M. C. Heaven, R. W. Field, and L. A. Kaledin, J. Mol. Spectrosc. **179**, 310 (1996).

Chapter 2

General theory

High resolution spectroscopy allows us to explore the processes inside the microscopic world of molecules by observing spacings between lines, their splittings and the deviations from periodic patterns. This chapter provides a brief explanation of the nature of such effects in diatomic molecules.

2.1 Born–Oppenheimer approximation

The solution of the Schrödinger equation $\hat{H}\psi = E\psi$ with a nonrelativistic molecular Hamiltonian is a hard task, since this Hamiltonian is a combination of nuclear kinetic energy, electronic kinetic energy, nuclear-nuclear repulsion energy, electron-nuclear attraction energy and electron-electron repulsion energy [1]. The solution can be simplified by the separation of the electronic and nuclear motions by invoking the Born–Oppenheimer approximation [2]. The Coulombic forces acting on nuclei and electrons are the same order of magnitude, but the masses of electrons are much smaller, and therefore they move faster. The electronic motion can therefore be separated from the much slower nuclear (vibration-rotation) motion. The vibration and rotation parts of the nuclear motion can be further separated in a similar way. As a result the total wavefunction of a molecule can be broken into components, i.e., $\psi = \psi_{el}\psi_{vib}\psi_{rot}...$ as an approximation.

2.2 Rotational structure

In the simplest approximation, a diatomic molecule (AB) can be considered as a rigid rotor, consisting of two point masses (A and B) connected by a rigid massless bar [1, 3, 4]. The discrete rotational energy levels are given by

$$F(J) = BJ(J+1), \tag{2.1}$$

where

$$B[\mathrm{cm}^{-1}] = \frac{h \times 10^{-2}}{8\pi^2 cI}, \tag{2.2}$$

with $I = \mu r^2$, where μ is a reduced mass

$$\mu = \frac{m_{\mathrm{A}} m_{\mathrm{B}}}{m_{\mathrm{A}} + m_{\mathrm{B}}}. \tag{2.3}$$

and r is an internuclear separation.

The molecule, of course, is not completely rigid, and as it rotates the centrifugal forces cause the internuclear distance to elongate slightly. The rotational-level energy expression thus has to have terms that account for the effect of centrifugal forces

$$F(J) = BJ(J+1) - D[J(J+1)]^2 + H[J(J+1)]^3 + L[J(J+1)]^4 + \ldots, \tag{2.4}$$

where $D, H, L, ...$ are centrifugal distortion constants [5]. The transitions between rotational levels of the same vibrational level (pure rotational spectra) can be observed in the microwave region of the spectrum; such transitions were not studied in this thesis.

2.3 Vibrational structure

The vibrational energy level expression can be written as [6]

$$G(\upsilon) = \omega_e(\upsilon + \frac{1}{2}) - \omega_e x_e(\upsilon + \frac{1}{2})^2 + \omega_e y_e(\upsilon + \frac{1}{2})^3 + \omega_e z_e(\upsilon + \frac{1}{2})^4 \ldots, \tag{2.5}$$

where υ is a vibrational quantum number, the $\omega_e(\upsilon + \frac{1}{2})$ term reflects the harmonic oscillator part of the potential energy function and the other terms account for the "anharmonicity" of real potentials. The value of the rotational constant B depends on the vibrational state of the molecule, since $B \propto 1/r^2$. The vibrational dependence of B can be modeled by the following expression [3]

$$B_v = B_e - \alpha_e(v + \frac{1}{2}) + \gamma_e(v + \frac{1}{2})^2 \ldots, \quad (2.6)$$

where B_e is the equilibrium rotational constant and α_e and γ_e are rotation-vibration interaction coefficients.

A popular expression for the energy levels of the vibrating rotor was introduced by Dunham [7] by using the first-order semi-classical quantization condition from WKB (Wentzel–Kramers–Brillouin) theory [8]

$$E(v, J) = \sum_{l,m} Y_{l,m}(v + \frac{1}{2})^l (J(J+1))^m. \quad (2.7)$$

The coefficients $Y_{l,m}$ can be related to the conventional spectroscopic constants [3, 7]. For example $Y_{10} \approx \omega_e$, $Y_{01} \approx B_e$ and $Y_{11} \approx \alpha_e$ [3].

The spectroscopic constants associated with vibration and rotation depend on the reduced mass; therefore, their values are different for different isotopologues of the same molecule. The isotopic dependence of the spectroscopic constants can be conveniently generalized for the Dunham $Y_{l,m}$ constants as

$$Y_{l,m} \propto \mu^{-(l+2m)/2}. \quad (2.8)$$

Therefore, within the Born–Oppenheimer approximation, the parameters associated with different isotopologues are related as

$$Y_{l,m}^{(\alpha)} = Y_{l,m}^{(1)}(\frac{\mu_1}{\mu_\alpha})^{m+l/2}, \quad (2.9)$$

where μ_1 is the reduced mass of the reference isotopologue and μ_α is the reduced mass of isotopologue-α. Equation (2.7) can be rewritten to express energy levels for any isotopologue through the Dunham $Y_{l,m}$ constants of the reference isotopologue as

$$E^{(\alpha)}(v, J) = \sum_{l,m} Y_{l,m}^{(1)}(\frac{\mu_1}{\mu_\alpha})^{m+l/2}(v + \frac{1}{2})^l (J(J+1))^m. \quad (2.10)$$

In the case of Born–Oppenheimer approximation breakdown, small correction terms [9–11] must be added to Eq. (2.10). In this thesis Le Roy's formalism [11] was used to account for the breakdown of the Born–Oppenheimer approximation in CoH and MnH.

The rotation-vibrational transitions are usually observed in the infrared region of the spectrum. In this thesis we have studied infrared spectra of MnH and MnD.

2.4 Electronic spectroscopy of diatomic molecules

2.4.1 Angular momenta in diatomic molecules

To understand the electronic spectrum of diatomic molecules, it is important to consider their angular momenta and the interaction between these momenta.

If one excludes nuclear spin, the total angular momentum of the diatomic molecule **J** is the vector sum of electron orbital **L**, electron spin **S**, and nuclear rotation **R** angular momenta (Figure 2.1a). The angular momenta and their projections on the internuclear axis are very important parameters, and the notation is summarized in Table 2.1.

Table 2.1: Angular momenta in diatomic molecules.

Angular momentum	Projection on molecular axis (units of $\hbar$)
J	$\Omega = \Lambda + \Sigma$
L	Λ
S	Σ
R	–
N=R+L	Λ

The $^{2S+1}\Lambda_\Omega$ symbol is used to denote different electronic states. For electronic states with $\Lambda > 0$ the circulation of electrons can be in a clockwise or counter-clockwise direction around the internuclear axis, which results in a double orbital degeneracy. This phenomena is usually called Λ-doubling. Analogously, for $\Omega > 0$ there is an Ω-doubling for which both values are represented by $|\Omega|$ for each of the $2S + 1$ spin components [1]. For the cases when $S > |\Lambda| > 0$ the labeling of each spin component becomes difficult and, $\Omega = |\Lambda| + \Sigma$ is used instead of $\Omega = |\Lambda + \Sigma|$.

2.4.2 Hund's coupling cases

The electronic spectra of molecules that do not have closed electron shells are usually quite complex because of the interaction of different angular momenta. In the absence of nuclear spin there are three "fine structure" interactions associated with the magnetic moments due to electrons, which are summarized in Table 2.2.

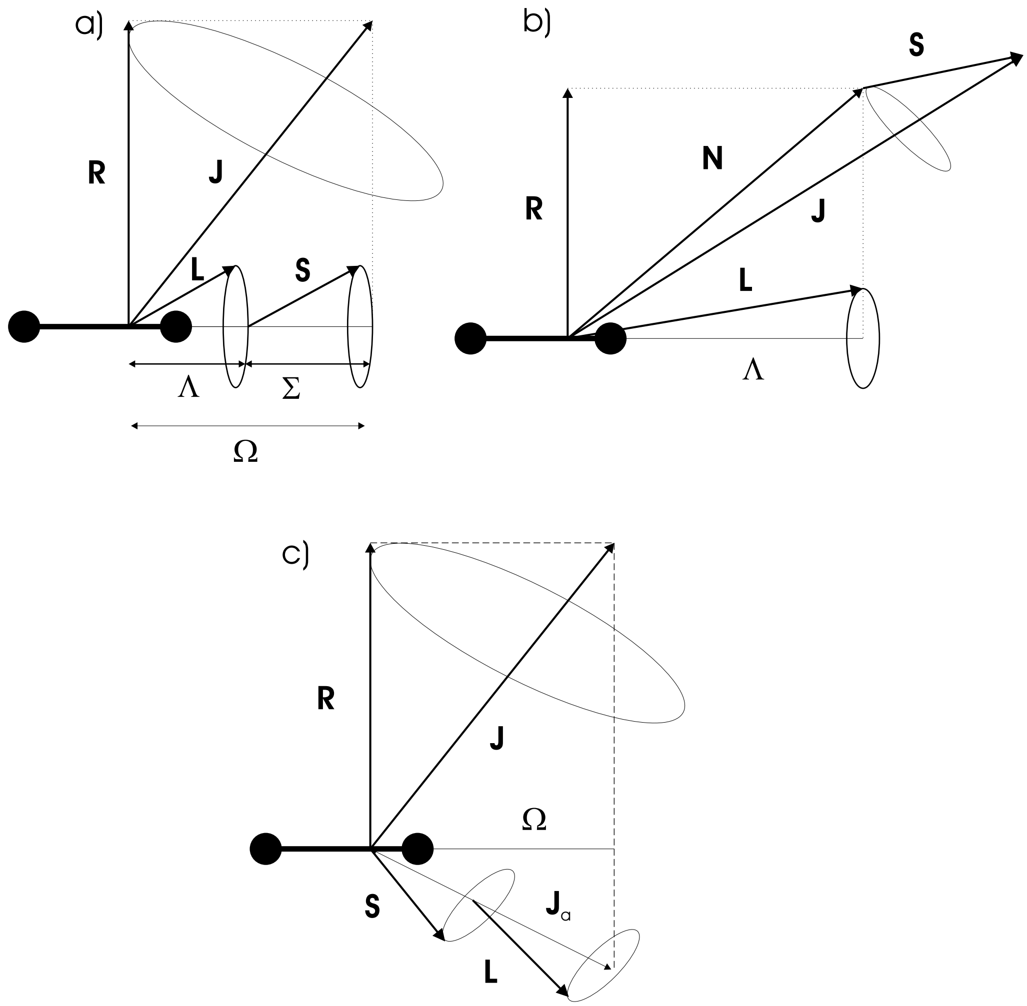

Figure 2.1: Hund's cases.

The effective Hamiltonian for a diatomic molecule can be therefore written as

$$\hat{H}_{\text{eff}} = \hat{H}_{\text{vib}} + \hat{H}_{\text{rot}} + \hat{H}_{\text{SO}} + \hat{H}_{\text{SR}} + \hat{H}_{\text{SS}} + \hat{H}_{\text{LD}}, \tag{2.11}$$

where

$$\hat{H}_{\text{SO}} = A\mathbf{L}\cdot\mathbf{S}, \tag{2.12}$$

$$\hat{H}_{\text{SR}} = \gamma\mathbf{N}\cdot\mathbf{S}, \tag{2.13}$$

Table 2.2: Coupling of angular momenta.

Interaction term	Designation	Description
R·**S**	Spin-Rotation (SR)	Total electron spin interacting with the magnetic fields created by nuclear motion
L·**S**	Spin-Orbit (SO)	Electron spin interacting with the magnetic fields created by electron motion
S·**S**	Spin-Spin (SS)	Interaction between magnetic moments of different unpaired electrons

$$\hat{H}_{\text{SS}} = \frac{2}{3}\lambda(3S_z^2 - \mathbf{S}^2), \tag{2.14}$$

and $\hat{H}_{\text{LD}}$ describes the Λ-doubling interaction. The constants A, γ, λ and their physical interpretation (as well as that of Λ-doubling) are discussed in more detail in the following chapters and in Refs. [1, 6, 12–14].

As the appearance of the spectra depends strongly on the strength of spin-orbit coupling, it is convenient to introduce several idealized situations classified as Hund's coupling schemes [15].

Hund's case (*a*)

The vector diagram of Hund's case (*a*) is shown in Figure 1.1a. The electron orbital angular momentum **L** is strongly coupled to the internuclear axis by electrostatic forces, and electron spin angular momentum **S** is coupled to **L** through strong spin orbit coupling. One can safely assume case (*a*) coupling whenever $A \gg BJ$, where A is the spin-orbit coupling constant. Obviously Hund's case (*a*) approximation becomes less appropriate as J increases. The "good" quantum numbers in Hund's case (*a*) are Λ, S, Σ, J and Ω. In a pure case (*a*) there are $2S+1$ spin components, each with their own Ω-value, and each of these spin components has a pattern of rotational energy levels given by $B_{\Omega,eff}J(J+1)$, with the lowest level having $J = \Omega$. Each J is doubly degenerate (for $\Omega > 0$), corresponding to e and f parities. Although Λ=0 for Σ states, second order spin-orbit coupling can split a $^{2S+1}\Sigma$ state into $S + 1$ spin components [5]. This situation is referred as Hund's coupling case (a') [16].

Hund's case (b)

In the case when $A \ll BJ$ the coupling of the electron spin to the internuclear axis is very weak and this situation is referred as Hund's case (b) (Figure (1.1b). As it is illustrated in Figure 1.1b, $\mathbf{L}$ (or its projection Λ) is coupled to $\mathbf{R}$ to form $\mathbf{N}$; $\mathbf{N}$ is then coupled with $\mathbf{S}$ to form the total angular momentum $\mathbf{J}$. The "good" quantum numbers in Hund's case (b) are Λ, N, S and J. The energy of the rotational levels is given by $BN(N+1)$, and each N-level is split into $2(2S+1)$ or $2S+1$ spin components for $\Lambda \neq 0$ and $\Lambda = 0$, respectively. Electronic states obeying Hund's case (b) coupling are described in more detail later in the thesis for the $X^7\Sigma^+$ state of MnH and the $X^9\Sigma^-$ state of EuH.

Hund's cases (a) and (b) are extreme cases, and there are many examples of electronic states that do not obey either coupling approximation closely. These states can be described as intermediate coupling cases [6].

Hund's case (c)

In electronic states that obey Hund's case (c) coupling, the spin-orbit coupling is so strong that $A \gg \Delta E_{\text{states}}$, where ΔE_{states} is the separation between the electronic states. As shown in Figure 1.1c, the electron orbital angular momentum $\mathbf{L}$ and electron spin $\mathbf{S}$ couple to form J_a whose projection on the internuclear axis is Ω. $\mathbf{J}_a$ (or its projection Ω) is then coupled to $\mathbf{R}$ to form the total angular momentum $\mathbf{J}$. The "good" quantum numbers in Hund's case (c) are therefore Ω and J. The $^{2S+1}\Lambda_\Omega$ spin components of a given $^{2S+1}\Lambda$ term can be considered as independent electronic states, because these components are usually a mixture of many $^{2S+1}\Lambda_\Omega$ basis functions coming from different electronic states. The spectroscopic constants for different Ω components of the same $^{2S+1}\Lambda$ term can be quite different, as we shall see for the electronic states of CoH. In fact, because of the aforementioned mixing of basis functions, the $^{2S+1}\Lambda_\Omega$ notation is not very appropriate for Hund's case (c) and the notation suggested by Linton *et al.* [17] is commonly used. In this notation states are labeled by $[T_0]\Omega$, where $[T_0]$ is the energy of the state in thousands of wavenumbers.

Just as in case (a), the rotational levels have relative energies $BJ(J+1)$ which are doubled for $\Omega \neq 0$.

Hund's cases ($a_{\beta J}$) and ($b_{\beta J}$)

If nuclear spin is present in at least one of the atoms, then one has to consider its coupling with other angular momenta in the molecule, and Hund's cases (a) and (b) are divided into various sub-classifications. In this thesis we encounter only Hund's cases ($a_{\beta J}$) and ($b_{\beta J}$). In both cases, the nuclear spin **I** couples with total angular momentum **J** to produce **F**. The subscript β implies that this quantization occurs only in the laboratory system of coordinates, and hyperfine components are expected to form a Landé-type pattern [18]; i.e., the spacing between them is proportional to the larger value of F.

2.4.3 Parity

It should be noted that the meaning of parity in molecular spectroscopy is slightly different from the one given in physics textbooks. The concept of parity as it applies to molecular spectroscopy is well explained in Refs. [1, 14]. In this thesis, the term parity usually refers to rotationless e and f parities.

All rovibronic energy levels can be divided into two types by applying the inversion operator $\hat{E}^*$, which inverts the laboratory coordinates of all electrons and nuclei:

$$\hat{E}^*\psi = \hat{E}^*(\psi_{\rm el}\psi_{\rm vib}\psi{\rm rot}) = (\pm)\psi. \tag{2.15}$$

All $(+)\psi$ energy states have positive total parity, while $(-)\psi$ energy states have negative total parity. Of course, the effects of $\hat{E}^*$ on the electronic, vibrational and electronic parts of the wavefunction need to be determined individually [1]. $\hat{E}^*$ is a symmetry operator, because all of the relative distances between particles are preserved.

The total parity alternates with J and it is useful to factor out this alternation by introducing rotationless e and f parities

$$\hat{E}^*\psi = +(-1)^J\psi, \tag{2.16}$$

$$\hat{E}^*\psi = -(-1)^J\psi. \tag{2.17}$$

Rotationless parity is more convenient to use as, for example all rotational energy levels of a $^1\Sigma^-$ state have f parity, while the sign of their total parity alternates with J.

2.4.4 Transitions between electronic states

Transitions between different electronic states of the molecule can be observed at a great range of frequencies, depending on the energy separation between these states. In this thesis, the electronic transitions of CoH, YbO, EuH, ErF, SmH, TmH and SmCl molecules are reported in Chapters 5, 6, 7 and 8.

Bibliography

[1] P. F. Bernath, *Spectra of Atoms and Molecules*, Oxford University Press, New York, 2nd edition, 2005.

[2] M. Born and J. R. Oppenheimer, Ann. Phys. **84**, 457 (1927).

[3] C. H. Townes and A. L. Schawlow, *Microwave Spectroscopy*, Dover, New York, 1975.

[4] W. Gordy and R. L. Cook, *Microwave Molecular Spectroscopy*, Interscience, New York, 1970.

[5] P. F. Bernath, *Spectra of Atoms and Molecules*, Oxford University Press, Oxford, 1995.

[6] G. Herzberg, *Spectra of Diatomic Molecules*, Van Nostrand, New York, 1950.

[7] J. L. Dunham, Phys. Rev. **41**, 721 (1932).

[8] J. L. Dunham, Phys. Rev. **41**, 713 (1932).

[9] A. H. M. Ross, R. S. Eng, and H. Kildal, Opt. Comm. **12**, 433 (1974).

[10] J. K. G. Watson, J. Mol. Spectrosc. **80**, 411 (1980).

[11] R. J. Le Roy, J. Mol. Spectrosc. **194**, 189 (1999).

[12] J. M. Hollas, *Modern Spectroscopy*, John Wiley & Sons, Chichester, England, 2nd edition, 1996.

[13] J. M. Brown and A. Carrington, *Rotational Spectroscopy of Diatomic Molecules*, Cambridge University Press, Cambridge, U.K., 2003.

[14] H. Lefebvre-Brion and R. W. Field, *Perturbations in the Spectra of Diatomic Molecules*, Academic Press, New York, 1986.

[15] F. Hund, Handbuch der Physik **24**, 561 (1933).

[16] I. Kopp and J. T. Hougen, Can. J. Phys. **45**, 2581 (1967).

[17] C. Linton et al., J. Mol. Spectrosc. **102**, 441 (1983).

[18] T. M. Dunn, Nuclear hyperfine structure in the electronic spectra of diatomic molecules, in *Molecular Spectroscopy- Modern Research*, edited by K. N. Rao and C. W. Mathews, pages 231–257, Academic Press, New York, 1978.

Chapter 3

Experimental

3.1 Fourier transform emission spectroscopy

3.1.1 Emission spectroscopy vs absorption spectroscopy

The majority of the experiments reported in this thesis were carried out in emission, and were recorded using a Bruker IFS 120HR Fourier transform spectrometer. The vibrational (infrared) and electronic (in the near infrared and visible parts of the spectrum) transitions were studied for different metal-containing diatomic molecules.

It is well known that emission spectroscopy is more sensitive than the absorption spectroscopy in the visible and ultraviolet regions. This is due to the fact that absorption spectroscopy requires intense broad band background radiation which introduces noise [1].

The advantages in the infrared regions are not that obvious. Our experiments on the metal containing molecules in the gas phase required the heating of the metal to produce the metal vapor. This heating results also in background blackbody radiation, even for emission experiments. Moreover, the Einstein A coefficient which determines the emission rate of photons is proportional to ν^3, and is therefore much smaller for the vibrational transitions than for electronic transitions [1]. Nevertheless, the emission experiments in the IR region proved to be very effective partly due to the fact that these experiments do not require high concentrations of the gas phase molecules (or very long absorption paths), unlike absorption experiments. In Ref. [2] the infrared spectrum of BaH was recorded both in emission and absorption. Those experiments demonstrated that in that particular case the emission measurement was 20 times more sensitive with all conditions being equal.

3.1.2 Fourier transform spectroscopy

Modern Fourier transform spectrometers employ the Michelson interferometer first proposed by Albert Michelson in 1891 [3]. A schematic diagram of a Michelson interferometer is shown in Figure 3.1.

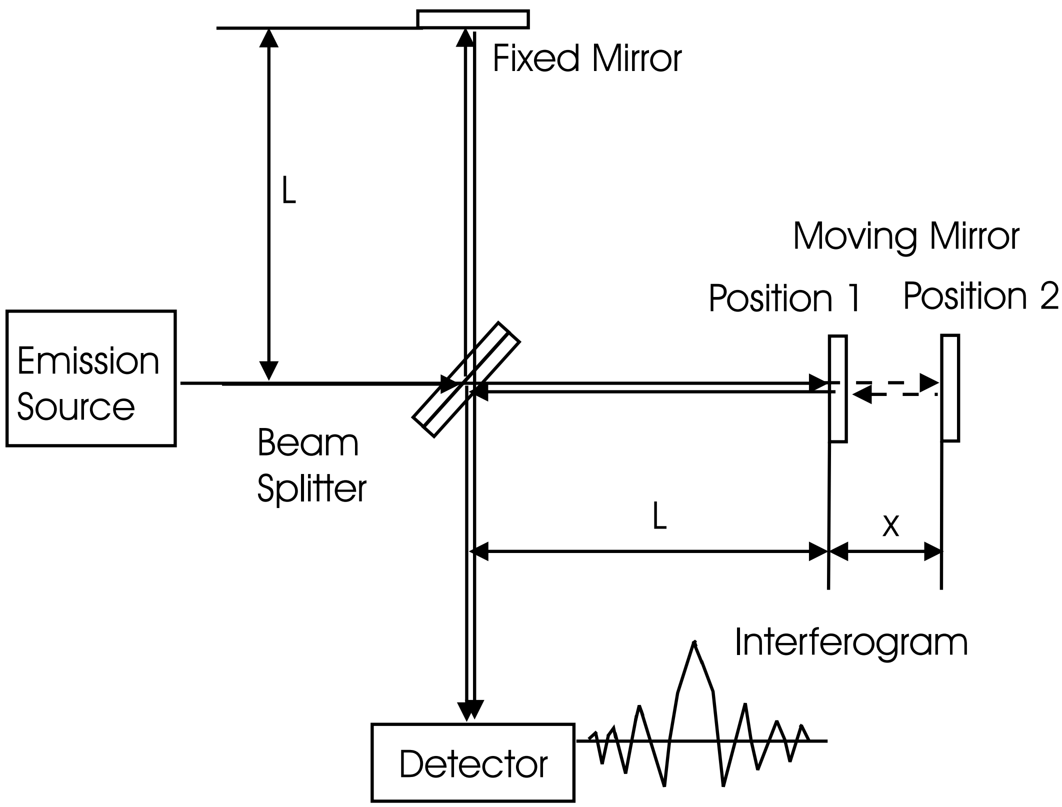

Figure 3.1: The schematic diagram of a Michelson interferometer. This figure is taken from Ref. [4].

When electromagnetic radiation from the source reaches the beamsplitter it splits into two beams. One beam is transmitted in the original direction while the other is reflected in the perpendicular direction. Both beams are reflected back from two mirrors and recombine at the detector after passing through the beamsplitter again. The two components of the recombined beam interfere with each other in a way that depends on the difference in the distances of the mirrors from the beamsplitter (optical path difference). For that purpose one of the mirrors is held fixed while the other one is moved to change the optical path difference between two beams. Although the optical design of our Bruker IFS 120 HR Fourier transform spectrometer is more sophisticated than that of classical Michelson interferometer, the general concept remains the same.

If the light source is monochromatic, then the relationship between the intensity of the interferogram $I(x)$ as a function of the optical path difference x between the two beams, and spectral intensity $B(\overline{\nu})$ as a function of wavenumber $\overline{\nu}$ is given by [5]

$$I(x) = B(\overline{\nu})[1 + cos(2\pi\overline{\nu}x)] \tag{3.1}$$

When the source contains more than one frequency the intensity of interferogram is given by [5]

$$I(x) = \int_{-\infty}^{+\infty} B(\overline{\nu})[1 + cos(2\pi\overline{\nu}x)]d\overline{\nu}. \tag{3.2}$$

This integral contains a mean intensity of the interferogram ($\int_{-\infty}^{+\infty} B(\overline{\nu})d\overline{\nu}$) and a so-called ac component

$$I(x) = \int_{-\infty}^{+\infty} B(\overline{\nu})cos(2\pi\overline{\nu}x)d\overline{\nu}, \tag{3.3}$$

which can be generalized as

$$I(x) = \int_{-\infty}^{+\infty} B(\overline{\nu})exp(2\pi i\overline{\nu}x)d\overline{\nu}. \tag{3.4}$$

The spectral distribution $B(\overline{\nu})$ can be obtained by the complex Fourier transform of the interferogram $I(x)$ as

$$B(\overline{\nu}) = \int_{-\infty}^{+\infty} I(x)exp(-2\pi i\overline{\nu}x)dx. \tag{3.5}$$

Since real spectrometers can produce only finite optical path differences, the spectra have a finite resolution. The maximum optical path difference ($OPD_{\max}$) of our Bruker IFS 120 HR FTS is about 5 m, which gives the highest resolution $\Delta\overline{\nu}_{\max}$ of $\sim$0.002 cm^{-1}, since $\Delta\overline{\nu}_{\max} \approx 1/OPD_{\max}$.

Another factor that has to be taken into account is a finite size of the entrance aperture of the spectrometer. The aperture introduces oblique rays in the nominally parallel beam, which results in circular fringes in the plane of the detector. Ideally, the detector should sample only the central fringe, because if the other interference rings fall on the detector the resolution is degraded. One therefore has a dilemma between choosing a large aperture to increase the light intensity at the detector, or choosing a smaller aperture to increase the resolution. In practice, the aperture is chosen to select as much as possible of the central region of the "bull's eye" pattern of interferogram. The following expression gives the maximum achievable resolution at the chosen aperture diameter d

$$\Delta\overline{\nu} = \frac{\overline{\nu}_{\max} d^2}{8F^2}, \tag{3.6}$$

where $\overline{\nu}_{\max}$ is the maximum wavenumber for which the interference is constructive over the OPD for a given aperture diameter and F is the focal length of the collimating mirror (F = 418 mm in our FTS). For example, for a resolution of 0.02 cm^{-1} at 5000 cm^{-1} the maximum aperture has a diameter of 2.4 mm, while for 0.002 cm^{-1} the maximum aperture is 0.75 mm. In our high-temperature experiments Doppler broadening was significant (as was pressure broadening for the experiments in the King furnace) and it was not necessary to use the maximum possible instrumental resolution. This allowed us to use larger diameters of the aperture to let more photons into the spectrometer.

Fourier transform spectrometers have two main advantages in comparison with grating spectrometers.

(1) Throughput Advantage (Jacquinot Advantage)

The optical throughput (also known as étendue) is equal to the product of the area A of the instrument aperture and the solid angle Ω subtended by the collimator. For the same spectral resolution, the circular aperture of an FTS has a larger area than that of the slit of a dispersive spectrometer; therefore the product $A\Omega$ is larger and the signal intensity is higher [5].

(2) Multiplex Advantage (Fellgett Advantage)

The total flux in the input beam falls on the detector of the FTS to give a large total signal, while in a grating spectrometer each frequency is dispersed (small signal falls on the detector) and scanned separately. The Fellgett advantage, however, applies only if the dominant source of noise is due to the detector or background radiation, which remains constant regardless of the level of signal entering the spectrometer.

(3) Precision Advantage

All modern FTSs have a built-in single mode laser (usually He-Ne) to control the mirror motion and to provide a convenient internal wavenumber standard.

The sensitivity of FTSs is however worse than that of diode lasers used for spectroscopic measurements in the infrared region. Nevertheless, an FTS is often the preferred instrument even in the infrared, because diode lasers have gaps in their tunable range and they do not have inherent means of calibration.

3.2 Emission sources

Three types of emission sources were used to generate the gas-phase molecules studied in this thesis. The choice of one source over another depends on the molecule that one wants to study. The main factors that have to be taken into account before choosing an experimental cell are the metal vapor pressures at the temperatures achievable in these sources, the reactivity of the metals and the oxidant gases with the experimental environment, and the stability of the created molecules under the experimental conditions. The temperature dependence of the vapor pressures of the metals studied in this thesis, calculated using interpolation equations from Ref. [6], is shown in Figure 3.2.

3.2.1 Broida oven

A flow system known as a Broida oven was introduced by West *et al*. [7] as a source for production of gas-phase diatomic metal oxides and halides. Broida ovens have been widely used by spectroscopists for many years in optical emission (chemiluminescence) and laser-induced fluorescence (LIF) experiments (see for example Ref. [8] - [12]).

The designs of this source vary slightly in different research groups, but the general idea remains the same. Figure 3.3 presents a schematic diagram of the Broida oven used in optical emission experiments in the Bernath laboratory.

About 5 g of metal sample is placed in an alumina (Al_2O_3) crucible which is surrounded by a tungsten heating basket. The current flowing through the basket is increased slowly over the period of 1-2 hours to a maximum value determined by the vapor pressure of the metal. Typically, few mTorr of metal vapor is adequate, and excessive metal vapor pressure will cause deposits that block the cone at the top of the crucible. An inert carrier gas (normally argon) is introduced through a small

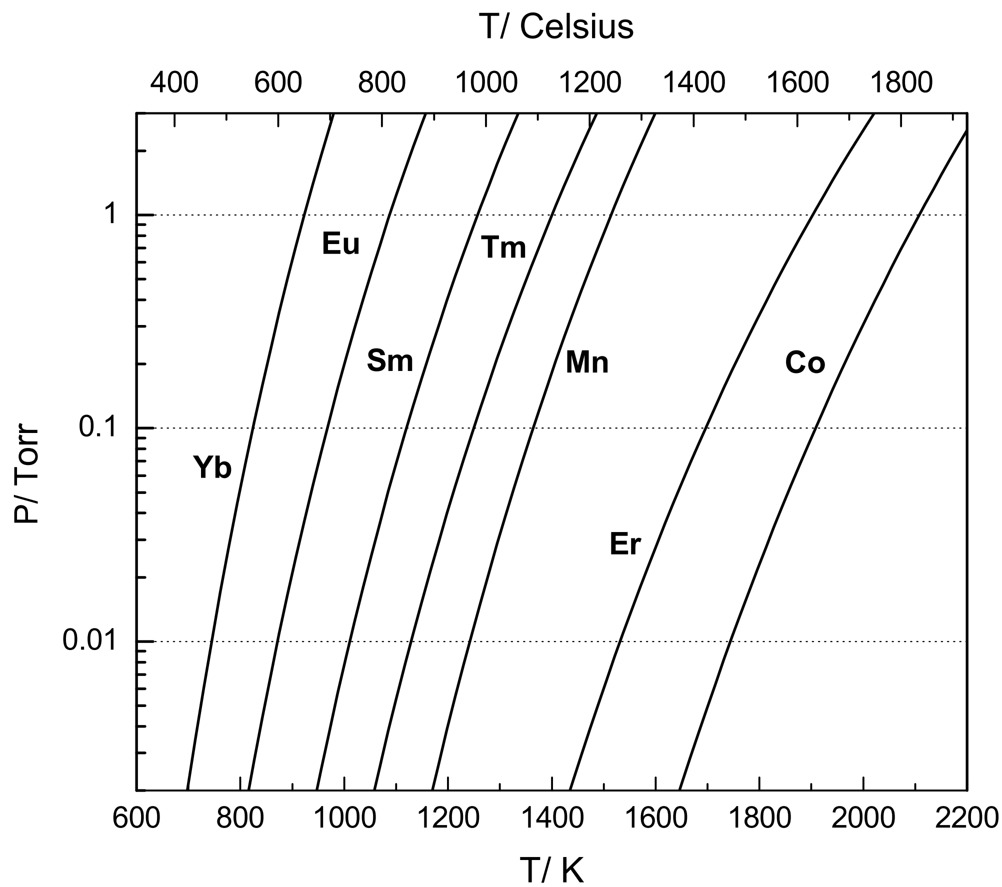

Figure 3.2: Selected metal vapor pressures as a function of temperature. Calculated using equations from Ref. [6].

stainless steel ring at the top of crucible just below the cone. The vaporized metal is carried out of the crucible by this inert gas through the stainless steel conical chimney. The chimney is about 5 mm in diameter at the top, and it reduces the cross sectional area of the flow. The tip of the chimney is surrounded by another ring through which an oxidant gas flows. The typical oxidant gases are: a) N_2O for production of metal oxides, b) SF_6 for metal fluorides, and c) HCl or CH_3Cl for metal chlorides. The heating system is placed inside a water-cooled stainless steel chamber which is constantly pumped while the inert gas pressure is usually kept at

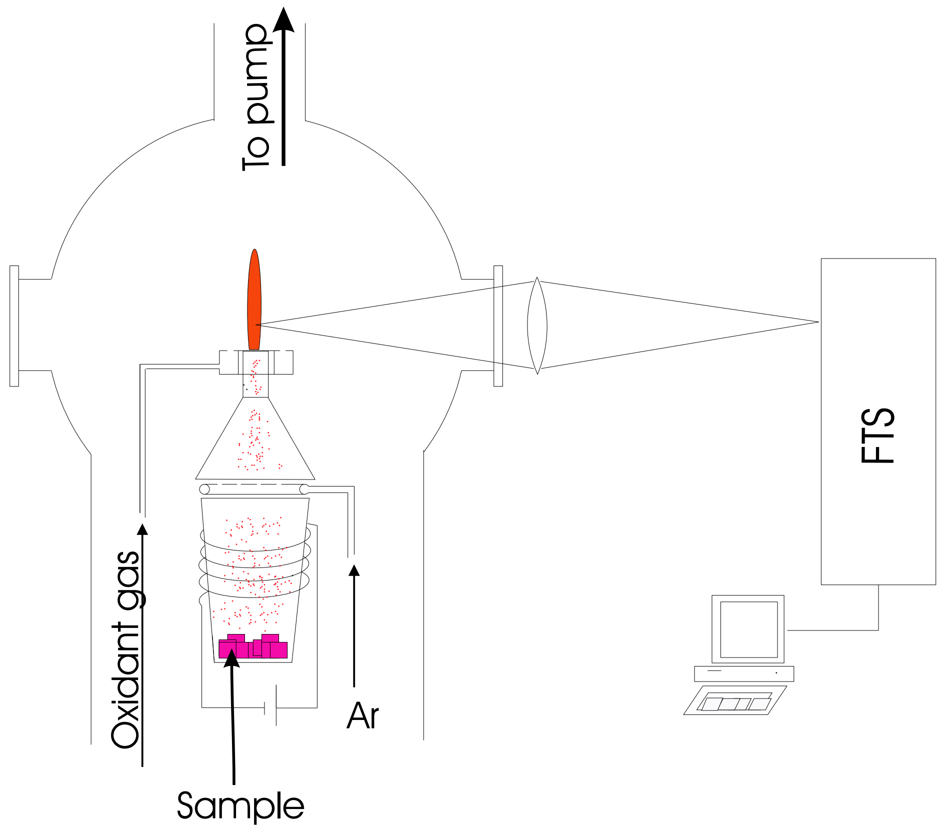

Figure 3.3: A schematic of the Broida oven at the University of Waterloo.

2-10 Torr and oxidant gas at ∼0.1 Torr. To avoid contamination of the pump oil with dust particles, a large diameter automobile air filter is used.

In order to prevent the escape of heat from the system, a cylindrical alumina heat shield is usually placed around the crucible (not shown on Figure 3.3). The space between the crucible and the heat shield is filled with zirconia or other fibrous ceramic materials. Care has to be taken because some ceramic materials become conductive at high temperatures and need to be isolated from the tungsten basket.

The diatomic molecules formed at the exit of the chimney usually produce a bright chemiluminescent flame. The shape and color of the flame depends on the metal and the oxidant gas as well as onthe pressures of the carrier gas and oxidant. In the emission experiments carried out in this work, the flame was imaged onto the entrance aperture of the FTS, and emission spectra were recorded.

Although the Broida oven is one of the most widely used sources for production of metal-containing diatomics for spectroscopic experiments, it has some disadvantages: a) the chemiluminescence is not very bright, which result in a poor signal-to-noise ratio in emission experiments; b) the operating temperatures are typically ≤ 1500°C (nevertheless some modifications can be made to achieve higher temperatures [7], [13]); c) it is best for experiments with metal oxides and halides.

3.2.2 The high temperature furnace/electrical discharge emission source

A combination of an electrical discharge with a high temperature furnace has proved to be an excellent emission source for the electronic and infrared spectroscopy of diatomic [14–17] and triatomic [18, 20] metal hydrides. A schematic diagram of the source is depicted in Figure 3.4.

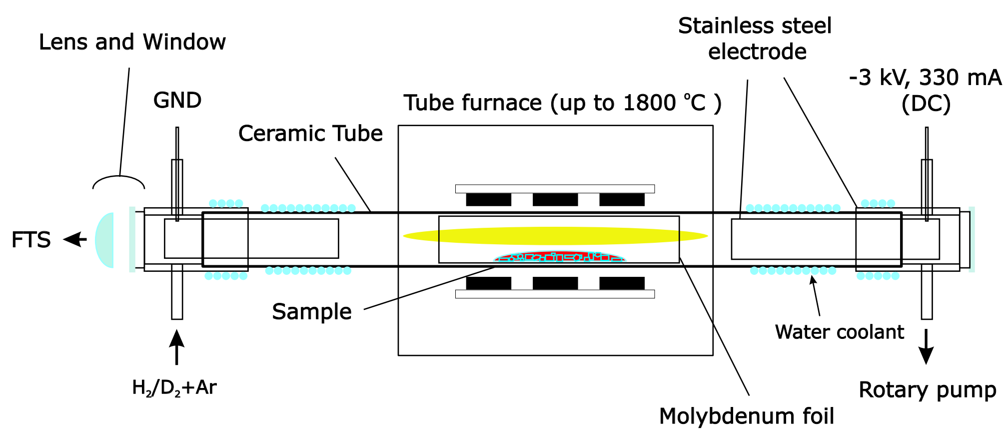

Figure 3.4: An illustration of the emission source that combines a dc discharge and a high temperature furnace.

The following procedure is used in our experiments. First, a sample of metal, 20-50 g, is placed in the center of the alumina (Al_2O_3) or mullite ($2Al_2O_3{\cdot}2SiO_2$) tube, and is then heated by the CM Rapid Temp furnace. In the case of rare earth metals, the hot part of the tube is wrapped inside with molybdenum foil to prevent the reaction between the metal and the ceramic. The furnace can be heated to temperatures ≤ 1800°C, depending on the experiment. Normally the temperature is chosen to achieve about 1 Torr of the metal vapor pressure. The heating rate was usually 250°C per hour, to avoid thermal shock of the alumina ceramic.

An electrical discharge (3 kV, 333 mA) was then applied between two cylindrical stainless steel electrodes inside the water-cooled ends of the tube. A mixture of Ar and H_2 gases flows slowly over the sample, typically at 3-12 Torr of total pressure, with the H_2 pressure being just 2% of the total. The high temperature together with a DC discharge not only facilitates the production of the molecules in the gas phase, but also populates excited vibrational levels and excited electronic states. Electronic transitions appear in the visible or near infrared parts of the spectral range, while transitions between vibrational levels of the same electronic state can be observed in the infrared region. The tube is sealed with windows made from different materials depending on the spectral range of interest. The emission from the tube is focused on the entrance aperture of the Fourier transform spectrometer by a lens made from the same material as the windows.

One of the disadvantages of this method is the reaction of the alumina (or mullite) with some of the metals at high temperatures. This sometimes results in deformation or even breaking of the tubes. Although there are some methods to avoid direct contact of the metal and the ceramic, i.e., carbon liners, tantalum or carbon boats, damage of the tubes sometimes occurs anyway. Unlike the Broida oven source, there are numerous impurities that can be seen in emission spectra produced in the discharge/furnace source. The most common impurities are AlH (with alumina tubes) and SiO (with mullite tubes). It is interesting that during an attempt to produce the infrared spectrum of scandium monohydride (ScH), a very intense spectrum of AlH was observed. The signal was in fact of the same quality as in the experiment that was aimed directly at observing the spectrum of AlH [21]. This was probably because Sc atoms were "replacing" the Al atoms in the walls of the tube.

Another disadvantage of the furnace/discharge source is that experiments to make molecules other than hydrides are difficult. This is mostly because the electrodes at the ends of the tube become contaminated rapidly and the discharge becomes very unstable.

3.2.3 The King furnace

One of the oldest tools for gas phase spectroscopy of atoms and molecules is a King furnace (a graphite tube furnace) originally introduced by Arthur King in 1908 [22]. The design of the King furnace at the University of Waterloo is depicted in Figure 3.5.

The furnace shell is a water jacket made from anodized aluminum. The end bulkheads were originally made from nickel-plated aluminum, but we had to replace

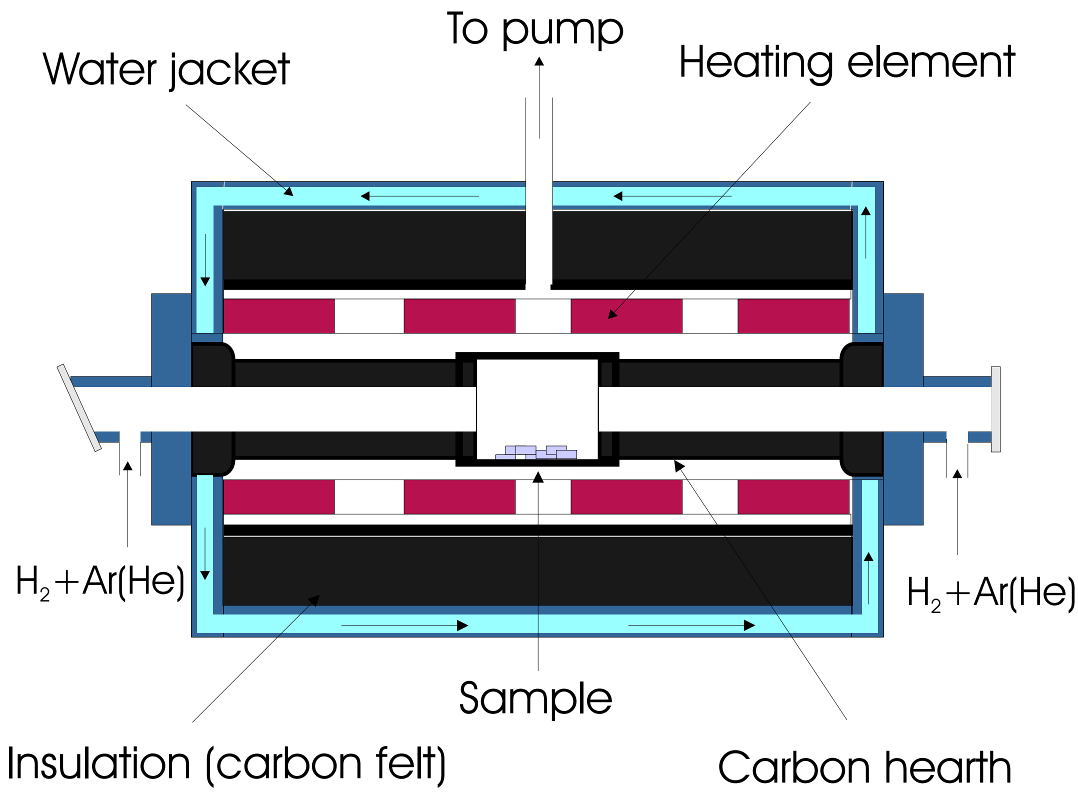

Figure 3.5: A schematic of the King furnace at the University of Waterloo.

them with new stainless steel bulkheads because the internal cooling water passages were clogged with deposits. Everything inside the outer shell is made of carbon. The active part of the furnace is a graphite heating element through which currents up to 65 A can flow. Thermal insulation between the heating element and the furnace shell is provided by carbon felt which is retained by a graphite radiation shield. Two carbon hearths (tubes) are inserted into each end of the furnace coaxial to the heating element. The graphite holder containing the metal sample connects the two hearths. The temperatures inside the furnace can reach 2700°C, depending on the operating gas and the current applied.

The heating process was started with about 100 Torr of operating gas. Hydrogen, helium and argon gases were used for the experiments in this thesis. It was found that when doing experiments on metal hydrides, the use of pure hydrogen does not yield intense spectra due to the relatively low temperature. This is due to the fact that at temperatures greater than 2 250°C molecular hydrogen dissociates to atomic hydrogen, which is an endothermic reaction. The addition of argon gas helps significantly in achieving higher temperatures (up to 2 800°C), but at high temperatures the argon gas proved to be harmful to the heating element. Helium gas yields a smaller increase in temperature, but it does not harm the heating element. In the experiments with metal fluorides, chlorides and sulfides, the furnace was heated with helium gas, and after the maximum temperature was achieved CF_4, HCl or CS_2 gases, respectively, were added. When the spectra were recorded the total pressure in the furnace was held at ∼200 Torr. The emission from the furnace was imaged onto the entrance aperture of the FTS with a lens.

It was found that the lanthanide metals are very reactive with the carbon environment of the King furnace. Some of the damage can be avoided by wrapping the inside of the sample holder first with tantalum and then with tungsten foils. However, the metal vapor can penetrate almost everywhere inside the furnace, causing severe damage to the heating element and radiation shield.

3.3 Laser ablation/molecular beam apparatus

The sub-Doppler spectrum of EuH was recorded in the laser ablation/molecular beam apparatus at the Arizona State University in the laboratory of Prof. T. C. Steimle. A brief description of this apparatus is given in section 7.2.2 of this thesis.

Bibliography

[1] P. Bernath, Chem. Soc. Rev **25**, 111 (1996).

[2] K. Walker, H. Hedderich, and P. Bernath, Mol. Phys. **78**, 577 (1993).

[3] A. Michelson, Phil. Mag. **31**, 256 (1891).

[4] G. Li, PhD thesis, University of Waterloo, Waterloo, ON, 2003.

[5] S. P. Davis, M. C. Abrams, and J. W. Brault, *Fourier Transform Spectrometry*, Academic Press, New York, 2001.

[6] O. Knacke, O. Kubaschewski, and K. Hesselmann, *Thermo-chemical Properties of Inorganic Substances*, volume 51, Springer-Verlag Berlin, Heidelberg, 2nd edition, 1991.

[7] J. West, R. Bradford, J. D. Eversole, and C. Jones, Rev. Sci. Instr. **46**, 164 (1975).

[8] T. Melville, I. Gordon, K. Tereszchuk, J. Coxon, and P. Bernath, J. Mol. Spectrosc. **218**, 235 (2003).

[9] H. Li, R. Skelton, C. Fosca, B. Pinchemel, and P. Bernath, J. Mol. Spectrosc. **203**, 188 (2000).

[10] S. A. McDonald, S. Rice, R. Field, and C. Linton, J. Chem. Phys. **93**, 7676 (1990).

[11] P. Carrette, A. Hocquet, M. Douay, and B. Pinchemel, J. Mol. Spectrosc. **124**, 243 (1987).

[12] M. J. Dick and C. Linton, J. Mol. Spectrosc. **217**, 26 (2003).

[13] P. Sheridan, PhD thesis, University of Arizona, Tucson, AZ, 2003.

[14] A. Shayesteh, D. Appadoo, I. Gordon, R. LeRoy, and P. Bernath, J. Chem. Phys. **120**, 10002 (2004).

[15] A. Shayesteh, K. Walker, I. Gordon, D. Appadoo, and P. Bernath, J. Mol. Struct. **695**, 23 (2004).

[16] S. Yu et al., J. Mol. Spectrosc. **229**, 257 (2005).

[17] I. E. Gordon, A. Shayesteh, D. Appadoo, K. Walker, and P. Bernath, J. Mol. Spectrosc. **229**, 269 (2005).

[18] P. Bernath, A. Shayesteh, and K. Tereszchuk, Science **297**, 1323 (2002).

[19] A. Shayesteh, D. Appadoo, I. Gordon, and P. Bernath, J. Chem. Phys. **119**, 7785 (2003).

[20] A. Shayesteh, D. Appadoo, I. Gordon, and P. Bernath, J. Am. Chem. Soc. **126**, 14356 (2004).

[21] J. White, M. Dulick, and P. Bernath, J. Chem. Phys. **99**, 8371.

[22] A. S. King, Astrophys. J. **28**, 300 (1908).

Chapter 4

Infrared emission spectra of MnH and MnD

4.1 Introduction

The search for infrared spectra of gas phase metal dihydride molecules using Fourier transform emission spectroscopy is a continuing project in the Bernath laboratory. So far we have been able to detect spectra of BeH_2 [1, 2], MgH_2 [3], ZnH_2 [4–6], HgH_2 and CdH_2 [6]. Similar experiments on MnH_2 were of particular interest, because early spectroscopic studies [7, 8] suggested a bent structure for MnH_2, whereas theory predicts a linear geometry [9–11]. The most recent experimental work on MnH_2 also favors a linear structure [12]. Unfortunately, we were not able to find the spectrum of manganese dihydride in our experiments. In our paper on CaH and SrH [13], we discuss the factors that promote the production of gaseous metal dihydrides. Nevertheless high quality spectra of manganese monohydride and monodeuteride were obtained in the course of our experiments, and we present the results in this chapter.

Molecules containing transition metal atoms are of interest to scientists, including spectroscopists. Apart from astrophysical interest, research on metal hydrides contributes to understanding of such topics as hydrogenation catalysis and the formation of the metal-hydrogen bond. Transition metal atoms have partially filled d-subshells, resulting in numerous low-lying electronic states that readily interact with each other. Manganese is an unusual transition element because it has a half-filled $3d$-subshell, and therefore manganese-containing molecules possess only a few low-lying electronic states. Manganese has high spin coupling that leads to high-multiplicity electronic states. Spectra of molecules with electronic states of high multiplicity are very complex, and are a challenge to analyze.

Manganese hydride is one of the most extensively studied high-spin molecules. The MnH $A^7\Pi$–$X^7\Sigma^+$ electronic transition alone has been the subject of more than a dozen experimental and theoretical papers. The first observation and identification of this spectrum was carried out by Heimer in 1936 [14]. Between 1942 and 1957, Nevin and co-workers recorded and rotationally analyzed the 0-0 and 0-1 bands of the $A^7\Pi$–$X^7\Sigma^+$ transition (near 568 and 624 nm) for MnH and MnD. This extensive work was published in six papers over a 15 year period [15–20]. The $A - X$ 0-0 band was revisited 50 years later by Varberg *et al.* [21–23] using laser excitation spectroscopy. Theye extended Nevin's rotational analysis to the lowest J values for every spin component, and studied the nuclear hyperfine interaction.

The first observation of transitions involving quintet states of MnH was in 1938 by Pearse and Gaydon [24]. Balfour *et al.* recorded a number of quintet bands using a Fourier transform spectrometer. They rotationally analyzed the $c^5\Sigma^+$–$a^5\Sigma^+$ 0-0 and 1-1 bands near 846 nm, the $b^5\Pi$–$a^5\Sigma^+$ 0-0 band at 1060 nm [25], the $d^5\Pi_i$–$a^5\Sigma^+$ 0-0, 1-1 and 2-2 bands at 480 nm, and the $e^5\Sigma^+$–$a^5\Sigma^+$ 0-0 band at 450 nm [26, 27]. Some of the corresponding MnD bands were also presented in these papers.

The ground $X^7\Sigma^+$ electronic state of MnH was probed by means of electron spin resonance (ESR) [7] and electron-nuclear double resonance (ENDOR) spectroscopy [28, 29]. Later Urban and Jones observed an infrared spectrum of MnH [30] and MnD [31] using a diode laser spectrometer. They recorded vibrational bands v=1←0 to v=3←2 with a nominal accuracy of 0.001 cm^{-1}. Urban and Jones [30, 31] determined equilibrium constants for both molecules and carried out a combined isotopologue fit to determine mass-independent parameters. Unfortunately, semiconductor diode lasers have certain limitations (mainly due to gaps in the tuning curve), which do not allow coverage of the whole spectral range. As a result, only relatively few infrared lines have been measured; for example only seven R-lines, that are all spin components of a single R(5) transition, were obtained for the fundamental band of MnH.

Theoretical studies of MnH began with work of Kovács and Pacher [32–34], who derived a molecular Hamiltonian for $A^7\Pi$ and $X^7\Sigma^+$ states. *Ab initio* calculations on MnH by Das [35], Walch and Bauschlicher [36] and Chong *et al.* [37] were performed for the ground $X^7\Sigma^+$ state. Bagus and Schaefer [38] investigated both the $A^7\Pi$ and $X^7\Sigma^+$ states, but in the absence of electron correlation. *Ab initio* calculations by Langhoff *et al.* [39] included all quintet and septet states below 30 000 cm^{-1}. The most recent *ab initio* calculations for the ground state were carried out by Harrison [40].

In this chapter, we report new infrared emission spectra of MnH and MnD recorded with a Fourier transform spectrometer. The vibrational bands $v = 1 \rightarrow 0$ to $v = 3 \rightarrow 2$ for MnH and $v = 1 \rightarrow 0$ to $v = 4 \rightarrow 3$ for MnD were observed. Analyses of the new spectra have provided improved ground state molecular constants for MnH and MnD.

4.2 Experimental

The same emission source that has proved to be very effective in providing spectra of other metal hydrides in our laboratory [4, 13, 41] was used for MnH and MnD. About 40 g of manganese metal was heated to 1 200°C in a sealed and evacuated alumina tube by a CM Rapid Temp furnace. This produced approximately 1 Torr pressure of manganese vapor. A mixture of hydrogen (or deuterium) and argon gases was introduced into the tube and an electrical discharge (3 kV, 333 mA) was applied between two cylindrical stainless steel electrodes inside the ends of the tube. The total pressure inside the system was maintained at about 3.5 Torr, with hydrogen gas being approximately 10 % of the total. Emission from the tube was focused onto the entrance aperture of a Bruker IFS 120 HR Fourier transform spectrometer. The windows at the ends of the tube and the lens were made from BaF_2. The infrared spectra of MnH/D were recorded between 800 and 1 700 cm^{-1} at a resolution of 0.0085 cm^{-1} using a KBr beamsplitter and a liquid nitrogen-cooled HgCdTe (MCT) detector. A 1 670 cm^{-1} red pass filter was used to limit the emission to the desired spectral range. The spectra contained MnH/D emission lines, as well as blackbody emission from the hot tube, and absorption lines from atmospheric water vapor, as one can see for the spectrum of MnH in Figure 4.1. Four hundred scans were co-added for each molecule in order to improve the signal-to-noise ratio.

4.3 Results and discussion

The recorded infrared emission spectrum of MnH/D contained vibration-rotation bands in the ground electronic $^7\Sigma^+$ state. The lines from $v = 1 \rightarrow 0$ to $v = 3 \rightarrow 2$ for MnH and the lines from $v = 1 \rightarrow 0$ to $v = 4 \rightarrow 3$ transitions for MnD were found and analyzed. An overview spectrum of MnD is shown on Fig. 4.2. In order to display the bands more clearly, the baseline was corrected by eliminating blackbody emission profile using the Bruker OPUS program.

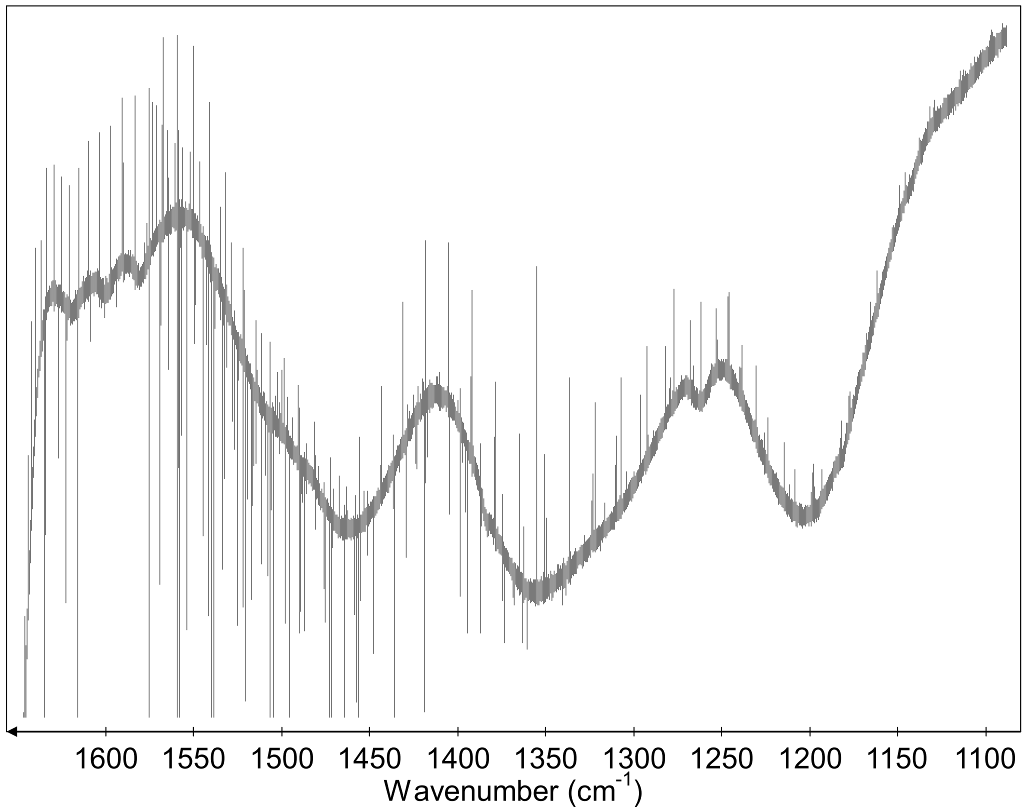

Figure 4.1: An overview of the infrared emission spectrum of MnH.

The $X^7\Sigma^+$state of MnH obeys Hund's case (b) coupling, so each rotational level (N) is split into seven spin components (for $N \geq 3$) labeled by J with **J=N+S**, where **J** is the total angular momentum, **N** is rotational angular momentum and **S** is the total electron spin. The fine structure splitting of $N = 0$ to 3 rotational levels is shown in Figure 4.3. An example showing seven spin components for R(5) and P(7) lines of the fundamental band of MnH are displayed in Fig. 4.4. It is fortunate that manganese has just one isotope (^{55}Mn with $I = 5/2$), otherwise the spectrum would be more complicated due to line overlaps. The spacing between the spin components in the R branches decreases with increasing N, causing transitions with $N > 20$ of fundamental band to be observed as single broad lines. This blending is observed to occur at lower N values as the vibrational quantum number increases. On one hand it is a disadvantage, since unblended lines are more desirable for analysis, but on the other hand, the intensity of blended lines is usually higher, allowing the measurement of the $v = 4 \rightarrow 3$ transition in MnD for which only single R-lines

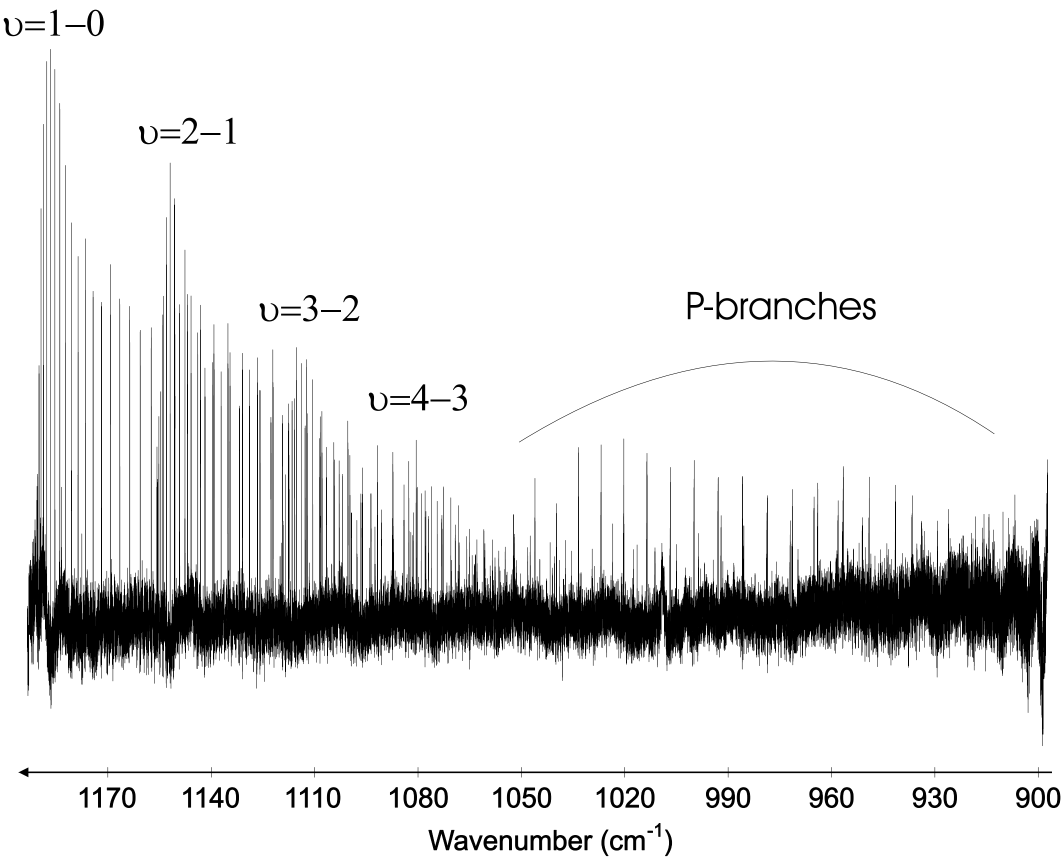

Figure 4.2: An overview of the infrared emission spectrum of MnD after baseline correction.

were observed without any trace of corresponding P-lines. The intensities of the spin components of each rotational line both in the P- and R-branches increase from $J = N - 3$ to $J = N + 3$, as shown in Figure 4.4 for R(5) and P(7) transitions of the fundamental band. These line intensities have the classic pattern given by coupling of two angular momenta such as **L** and **S** to give **J** for atoms [42]. Urban and Jones [30] observed deviations from this expected intensity pattern. In the present FT spectrum, however, this intensity pattern seems to be consistent throughout the spectrum with the exception of a few lines that are overlapped with water absorption lines or atomic emission lines. As an illustration, the lines in Fig. 4.4 were chosen to be the same as the ones shown by Urban and Jones [30]. In our spectrum we were also able to observe a few satellite lines (transitions across spin components) at low N values.

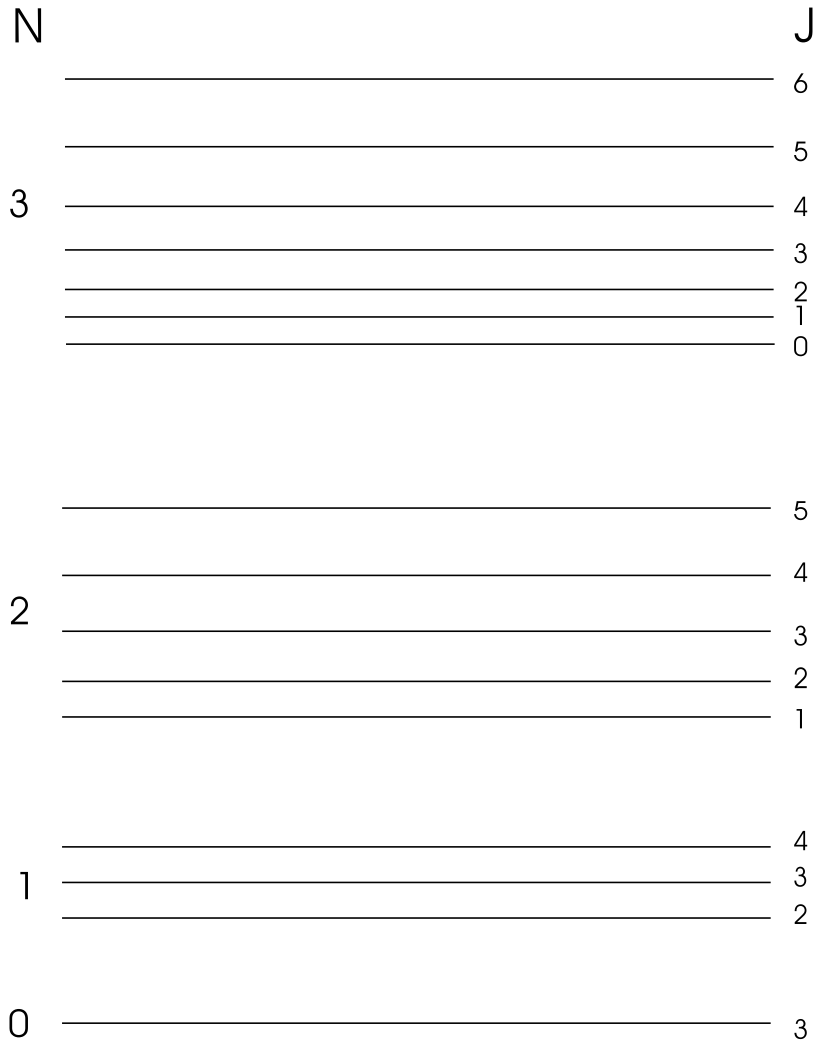

Figure 4.3: Fine structure of the low rotational levels of the $X^7\Sigma^+$state of MnH.

A zero filling factor of 8 was used during the Fourier transformation to improve data reduction. Zero filling in the interferogram interpolates the spectrum by increasing the number of sampling points. The line positions were determined using the program WSpectra written by M. Carleer. The MnH/D spectra were calibrated using the line positions of the previous diode laser infrared measurements [30, 31]. The effect of blending at higher N values forced us to assign an experimental uncertainty ranging from 0.001 cm^{-1} for strong unblended lines to 0.003 cm^{-1} for completely blended lines (i.e., lines corresponding to seven spin

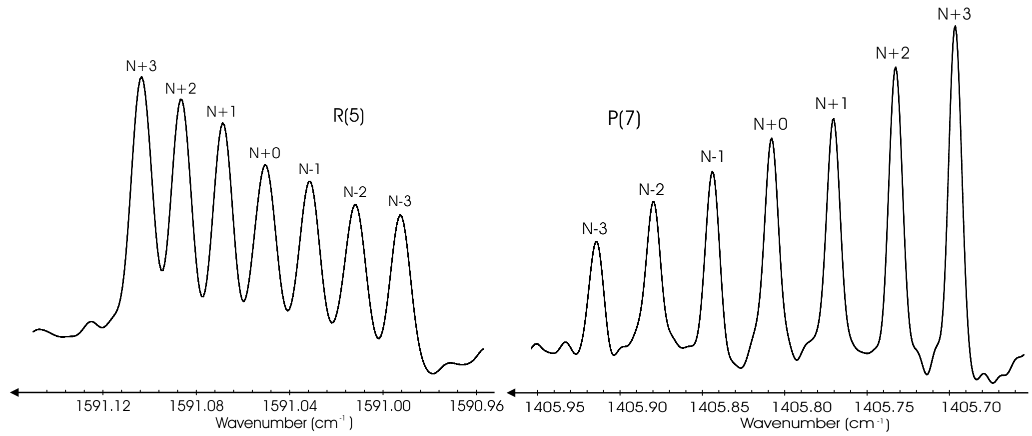

Figure 4.4: Example of spin-splitting in MnH lines: R(5) and P(7) transitions of the fundamental band. The intensities of the spin components of each rotational line both in the P- and R-branches increase from $J = N - 3$ to $J = N + 3$. The spin components are labeled by J values.

components blended into one feature) for MnH, and 0.001 to 0.005 cm^{-1} for MnD. For the blended lines, the same line position was used for all seven spin-components but with different uncertainties. This procedure proved to be more effective than assigning a blended line to a single transition. The bands were picked out and assigned using a color Loomis-Wood program. Assignments were made for the fundamental band up to N''=27 for MnH, for the υ=2→1 transition up to N''=24 and for the υ=3→2 transition up to N''=21. The corresponding bands of MnD were assigned up to N''=37, N''=36 and N''=33 respectively, while the weak R-branch of the υ=4→3 transition of MnD was followed up to N''=29. In total, 874 MnH lines and 953 MnD lines were assigned.

The high multiplicity septet ground state of MnH caused some difficulties at the beginning in the fitting of the experimental data. Urban and Jones [30, 31] fitted their data using expressions similar to the Dunham expansion for spin-rotation and spin-spin interactions, along with a regular Dunham expression for the rovibrational energy levels. In this way they were able to determine equilibrium constants for MnH and MnD.

Instead we chose to update our existing fitting program by inclusion of a Hamiltonian matrix for $^7\Sigma^+$ states. We derived a matrix using Hund case (a) basis functions, similar to that of Ref. [23], but with the addition of the H and L centrifugal distortion constants required for fitting data with higher N values. It should be noted that there is a small typographical error in Table II of Ref. [23]: a part of the $< 3|2 >$ element should be $-2D(x-1)$ instead of $-2D(2x-2)$. The updated Hamiltonian matrix for a $^7\Sigma^+$ electronic state is given in Table 4.1. However, it turned to be very tedious to update the existing code to perform Dunham-type fits for MnH and MnD. It was therefore decided to employ Pickett's program SPFIT [43], which is widely used to fit microwave spectra.

SPFIT was used to carry out a Dunham-type fit to obtain equilibrium parameters for MnH and MnD using transitions up to $\upsilon = 3 \rightarrow 2$. The $\upsilon = 4 \rightarrow 3$ band of MnD was excluded because almost all of the observed lines were blended and the inclusion of these transitions led to an unsatisfactory fit. In this Dunham-type fit, each parameter X was assumed to have the usual vibrational dependence,

$$X_{ij} = X_{0j} + X_{1j}(\upsilon + \tfrac{1}{2}) + X_{2j}(\upsilon + \tfrac{1}{2})^2 + ... \qquad (4.1)$$

indicated by first index for each parameter. The second index for each parameter indicates the order of the rotational dependence. The calculated equilibrium constants are provided in Table 4.2 for MnH and Table 4.3 for MnD. Then a fit was carried out with SPFIT to determine band constants and the results are presented in Table 4.4 for MnH and Table 4.5 for MnD. This time the υ=4→3 band was included for MnD in the fit with spin-spin and spin-rotation constants fixed to the values calculated using equilibrium constants from Table 4.3.

No higher order parameters such as θ and γ_s were required to obtain a good fit. The diode laser lines of Urban and Jones [30, 31] were included in the fits; this was particularly helpful in the case of MnD since the diode laser spectrum was recorded at higher resolution than our Fourier transform measurements and some lines that were blended in our spectrum were resolved. The corresponding lines in our spectrum were given lower weight. It appears that the P(17) lines of the fundamental band in Ref. [30] are mistyped. Tables 4.2 and 4.3 list constants obtained by Urban and Jones [30, 31] for comparison.

Table 4.1: $^7\Sigma^+$ Hamiltonian matrix (Hund's case (a) basis), $x = J(J+1)$.

	$\|3>$	$\|2>$	$\|1>$	$\|0>$
$\|3>$	$10\lambda + 15\theta - 3\gamma + 90\gamma_s + (B + 10\lambda_D - 6\gamma_D)(x - 6) - D(x^2 - 6x) + H(x^3 - 48x + 72) + L(x^4 + 12x^3 - 96x^2 - 168x + 576)$	$-(6(x-6))^{1/2}[B - \frac{1}{2}\gamma - 10\gamma_s + 5\lambda_D - \gamma_D(\frac{1}{2}x + 5) - 2D(x-1) + H(3x^2 + 10x - 28) + 4L(x^3 + 13x^2 + 4x + 50)]$	$(15(x-2)(x-6))^{1/2}(-\gamma_D - 2D + 2H(3x+8) + 2L(6x^2 + 60x + 52 \mp 12x))$	$-(15(x-2)x(x-6))^{1/2}(4H + 16L(x+5))$
$\|2>$		$-35\theta - 8\gamma - 60\gamma_s + B(x+4) - D(x^2 + 24x - 40) - 4\gamma_D(4x+1) + H(x^3 + 60x^2 + 72x - 368) + L(x^4 + 112x^3 + 904x^2 - 1008x - 2464 \mp (120x^2 - 240x))$	$-(10(x-2))^{1/2}[B - \frac{1}{2}\gamma - 3\lambda_D - \gamma_D(\frac{1}{2}x + 13) - D(2x+14) + H(3x^2 + 70x + 100 \mp 12x) + 4L(x^3 + 49x^2 + 296x + 158 \mp (12x^2 + 108x)]$	$(15x(x-2))^{1/2}(-2\gamma_D - 4D + 2H(6x+52) + 2L(12x^2 + 288x + 824)$
$\|1>$	Symmetric		$-6\lambda + 5\theta - 11\gamma - 30\gamma_s + (B - 6\lambda_D)(x+10) - D(x^2 + 42x + 80 \mp 12x) - 2\gamma_D(11x + 50 \mp 3x) + H(x^3 + 96x^2 + 864x + 520 \mp (36x^2 + 384x)) + L(x^4 + 172x^3 + 3664x^2 + 1288x + 3200 \mp (72x^3 + 2064x^2 + 7728x))$	$-(24x)^{1/2}[B - \frac{1}{2}\gamma + 5\gamma_s - \gamma_D(\frac{1}{2}x + 17) - 7\lambda_D - D(2x + 22) + H(3x^2 + 100x + 344) + L(4x^3 + 268x^2 + 2792x + 4648)]$
$\|0>$				$-8\lambda + 30\theta - 12\gamma + (B - 8\lambda_D)(x+12) - D(x^2 + 48x + 144) - 24\gamma_D(x+6) + H(x^3 + 108x^2 + 1248x - 1728) + L(x^4 + 192x^3 - 4944x^2 - 24960x + 20736)$

Table 4.2: Equilibrium constants (in cm^{-1}) for MnH. Numbers in parentheses represent one standard deviation in units of the last digit.

Constant	This work	Ref. [37]
$Y_{1,0}$	1546.84518(65)	1546.8536(15)
$Y_{2,0}$	-27.59744(39)	-27.60280(91)
$Y_{3,0}$	-0.309037(67)	-0.30822(15)
$Y_{0,1}$	5.6856789(103)	5.685795(37)
$Y_{1,1}$	-0.1602038(70)	-0.160488(22)
$10^4 Y_{2,1}$	-1.200(40)	0.405(91)
$10^4 Y_{3,1}$	-3.0252(72)	-3.255(13)
$10^4 Y_{0,2}$	-3.05384(58)	-3.0630(30)
$10^6 Y_{1,2}$	1.397(22)	2.983(68)
$10^7 Y_{2,2}$	-2.823(83)	-12.01(16)
$10^7 Y_{3,2}$	-1.225(16)	-
$10^9 Y_{0,3}$	9.4670(128)	8.68(60)
$10^9 Y_{1,3}$	-1.551(48)	-
$10^{12} Y_{0,4}$	1.360(89)	-
$10^{13} Y_{1,4}$	9.16(39)	-
$10^2 \gamma_{0,1}$	3.1749(35)	3.2055(83)
$10^4 \gamma_{1,1}$	-7.698(54)	-8.32(13)
$10^5 \gamma_{2,1}$	-4.100(101)	-3.40(33)
$10^6 \gamma_{0,2}$	-6.763(53)	-7.54(21)
$10^7 \gamma_{1,2}$	-2.554(98)	-
$10^3 \lambda_{0,0}$	-3.758(92)	-3.35(12)$^{a)}$
$10^4 \lambda_{1,0}$	-2.623(117)	-
$10^6 \lambda_{0,1}$	-5.39(43)	-0.0195(27)$^{a)}$

$^{a)}$ Calculated from values of $\varepsilon_{0,1}$ and $\varepsilon_{1,1}$ listed in Ref. [30].

A few lines for certain low N values could not be fitted within the experimental uncertainty. This can be attributed to the internal hyperfine perturbations discussed by Varberg *et al.* [23]. Therefore, a larger uncertainty was assigned to those

Table 4.3: Equilibrium constants for MnD and Born–Oppenheimer breakdown parameters estimated using Eq. 4.2 (in cm^{-1}). Numbers in parentheses represent one standard deviation in units of the last digit.

Constant	This work	Ref. [38]	Calculated [a)]	$\delta^H_{l,m}$	
$Y_{1,0}$	1104.65312(51)	1104.65225(93)	1104.0017	$\delta^H_{1,0}$	1.8268
$Y_{2,0}$	-14.22657(31)	-14.22656(54)	-14.05771	$\delta^H_{2,0}$	-0.6635
$Y_{3,0}$	-0.085848(52)	-0.085813(90)	-0.112351	$\delta^H_{3,0}$	0.14591
$Y_{0,1}$	2.8987214 (57)	2.898685(12)	2.8961972	$\delta^H_{0,1}$	0.009919
$Y_{1,1}$	-0.0581028(33)	-0.0580972(79)	-0.0582427	$\delta^H_{1,1}$	-0.159557
$10^4Y_{2,1}$	-1.065(20)	-0.943(31)	-0.3115	$10^4\delta^H_{2,1}$	-5.8150
$10^4Y_{3,1}$	-0.4500(35)	-0.4784(44)	-0.5602	$10^4\delta^H_{3,1}$	1.1914
$10^4Y_{0,2}$	-0.796939(190)	-0.79584(54)	-0.79239	$10^4\delta^H_{0,2}$	0.03511
$10^6Y_{1,2}$	0.2543(41)	0.201(21)	0.259	$10^6\delta^H_{1,2}$	-0.048
$10^7Y_{2,2}$	-0.521(22)	-0.897(40)	-0.373	$10^7\delta^H_{2,2}$	-2.239
$10^7Y_{3,2}$	-0.0870(38)	-	-0.1156	$10^7\delta^H_{3,2}$	0.6059
$10^9Y_{0,3}$	1.5713(197)	1.58(12)	1.2513	$10^9\delta^H_{0,3}$	4.8464
$10^9Y_{1,3}$	-0.0957(30)	-	-0.1463	$10^9\delta^H_{1,3}$	1.0738
$10^2\gamma_{0,1}$	1.6234(30)	1.6388(67)	1.6172		
$10^4\gamma_{1,1}$	-3.026(37)	-2.954(76)	-2.799		
$10^5\gamma_{2,1}$	-0.831(99)	-	-1.06		
$10^6\gamma_{0,2}$	-1.968(39)	-2.19(13)	-1.755		
$10^3\lambda_{0,0}$	-1.823(55)	-1.44(21)[b)]	-3.758		
$10^4\lambda_{1,0}$	-1.17(11)	-1.33(19)[b)]	-1.87		

[a)]Calculated from MnH constants from Table 4.2 using Eq. 4.1.

[b)] Calculated from values of $\alpha_{0,1}$ and $\alpha_{1,1}$ listed in Ref. [31].

lines. This problem affected most of the observed satellite lines as well, which is particularly disadvantageous since these lines are very useful in determining better values for the spin-spin constants. Line lists for MnH and MnD spectra are given in Appendix A. Input and output files of SPFIT program are available on ScienceDirect (www.sciencedirect.com) and as part of the Ohio State University

Table 4.4: Spectroscopic constants (in cm^{-1}) for the $X^7\Sigma^+$ ground state of MnH. Numbers in parentheses represent one standard deviation in units of the last digit.

Constant	υ=0	$0^{a)}$	1	2	3
T_υ	0	-	1490.644889(21)	2923.31542(34)	4296.15620(55)
B_υ	5.6055050(96)	5.605746(71)	5.4441092(96)	5.2797006(106)	5.1104876(160)
$10^4 D_\upsilon$	3.04743(57)	3.0413(61)	3.04512(62)	3.05665(76)	3.08943(128)
$10^9 H_\upsilon$	8.639(131)	-	7.532(152)	5.926(196)	3.38(39)
$10^{12} L_\upsilon$	1.861(96)	-	2.473(122)	3.324(174)	5.12(39)
γ_υ	0.031349(36)	0.030341(82)	0.030497(37)	0.029559(38)	0.028548(38)
$10^6 \gamma_{D\upsilon}$	-6.902(58)	-11.0(12)	-7.159(64)	-7.399(71)	-7.681(80)
λ_υ	-0.004020(92)	-0.00325(10)	-0.004230(92)	-0.004462(95)	-0.004778(103)
$10^6 \lambda_{D\upsilon}$	-5.20(46)	0.0 (fixed)	-5.22(49)	-5.40(55)	-5.32(60)

$^{a)}$Constants for υ=0 from Ref. [23].

Table 4.5: Spectroscopic constants (in cm^{-1}) for the $X^7\Sigma^+$ ground state of MnD. Numbers in parentheses represent one standard deviation in units of the last digit.

Constant	v=0	1	2	3	4
T_v	0	1075.920727(133)	2122.616176(206)	3139.57067(27)	4126.0780(25)
B_v	2.8696280(55)	2.8111700(52)	2.7520865(50)	2.6921167(51)	2.6310263(193)
$10^5 D_v$	7.95559(189)	7.94459(167)	7.94981(155)	7.97910(153)	8.0685(42)
$10^9 H_v$	1.5025(191)	1.4147(160)	1.3148(139)	1.2189(126)	1.295(27)
γ_v	0.0164400(181)	0.0161162(173)	0.0157850(166)	0.0154373(161)	0.014704[a)]
$10^6 \gamma_{Dv}$	-2.418(34)	-2.410(31)	-2.396(28)	-2.403(25)	-1.97[a)]
λ_v	-0.001637(58)	-0.001698(58)	-0.001855(58)	-0.002005(57)	-0.002350[a)]

[a)] Fixed to the values calculated from Table 4.3 using Eq. 4.1

Molecular Spectroscopy Archives (http : //msa.lib.ohio − state.edu/jmsa_hp.htm) as supplementary data for Ref. [44].

The Dunham constants of MnH and MnD display evidence for the breakdown of the Born–Oppenheimer approximation. In order to demonstrate this, MnD equilibrium constants were calculated from those of MnH using the reduced mass relationship:

$$Y_{l,m}^{\mathrm{MnD}} = Y_{l,m}^{\mathrm{MnH}} \left(\frac{\mu_{\mathrm{MnH}}}{\mu_{\mathrm{MnD}}}\right)^{(l+2m)/2} . \qquad (4.2)$$

Calculated MnD constants are shown in Table 4.3. There is a significant difference between the constants obtained from the fit of the experimental data and the ones calculated from the MnH constants. The Born–Oppenheimer breakdown constants were estimated using Le Roy's formalism [45]:

$$Y_{l,m}^{\mathrm{MnD}} = \left\{ Y_{l,m}^{\mathrm{MnH}} + \frac{M_D - M_H}{M_D} \delta_{l,m}^{H} \right\} \left(\frac{\mu_{\mathrm{MnH}}}{\mu_{\mathrm{MnD}}}\right)^{(l+2m)/2} . \qquad (4.3)$$

The estimated Born–Oppenheimer breakdown constants ($\delta_{l,m}^{H}$) obtained are also given in Table 4.3.

The fit of the new and extensive dataset has provided an improved set of constants for the ground states of MnH and MnD, and allowed us to determine higher-order expansion constants in the Dunham-type fit. The equilibrium bond distance was determined to be 1.7308601(47) Å for MnH, based on the value of B_e calculated in the fit. Our spectroscopic constants for v=0 can also be compared with those of Varberg *et al.* [21] in Table 4.4. Of the series of spin-orbit parameters A, λ, η, θ (corresponding to first through fourth order in perturbation theory) only λ was required. For Σ states the constants A and η are zero. Varberg *et al.* [23] determined a value for θ and for γ_s (a cross-term between spin-rotation and spin-spin terms) that we find unnecessary. We find that the Born–Oppenheimer breakdown correction parameters ($\delta_{l,m}^{H}$) are relatively large, as is usually the case for metal hydrides [41].

One of the most prominent features that distinguish manganese hydride from other transition metal hydrides is a very small spin-spin interaction constant $\lambda_e = -0.003758(92)\ \mathrm{cm}^{-1}$. As discussed by Varberg *et al.* [23], the spin-spin interaction in the ground state of manganese hydride is a sum of the first order electron spin-spin interaction and the second order spin-orbit interaction with other states, with the latter usually dominating in other metal hydrides. The selection rules for the second order spin-orbit interaction are ΔS=0,$\pm$1; $\Sigma^{\pm} \sim \Sigma^{\mp}$; $\Delta\Omega$=0, hence among states known from experiment, only the $b^5\Pi_i$ (lying at 11 000 cm^{-1}), $d^5\Pi_i$ (at 23000 cm^{-1})

and $A^7\Pi_r$ (at 18 000 cm^{-1}) states can be involved in this second order interaction. Since $b^5\Pi_i$ arises from the $3d^6$ electron configuration, it therefore does not interact with the $3d^5$ ground $^7\Sigma^+$ electronic state. The $d^5\Pi_i$ state arises from the $3d^5$ electron configuration, but it lies far from the ground state. This leaves the $A^7\Pi_r$ state as the dominant perturber. The second order spin-orbit interaction between $A^7\Pi_r$ and $X^7\Sigma^+$ states can be expressed as [46]:

$$\lambda = \frac{|< A^7\Pi|\, \hat{H}_{SO}\, |X^7\Sigma^+ >|^2}{E(X^7\Sigma^+) - E(A^7\Pi)} \tag{4.4}$$

The denominator of Eq. (4.4) is large (18 000 cm^{-1}) and the numerator is relatively small, as discussed in the MnF case [46], which leads to the small value of λ.

The spin-rotation constant γ is an order of magnitude larger than λ, and this leads to the simple appearance of the rotational lines (Fig. 4.4). The seven spin components for each N appear in order of increasing J.

Surprisingly, no microwave experiments have been carried out yet on MnH. The rotational spectra will be complex because of fine and hyperfine structure. Every rotational level will be split into $(2S{+}1)(2I_{\mathrm{Mn}}{+}1)(2I_{\mathrm{H}}{+}1){=}84$ energy levels, where $I_{\mathrm{Mn}}{=}5/2$ and $I_{\mathrm{H}}{=}1/2$. This will lead to many lines, overlapped due to the fact that spin-spin interaction in MnH is fairly small, as observed for the similar spectrum of MnF [46].

4.4 Conclusions

New infrared emission spectra of manganese hydride and deuteride were recorded at high resolution using a Fourier transform spectrometer. Improved sets of band constants and equilibrium parameters for the ground $^7\Sigma^+$ state of MnH and MnD were determined. The Born–Oppenheimer breakdown constants ($\delta^H_{l,m}$) were estimated. Our search for the manganese dihydride molecule in the gas phase was not successful.

Bibliography

[1] P. Bernath, A. Shayesteh, and K. Tereszchuk, Science **297**, 1323 (2002).

[2] A. Shayesteh, K. Tereszchuk, R. Colin, and P. Bernath, J. Chem. Phys. **118**, 3622 (2003).

[3] A. Shayesteh, D. Appadoo, I. Gordon, and P. Bernath, J. Chem. Phys. **119**, 7785 (2003).

[4] A. Shayesteh, D. Appadoo, I. Gordon, and P. Bernath, J. Am. Chem. Soc. **126**, 14356 (2004).

[5] A. Shayesteh, D. Appadoo, I. Gordon, and P. Bernath, Phys. Chem. Chem. Phys. **7**, 3132 (2005).

[6] A. Shayesteh, S. Yu, and P. Bernath, Chemistry - A European Journal **11**, 4709 (2005).

[7] R. Van Zee, T. DeVore, J. Willkerson, and W. Weltner Jr, J. Chem. Phys. **69**, 1869 (1978).

[8] R. Van Zee, C. M. Brown, and W. Weltner Jr, Chem. Phys. Lett. **64**, 325 (1979).

[9] J. Demuynck and H. Schaefer, J. Chem. Phys. **72**, 72 (1980).

[10] J. A. Platts, J. Mol. Struct. (Theochem) **545**, 111 (2001).

[11] N. Balabanov and J. Boggs, J. Phys. Chem. **106**, 6839 (2002).

[12] X. Wang and L. Andrews, J. Phys. Chem. **107**, 4081 (2003).

[13] A. Shayesteh, K. Walker, I. Gordon, D. Appadoo, and P. Bernath, J. Mol. Struct. **695**, 23 (2004).

[14] T. Heimer, Naturwiss. **24**, 521 (1936).

[15] T. Nevin, Proc. R. Irish Acad. **48**, 1 (1942).

[16] T. Nevin, Proc. R. Irish Acad. **50**, 123 (1945).

[17] T. Nevin, M. Conway, and M. Cranley, Proc. Roy. Soc. (London) A **65**, 115 (1952).

[18] T. Nevin and P. G. Doyle, Proc. R. Irish Acad. **52**, 35 (1948).

[19] T. Nevin and D. V. Stevens, Proc. R. Irish Acad. **55**, 109 (1953).

[20] W. Hayes, P. McCarvill, and T. Nevin, Proc. Roy. Soc. (London) A **70**, 904 (1957).

[21] T. Varberg, R. Field, and A. Merer, J. Chem. Phys. **92**, 7123 (1990).

[22] T. Varberg, R. Field, and A. Merer, J. Chem. Phys. **95**, 1563 (1991).

[23] T. Varberg, J. A. Gray, R. Field, and A. Merer, J. Mol. Spectrosc. **156**, 296 (1992).

[24] R. Pearse and A. Gaydon, Proc. Phys. Soc. (London) **50**, 201 (1938).

[25] W. Balfour, O. Launila, and L. Klynning, Mol. Phys. **69**, 443 (1990).

[26] W. Balfour, J. Chem. Phys. **88**, 5242 (1988).

[27] W. Balfour, B. Lindgren, O.Launila, S. O'Connor, and E. Cusack, J. Mol. Spectrosc. **154**, 177 (1992).

[28] R. Van Zee, D. Garland, and W. Weltner Jr, J. Chem. Phys. **84**, 5968 (1986).

[29] R. Van Zee, D. Garland, and W. Weltner Jr, J. Chem. Phys. **85**, 3237 (1986).

[30] R.-D. Urban and H. Jones, Chem. Phys. Lett. **163**, 34 (1989).

[31] R.-D. Urban and H. Jones, Chem. Phys. Lett. **178**, 295 (1991).

[32] I. Kovács and O. Scari, Acta Phys. Acad. Sci. Hung. **9**, 423 (1959).

[33] P. Pacher, Acta Phys. Acad. Sci. Hung. **35**, 73 (1974).

[34] I. Kovács and P. Pacher, J. Phys. B **35**, 796 (1975).

[35] G. Das, J. Chem. Phys. **74**, 5766 (1981).

[36] S. Walch and C. Bauschlicher Jr., J. Chem. Phys. **78**, 4597 (1983).

[37] D. Chong, S. Langhoff, C. Bauschlicher Jr, S. Walch, and H. Partridge, J. Chem. Phys. **85**, 2850 (1986).

[38] P. Bagus and H. Schaefer III, J. Chem. Phys. **58**, 1844 (1973).

[39] S. Langhoff, C. Bauschlicher, and A. Rendell, J. Mol. Spectrosc. **138**, 108 (1989).

[40] J. Harrison, Chem. Rev. **100**, 679 (2000).

[41] A. Shayesteh, D. Appadoo, I. Gordon, R. LeRoy, and P. Bernath, J. Chem. Phys. **120**, 10002 (2004).

[42] E. U. Condon and G. Shortley, *The Theory of Atomic Spectra*, Cambridge University Press, Cambridge, England, 1951.

[43] H. M. Pickett, J. Mol. Spectrosc. **148**, 371 (1991).

[44] I. E. Gordon, A. Shayesteh, D. Appadoo, K. Walker, and P. Bernath, J. Mol. Spectrosc. **229**, 269 (2005).

[45] R. J. Le Roy, J. Mol. Spectrosc. **194**, 189 (1999).

[46] P. Sheridan and L. Ziurys, Chem. Phys. Lett. **380**, 632 (2003).

Chapter 5

Electronic emission spectra of CoH and CoD

5.1 Introduction

Molecules containing $3d$-transition metal atoms usually have many low-lying electronic states with complex structure due to the open d-shells. As a result the electronic spectra are complicated because of the perturbations caused by interactions of close-lying electronic states. Spectra of the cobalt-containing molecules (including cobalt monohydride) are a perfect example of such complexity.

The first observation of the electronic spectra of CoH was reported by Heimer in 1937 [1]. The spectra were recorded in emission from a King furnace (carbon tube furnace), and Heimer was able to assign two of the observed bands (at 420.3 and 449.2 nm) as the (1,0) and (0,0) bands of the $A\,^3\Phi_4 \rightarrow X\,^3\Phi_4$ transition. Despite a suggestion in Ref. [2] (based on the electronic configuration proposed in Ref. [1]) that the ground electronic state of CoH should be a $^1\Gamma$ state, it was proved in subsequent work that it is in fact a $^3\Phi$ state. Klynning and co-workers [3–6] significantly extended Heimer's results for the $A - X$ transition by recording the (1,1) band of CoH and several bands of the corresponding system of CoD. In these experiments they were also able to observe the (0,0) transition between $\Omega'' = \Omega' = 3$ spin components for CoH and the analogous (0,0) and (1,0) bands of CoD. However, only one parity component of the $\Omega = 3$ transitions was observed for CoH. Smith [7] was also able to see some of these transitions in absorption behind reflected shock waves.

Later, Varberg *et al.* [8, 9] recorded several new bands via laser excitation spectroscopy. Two of the analyzed $\Omega' = 4 - X^3\Phi_4$ transitions were later identified by Barnes *et al.* [10] as (3,0) and (4,0) bands of the $A'^3\Phi_4 - X^3\Phi_4$ electronic transition. Varberg *et al.* [8] had also observed resolved fluorescence from an excited [16.0]3 state, which enabled them to find a new electronic state (presumably $^3\Delta_3$) lying 2469 cm^{-1} above $X^3\Phi_4$, as well as to determine spin-orbit splitting between the $\Omega'' = 4$ and 3 spin components as 728(±3) cm^{-1}. A little later, Barnes *et al.* [10] carried out laser excitation experiments on CoH and CoD generated in a laser ablation/molecular beam source, and recorded the (0,0) to (5,0) bands of the $A'^3\Phi_4 - X^3\Phi_4$ electronic transition. The (0,0) bands were recorded at high resolution and a hyperfine analysis was carried out for both molecules. The electron configuration of the $A'^3\Phi$ state was found to be $(7\sigma)^1(3d\delta)^3(3d\pi)^3(8\sigma)^1$. In addition, Barnes *et al.* carried out resolved fluorescence experiments and determined the spin-orbit splitting in the ground state of the CoD molecule.

The $A'^3\Phi - X^3\Phi$ transition in CoH was also studied by Ram *et al.* [11] in emission using Fourier transform spectrometer. For the $A'\,^3\Phi_4 - X\,^3\Phi_4$ electronic transition the (0,0) and (0,1) bands were observed, while the (0,0) band was observed for the $A'\,^3\Phi_3 - X\,^3\Phi_3$ transition, although one of its parity components was missing as it had been in Ref. [6]. Photoelectron spectroscopy of CoH^- [12] showed the existence of an excited electronic state of quintet multiplicity lying 0.8 eV above the ground state of CoH. The ground $X^3\Phi$ electronic state of CoH was studied by laser magnetic resonance (LMR). Lipus *et al.* [13] reported the infrared spectrum of the fundamental band of the $X^3\Phi_4$ substate, and Beaton *et al.* [14, 15] carried out far-infrared LMR experiments to perform a hyperfine analysis of the $X^3\Phi_4$ and $X^3\Phi_3$ substates.

The first theoretical work on CoH was reported by Chong *et al.* [16], in which some spectroscopic parameters for the ground $X^3\Phi$ state have been predicted using the modified coupled pair functional (MCPF) method. Anglada *et al.* [17] carried out calculations mainly for the low-lying electronic states of CoH^+, but the ionization potential for the $X^3\Phi$ state of CoH was also calculated. A set of very thorough *ab initio* calculations was performed by Freindorf *et al.* [18] in which 30 electronic states of singlet, triplet and quintet multiplicity below 4 eV were studied. The latest theoretical work was reported by Barone and Adamo [19], who calculated some properties of CoH and other first-row transition metal hydrides in order to test a new density functional method. Theoretical calculations on the CoH molecule are also currently in progress in the group of Hirano [20].

None of the aforementioned experimental studies were able to locate the $\Omega = 2$ spin component for the ground state or for any of the observed excited electronic states. Also $\Delta\Omega = \pm 1$ transitions were not observed at high resolution, and there was not enough vibrational data to allow a combined-isotopologue fit of data for CoH and CoD. It was therefore decided to revisit the $A'\,^3\Phi - X\,^3\Phi$ system in order to obtain the missing information.

In this thesis, the analysis of numerous bands of CoH and CoD in the near infrared region is reported. This work significantly extends the available vibrational and rotational information for the $A'^3\Phi$ and $X^3\Phi$ electronic states, allowing us to perform Dunham-type and combined isotopologue fits. The $\Delta\Omega = -1$ transition was also observed and analyzed for the CoH molecule. In addition, new $[13.3]4 - X^3\Phi_3$ and $[13.3]4 - X^3\Phi_4$ transitions were observed for the CoD molecule.

5.2 Experimental details

About 40 g of cobalt metal was heated in the King furnace to a temperature of ~2 600°C with a mixture of hydrogen (or deuterium) and helium gases flowing slowly through the system. The total pressure inside the furnace was kept between 150 and 200 Torr. It was found that the use of argon instead of helium allows higher temperatures to be achieved, but can be harmful to the carbon heating element. A BaF_2 lens was employed to image emission from the King furnace onto the entrance aperture of a Bruker IFS 120 HR Fourier transform spectrometer. The CoH/D emission spectra were recorded in two parts. The region $8\,000 - 15\,700$ cm^{-1} was recorded using a silicon photodiode detector, a quartz beamsplitter and a 640 nm red pass optical filter that blocked the signal from the He-Ne laser of the spectrometer. The region $1\,800 - 10\,000$ cm^{-1} was recorded using a CaF_2 beamsplitter and an InSb detector cooled with liquid nitrogen. A total of $100 - 200$ scans (depending on the experiment) were co-added at a resolution of 0.05 cm^{-1} in order to obtain a good signal-to-noise ratio (S/N). An overview spectrum of CoD in the near infrared region is shown on Fig. 5.1. In order to display the bands more clearly, the baseline was corrected by eliminating the blackbody emission profile using the Bruker OPUS program.

Line positions were measured using a Windows-based program called WSpectra, written by M. Carleer (Université Libre de Bruxelles). The width of the individual lines in different bands vary from 0.05 to 0.8 cm^{-1}. Apart from Doppler and pressure broadening, the lines are broadened by unresolved hyperfine and Ω-doubling splittings. Significant broadening due to hyperfine structure (^{59}Co has large nuclear spin $I = \frac{7}{2}$ and a large magnetic moment, $\mu = 4.627$ nuclear magnetons) is present not only in the lower J lines, but also for some higher J lines of the transitions terminating on the Ω=3 component of the ground $X^3\Phi$ state (see discussion).

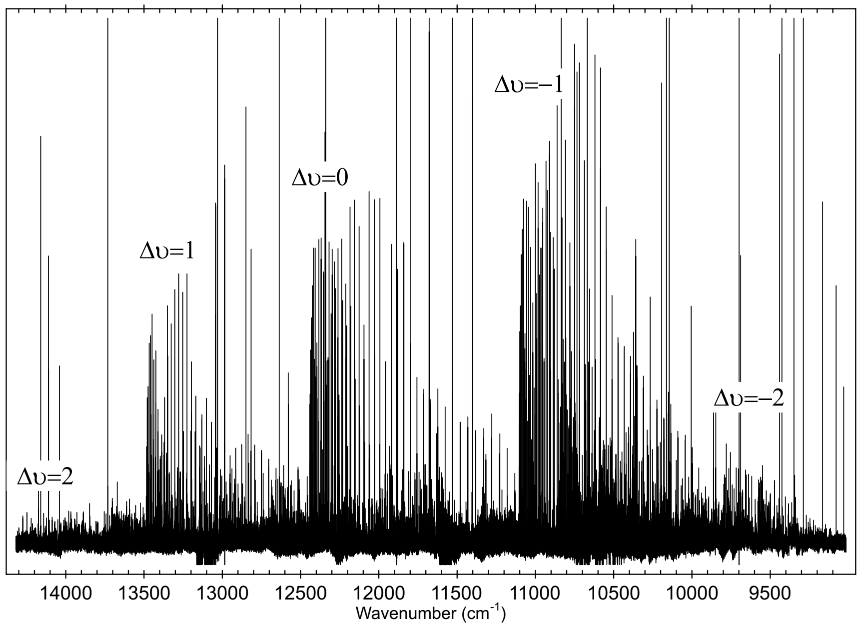

Figure 5.1: An overview spectrum of CoD after baseline correction.

The CoH spectrum in the 8 000 − 15 700 cm^{-1} region was calibrated using lines reprorted in Ref. [11]. The corresponding spectrum of CoD was calibrated using lines common to the spectra of both molecules. The infrared part of the spectrum was calibrated using lines of HF impurity [21]. The accuracy of the measured lines is estimated to vary from ±0.002 cm^{-1} to ±0.01 cm^{-1}, depending on the S/N ratio.

5.3 Observations and analysis

For the $A'^3\Phi_4 \rightarrow X^3\Phi_4$ transition of CoH, the (2,0), (1,0), (0,0), (0,1) and (1,2) bands were assigned. For the $\upsilon'' = 0$ level the lines were followed up to J_e''=26 for the e-parity component and $J_f'' = 33$ for the f-parity component, for $\upsilon'' = 1$ up to $J_e'' = 26$ and $J_f'' = 31$, and for $\upsilon'' = 2$ up to $J_e'' = 21$ and $J_f'' = 18$. For the corresponding transition of CoD the (2,0), (1,0), (2,1), (0,0), (0,1), (1,2), (2,3), (0,2) and (1,3) bands were analyzed. Assignments were made up to J_e''=$J_f'' = 37$ for $\upsilon'' = 0$ and 1, up to J_e''=J_f''=22 for υ''=2, and up to J_e''=J_f''=16 for $\upsilon'' = 3$. For the $A'^3\Phi_3 \rightarrow X^3\Phi_3$ transitions of both CoH and CoD and for the [13.3]4→$X^3\Phi_3$ and [13.3]4→$X^3\Phi_4$ transitions of CoD only the (0,0) bands were observed. The

(0,0) and (0,1) bands were analyzed for the $A'^3\Phi_3 \rightarrow X^3\Phi_4$ transition of CoH. For the $\Omega'' = 3$ component lines were found corresponding to J's up to $J_e'' = 16$ and $J_f'' = 23$ for CoH and up to $J_e''=J_f'' = 21$ for CoD.

In all transitions with $\Delta\Omega$=0, P and R branches appear to have similar relative intensities while Q branches disappear rapidly with increasing J. In the [13.3]4$\rightarrow X^3\Phi_4$ transition in CoD the lines start to appear only from J=13, and the Q branch was not observed. The [13.3]4$\rightarrow X^3\Phi_3$ transition has a P branch much weaker than R and Q branches. In addition, the overall intensity of this band is weaker than that of the [13.3]4$\rightarrow X^3\Phi_4$ transition. These observations led us to the conclusion that Ω' is equal to 4.

The $A'^3\Phi_3 \rightarrow X^3\Phi_4$ transition of CoH has strong R and Q branches, but the P branch is so weak that we were able to assign only two P-lines. This is not consistent with a pattern one would expect for a transition with $\Delta\Omega = -1$ where the P branch should be stronger than R, but strong interactions between close-lying states in CoH may be responsible for the deviations in the intensity pattern. Most of the recorded bands are severely perturbed, especially the ones from the [13.3]4 state in CoD. The assignments of the lines were made by the application of combination differences starting from the ground state values for CoD and CoH known from the previous experimental papers [4, 11]. We were unable to find transitions to the $\Omega'' = 2$ component of the ground state, probably because it is extremely perturbed as suggested in Ref. [11]. There are many unassigned lines in the spectra of both molecules. The most intense unassigned bands are in the $7\,500 - 8\,500$ cm^{-1} region; it is unclear what states are involved in these transitions, but certainly they are not known states. Figure 5.2 shows these unassigned bands for CoH.

Because the spectroscopic constants for $\Omega = 3$ and Ω=4 spin components in the ground and in the excited electronic states are quite different, it was decided to use empirical Hund's case (c) expressions when fitting the data. We have performed band constant and Dunham-type fits for CoH and CoD separately and then a combined isotopologue fit, using the DParfit 3.3 program [22]. An experimental uncertainty of ± 0.007 cm^{-1} was assigned to most of the lines. The data of Heimer [1], and Klynning and Kronekvist [4, 5] were included in our fit in order to obtain a consistent set of spectroscopic constants. However, some published lines were not included in the fit because of discrepancies in the combination differences.

For the band-constant fits, we first fitted the severely perturbed upper states to individual term values, while the ground state was fitted with the following Hund's case (c) expression:

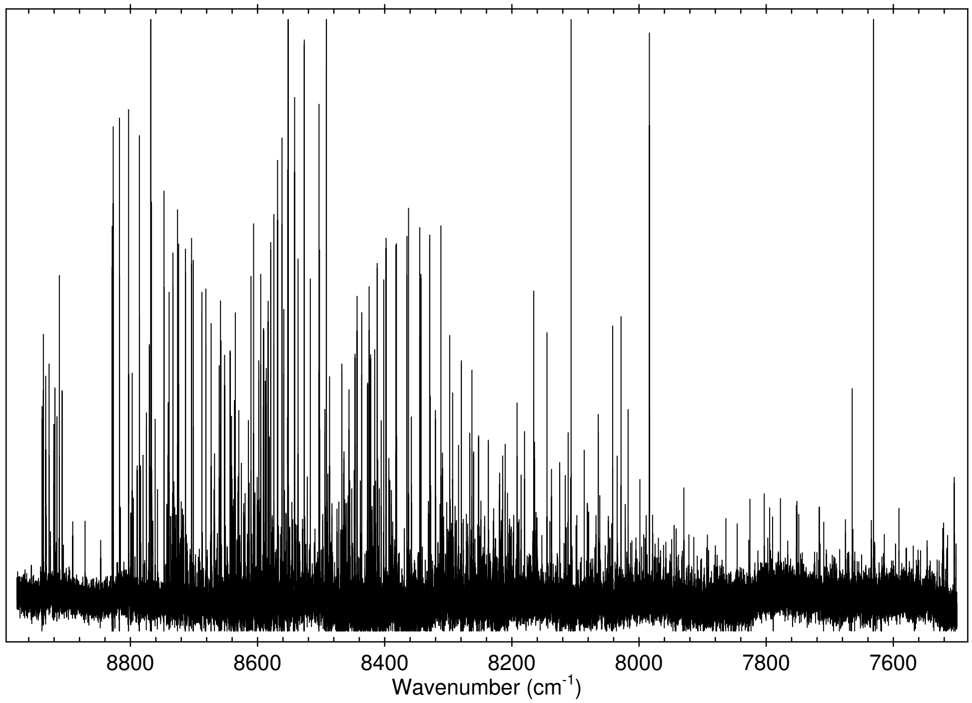

Figure 5.2: Unassigned bands of CoH at 8000 cm^{-1}.

$$F_v(J) = T_v + B_v[J(J+1) - \Omega^2] - D_v[J(J+1) - \Omega^2]^2 + H_v[J(J+1) - \Omega^2]^3 + L_v[J(J+1) - \Omega^2]^4 \pm \frac{1}{2}[J(J+1)]^\Omega \sum_{m=\Omega} q_m[J(J+1) - \Omega^2]^{m-\Omega}. \quad (5.1)$$

The last term in this equation reflects the fact that the Ω-doubling splitting increases as $\sim J^{2\Omega}$ [23]. In particular, it implies that if $\Omega = 3$ then the leading Ω-doubling splitting term is $q_H[J(J+1)]^3$, while if $\Omega = 4$ it would be $q_L[J(J+1)]^4$. The summation in Eq. 5.1 starts from the leading term and the upper limit is determined by the quality of the fit, i.e., there is no necessity to add more Ω-doubling splitting terms if the quality of the fit is good. Note that following the common practice the m-subscript in q is replaced by the label for the mechanical rotational constant of the same order of $J(J+1)$.

It is interesting to observe the effect of using an Ω-doubling constant of the incorrect order on the quality of the fit. The quality of the fit of N data $y_{\rm obs}(i)$ with associated uncertainties $u(i)$ is indicated by the value of the dimensionless root mean square deviation (DRMSD),

$$\text{DRMSD} \equiv \left\{ \frac{1}{N} \sum_{i=1}^{N} \left[\frac{y_{\text{calc}}(i) - y_{\text{obs}}(i)}{u(i)} \right]^2 \right\}^{1/2}, \tag{5.2}$$

in which $y_{\text{calc}}(i)$ is the value of datum-i calculated from the model. For illustrative purposes the (0,0) band of $A'^3\Phi_4 \rightarrow X^3\Phi_4$ transition of CoH was fitted using Eq. 5.1 with only a single Ω-doubling constant but of different orders (the number of rotational constants was the same). Fig. 5.3 shows the dependence of DRMSD on the order of the Ω-doubling constant used, and it is clear that the best fit corresponds to the use of a q_L constant. This shows that the dependence of the DRMSD on the leading Ω-doubling constant can be a useful tool in assigning new electronic transitions in order to determine the Ω values of the states involved.

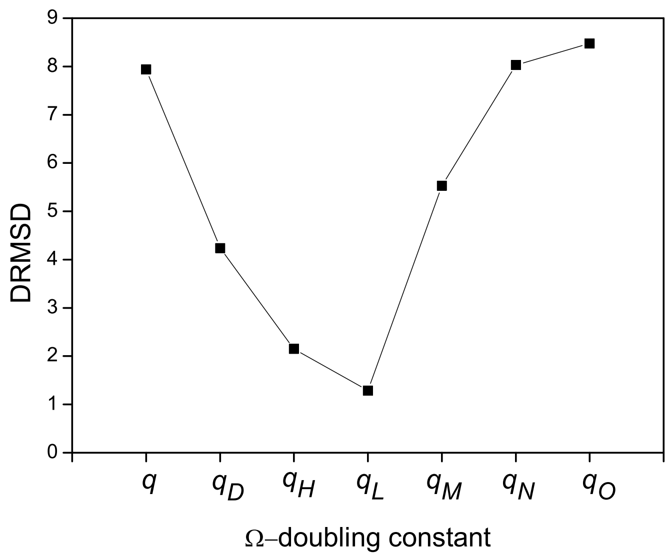

Figure 5.3: The dependence of DRMSD as defined in Eq. 5.2 on the lower state Ω-doubling constant used to fit (0,0) band of $A'^3\Phi_4 \rightarrow X^3\Phi_4$ transition of CoH.

The $v = 1$ vibrational level of the $X^3\Phi_4$ sub-state appears to be slightly perturbed between $J'' = 13$ and $J'' = 21$, so the corresponding lines were fitted with larger uncertainties assigned to them. Despite the fact that the $v = 2$ state fits well, it is probably slightly perturbed as well because the values of the constants do not follow the trend established by $v = 0$ and $v = 1$.

The results of the band-constant fits for CoH and CoD are presented in Table 5.1. The modified output files of DParfit 3.3 containing line positions are given in Appendix B.

The ground state constants obtained (Table 5.1) were then held fixed, while the upper states were fitted using Eq. 5.1. Since all upper states are perturbed, we employed Watson's "robust" fit method [24] which iteratively minimizes the contribution to the fit from the lines with large discrepancies from the model. This approach worked fairly well for CoD, but required some "manual" help for the CoH, i.e., some lines had to be assigned larger uncertainties before performing the fit. The constants for the upper states are listed in Tables 5.2 and 5.3. One can immediately note the large difference between B-values for the $A'^3\Phi_4$ and $A'^3\Phi_3$ spin components. This means that the Ω-components of the excited state are mixed with the sub-states of other electronic states and the use of Hund's case (c) expressions is justified.

The CoH molecule was used as a reference isotopologue for the combined-isotopologue fit of the data involving $X^3\Phi_4$ state. The fit was carried out using following expression

$$\begin{aligned} E^{\alpha}(\upsilon, J) \;=\; & \sum_{m=0}\sum_{l=0}\left\{Y_{l,m}^{(\mathrm{CoH})} + \frac{\Delta M_H^{(\alpha)}}{M_H^{(\alpha)}}\delta_{l,m}^{H}\right\}(\mu_{\mathrm{CoH}}/\mu_{\alpha})^{m+l/2} \\ & \times(\upsilon+\frac{1}{2})^{l}[J(J+1)-\Omega^2]^{m} \\ & \pm\frac{1}{2}[J(J+1)]^{\Omega}\sum_{m=\Omega}\sum_{l=0} q_{l,m}^{(\mathrm{CoH})}(\mu_{\mathrm{CoH}}/\mu_{\alpha})^{\Omega+m+l/2} \\ & \times(\upsilon+\frac{1}{2})^{l}[J(J+1)-\Omega^2]^{m-\Omega}, \end{aligned} \tag{5.3}$$

in which α labels to a particular isotopologue and $\Delta M_A^{(\alpha)}$ is the difference between the atomic mass of atom A in isotopologue-α and in the reference isotopologue. The Born–Oppenheimer breakdown terms are represented using the formalism of Ref. [25]. The severely perturbed upper states were fitted to individual term values. The results of this fit are presented in Table 5.4. A large number (8) of Born–Oppenheimer breakdown correction parameters ($\delta_{l,m}^{H}$) was required, and their values are relatively large, which is usually the case for metal hydrides [26]. This fit was also carried out using "robust" routine because of the perturbations in CoH.

A Dunham-type fit was also carried out using Eq. 5.3 for each molecule separately, because the $X^3\Phi_4$ state of the CoH molecule is slightly perturbed for υ=1

Table 5.1: Spectroscopic constants (in cm^{-1}) for the $X^3\Phi_4$ and $X^3\Phi_3$ states of CoH and CoD. The numbers in parentheses are 95% confidence limit (approximately two standard deviations, in units of the last significant digit quoted).

v	T_v	B_v	$-10^4 D_v$	$10^9 H_v$	$10^{11} L_v$	$10^8 q_H$	$10^{11} q_L$	$10^{14} q_M$
			CoH $X^3\Phi_4$					
0	0.0	7.136591(160)	−4.0096(93)	8.4(2.1)	−1.34(12)	...	−1.167(100)	−8.7(1.5)
1	1855.3720(64)	6.925110(180)	−4.0672(97)	33.8(2.0)	−3.47(14)	...	2.37(97)	−5.09(13)
2	3641.603(95)	6.71168(38)	−3.948(42)	61.(18)	−18.7(2.6)	...	1.3(1.3)	31.(41)
			CoH $X^3\Phi_3$					
0	675.564(14)	7.27614(21)	−5.3253(79)	−8.6290(130)	...	−169.32(25)		
			CoD $X^3\Phi_4$					
0	0.0	3.719474(59)	−1.11330(110)	1.65(53)	...	...	−0.00900(110)	
1	1338.0940(40)	3.641032(64)	−1.10797(120)	1.68(61)	...	...	−0.01870(120)	
2	2640.9270(52)	3.56283(16)	−1.08400(180)	...	...	...	−0.170(55)	
3	3908.6000(120)	3.48426(20)	−1.0690(72)	...	...	...	−0.30(37)	
			CoD $X^3\Phi_3$					
0	669.045(50)	3.75536(54)	−1.1792(230)	−7.9(4.0)	−3.56(27)	−0.437(110)	8.20(26)	

Table 5.2: Spectroscopic constants (in cm^{-1}) for the excited states of CoH. Uncertainties are defined as in Table 5.1.

v	T_v	B_v	$-10^4 D_v$	$10^7 H_v$	$10^9 L_v$	$10^8 q_H$	$10^{10} q_L$	$10^{13} q_M$
		CoH $A'^3\Phi_4$						
0	12358.4390(85)	5.47693(69)	4.28(14)	1.760(73)	...	...	1.003(39)	−8.30(35)
1	13796.574(13)	5.28919(190)	3.68(66)	9.33(75)	6.20(24)	...	5.32(55)	−3.10(28)
2	15136.047(150)	5.1564(40)	−8.43(33)	6.04(85)	...	...	4.72(99)	−2.010(53)
		CoH $A'^3\Phi_3$						
0	12644.977(18)	6.36226(49)	−10.6810(43)	8.26(11)	...	−5.380(68)	1.580(32)	
		CoH $A^3\Phi_4$[a]						
0	22243.210(43)	6.5197(14)	−5.260(74)	−3.5(1.6)	...	...	−6.(2)	

[a] These constants are calculated using the line lists from Ref. [1].

Table 5.3: Spectroscopic constants (in cm^{-1}) for the excited states of CoD. Uncertainties are defined as in Table 5.1.

v	T_v	B_v	$-10^4 D_v$	$10^7 H_v$	$10^9 L_v$	$10^8 q_H$	$10^{10} q_L$	$10^{13} q_M$
		CoD $A'^3\Phi_4$						
0	12415.6620(37)	2.935920(64)	−0.3863(270)	−0.2731(40)	0.01240(18)	...	0.01547(83)	−0.0082(69)
1	13460.6260(100)	2.90166(53)	6.89(73)	−5.37(30)	1.230(38)	...	−0.942(110)	−3.40(31)
2	14459.2060(81)	2.87454(27)	0.469(31)	2.100(90)	...	...	0.0	...
		CoD $A'^3\Phi_3$						
0	12687.207(250)	3.22093(54)	−8.166(38)	20.44(11)	−1.900(110)	4.07(45)	−2.00(12)	
		CoD [13.3]4						
0	13293.008(160)	3.6180(15)	−14.833(48)	13.951(69)	−0.5988(39)	...	−1.6909(15)	2.640(22)
		CoD $A^3\Phi_4$[a]						
0	22267.480(18)	3.34007(46)	−1.076(29)	−0.520(61)	0.0460(40)	...	−0.0130(12)	
1	23383.261(22)	3.23602(67)	−0.776(58)	−2.06(19)	0.240(20)	...	1.824(11)	−3.90(21)
2	24433.450(86)	3.1212(51)	−2.010(97)	15.(10)	...	...	−1.10(52)	
		CoD $A^3\Phi_3$[a]						
0	22598.221(19)	3.37874(38)	−1.291(18)	5.0(2.1)	...	1.23(21)	−0.760(36)	
1	23708.644(25)	3.27127(64)	−1.208(41)	−2.10(68)	...	−1.60(11)		

[a] These constants are calculated using the line lists from Refs. [4] and [5].

Table 5.4: Dunham-type parameters and Born-Oppenheimer breakdown parameters (in cm^{-1}) for the $X^3\Phi_4$ state of CoH determined from the combined-isotopologue analysis. Uncertainties are defined as in Table 5.1.

constant	CoH	CoD
$\tilde{T}_{v=-1/2}$	953.730825	682.294956
$Y_{1,0}$	1924.8598(230)	1373.4397(140)
$Y_{2,0}$	−34.8214(150)	−17.7087(73)
$10^2\times Y_{3,0}$	5.02(32)	1.821(120)
$Y_{0,1}$	7.242385(74)	3.758673(73)
$Y_{1,1}$	−0.212336(270)	−0.078031(82)
$10^4\times Y_{2,1}$	2.87(99)	−0.67(26)
$10^4\times Y_{0,2}$	−3.9856(83)	−1.1132(23)
$10^6\times Y_{1,2}$	0.210(94)	−2.11(21)
$10^6\times Y_{2,2}$	−2.11(25)	0.656(66)
$10^8\times Y_{0,3}$	−0.672(170)	0.188(24)
$10^8\times Y_{1,3}$	2.188(130)	0.2055(120)
$10^{13}\times Y_{0,4}$	−0.10(13)	−0.67(89)
$10^{11}\times Y_{1,4}$	−1.910(100)	−0.0913(49)
$q_{0,4}$	$-0.56(11)\times 10^{-11}$	$-2.36(47)\times 10^{-15}$
$q_{1,4}$	$-3.278(180)\times 10^{-11}$	$-1.220(67)\times 10^{-16}$
$q_{2,4}$	$3.370(70)\times 10^{-11}$	$1.107(23)\times 10^{-18}$
$q_{0,5}$	$1.440(130)\times 10^{-14}$	$4.18(39)\times 10^{-24}$
$q_{1,5}$	$-4.120(98)\times 10^{-14}$	$-1.054(25)\times 10^{-27}$
$\delta^H_{1,0}$	1.273(32)	
$10^3\times \delta^H_{2,0}$	0.310(130)	
$10^1\times \delta^H_{0,1}$	2.90555(34)	
$10^3\times \delta^H_{1,1}$	−5.36(47)	
$10^3\times \delta^H_{2,1}$	−1.10(23)	
$10^5\times \delta^H_{0,2}$	−6.303(110)	
$10^5\times \delta^H_{1,2}$	−2.330(150)	
$10^5\times \delta^H_{2,2}$	1.420(97)	
$10^8\times \delta^H_{0,3}$	4.200(100)	

and 2, and it definitely affects the combined-isotopologue fit. The results of the Dunham-type fits are presented in Table 5.4. The equilibrium bond lengths (r_e) for CoH and CoD were found to be 1.532731(27) Å and 1.517506(13) Å , respectively. The difference between r_e values of the two isotopologues is about 1%, which is

Table 5.5: Dunham-type parameters for the $X^3\Phi_4$ state of CoH and CoD, all in cm^{-1}. Uncertainties are defined as in Table 5.1.

Constant	CoH	CoD
$\tilde{T}_{v=-1/2}$	953.6188875	682.303188
$Y_{1,0}$	1924.5256(21)	1373.4556(150)
$Y_{2,0}$	−34.5757(76)	−17.7063(86)
$10^2\times Y_{3,0}$	...	1.570(140)
$Y_{0,1}$	7.24175(26)	3.758823(69)
$10\times Y_{1,1}$	−2.0984(42)	−0.78765(52)
$10^3\times Y_{2,1}$	−0.851(160)	0.1480(120)
$10^4\times Y_{0,2}$	−3.9069(140)	−1.11661(120)
$10^5\times Y_{1,2}$	−2.618(210)	0.0625(69)
$10^5\times Y_{2,2}$	1.045(79)	...
$10^8\times Y_{0,3}$	−2.287(30)	0.168(63)
$10^8\times Y_{1,3}$	7.697(35)	−0.0030(39)
$10^8\times Y_{2,3}$	−2.640(120)	...
$10^{12}\times Y_{0,4}$	−3.8(2.2)	...
$10^{11}\times Y_{1,4}$	−2.03(15)	...
$10^{11}\times q_{0,4}$	0.349(170)	0.0039(11)
$10^{11}\times q_{1,4}$	−5.118(24)	−0.00970(57)
$10^{11}\times q_{2,4}$	−4.300(93)	...
$10^{14}\times q_{0,5}$	1.14(21)	...
$10^{14}\times q_{1,5}$	−4.130(150)	...
$\overline{dd}$	1.058	1.040

due to the breakdown of the Born–Oppenheimer approximation and to the effect of perturbations.

5.4 Discussion

When comparing our spectroscopic constants with those derived in previous experimental work [1, 3–11], one has to be very cautious because of the different energy level expressions used. For instance, band origins for the excited $A'\,^3\Phi_4$ state reported by Barnes *et al.* [10] and Ram *et al.* [11] differ by as much as ~ 30 cm^{-1}. However, this is merely because Ram *et al.* [11] did not include the term Ω^2 in the rotational angular momentum factor $[J(J+1)-\Omega^2]$ in their versions of Eq. 5.1.

One can compare values of the spin-orbit splitting in the ground state obtained in this work with values determined in the laser experiments [8, 10]. If one considers the ground-state term values of CoH calculated using constants from Table 5.1, the difference between the energy levels $J = 4$ in $\Omega = 3$ and $J = 4$ in $\Omega = 4$ is found to be 726.996 cm^{-1}, which is in excellent agreement with the value of 728 ($\pm$3) cm^{-1} reported in Ref. [8]. However for CoD our difference between $J = 4$ in $\Omega = 3$ and $J = 4$ in $\Omega = 4$ levels is found to be 695.464 cm^{-1}, which is significantly different from the value of 729 ($\pm$2) cm^{-1} reported by Barnes *et al.* [10]. The reason for this discreapancy is not yet understood.

The fact that only one parity component of the $X^3\Phi_3$ state of the CoH molecule is perturbed leads to the assumption that the perturbing state has only one parity component. *Ab initio* calculations [18] predict a $^3\Sigma^-$ state 0.14 eV above the ground electronic state. This state has a 0^+ spin component of e-parity and we believe that despite the difference in Ω-values, it is a perturber of the $X^3\Phi_3$ state. That means that the perturbed levels belong to the e-parity component, and this makes it possible to assign the parities of all observed energy levels in the ground and excited electronic states. The tentative parity assignment of the levels given in Ref. [11] has to be changed to satisfy the arguments above. Also, one can assume that the 0^+ spin component of the $^3\Sigma^-$ is located $\sim$700 cm^{-1} above the $X^3\Phi_4$ state. Nevertheless, it should be noted that since the e and f levels of the same J of the Ω=1 component of the $^3\Sigma^-$ state are widely separated, one of these components could also be responsible for perturbing only one parity component of the $X^3\Phi_3$ sub-state.

The anomalous broadening of the high-J lines of the transitions terminating on the $X^3\Phi_3$ state that was observed in this work was also noticed by Klynning and Kronekvist [5] in the $A^3\Phi_3$- $X^3\Phi_3$ transition of CoH. They suggested that it may be caused by predissociation of the upper state. However, the experiments in Ref. [5] were done in absorption, and since we are observing the same broadening in emission it is unlikely that it is caused by predissociation. More likely, this broadening is evidence for hyperfine perturbations which were also observed in the $X^3\Phi_3$ state of the CoCl molecule by Flory *et al.* [27]. In the case of CoCl it was suggested that these perturbations are caused by second-order spin-orbit mixing with a nearby isoconfigurational $^1\Phi_3$ state, but theoretical predictions [18] suggest that for the CoH molecule $^1\Phi$ state is located 2.60 eV above the ground state; therefore, that state can not be responsible for the hyperfine perturbations.

The [13.3]4 state of CoD observed in this work is most probably a $^1\Gamma_4$ state, as it is the only state within 5000 cm^{-1} that has an Ω=4 spin component, according to theory [18]. Fig. 5.4 illustrates electronic states of CoH molecule observed in all previous optical experiments [1, 3–11] and this work. The transitions observed in this work are marked with arrows. The [15.5]3, [16.0]3 and [16.6]3 states observed in Ref. [9] are probably higher vibrational levels of the $A'^3\Phi_3$ and $^1\Gamma_3$ states.

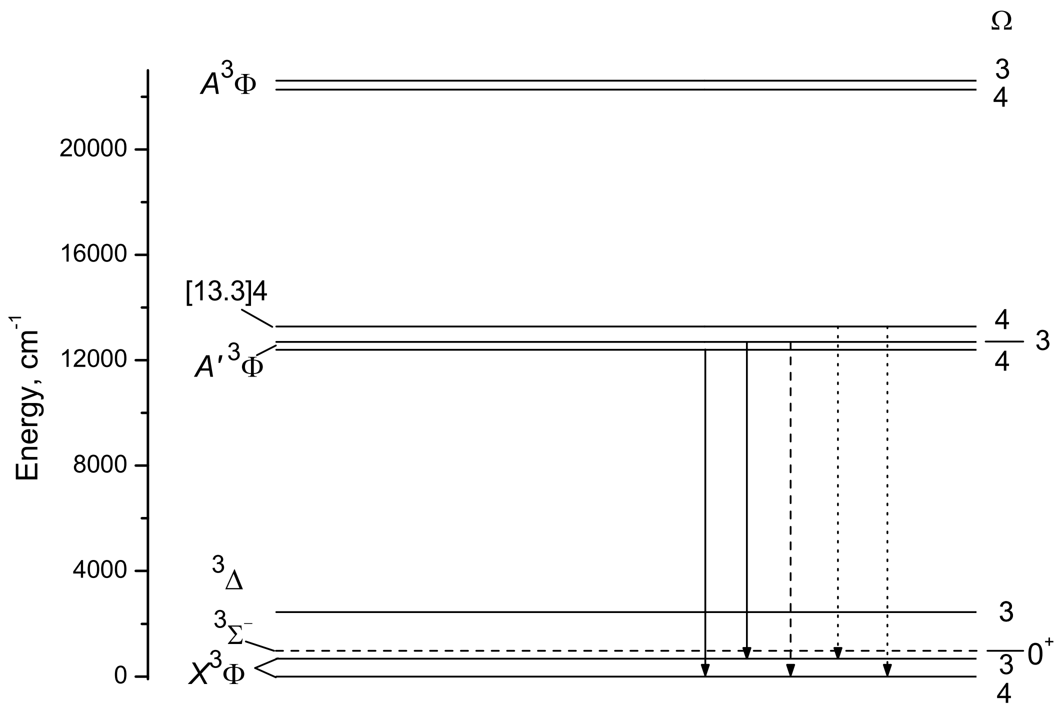

Figure 5.4: An energy level diagram showing the electronic states found in the Refs. [1, 3–11] and this work. The transitions observed in this work are marked with arrows. The solid arrows correspond to transitions observed for both CoH and CoD, dash arrows-only for CoH and dot arrows-only for CoD.

5.5 Conclusions

The Fourier transform emission spectra of CoH and CoD have been investigated in the near infrared region. A detailed analysis of bands of the $A'^3\Phi \rightarrow X^3\Phi$ transitions in both molecules has provided an improved set of ground state band and Dunham-type constants for the Ω=4 component. A combined-isotopologue fit was also performed for the $X^3\Phi_4$ spin component. The global fit of all transitions (including those from the previous optical experiments) has provided more precise values for the spin-orbit splittings between Ω=4 and Ω=3 in the ground and excited electronic states. We find no trace of any spin components with Ω=2. This is probably due to the fact that these sub-states are more perturbed than those with higher Ω-values because there are more possible perturbers available (according to the *ab initio* calculations [18]).

Bibliography

[1] A. Heimer, Z. Physik **104**, 448 (1937).

[2] G. Herzberg, *Spectra of Diatomic Molecules*, Van Nostrand, New York, 1950.

[3] L. Klynning and H. Neuhaus, Z. Naturforsch. **18**, 1142 (1963).

[4] L. Klynning and M. Kroneqvist, Physica Scripta **6**, 61 (1972).

[5] L. Klynning and M. Kroneqvist, Physica Scripta **7**, 72 (1973).

[6] L. Klynning and M. Kroneqvist, Physica Scripta **24**, 21 (1981).

[7] R. E. Smith, Proc. Roy. Soc. (London) A **322**, 113 (1973).

[8] T. D. Varberg, E. J. Hill, and R. W. Field, J. Mol. Spectrosc. **138**, 630 (1989).

[9] T. D. Varberg, PhD thesis, MIT, Cambridge, MA, 1992.

[10] M. Barnes, A. J. Merer, and G. F. Metha, J. Mol. Spectrosc. **173**, 100 (1995).

[11] R. S. Ram, P. F. Bernath, and S. P. Davis, J. Mol. Spectrosc. **175**, 1 (1996).

[12] A. E. S. Miller, C. S. Feigerle, and W. C. Lineberger, J. Chem. Phys. **87**, 1549 (1987).

[13] K. Lipus, T. Nelis, E. Bachem, and W. Urban, Mol. Phys. **68**, 1171 (1989).

[14] S. A. Beaton, K. M. Evenson, T. Nelis, and J. M. Brown, J. Chem. Phys. **89**, 4446 (1988).

[15] S. A. Beaton, K. M. Evenson, and J. M. Brown, J. Mol. Spectrosc. **164**, 395 (1994).

[16] D. Chong, S. Langhoff, C. Bauschlicher Jr, S. Walch, and H. Partridge, J. Chem. Phys. **85**, 2850 (1986).

[17] J. Anglada, P. J. Bruna, and F. Grein, J. Chem. Phys. **92**, 6732 (1990).

[18] M. Freindorf, C. M. Marian, and B. A. Hess, J. Chem. Phys. **99**, 1215 (1993).

[19] V. Barone and C. Adamo, Int. J. Quant. Chem. **61**, 443 (1997).

[20] T. Hirano, private communication.

[21] R. B. Le Blanc, J. B. White, and P. F. Bernath, J. Mol. Spectrosc. **164**, 574 (1994).

[22] R. J. L. Roy, *DParFit 3.3: A Computer Program for Fitting Multi-Isotopologue Diatomic Molecule Spectra*, University of Waterloo Chemical Physics Research Report CP-660 (2005). http://leroy.uwaterloo.ca.

[23] J. M. Brown and A. Carrington, *Rotational Spectroscopy of Diatomic Molecules*, Cambridge University Press, Cambridge, U.K., 2003.

[24] J. K. G. Watson, J. Mol. Spectrosc. **219**, 326 (2003).

[25] R. J. Le Roy, J. Mol. Spectrosc. **194**, 189 (1999).

[26] A. Shayesteh, D. Appadoo, I. Gordon, R. LeRoy, and P. Bernath, J. Chem. Phys. **120**, 10002 (2004).

[27] M. Flory, D. T. Halfen, and L. M. Ziurys, J. Chem. Phys. **121**, 8385 (2004).

Chapter 6

Fourier transform spectroscopy of ytterbium monoxide

6.1 Introduction

A considerable interest in lanthanide-containing molecules has arisen during past two decades [1]. For diatomic molecules, the lanthanide monoxides were studied most extensively, both theoretically and experimentally. The spectra are difficult to interpret because of the huge number of electronic states arising from open $4f$ configurations. Moreover, large spin-orbit coupling effects split and mix the various spin components that arise from the numerous ${}^{2S+1}\Lambda$ terms. The only remaining good quantum numbers are thus J and Ω, in the absence of nuclear spin. *Ab initio* calculations thus need to include relativistic effects before any meaningful comparison with experiment can be made.

The first experimental work on YbO, apart from band head positions found in the Vatican plates [2], was by Linton *et al.* [3]. They recorded a number of visible bands by laser excitation spectroscopy and examined some of the low-lying states by dispersing the laser-induced fluorescence. The ground state of YbO was found to be $X^1\Sigma^+$, arising from the $4f^{14}$ Yb^{2+} configuration, as predicted from a ligand-field calculation [3, 4] on $Yb^{2+}O^{2-}$. Such a closed-shell ground state was unusual because all lanthanide oxides except EuO and YbO have ground states that arise from M^{2+} $4f^n6s^1$ configurations rather than $4f^{n+1}$ configurations [4, 5]. The extra stability of the half-filled $4f^7$ Eu^{2+} and the filled $4f^{14}$ Yb^{2+} leads to $X^8\Sigma^-$ and $X^1\Sigma^+$ ground states, respectively, for EuO and YbO.

The combination of ligand field theory [4, 5] and laser spectroscopy [3, 6] has led to a rather satisfactory picture of the first few low-lying electronic states of YbO. In spite of a large number of papers [7–14], *ab initio* calculations do not predict a $X^1\Sigma^+$ ground state but rather a 0^- ground state that correlates with the $4f^{13}6s^1$ configuration of Yb^{2+}. Experimentally, this 0^- state is found at just 910 cm^{-1} above the $X^1\Sigma^+$ state [6], so it is not surprising that calculations have difficulty obtaining the correct energy ordering. There is also substantial configuration mixing between the $4f^{13}1\sigma^2 2\sigma^2 1\pi^4 3\sigma^1$ and $4f^{14}1\sigma^2 2\sigma^2 1\pi^4$ configurations (i.e., $4f^{13}6s^1$ and $4f^{14}$ on Yb^{2+}) in the ground state, as deduced from the dipole moment of 5.89 D [15]. The most recent experimental work was the detection of the infrared vibrational fundamentals of both YbO and YbO^+ in an argon matrix [16]. The exited states of YbO seen in the visible bands are ascribed to states correlating with the $4f^{13}5d^1$ and $4f^{13}6p^1$ configurations of Yb^{2+}, as well as to charge transfer states associated with Yb^+O^- [6]. The details are uncertain, however, and it would be helpful to locate additional transitions in the near infrared region where the density of states is lower. We, therefore, report the obserfation of 8 new bands near 1 micron. A rotational analysis was possible for 3 of these bands.

6.2 Experimental Arrangement

Gas-phase YbO was generated in a Broida-type oven [17] by the reaction of ytterbium metal vapor with N_2O. About 10 g of ytterbium metal was resistively heated in an alumina crucible with a current of about 45 A. A flow of argon gas carried the Yb metal vapor from the crucible to the reaction region where it was mixed with the oxidant gas. The partial pressures of the argon and nitrous oxide were adjusted to optimize the reddish chemiluminescent flame. Total pressures in the oven were approximately 6 – 8 Torr, with the oxidant gas making up a small fraction of this total. Little can be said about the exact chemistry inside the flame, but the mechanism of reaction is straightforward. The N_2-O bond dissociation energy is 70 kcal/mole, while the dissociation energy of YbO is ~100 kcal/mole [18] and the exothermic reaction proceeds quite readily. For the reaction of N_2O with ytterbium metal $\Delta H = -30$ kcal/mole [19]. The energy released is available to cause excited electronic states to be populated, and is responsible for the observed chemiluminescence.

The chemiluminescence from the flame was imaged onto the entrance aperture of a Bruker IFS 120 HR Fourier transform spectrometer. The YbO emission spectrum was recorded in the range 9 000-12 000 cm^{-1} using a silicon photodiode detector. An 800 nm red pass filter was used to eliminate the signal from the He-Ne laser of the spectrometer. To obtain a good signal-to-noise ratio (S/N), a total of 50 scans were co-added at a resolution of 0.04 cm^{-1}. Line positions were measured using a Windows-based program called WSpectra, written by Dr. Michel Carleer (Laboratoire Chimie Physique Moléculaire, Université Libre de Bruxelles, Belgium). A zero filling factor of 4 was used to generate enough points for good data reduction, and Voigt lineshape functions were fitted to the observed rotational lines. For calibration, argon atomic lines were recorded from an argon pen lamp immediately after the experiment and compared to the list of Norlén [20]. The accuracy of measurements in similar previous work of this nature is typically 0.005 cm^{-1} (or better) for strong, unblended lines.

6.3 Results and Discussion

An overview of YbO chemiluminescence spectrum obtained in the present work is displayed in Figure 6.1. A total of 8 red-degraded bands were identified in the 9 800 − 11 300 cm^{-1} region . However due to the presence of several isotopomers, as well as perturbations in some of the bands, only 3 were rotationally analyzed. The bandhead positions of all the observed bands are listed in Table 1, along with the band origins for the 3 analyzed systems.

Table 6.1: Observed YbO bandhead positions (cm^{-1}).

Bandhead	Type	Band origin	Note
9888.40	R-head	–	–
10200.28	R-head?	–	–
10256.08	Q-head	10256.11	System 1
10537.02	R-head	–	–
10862.66	R-head	–	–
10963.13	R-head	–	perturbed
10992.03	R-head	10943.04	System 2
11200.26	R-head	11196.90	System 3

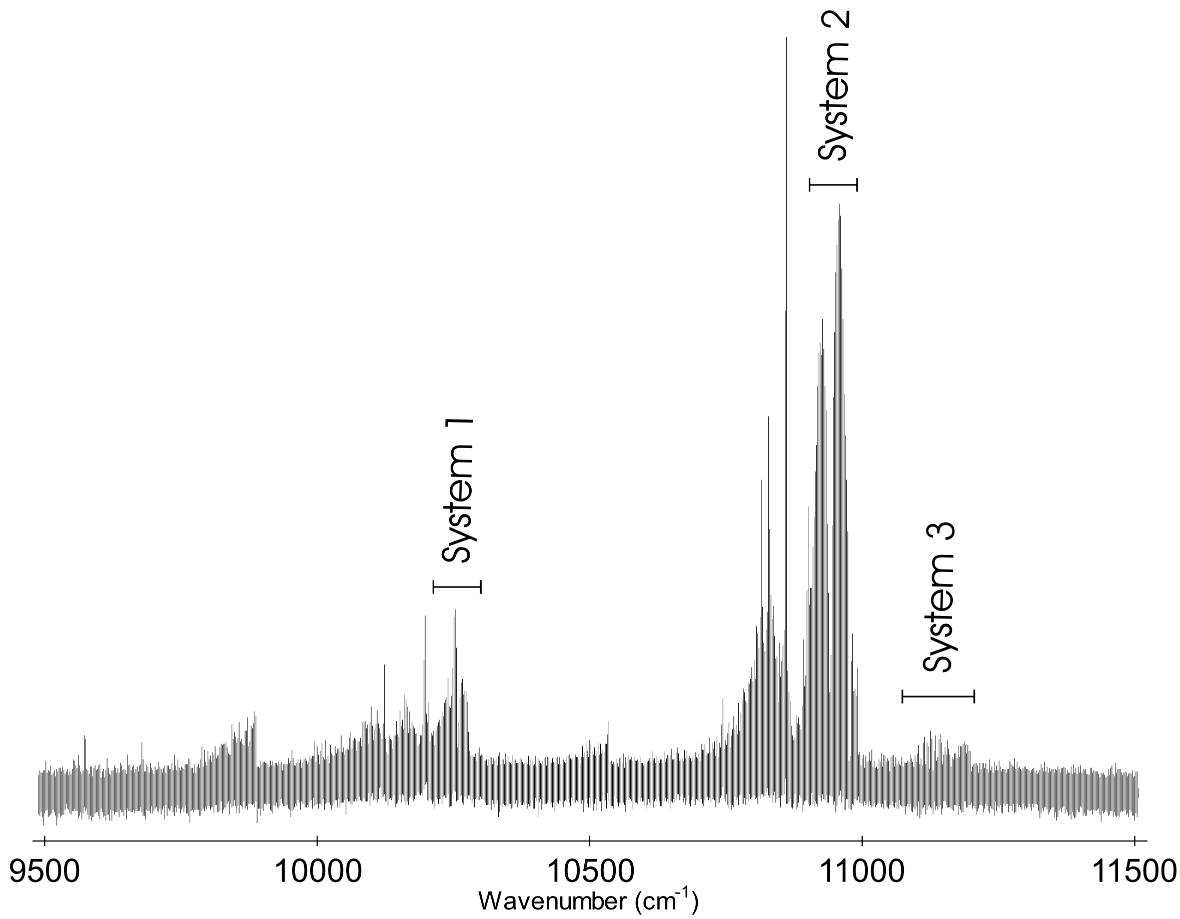

Figure 6.1: An overview of the emission spectrum of YbO.

Once the spectrum was recorded and measured, preliminary assignments of the rotational numbering were achieved by using graphical methods [21]. Since the splitting of the spectral lines due to the different isotopes was not resolved the analysis (by convention) was assumed to be for the principal isotopologue (^{174}YbO). In addition, for systems 1 and 2 it was possible to observe the "first lines" of the bands, which confirmed our initial rotational assignments. System 1 has a simple P-Q-R branch structure, which is typical for a $^1\Pi -^1 \Sigma$ transition, while systems 2 and 3 possess only P- and R-branches, indicative of a $^1\Sigma -^1 \Sigma$ transition. The data for system 3 and the combined data for the systems 1 and 2 were then employed in least-squares fits that contained the usual analytical expressions for $^1\Sigma^+$ and $^1\Pi$ states.

$$F_v(J) = \nu_0 + BJ(J+1) - D[J(J+1)]^2 + H[J(J+1)]^3 \quad (6.1)$$

$$\begin{aligned} F_v(J) &= \nu_0 + BJ(J+1) - D[J(J+1)]^2 + H[J(J+1)]^3 \\ &\pm \frac{1}{2}\{qJ(J+1) + q_D[J(J+1)]^2\}. \end{aligned} \quad (6.2)$$

For the lower states, the fitted parameters were the rotational parameters B and D, and for upper states: the band origin, ν_0, rotational parameters B, D and H, and the lambda-doubling parameters, q and q_D for system 1.

System 1: $\nu_0 = 10\,256$ cm^{-1}

As mentioned above, this band has a simple P-Q-R branch structure, and no perturbations were identified in the observed J-range ($1 \leq J \leq 50$). In total, more than 100 lines were assigned for this band. By comparing combination differences for the lower state to those from the work of Linton *et al.* [3], it was determined that this band connects to the $X^1\Sigma^+$ $v = 0$ level.

System 2: $\nu_0 = 10\,943$ cm^{-1}

System 2 has the best S/N of all of the observed bands, and the first lines of this system were easily identified. Furthermore, a strong perturbation was immediately obvious in the spectrum at high-J (see Figure 6.2). The perturbation appears to be a classic level crossing, although attempts to assign the more severely perturbed lines were met with frustration. The shifts in the line positions indicate that the perturber's origin lies at higher energy, but the identity of the perturbing state is unknown. Assignments were made for both branches up to $J' = 55$ and it is believed the perturbation occurs at $J' \geq 56$.

Because we were unable to completely assign the perturbation, the perturbed lines were omitted from the data set in order to obtain a satisfactory fit. The lower state of this band was found to be the $X^1\Sigma^+$ $v = 0$ level.

System 3: $\nu_0 = 11\,197$ cm^{-1}

Of the 3 analyzed bands, system 3 had the poorest S/N, and we were only able to assign about 60 lines to ^{174}YbO. Least-squares fitting of the data revealed a perturbation at high-J, occurring at $J' \geq 44$. As with system 2, the more severely perturbed lines were omitted from the final least-squares fits. It should be noted that the perturbation found in this band is not due to system 1, that is, they are

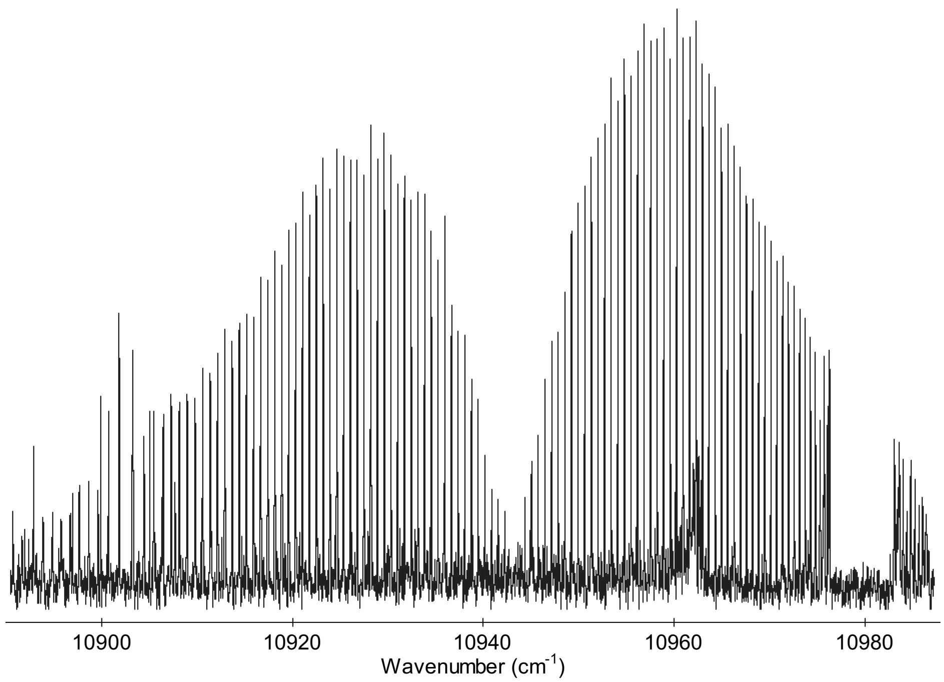

Figure 6.2: The observed YbO chemiluminescence spectrum of the strongest band with a perturbation clearly visible in the R-branch near 10980 cm^{-1}.

not the same perturbation. The lower state of this band was determined to be the $X^1\Sigma^+$ υ=1 level located 683.107 cm^{-1} above υ=0 [3].

The molecular parameters for all 3 of the bands analyzed in the present work are summarized in Table 2. A complete list of the line positions used in the fits, as well as residuals between the measured lines and those calculated using the parameters in Table 2, is available in Appendix C. Our ground state rotational constants are in agreement with those of Linton *et al.* [3].

The standard deviations of the fits were on the order of 0.005 cm^{-1}, indicating that the deviations between the calculated and measured line positions were consistent, on average, with the estimated measurement precision.

The results from the study of YbO by McDonald *et al.* [6], which includes laser-induced fluorescence results and ligand field predictions, can shed some light on the transitions observed in the present study. In their work, McDonald *et al.* showed that the ground state of YbO arises primarily from the $Yb^{2+}(4f^{14})O^{2-}$ electronic

Table 6.2: Molecular parameters (cm^{-1}) for the observed ^{174}YbO bands.

Parameter	System 1	System 2	System 3
ν_0	10256.1246(19)	10943.0413(20)	11196.9197(30)
B'	0.346383(30)	0.350130(30)	0.310778(47)
$10^7 D'$	4.99(12)	4.27(15)	2.31(27)
$10^{11} H'$	-1.53(17)	-6.71(36)	-22.84(81)
$10^4 q'$	-9.516 (4)	–	–
$10^8 q_D'$	4.59 (21)	–	–
B''	0.350326(27)		0.346116(48)
$10^7 D''$	3.91(9)		4.45(23)
Lower state	$X^1\Sigma^+$ v = 0		$X^1\Sigma^+$ v = 1

configuration. In addition, they investigated the manifold of electronic states arising from the $Yb^{2+}(4f^{13}6s)O^{2-}$ configuration. Based on the magnitude of the rotational constant, B, for the upper state of system 3 from the present work, it seems unlikely that it arises from the $f^{13}s$ configuration, since all of the observed $f^{13}s$ states in the work of McDonald *et al.* have $B \approx 0.35$ cm^{-1}. Also noted by those authors is the fact that all states with $f^{13}s$ electronic configurations have a vibrational spacing of about 830 cm^{-1}. In the present work, unfortunately, we have observed only one vibrational level, and therefore could not determine a vibrational spacing for any of the observed states. At this point it is unclear what type of electronic configuration would give rise to a rotational parameter with a value similar to that observed for the upper state of system 3 ($B' \approx 0.31$ cm^{-1}, $r \sim 1.92$ Å). Unlike system 3, both systems 1 and 2 have $B' \approx 0.35$ cm^{-1} ($r \sim 1.81$ Å), so it is plausible that these upper states could arise primarily from the $Yb^{2+}(f^{13}s)O^{2-}$ electronic configuration. Interestingly, the ligand-field fit of the low-lying states in YbO by McDonald *et al.* [6] predicts that an electronic state with $\Omega = 0^+$ will lie at 11981 cm^{-1} and one with $\Omega = 1$ at 11675 cm^{-1}. These calculated states are close to the states observed in the present work in which system 2 ($\Omega = 0^+$) lies at about 11000 cm^{-1} and system 1 ($\Omega = 1$) at about 10250 cm^{-1}.

After our work was completed we learned of an unpublished ligand field calculation for YbO that uses relativistic atomic wavefunctions [22]. The use of relativistic wavefunctions rather than the usual non-relativistic electronic wavefunctions cause small shifts in the YbO energy levels. For example the $\Omega = 0^+$ and 1 states from the $Yb^{2+}(f^{13}s)O^{2-}$ configuration predicted by McDonald *et al.* [6] shift from 11 981 cm^{-1} and 11 675 cm^{-1} to 11 884 cm^{-1} and 11 708 cm^{-1}, respectively.

Kaledin *et al.*'s calculations [22] show that the states arising from the $Yb^{2+}(f^{13}p)O^{2-}$ and $Yb^{2+}(f^{13}d)O^{2-}$ configurations lie too high in energy to be responsible for any of our new states, although the integer charge model may not be very reliable for these configurations. However, the singly charged configurations $Yb^{1+}(f^{14}s)O^{1-}(p^5)$ and $Yb^{1+}(f^{13}s^2)O^{1-}(p^5)$ give rise to a number of electronic states in the 10 000-13 000 cm^{-1} region. In particular, the $Yb^{1+}(f^{14}s)O^{1-}(p^5)$ configuration has a [12.3]1 ($A'^1\Pi_1$) state at 12 283 cm^{-1}, [12.0]0 ($a^3\Pi_0$) at 12026 cm^{-1} and [11.9]1 ($a^3\Pi_1$) at 11 950 cm^{-1}, while the $Yb^{1+}(f^{13}s^2)O^{1-}(p^5)$ configuration has states with $\Omega =$ 2,1,1,0,0 (probably $^3\Pi$ and $^1\Pi$ states) around 12 565 cm^{-1}. The square bracket notation corresponds to $[T_0]\Omega$, and the A' and a notation is based on a comparison with CaO [22]. The upper state of system 3 probably originates from one of the singly charged Yb^+ configurations, and the $A'^1\Pi$ state at 12 283 cm^{-1} is a plausible match. Note, however, that the $A^1\Sigma^+$ state of YbO with $r = 2.062$ Å is attributed to the same $Yb^{1+}(f^{14}s)O^{1-}(p^5)$ configuration as the $A'^1\Pi$ state, and hence should have the same bond length, while the observed r value for the upper state of system 3 is only 1.92 Å.

In conclusion, we have made the first observation of several electronic transitions in the near-infrared spectrum of YbO using Fourier transform emission spectroscopy. A rotational analysis of three transitions identified the lower states as the ground electronic state of YbO. While two of the upper states involved in the transitions appear to arise primarily from the $f^{13}s$ electronic configuration, it is unclear which configuration gives rise to the third observed state. Additional calculations, both ligand field and *ab initio*, are required to provide more information about low-lying states. Experimental work for transitions in infrared region will be very helpful as well.

Bibliography

[1] M. Dolg and H. Stoll, *Electronic Structure Calculations for Molecules Containing Lanthanide Atoms*, volume 22, Elsevier, Amsterdam.

[2] A. Gatterer, J. Junkes, E. Salpeter, and B. Rosen, *Molecular Spectra of Metallic Oxides*, Specola Vaticana, Vatican City, 1957.

[3] C. Linton et al., J. Mol. Spectrosc. **101**, 332 (1983).

[4] M. Dulick, E. Murad, and R. Barrow, J. Chem. Phys. **85**, 385 (1986).

[5] P. Carette and A. Hocquet, J. Mol. Spectrosc. **131**, 301 (1988).

[6] S. A. McDonald, S. Rice, R. Field, and C. Linton, J. Chem. Phys. **93**, 7676 (1990).

[7] M. Dolg and H. Stoll, Theor. Chem. Acta **75**, 369 (1989).

[8] M. Dolg, H.-J. Flad, H. Stoll, and H. Preuss, J. Chem. Phys. **97**, 1162 (1992).

[9] M. Dolg, H. Stoll, and H. Preuss, Theor. Chem. Acta **85**, 441 (1993).

[10] S. G. Wang and W. Schwarz, J. Phys. Chem. **99**, 11687 (1995).

[11] S. G. Wang, D. K. Pan, and W. Schwarz, J. Chem. Phys. **102**, 9296 (1995).

[12] W. Liu, G. Hong, D. Dai, L. Li, and M. Dolg, Theor. Chem. Acc **96**, 75 (1997).

[13] W. Liu, M. Dolg, and L. Li, J. Chem. Phys. **108**, 2886 (1998).

[14] X. Cao, W. Liu, and M. Dolg, Science in China (Series B) **31**, 6 (2001).

[15] T. C. Steimle, D. M. Goodridge, and C. Linton, J. Chem. Phys. **107**, 3723 (1997).

[16] S. Willson and L. Andrews, J. Phys. Chem. **103**, 6972 (1999).

[17] J. West, R. Bradford, J. D. Eversole, and C. Jones, Rev. Sci. Instr. **46**, 164 (1975).

[18] C. B. Cosmovici et al., Chem. Phys. Lett. **47**, 241.

[19] S. McDonald, PhD thesis, MIT, Cambridge, MA, 1985.

[20] G. Norlén, Physica Scripta **8**, 249.

[21] G. Herzberg, *Spectra of Diatomic Molecules*, Van Nostrand, New York, 1950.

[22] L. Kaledin, M. Heaven, and R. W. Field, unpublished manuscript.

Chapter 7

Electronic spectra of europium monohydride

7.1 Introduction

The lanthanide hydrides have attracted recently much interest because of their use in semiconducting and magnetic materials [1, 2]. Lanthanide metals are also being considered as hydrogen storage materials [3]. It is therefore important to study small lanthanide hydrides in order to extend our knowledge of the hydrogen chemistry of these compounds.

Unfortunately, spectroscopic experiments with rare-earth metals are difficult. Apart from the fact that lanthanides are expensive, they are also very reactive, and it is hard to control the chemistry during an experiment. Gas-phase experiments are also difficult due to the low vapor pressures of most of these metals at the temperatures that can be achieved by conventional methods. When the experiments are successful, the interpretation of the obtained spectra is also difficult. The main reason is that the partially filled $4f$ orbitals of lanthanide metal atoms result in many low-lying molecular electronic states with complex structures. The great number of these states results in band overlaps in electronic spectra in addition to perturbations caused by interactions between the states. *Ab initio* calculations are not straightforward, because of the necessity of including relativistic and electron correlation effects when dealing with the atoms of heavy rare earth elements.

So far, the only lanthanide metal hydrides that have been studied in the gas phase are YbH and LuH [4–11]. Matrix isolation experiments were carried out by Willson and Andrews [12], who studied the vibrational fundamentals of several lanthanide metal polyhydrides as well as of NdH, CeH and TbH. In the experiments with europium metal, only EuH_2 and EuH_3 molecules were observed.

The first theoretical investigation of rare earth hydrides was carried out by Pyykkö [13] who estimated some spectroscopic parameters of LuH and TmH using Hartree-Fock (HF) and Dirac-Hartree-Fock (DHF) calculations. A series of pseudopotenial calculations on rare earth oxides, hydrides and halides were reported by Dolg and co-workers [14–17]. Most of these calculations were performed with nonrelativistic pseudopotentials, but for some molecules (including EuH), quasirelativistic pseudopotentials were used as well. Dolg and Stoll summarized the results of all calculations on lanthanide monohydrides in Table 15 of Ref. [16]. The calculated parameters for the ground electronic state of EuH range from 1.55 to 1.82 eV for dissociation energies, from 2.150 to 2.235 Å for bond lengths and from 1102 to 1215 cm^{-1} for the vibrational frequencies (ω_e), depending on the basis sets and pseudopotentials that were used. In Ref. [17] the molecular constants of selected lanthanide compounds (including EuH) have been calculated using relativistic small core pseudopotentials and optimized valence basis sets. All available theoretical calculations on EuH are limited to the ground electronic state. The lack of experimental and theoretical data forces us to use experiments and ligand field theory calculations on related molecules such as GdO [18–20] and EuF [18, 21] as a guide. New *ab initio* calculations on EuH by Yang and Pitzer are in progress at the Ohio State University [22].

In our work the EuH molecular spectrum was observed for the first time.

7.2 Experimental

7.2.1 Fourier transform spectra of EuH and EuD

The first set of experiments on EuH and EuD was carried out at the University of Waterloo. An emission source described in section 3.2.2 was used to generate an electronic spectrum. The inside of the alumina tube was wrapped with molybdenum foil to prevent the reaction between the metal and ceramic. The tube furnace was heated to 750°C and a mixture of Ar (∼13 Torr) and H_2 or D_2 (∼2 Torr) gases flowed slowly over the metal. The melting point of Eu is 1150°C so during our experiment the metal was in the solid phase. An electrical discharge (3 kV, 333 mA) was applied between two cylindrical stainless steel electrodes inside the ends of the tube. The argon pressure had to be much higher than in other experiments on metal hydrides carried out in our laboratory [23–25]. In this experiment as well as in experiments with other rare earth metals, the metal surface absorbed hydrogen gas, presumably forming solid EuH_2. For europium, the hydrogen absorption occurred at all temperatures but after some time the pressure inside the system stabilized probably after saturation of the metal surface with hydrogen. Nevertheless, the pressure in the system would occasionally increase suddenly, presumably because of a rapid release of hydrogen from the europium sample. The chemistry of this process was unfortunately beyond our control. After the experiment with hydrogen gas, deuterium gas was used the following day, but for the first two hours only EuH emission lines were observed, due to the fact that a considerable amount of hydrogen was still trapped in the metal from the previous experiment. Only after four hours of heating was the EuH signal completely replaced by that of EuD. It is worth noting that the Eu metal did not melt during the experiment, so the vapor was subliming from the surface.

Emission from the tube was focused onto the entrance aperture of a Bruker IFS 120 HR Fourier transform spectrometer. The windows at the ends of the tube and the lens were made from BaF_2. The EuH emission spectrum was recorded in the $10\,000-18\,000$ cm^{-1} region using a silicon photodiode detector, quartz beamsplitter and 550 nm red-pass filter. The EuD spectrum was recorded in the $8\,000 - 16\,000$ cm^{-1} region. A total of 100 scans for both molecules were co-added at a resolution of 0.04 cm^{-1} in order to obtain a good signal-to-noise ratio. Overview spectra of EuD and EuH are shown in Fig. 7.1. The dense features in the spectrum are molecular emission lines, while sparse and intense lines are europium and argon atomic emission lines.

Line positions were measured using a Windows-based program called WSpectra, written by M. Carleer (Université Libre de Bruxelles). The spectrometer was not under vacuum and the "air-to-vacuum" wavenumber correction [26] had to be made before the lines were calibrated against argon atomic lines present in the spectrum [27]. There are many bands present in the spectrum, as can be seen from Fig. 7.1. This results in line overlaps which make assignment of the lines difficult. Therefore it was decided to record a "cold" spectrum (when molecules are at ~ 5 K) of EuH in order to populate only the first few rotational levels, which will result in less lines in the electronic spectrum and simplify the line assignment.

7.2.2 Laser ablation/molecular beam experiment

The sub-Doppler spectrum of EuH was recorded in the laser ablation/molecular beam apparatus at the Arizona State University in the laboratory of Prof. T. C. Steimle. A europium metal rod (approximately $1''$ long and $0.25''$ in diameter) was

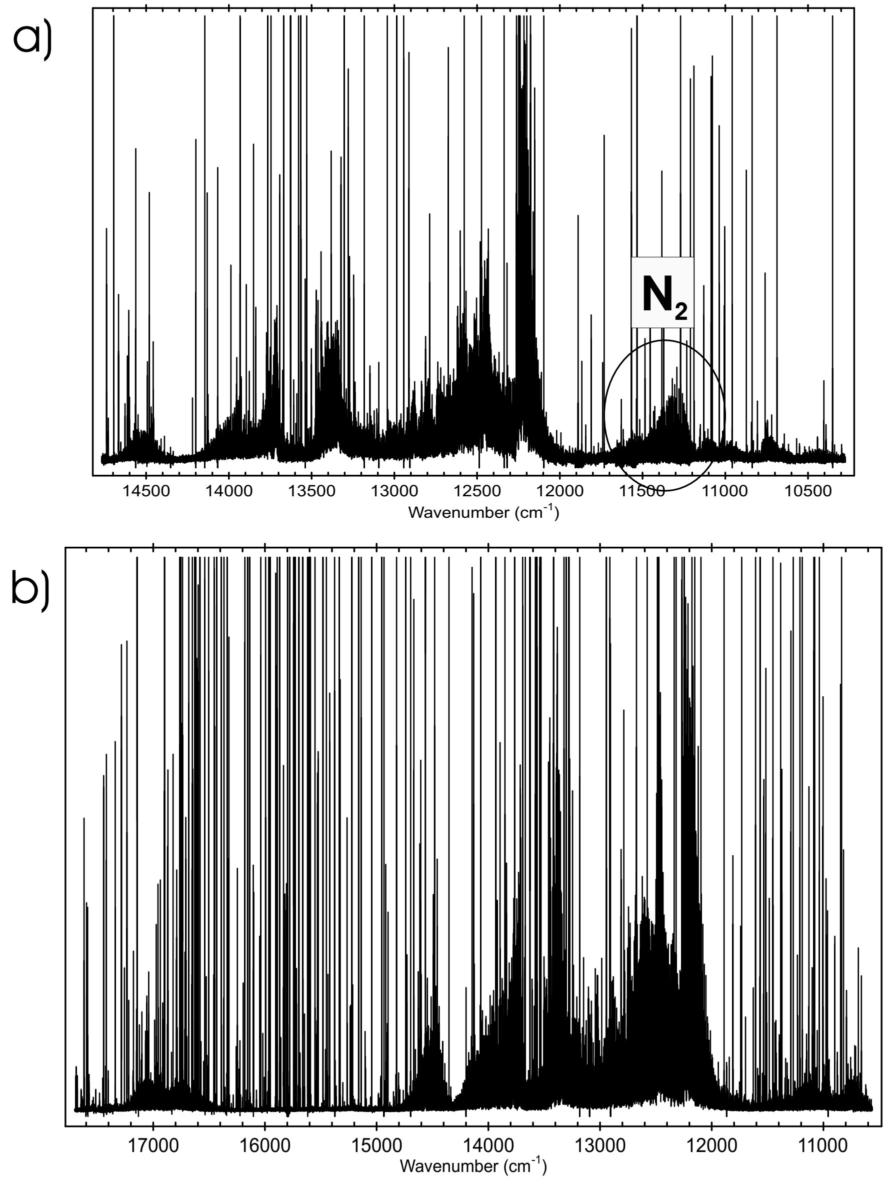

Figure 7.1: An overview of the FT spectrum of a) EuD and b) EuH. The dense features in the spectrum are molecular emission lines, while sparse and intense lines are europium and argon atomic lines. Note that the wavenumber ranges covered in EuD and EuH experiments are different (see text for details).

ablated by the third harmonic (355 nm) of a Q-switched Nd:YAG laser operating at approximately 10 mJ/pulse with a 20 Hz frequency of the pulses. In order to obtain stable shot-to-shot production of the metal vapor and to extend the life time of the sample, the rod was rotated and translated during the experiment. A quartz lens of 0.5 m focal length was used to focus the laser pulses onto the Eu sample. A solenoid pulsed valve was used to introduce the mixture of He and H_2 gases. After trying different proportions of gases in the mixture and different total backing pressures, it was found that a 50:50 mixture at ∼2300 kPa yields the best signal. As an alternative to helium, argon gas was used as well but the signal was much weaker. The created EuH molecules were skimmed about 15 cm downstream by a 5 mm diameter "skimmer" that separates source and detection chambers operated at approximately 5×10^{-5} Torr and 1×10^{-6} Torr pressures, respectively.

The dye laser radiation intersected the molecular beam at a right angle 10 cm downstream from the skimmer. A lens assembly was used to collect and collimate the resulting total laser-induced fluorescence through the band-pass filter, which minimized the background light associated with the ablation plasma. The cooled photomultiplier tube (PMT) detector was placed perpendicular to both the molecular beam and the probe laser. The signal from the PMT was processed using gated, single-photon-counting techniques.

First we made a number of survey scans (> 100 cm^{-1}) of the $13\,000 - 18\,000$ cm^{-1} region. For that purpose a Ti:Sapphire laser and a continuous wave, linear dye laser (operating with different dyes) were employed. This was done in an attempt to cover the range of the FT spectrum. Only the band at ∼17 000 cm^{-1} was found in these low resolution LIF scans. The bandwidth of the linear dye laser is approximately 5 GHz. A commercial wavemeter accurate to ± 0.01 cm^{-1} was employed for the wavelength calibration. An overview of the survey scan of this band is shown on Figure 7.2. As can be seen, this band has several intense features in a somewhat periodic pattern. It was decided to perform high resolution scans of these strong features.

Unfortunately, the condition of the rod could not allow a high resolution scan of the entire $16\,980 - 17\,125$ cm^{-1} region. The narrow scans (< 2 cm^{-1}) were carried out using a stabilized single mode, continuous wave ring dye laser. The bandwidth of this laser system was approximately 1 MHz. An absorption spectrum of a heated gaseous I_2 cell was recorded simultaneously with EuH laser induced fluorescence spectrum for wavelength calibration [28, 29] in narrow scans. An example of the "raw" high resolution scan is shown in Figure 7.3. The regions of the spectrum covered by the series of narrow scans are listed in Table 7.1.

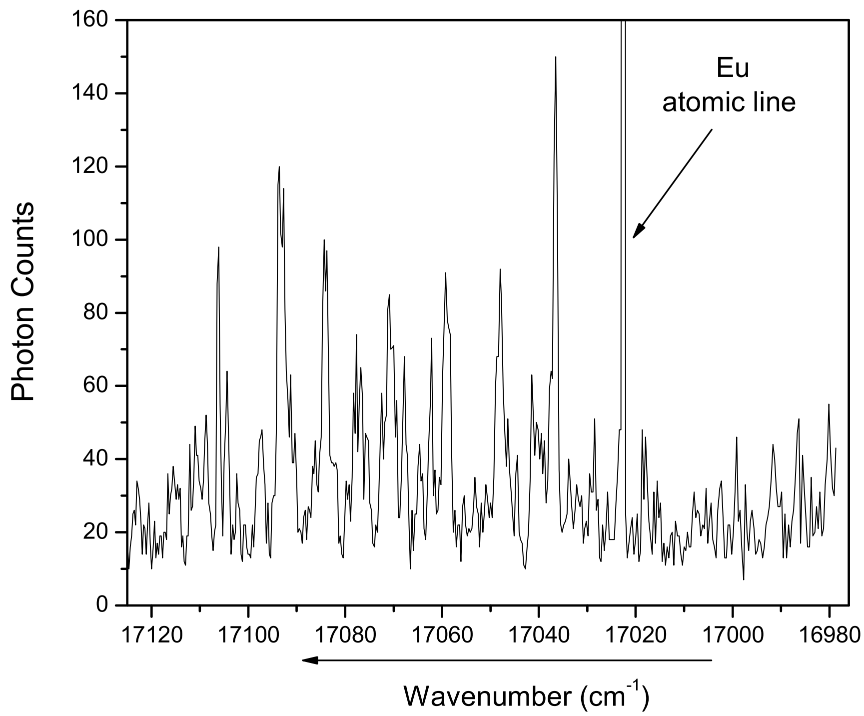

Figure 7.2: A survey laser excitation scan of the 16 975-17 125 cm^{-1}

7.3 Results and Discussion

7.3.1 Electronic states of EuH

The lack of available theoretical calculations, especially for excited electronic states, makes the interpretation of the EuH emission spectrum very difficult. In order to understand the electronic spectrum of EuH, we need to make some assumptions and educated guesses based on ligand field theory (LFT) and papers on EuF [18, 21] and GdO [18–20].

The ground-state atomic electron configuration is assumed to be $\mathrm{Eu}^{+}\{4f^{7}6s^{1}\}\mathrm{H}^{-}$. There are 8 unpaired electrons with parallel spins in the lowest energy configuration, which gives rise to a $^{9}\Sigma^{-}$ state [30]. In first excited electronic state, the spin of the s-electron flips to give a $^{7}\Sigma^{-}$ state. The next electronic configuration would be $4f^{7}5d^{1}$, which gives rise to nonet and septet Σ^{-}, Π and Δ states, and the nearby

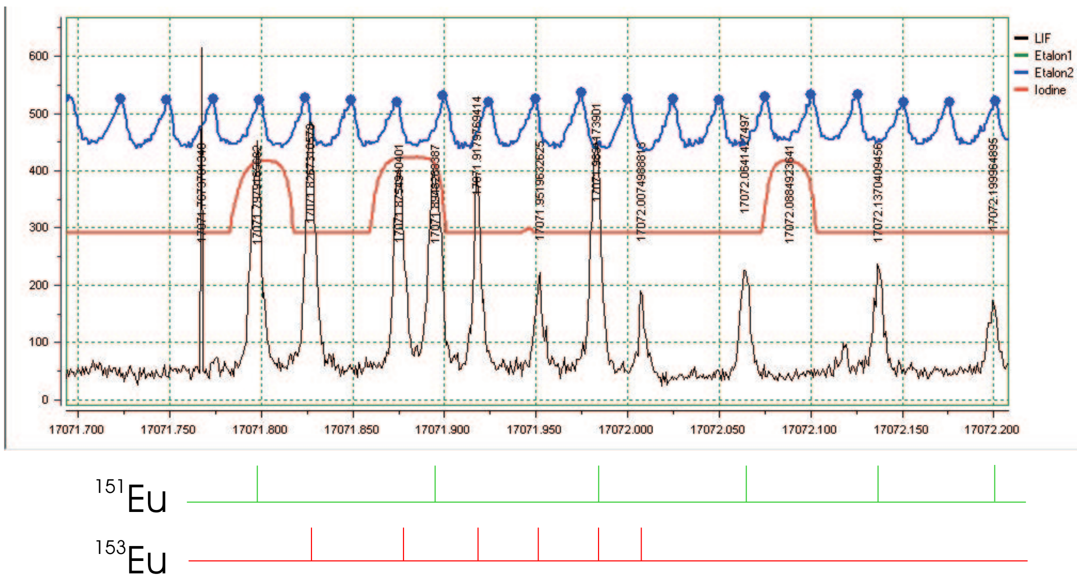

Figure 7.3: An example of "raw" high resolution LIF scan. Hyperfine and isotope splittings in EuH can be easily seen in the lower panel of this figure. The top panel are the fringes of an etalon and the middle panel is the spectrum of I_2 used for calibration.

$4f^7 6p^1$ configuration gives rise to the $^7\Sigma^-$, $^7\Pi$, $^9\Sigma^-$ and $^9\Pi$ states. Other possible excited electronic configurations are f^6s^2, $f^6s^1d^1$, *etc.*, which will give rise to numerous additional states. The absolute and relative positions of these states are hard to determine based on the simple LFT model. The main difficulty is that LFT is probably not a reliable model for the prediction of energy levels because EuH is not ionic. Some LFT predictions can be taken from Table 1 of Ref. [21], in which the results of LFT calculations for the low-lying states of EuF are listed. The $^7\Sigma^-$ state of EuF is predicted to lie 1420 cm^{-1} above the ground electronic state. Therefore, it was assumed initially that the majority of the observed transitions are from the excited $^7\Sigma^-$, $^9\Sigma^-$ and $^9\Pi$ states to the ground X $^9\Sigma^-$ state.

It is believed that the spin-spin interaction in the ground state is small and that this state obeys Hund's case (b) coupling. This is based on the fact that the spin-spin interaction is a sum of the first order electron spin-spin interaction and the second-order spin-orbit interaction with other states, with the latter usually dominating in heavy molecules [31]. The selection rules for the second order spin-orbit interaction are ΔS=0,$\pm$1; $\Sigma^\pm \sim \Sigma^\mp$; $\Delta\Omega$=0. Of the low-lying states, the best

Table 7.1: The regions covered by high-resolution scans (in cm^{-1})

Start	End
16982.7	16984.7
16986	16986.31
17012.5	17013.5
17037.6	17038.7
17040.2	17041.7
17051.05	17053.1
17060.45	17063.1
17067.29	17067.95
17070.25	17073.4
17082.9	17084.85
17091.97	17092.9
17094.3	17095.2
17105.3	17105.6
17108.8	17109.1
17112.3	17113.14

candidates for such an interaction with the ground state are $^9\Pi$ and $^7\Pi$ states arising from $4f^75d^1$ and $4f^75p^1$ configurations. According to the LFT predictions for EuF [21], the states arising from these configurations are located ~16 200 and ~18 900 cm^{-1}, above the ground $X\ ^9\Sigma^-$ electronic state, respectively; hence the interaction with these states is small. A similar situation was discussed in Chapter 4 in the case of $X\ ^7\Sigma^+$ state of MnH. Notice that the ground state atomic configuration of MnH is $Mn^+\{3d^54s^1\}H^-$, and so MnH is the transition metal analog of EuH. Also, according to Ref. [20] the value of spin-spin interaction constant λ of EuF was determined to be -0.13 cm^{-1} for an excited $^7\Sigma^-$ state, while the value for ground state was "very much" smaller (the exact value could not be determined from the available spectra).

In the Hund's case (b) coupling scheme, each rotational level (N) is split into nine spin components (for N>4) labeled by J, with **J**=**N**+**S**, where **J** is the total angular momentum, **N** is rotational angular momentum and **S** is the total electron spin. The excited septet and nonet states most probably obey Hund's case (a) (or (a′) for Σ states) coupling which spin "uncouples" to Hund's case (b) at higher J-values, just like the $A^7\Pi$ state of MnH [32]. At low J values the excited states of EuH will therefore be split into $2S$+1 well-separated spin components for non-Σ

states and into $S+1$ components for Σ states. That means that for lower J-values the excited $^9\Sigma^-$ state will be split into 5 relatively isolated spin components with $\Omega=0^-$, 1, 2, 3 and 4. The 4 last components ($\Omega > 0$) will have both e and f parity levels.

7.3.2 FT spectra of EuH/D

Guided by these ideas when scrutinizing the FT spectrum of EuH (Fig. 7.1b), it was noted that the band at 14 500 cm^{-1} (by coincidence this band is also the only band with a clear rotational structure, not overlapped by other bands) has the general appearance one would expect for $^9\Sigma^-$–$^9\Sigma^-$ transition, because it has 5 band heads (corresponding to 5 Ω-values). The spectrum of this band is shown in Figure 7.4.

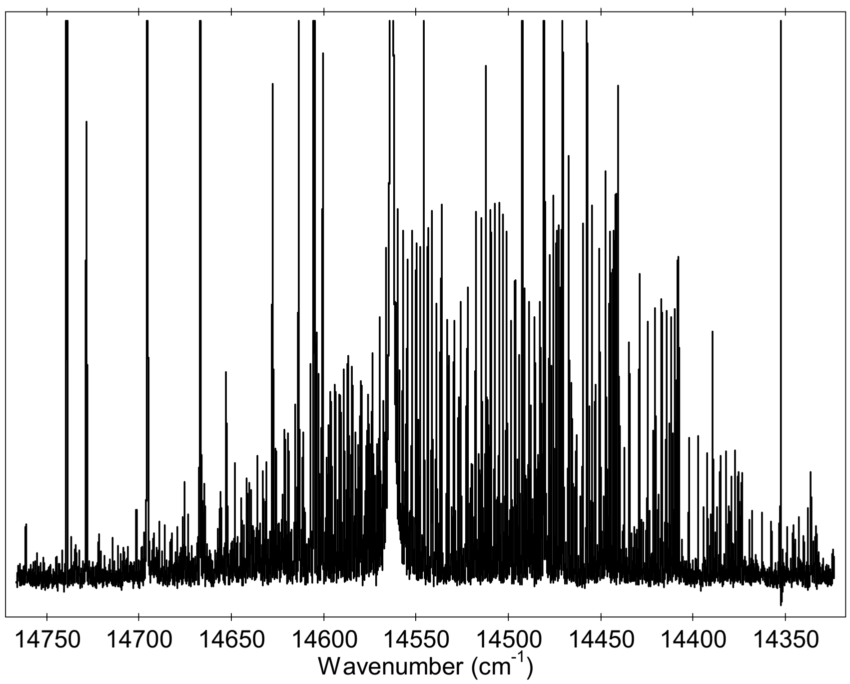

Figure 7.4: The 14 500 cm^{-1} transition of EuH observed by FT emission spectroscopy.

However, we have failed to assign this band because the branches are perturbed and exhibit behavior typical for transitions involving states with spin uncoupling, i.e., the spacing between the lines can increase and then decrease in the same branch [32].

7.3.3 The "cold" spectrum of EuH

Our failure to assign the FT spectrum of EuH, led us to record the sub-Doppler spectrum at Arizona State University. It was somewhat surprising that only the band at $\sim$17 000 cm^{-1} was seen with the laser ablation-molecular beam spectrometer. This implies that all other transitions in the FT spectrum (Fig. 7.1b) are not to the ground electronic state. The corresponding transition (at $\sim$17 000 cm^{-1}) was also observed for the EuF molecule [33], and most probably is a $^9\Sigma^-$–$X^9\Sigma^-$ or a $^9\Pi$–$X^9\Sigma^-$ transition.

When using the H_2-He gas mixture in the apparatus at the Arizona State University, an increase in the percentage of hydrogen leads to an increase in rotational temperature. Therefore the use of a 50:50 mixture of He and H_2 not only increases the production efficiency but unfortunately also increases the rotational temperature. This temperature is estimated to be 70 K by analogy with an experiment on CaH performed under similar conditions [34], while the desired rotational temperature was about 10 K. It is interesting to estimate the population distribution in the rotational levels at these temperatures. For that purpose the $X^9\Sigma^-$ ground state term values $E(J)$ were calculated using the SPCAT program [35]. The rotational constant B was taken to be 5.33 cm^{-1}, the spin-spin interaction constant λ=0.022 cm^{-1} and spin-rotation interaction constant γ=0. Then the rotational partition function was calculated using the following equation:

$$q_r = \sum_J (2J+1)e^{-\frac{E(J)}{kT}}, \tag{7.1}$$

in which k is the Boltzmann constant and the summation was taken over all J values corresponding to N having values from 0 to 7 (the population of the J levels corresponding to $N > 7$ is negligible). Now the population of every N level can be calculated as

$$p(N) = \sum_J p(J), \tag{7.2}$$

where $p(J)$ is a population of a particular J level given by

$$p(J) = (2J+1)\frac{e^{-\frac{E(J)}{kT}}}{q_r}. \tag{7.3}$$

Note that the summation in Eq. (7.2) is over the J values corresponding to a particular N.

The distribution of population calculated using Eq. (7.1-7.3) for 10 and 70 K is shown on Figure 7.5. As can be seen from the picture the N=0 to 6 levels have sufficient population at 70 K to contribute to the spectrum. Since the ground state obeys Hund's case (b) these levels are split into 4 to 9 J values.

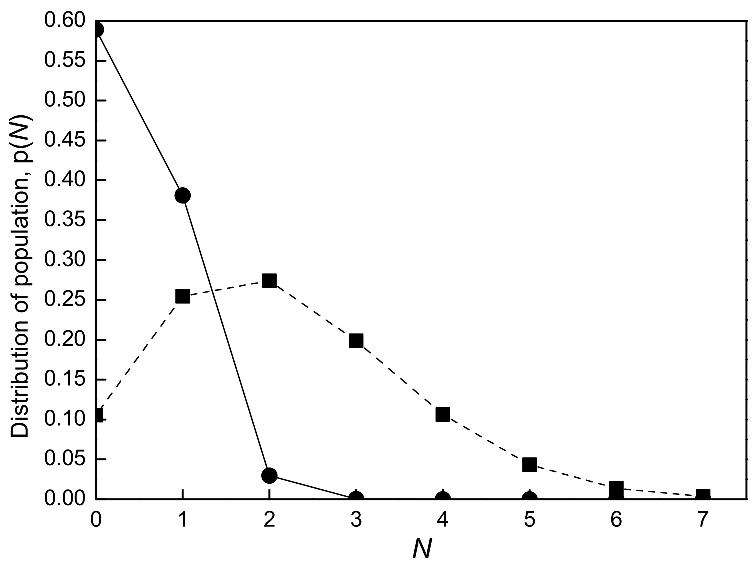

Figure 7.5: Distribution of population for the rotational temperature of 10 K (solid line) and 70 K (dashed line).

When considering our scan regions reported in Table 7.1, one must keep in mind that the isotope and hyperfine splittings are present at high resolution. Europium has two stable isotopes of similar abundance. Both isotopes have nuclear spins of $\frac{5}{2}$ and large nuclear magnetic moments. Table 7.2 provides nuclear data for isotopes of europium [36].

Table 7.2: The Eu data from the Ref. [36].

Isotope	Abundance (%)	Nuclear spin, I	Nuclear magnetic moment, μ/nuclear magnetons	Quadrupole moment, Q/fm^2
^{151}Eu	47.8	5/2	+3.4718	+116
^{153}Eu	52.2	5/2	+1.5331	+294

The nuclear spin of the H atom is $\frac{1}{2}$ but because the proton spin contribution to the hyperfine splitting is much smaller than that from the europium we can completely resolve only the Eu hyperfine splitting. We expect that the $X^9\Sigma^-$ state obeys Hund's case ($b_{\beta J}$) coupling [37], because it is a most common case for this type of molecules. For Hund's case ($b_{\beta J}$) coupling in addition to **J=N+S** coupling there is also a coupling of total angular momentum with nuclear spin: **F=J+I**. For the ground $X^9\Sigma^-$ state, each N level is split into $2S$+1=9 components (for N>4) and each J level is further split into $2I$+1=6 hyperfine components for each isotope. There are thus a total of 54×2=108 levels for each N counting each isotope separately. The upper state most probably follows Hund's case (a_β) coupling [37]. For both upper and lower states the $J = 0$ level splits into 3 hyperfine components (for each isotope), $J = 1$ into 4, $J = 2$ into 5 and $J \geq 3$ splits into 6 hyperfine components. The rotational selection rule for the electronic transition in this case will be $\Delta J = 0, \pm 1$. The selection rule for the transitions between upper and lower hyperfine levels is $\Delta F = 0, \pm 1$ with spectral lines with $\Delta J = \Delta F$ being the strongest. For higher J values only transitions with $\Delta J = \Delta F$ can be observed. As an example, hyperfine transitions from the $J' = 8$ level in the upper state to the $J'' = 9$ component for $N'' = 5$ rotational level of the ground state are shown in Figure 7.6. It follows from the figure that the transitions involving higher J values will appear in the spectrum with 6 hyperfine lines for each isotope (therefore 12 lines in total). The transition shown in Figure 7.3 is a clear illustration of these predictions as it is split into 12 hyperfine lines.

The lines in Fig. 7.3 appear in a "flag" or Landé pattern [38]. Before assigning the lines it is useful to consider the form of hyperfine interactions in the $^9\Sigma^-$ state. The hyperfine Hamiltonian for this state can be written as:

$$H_{hfs} = b_F \mathbf{I} \cdot \mathbf{S} + c(I_z S_z - \frac{1}{3}\mathbf{I} \cdot \mathbf{S}), \tag{7.4}$$

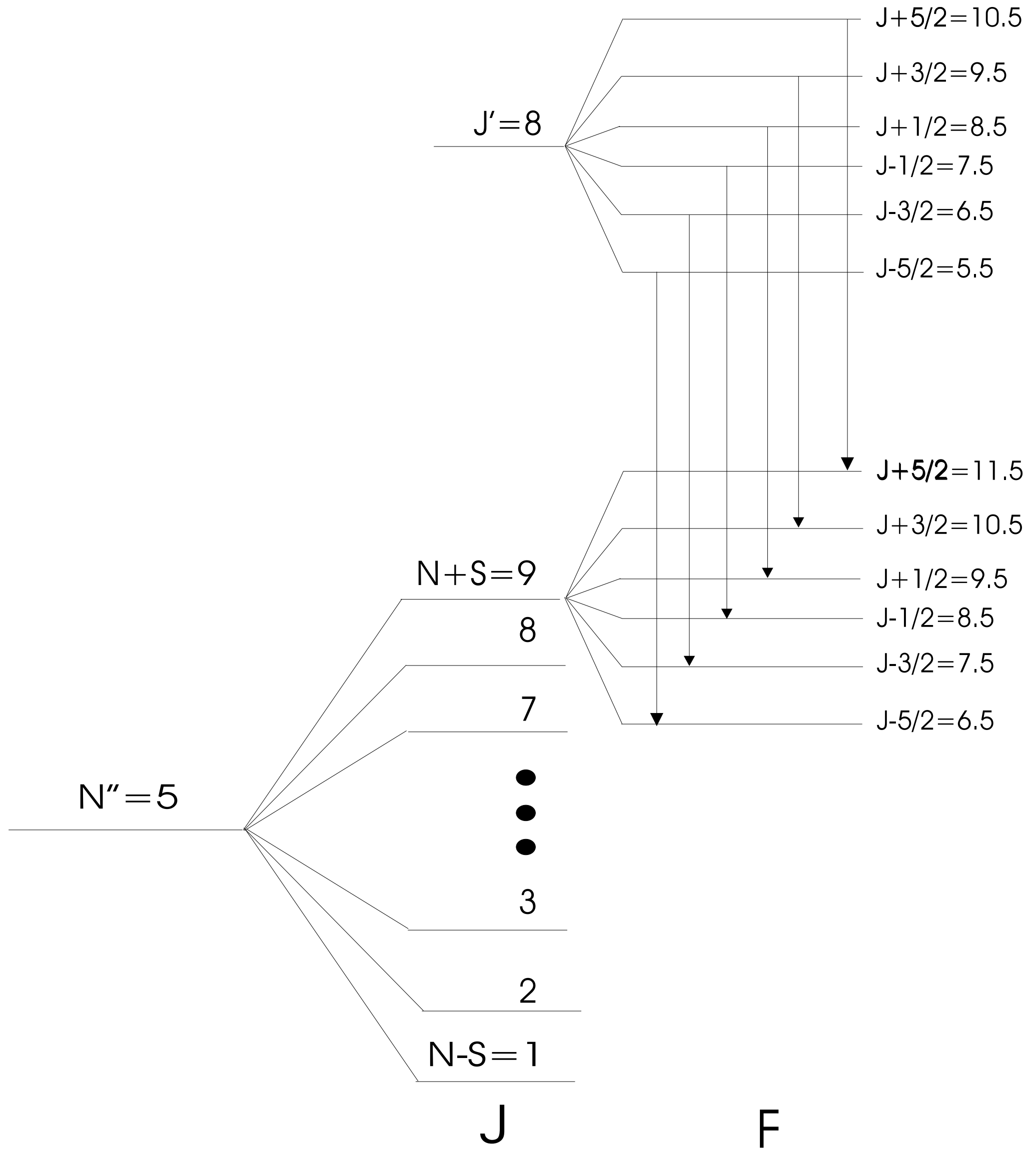

Figure 7.6: An example of the transitions between hyperfine levels in excited and ground electronic states.

where b_F is the Fermi contact parameter defined by

$$b_F = \frac{1}{hc}\frac{8\pi}{3} g\mu_B g_N \mu_N \sum_i \mid \langle \psi_i(r_i = 0) \rangle \mid^2 \qquad (7.5)$$

and the dipolar parameter c by

$$c = \frac{1}{hc}\frac{3}{2}g\mu_B g_N \mu_N \sum_i \langle (3cos^2\theta_i - 1) r_i^{-3} \rangle. \tag{7.6}$$

The expressions (7.5) and (7.6) are written in wavenumbers and μ_B and μ_N are the Bohr and nuclear magnetons, g and g_N are the electron and nuclear spin g-factors and (r_i, θ_i) are the spherical polar coordinates of the electron i, defined with respect to the Eu nucleus. The angle brackets imply the expectation value and the summations are over the unpaired electrons. The Fermi contact parameter basically describes the contribution of any s-electron density at the nucleus to the hyperfine interactions. Eq. (7.5) implies that $b''_F \gg b'_F$ for EuH since the ground state arises from an f^7s^1 configuration while the upper state is caused by f^7d^1 or f^7p^1 configurations. The difference in b_F values for the two isotopes of europium arise from the difference in g_N values. For ^{151}Eu $g_N = \frac{\mu_I}{I} = 1.38872$ and for ^{153}Eu $g_N = \frac{\mu_I}{I} = 0.61324$ and the ratio between the b_F values for ^{151}Eu and ^{153}Eu will be equal to 2.2646. In the spectrum the spacing between hyperfine lines of ^{151}EuH isotopologue will be a factor of ∼2.2646 larger than that of ^{153}EuH. This fact helps significantly in assigning the lines in hyperfine multiplets as can be seen in Fig. 7.3 (the isotope assignment is at the bottom of the Fig. 7.3). Notice that the f^7s^1 ground state configuration has a mainly spherical electron distribution so c'' is very small but c' can be significantly larger.

The diagonal matrix element of the Fermi contact interaction was derived by Varberg *et al*. [39] using the formulas of Ref. [40] as

$$\begin{aligned} \langle \Lambda NSJIF \mid b_F \mathbf{I}\cdot\mathbf{S} \mid \Lambda NSJIF \rangle &= -b_F\left[\frac{N(N+1) - S(S+1) - J(J+1)}{4J(J+1)}\right] \\ &\quad \times [F(F+1) - I(I+1) - J(J+1)]. \end{aligned} \tag{7.7}$$

This equation was derived for a $^7\Sigma^+$ state but it is also correct for a $^9\Sigma^-$ state.

It is clear that the hyperfine energies depend on which spin component they belong to (for simplicity we will denote $N+S$ (where S=4) electron spin components as F_1, $N+S-1$ as F_2,...$N-S$ as F_9). Nevertheless in order to make J-assignments of the lines we will temporarily neglect this dependence. For that matter one can imagine that we are dealing with atomic rather than molecular lines and use the energy expression for atomic nuclear magnetic interaction

$$W_F = \frac{1}{2} A_F [F(F+1) - I(I+1) - J(J+1)], \tag{7.8}$$

and in our case A_F is proportional to the b_F value (as it follows from comparison of Eq. (7.7) and (7.8)).

The difference between two adjacent hyperfine levels (and hence the difference between adjacent hyperfine lines in the spectrum) will therefore be

$$\Delta W_F = A_F(F+1) \tag{7.9}$$

as long as the dominant hyperfine parameter is b''_F. Eq. (7.9) implies that one can take the differences between adjacent hyperfine lines in each transition and assign different F values to them until the plot ΔW_F vs $F+1$ yields a straight line going through the origin with a slope equal to A_F. This way the J'' and F''-assignments can be made. Figure 7.7 shows such a plot for both isotopologues of EuH using one of the lines observed at $\sim$17108 cm^{-1} as an example.

The ratio between extracted from the two slopes A_F values has to correspond roughly to the expected ratio of 2.265. The lines that we were able to assign in this way are listed in Table 7.3. The first column of this table corresponds to the range in which the lines are observed, then A_F values for both isotopologues are followed by their ratio and tentative J-assignment based on the method described above. As can be seen from the table, some of the lines do not have the same J-assignment for the two isotopologues. These deviations may be caused by electric quadrupole interactions or (and) hyperfine perturbations.

If one takes the electric quadrupole interaction into account Eq. (7.4) changes to

$$H_{hfs} = b_F \mathbf{I} \cdot \mathbf{S} + c(I_z S_z - \frac{1}{3} \mathbf{I} \cdot \mathbf{S}) + \frac{e^2 Qq(3I_z^2 - I(I+1))}{4I(2I-1)}, \tag{7.10}$$

in which

$$e^2 Qq = -\frac{e^2 Q}{hc} \sum_i \langle (3cos^2\theta_i - 1) r_i^{-3} \rangle. \tag{7.11}$$

Table 7.3: The assigned lines, and some parameters associated with them. See text for details.

Region	A_F^{151}	A_F^{153}	$\frac{A_F^{151}}{A_F^{153}}$	J^{151}	J^{153}	ΔW^{151}	ΔW^{153}	$\frac{\Delta W^{151}}{\Delta W^{153}}$
16983.1-16982.7	0.0072	0.0071		10	4	0.3808	0.1606	2.37
16983.3-16983.8	0.0095	0.0088		9	4	0.4489	0.1973	2.27
16986.03-16986.3	0.0051	0.0044		10	5	0.2708	0.1201	2.25
17012.6-17013.33	0.0185	0.0081	2.28	5	5	0.5032	0.2246	2.24
17037.89-17038.3	0.0078	0.0073		9	4	0.3698	0.1657	2.23
17052.1-17052.6	0.0263	0.0118	2.23	3	3	0.4524	0.2026	2.23
17062.4-17062.93	0.0212	0.0093	2.28	4	4	0.4787	0.2142	2.25
17067.29-17067.75	0.0164	0.0074	2.22	5	5	0.4537	0.1998	2.27
17071.15-17071.59	0.0265	0.0108	2.45	3	3	0.4362	0.1875	2.32
17072.0-17072.83	0.0106	0.0049	2.16	7	7	0.4020	0.1808	2.22
17083.4-17083.73	0.0074	0.0078		8	3	0.3174	0.1387	2.28
17084.0-17084.6	0.0216	0.0096	2.25	4	4	0.4857	0.2146	2.26
17108.45-17108.91	0.0167	0.0078	2.14	4	4	0.4522	0.2061	2.19
17108.61-17109.1	0.0168	0.0078	2.15	5	5	0.4620	0.2067	2.23

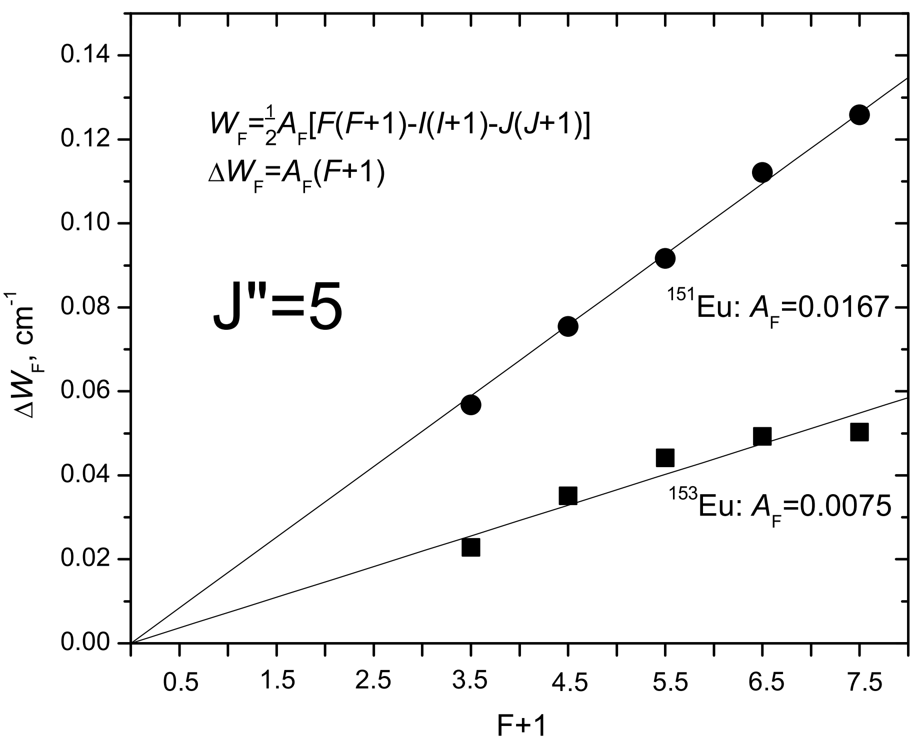

Figure 7.7: An example of the graphical method for making the J'' assignments in the observed transitions. See text for details.

In Eq. (7.11) q is the gradient of the electric field acting at the nucleus that is trying to orient the nucleus. Unlike magnetic hyperfine interactions which arise only from the unpaired electrons, the electric quadrupole interaction arises from *all* valence electrons. Therefore the contribution of the quadrupole interaction from the excited electronic state should be bigger than that in the more spherical ground state. Electric quadrupole hyperfine structure is definitely not negligible in our spectrum since for some of the lines the deviation from the Landé pattern is clearly larger in ^{153}Eu lines which is consistent with the fact that the ^{153}Eu nucleus has a larger quadrupole moment (see Table 7.2).

The effect of hyperfine perturbations is also easily observable in our spectrum. These perturbations occur due to the fact that at low N values the fine structure splitting between spin components of each N in the ground $^9\Sigma^-$ state is comparable to the size of the hyperfine splitting. That implies that for the same N level the hyperfine levels with the same F value but from different spin components could be located close to each other and cause perturbations. The selection rule for these perturbations is ΔF=0. The $F = J + I$ hyperfine level of each spin component can be perturbed only from above since no levels with the same F value exist in the spin components that lie lower in energy. The analogous hyperfine perturbations were observed in the $X^7\Sigma^-$ state of MnH by Varberg *et al.* [39].

Table 7.4: Overall widths of magnetic hyperfine energy multiplets of $^9\Sigma^-$ state for Hund's case ($b_{\beta J}$) coupling. See text for details.

$$\Delta W(F_1) = \frac{4Ib_F(2N+9)}{(N+4)}$$

$$\Delta W(F_2) = \frac{Ib_F(3N+16)(2N+7)}{(N+4)(N+3)}$$

$$\Delta W(F_3) = \frac{Ib_F(2N+13)(2N+5)}{(N+2)(N+3)}$$

$$\Delta W(F_4) = \frac{Ib_F(N+11)(2N+3)}{(N+1)(N+2)}$$

$$\Delta W(F_5) = \frac{10Ib_F(2N+1)}{N(N+1)}$$

$$\Delta W(F_6) = -\frac{Ib_F(N-10)(2N-1)}{N(N-1)}$$

$$\Delta W(F_7) = -\frac{Ib_F(2N-11)(2N-3)}{(N-1)(N-2)}$$

$$\Delta W(F_8) = -\frac{Ib_F(3N-13)(2N-5)}{(N-3)(N-2)}$$

$$\Delta W(F_9) = -\frac{4Ib_F(2N-7)}{(N-3)}$$

The overall width ΔW of the hyperfine multiplet due to the europium Fermi contact interaction is defined as the energy difference between the $F = J + I$ and $F = J - I$ levels and depends on the spin component. The overall hyperfine widths for all nine spin components were derived using Eq. (7.7) and are listed in Table 7.4. The negative signs in front of the expressions for the widths of F_6 to F_9 spin components indicates that after the N value exceeds a certain number the hyperfine pattern is reversed. For the F_6 component it will happen at $N > 10$, for the F_7 at $N > 5$, for the F_8 at $N > 4$ and for the F_9 at $N > 3$. Considering that in our spectrum we are populating only $N = 0$ to 6 rotational levels, theoretically we should expect to see inverted patterns only for the F_7, F_8 and F_9 spin components. However, we were unable to find any inverted patterns in the scanned spectral ranges.

The widths of the hyperfine multiplets for both isotopologues and their ratios for every assigned line are also listed in Table 7.3. Since the ratios between widths in almost all cases are close to the expected values, it was decided to attempt to get a rough estimate of the b_F values. For that purpose we took the lines that seemed to be least perturbed and had consistent J assignments based on the graphical method described above for both isotopologues, and applied to them all equations from Table 7.4 changing values of N so all spin components will yield consistent J values. For example if the line at $\sim$17084 cm^{-1} is assigned to have $J'' = 4$ then the F_1 component would have $N = 0$, F_2 would have $N = 1$,...,F_9 would have $N = 5$. Then we calculate b_F values using equations from the Table 7.4 for all lines and after that look for a number that would be roughly the same for every line. The average of these roughly matching numbers was taken as a b_F value. This procedure also provides N'' and more reliable J'' and F'' assignments of the observed lines, which are given in Table 7.5 together with approximate J' values. For some of the lines, the results are ambiguous and their assignments are not listed.

As one can see from Table 7.5 both transitions at 17 108 cm^{-1} terminate at the N''=1 rotational level of the ground state but at two different spin components (F_1, $J = 5$ and F_2, $J = 4$). Both of these transitions are most probably from the same upper state J'-level and the lines appear close to each other because of the small magnitude of the spin-spin interaction constant λ in the ground electronic state. The upper state J value could be 4 or 5 but since we do not observe a transition to the $N'' = 1$, $J'' = 3$ level around 17108 cm^{-1}, J' is most certainly equal to 5. This information is sufficient to determine the values for the Fermi contact interaction (b_F) and spin-spin interaction (λ) parameters. A fit was performed using the SPFIT program [35] with the hyperfine parameters of the upper state assumed to be negligible. However, one has to keep in mind that despite the fact that $b''_F \gg b'_F$, the magnetic dipolar and electric quadrupole interactions in the upper state could be significant. Nevertheless all 12 lines for both isotopologues fit very well with the quadrupole interaction neglected in both states. From this fit we found that for ^{151}EuH $\lambda'' = 0.0224(21)$ cm^{-1} and $b''_F = 0.020930(190)$ cm^{-1}, whilst for ^{153}EuH $\lambda'' = 0.0232(21)$ cm^{-1} and $b''_F = 0.009477(191)$ cm^{-1}. The ratio between b''_F values for 2 isotopologues is 2.21 which is a little different from the expected ratio of 2.265. This deviation may be due to the fact that we neglected the quadrupole interaction parameters in our fit (particularly for ^{153}EuH, which is consistent with the fact that ^{153}Eu has a larger Q value in Table 7.2). The λ'' values for ^{151}EuH and ^{153}EuH are the same within the estimated uncertainty as expected because this parameter does not depend on the reduced mass. Other lines from Table 7.5 were fitted separately and these fits yield the same (within calculated uncertainty) b''_F values as from the fit of lines at 17 108 cm^{-1}. Unfortunately a global fit of all lines in Table 7.5 was not possible since it was difficult to make an unambiguous assignment of the upper state quantum numbers for these transitions based on the available information, and the difficulty in fitting Hund's case (a)–case (b) transitions with the SPFIT program.

Table 7.5: Assignment of some of the transitions observed in the high-resolution LIF scans. The values of J' for some of the lines are not clear but the most probable assignment is given in bold font.

J'	F'	N''	J''	F''	Wavenumber (^{151}Eu)	Wavenumber (^{153}Eu)
5	7.5	1	4	6.5	17108.4563	17108.4912
5	6.5	1	4	5.5	17108.5875	17108.5415
5	5.5	1	4	4.5	17108.6979	17108.5908
5	4.5	1	4	3.5	17108.7862	17108.6394
5	3.5	1	4	2.5	17108.8590	17108.6701
5	2.5	1	4	1.5	17108.9085	17108.6979
5	7.5	1	5	7.5	17108.6121	17108.6529
5	6.5	1	5	6.5	17108.7379	17108.7118
5	5.5	1	5	5.5	17108.8501	17108.7608
5	4.5	1	5	4.5	17108.9418	17108.7992
5	3.5	1	5	3.5	17109.0172	17108.8319
5	2.5	1	5	2.5	17109.0740	17108.8590
3, **4** or 5	-	0	4	6.5	17084.0731	17084.0932
3, **4** or 5	-	0	4	5.5	17084.2118	17084.1561
3, **4** or 5	-	0	4	4.5	17084.3320	17084.2117

Table 7.5: Assignment of some of the transitions observed in the high-resolution LIF scans. The values of J' for some of the lines are not clear but the most probable assignment is given in bold font.

J'	F'	N''	J''	F''	Wavenumber (^{151}Eu)	Wavenumber (^{153}Eu)
3, **4** or 5	-	0	4	3.5	17084.4297	17084.2509
3, **4** or 5	-	0	4	2.5	17084.5045	17084.2861
3, **4** or 5	-	0	4	1.5	17084.5588	17084.3078
3, **4** or 5	-	1	4	6.5	17067.2922	17067.3341
3, **4** or 5	-	1	4	5.5	17067.4162	17067.3950
3, **4** or 5	-	1	4	4.5	17067.5224	17067.4433
3, **4** or 5	-	1	4	3.5	17067.6108	17067.4814
3, **4** or 5	-	1	4	2.5	17067.6832	17067.5116
3, **4** or 5	-	1	4	1.5	17067.7459	17067.5339
3, 4 or 5	-	0	4	6.5	17062.4600	17062.5071
3, 4 or 5	-	0	4	5.5	17062.5967	17062.5613
3, 4 or 5	-	0	4	4.5	17062.7112	17062.6144
3, 4 or 5	-	0	4	3.5	17062.8079	17062.6596
3, 4 or 5	-	0	4	2.5	17062.8838	17062.6941
3, 4 or 5	-	0	4	1.5	17062.9387	17062.7213
3 or **4**	-	1	3	5.5	17052.0923	17052.1289
3 or **4**	-	1	3	4.5	17052.2384	17052.1978
3 or **4**	-	1	3	3.5	17052.3580	17052.2526
3 or **4**	-	1	3	2.5	17052.4531	17052.2866
3 or **4**	-	1	3	1.5	17052.5150	17052.3140
3 or **4**	-	1	3	0.5	17052.5447	17052.3314
3 or **4**	-	2	3	5.5	17037.8903	17037.9108
3 or **4**	-	2	3	4.5	17037.9764	17037.9592
3 or **4**	-	2	3	3.5	17038.0568	17037.9969
3 or **4**	-	2	3	2.5	17038.1339	17038.0322
3 or **4**	-	2	3	1.5	17038.2027	17038.0568
3 or **4**	-	2	3	0.5	17038.2601	17038.0765
3 or 4	-	1	4	6.5	16983.3335	16983.3704
3 or 4	-	1	4	5.5	16983.4452	16983.4303
3 or 4	-	1	4	4.5	16983.5453	16983.4777
3 or 4	-	1	4	3.5	16983.6320	16983.5159
3 or 4	-	1	4	2.5	16983.7112	16983.5453

Table 7.5: Assignment of some of the transitions observed in the high-resolution LIF scans. The values of J' for some of the lines are not clear but the most probable assignment is given in bold font.

J'	F'	N''	J''	F''	Wavenumber (^{151}Eu)	Wavenumber (^{153}Eu)
3 or 4	-	1	4	1.5	16983.7824	16983.5677
3 or 4	-	2	3	5.5	16982.7053	16982.7334
3 or 4	-	2	3	4.5	16982.7929	16982.7786
3 or 4	-	2	3	3.5	16982.8774	16982.8179
3 or 4	-	2	3	2.5	16982.9512	16982.8487
3 or 4	-	2	3	1.5	16983.0212	16982.8740
3 or 4	-	2	3	0.5	16983.0861	16982.8989

It is interesting to compare the molecular Fermi contact interaction parameters to those of the free Eu^+ ion. The values for both isotopes are taken from Ref. [41] where for the $^{151}Eu^+$ ion the coupling constant for the magnetic-dipole interaction (A) was found to be 0.0514 cm^{-1} and for the $^{153}Eu^+$ ion it was found to be 0.0228 cm^{-1}. The value of A is a sum of the isotropic constant $A_{\rm iso}$ (which is analogous to molecular b_F) and the dipolar hyperfine interaction $A_{\rm dip}$ [42]. The $A_{\rm dip}$ value is expected to be very small for the ground configuration of Eu^+ and one can assume that $A \approx A_{\rm iso}$. Therefore the ratio between molecular and ionic Fermi contact interaction parameters is 0.41 for both isotopologues or in other words the ground state configuration has 41% 6s character, which is reasonable considering that the electric field of the H^- ion in the molecule polarizes the Eu^+ ion.

One can speculate about the values of the B rotational constant based on the available information. As can be seen from the Table 7.5 there are lines at 17 108 and 16 983 cm^{-1} that have common lower state level ($N'' = 1$, $J'' = 4$). If one assumes that the upper state levels of these transitions are $J' = 5$ and $J' = 3$ of the same Ω-component then the B' value can be estimated to be ∼6.94 cm^{-1}. Based on that value we can predict that the $J' = 4$ to $N'' = 1$, $J'' = 4$ transition will be at ∼17 038.5 cm^{-1} and there are indeed a number of lines in that area, but they are in a congested region, making their assignment difficult.

Finally a low resolution dispersed-fluorescence experiment enabled us to determine the vibrational spacing between the υ''=0 and υ''=1 levels in the ground state as 1 145(±5) cm^{-1}.

7.4 Conclusions and future work

We have recorded FT and LIF spectra of the EuH molecule. In the FT spectrum we have observed many transitions in the $10\,000 - 18\,000$ cm^{-1} region. The lack of any information about the electronic states of EuH together with the perturbations, band overlaps and other difficulties in the spectrum make the assignment difficult. The "cold" spectrum of EuH recorded in the laser ablation/molecular beam setup showed that in the FT spectrum only the transition at $\sim$17 000 cm^{-1} terminates at the ground $X\ ^9\Sigma^-$ electronic state. Unfortunately we were unable to perform a continuous high resolution scan of this band because it spreads over a $\sim$100 cm^{-1} region, and the condition of the Eu rod did not allow coverage of such a wide region. Instead we have recorded only the most intense features at high resolution. This enabled us to extract some information about the spectroscopic parameters of the ground and excited states in this transition, but still more information is required to obtain a full analysis. Therefore it is necessary to record a high resolution LIF spectrum of this band: however, the price of Eu metal is very high and it is important to have more information about the electronic states involved. In other words, reliable *ab initio* calculations are needed before experiments on the EuH molecule can be resumed.

Bibliography

[1] P. Vaida and J. N. Daou, Phys. Rev. B **49**, 3275 (1994).

[2] W. Bauhofer, W. Joss, R. K. Kremer, H. J. Mattausch, and A. Simon, J. Magn. Mater. **104**, 1243 (1992).

[3] C. Rao and J. Gopalkrishnan, *New Directions in Solid State Chemistry*, CUP, London, 3rd edition, 1986.

[4] L. Hagland, I. Kopp, and N. Åslund, Arkiv för Fysik **32**, 321 (1966).

[5] I. Kopp, L. Hagland, and B. Rydh, Can. J. Phys. **53**, 2242 (1975).

[6] A. Bahmaier, R.-D. Urban, and H. Jones, Chem. Phys. Lett. **195**, 609 (1992).

[7] C. Effantin and J. D'Incan, Can. J. Phys. **51**, 1394 (1973).

[8] J. D'Incan, C. Effantin, and R. Bacis, Can. J. Phys. **50**, 1810 (1972).

[9] C. Effantin and J. D'Incan, Can. J. Phys. **52**, 523 (1974).

[10] J. D'Incan, C. Effantin, and R. Bacis, Can. J. Phys. **55**, 1654 (1977).

[11] J. D'Incan, C. Effantin, and R. Bacis, J. Phys. B **5**, L187 (1972).

[12] S. P. Willson and L. Andrews, J. Chem. Phys. **104**, 1640 (2000).

[13] P. Pyykkö, Physica Scripta **20**, 647 (1979).

[14] M. Dolg and H. Stoll, Theor. Chem. Acta **75**, 369 (1989).

[15] M. Dolg, H. Stoll, and H. Preuss, Chem. Phys. **165**, 321 (1992).

[16] M. Dolg and H. Stoll, *Electronic Structure Calculations for Molecules Containing Lanthanide Atoms*, volume 22, Elsevier, Amsterdam.

[17] X. Cao, W. Liu, and M. Dolg, Science in China (Series B) **31**, 6 (2001).

[18] Y. N. Dmitriev et al., Acta Physics Hungarica **61**, 51 (1987).

[19] P. Carrette, A. Hocquet, M. Douay, and B. Pinchemel, J. Mol. Spectrosc. **124**, 243 (1987).

[20] L. A. Kaledin, M. Erickson, and M. C. Heaven, J. Mol. Spectrosc. **165**, 323 (1994).

[21] A. L. Kaledin, M. C. Heaven, R. W. Field, and L. A. Kaledin, J. Mol. Spectrosc. **179**, 310 (1996).

[22] T. Yang and R. Pitzer, private communication.

[23] A. Shayesteh, D. Appadoo, I. Gordon, R. LeRoy, and P. Bernath, J. Chem. Phys. **120**, 10002 (2004).

[24] A. Shayesteh, K. Walker, I. Gordon, D. Appadoo, and P. Bernath, J. Mol. Struct. **695**, 23 (2004).

[25] I. E. Gordon, A. Shayesteh, D. Appadoo, K. Walker, and P. Bernath, J. Mol. Spectrosc. **229**, 269 (2005).

[26] B. Elden, Metrologia **2**, 71.

[27] W. Whaling, W. Anderson, M. Carle, J. Brault, and H. Zarem, J. Res. Natl. Inst. Stand. Technol. **107**, 149.

[28] S. Gerstenkorn and P. Luc, *Atlas du spectre d'absorption de la molécule de d'iode*, Editions du C. N. R. S., Paris, 1978.

[29] S. Gerstenkorn, P. Luc, and R. Vetter, Rev. Phys. Appl. **16**, 529 (1981).

[30] E. Wigner and E. E. Witmer, Z. Physik **51**, 859 (1928).

[31] H. Lefebvre-Brion and R. W. Field, *Perturbations in the Spectra of Diatomic Molecules*, Academic Press, New York, 1986.

[32] T. Varberg, J. A. Gray, R. Field, and A. Merer, J. Mol. Spectrosc. **156**, 296 (1992).

[33] M. J. Dick, J.-G. Wang, J. Tang, and P. F. Bernath, Laser spectroscopy of europium monoflouride, in *59th Ohio State University International Symposium on Molecular Spectroscopy*, page TB04, Columbus, Ohio, 2004.

[34] T. C. Steimle, J. Gengler, and J. Chen, Can. J. Chem. **82**, 779 (2004).

[35] H. M. Pickett, J. Mol. Spectrosc. **148**, 371 (1991).

[36] I. Mills, T. Cvitaš, K. Homann, N. Kallay, and K. Kuchitsu, *Quantities, Units and Symbols in Physical Chemistry*, Blackwell Science, Oxford, 2nd edition, 1993.

[37] C. H. Townes and A. L. Schawlow, *Microwave Spectroscopy*, Dover, New York, 1975.

[38] T. M. Dunn, Nuclear hyperfine structure in the electronic spectra of diatomic molecules, in *Molecular Spectroscopy- Modern Research*, edited by K. N. Rao and C. W. Mathews, pages 231–257, Academic Press, New York, 1978.

[39] T. Varberg, R. Field, and A. Merer, J. Chem. Phys. **95**, 1563 (1991).

[40] C. Ryzlewicz, H.-U. Schutze-Pahlmann, J. Hoeft, and T. Torring, Chem. Phys. **71**, 389 (1982).

[41] O. Becker, K. Enders, G. Werth, and J. Dembczynski, Phys. Rev. A **48**, 3546 (1993).

[42] W. Weltner, *Magnetic atoms and molecules*, Van Nostrand Reinhold, New York, 1983.

Chapter 8

First observations of the gas-phase spectra of SmH, SmCl, TmH and ErF

8.1 Samarium monohydride

The gas phase SmH molecule was generated in the high temperature furnace/electrical discharge emission source described in section 3.2.2. The inside of the alumina tube was wrapped with molybdenum foil to prevent the reaction between the metal and ceramic. The tube furnace was heated to 950°C and a mixture of Ar (∼5 Torr) and H_2 (or D_2 for SmD) (∼2 Torr) gases flowed slowly over the metal. The melting point of samarium metal is 1072°C so during our experiment the metal was in the solid phase. The surface of samarium metal was absorbing hydrogen just as in experiments with europium metal (see Chapter 7). An electrical discharge (3 kV, 333 mA) was applied between two cylindrical stainless steel electrodes inside the ends of the tube. Emission from the tube was focused onto the entrance aperture of a Bruker IFS HR 120 Fourier transform spectrometer. The windows at the ends of the tube and the lens were made from BaF_2. The SmH emission spectrum was recorded in the 8 000-15 800 cm^{-1} region using a silicon photodiode detector, CaF_2 beamsplitter and 640 nm red-pass filter. The molecular emission was observed in the 11 000 cm^{-1} region (see Fig 8.1). The observed bandheads are at 10575.03 cm^{-1} (red degraded), 10620.11 cm^{-1} (red degraded) and 10700.42 cm^{-1} (blue degraded). A total of 180 scans for both molecules were co-added at a resolution of 0.04 cm^{-1} in order to obtain a good signal-to-noise ratio. The observed lines (or at least the strongest lines) appear to belong to two different bands (further referred to as the red system and the blue system). Line positions were measured using a Windows-based program called WSpectra, written by M. Carleer (Université Libre de Bruxelles). The spectrometer was not under vacuum and the "air-to-vacuum" wavenumber correction [1] had to be made before the lines were calibrated against argon atomic lines present in the spectrum [2].

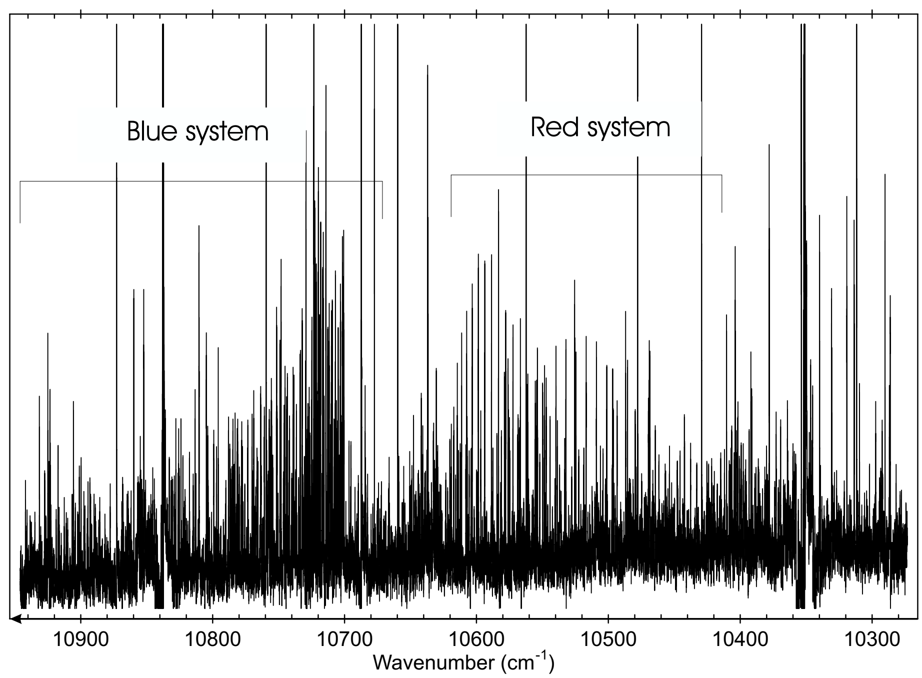

Figure 8.1: An overview of the SmH electronic transitions.

In order to analyze the recorded spectrum of SmH it is necessary to consider what electronic states may be involved in the observed transitions. The ground state configuration of the Sm^+ ion is $4f^66s^1$ [3]. The lowest lying state of this configuration is an ^{8}F [4], where spins of all seven unpaired electrons are parallel. This ionic state gives rise to $^8\Phi$, $^8\Delta$, $^8\Pi$ and $^8\Sigma^+$ molecular electronic states. When the spin of s electron flips (^{6}F state) the resultant molecular states will be $^6\Phi$, $^6\Delta$, $^6\Pi$ and $^6\Sigma^+$. It is hard to determine the relative positions of these states and it is convenient to consider separate Ω-components in the frame of ligand field theory (LFT). As it was mentioned earlier ligand field theory does not apply very well to lanthanide hydrides because hydrogen can not be considered as a point charge, nevertheless LFT can provide qualitative information about the low-lying states of SmH. The ^{8}F term has $^8\mathrm{F}_{1/2}$, $^8\mathrm{F}_{3/2}$, $^8\mathrm{F}_{5/2}$, $^8\mathrm{F}_{7/2}$, $^8\mathrm{F}_{9/2}$, $^8\mathrm{F}_{11/2}$ and $^8\mathrm{F}_{13/2}$ J-components, with the $^8F_{1/2}$ state being lowest in energy because the f shell is less than half-filled. Each of these states is split into several doubly degenerate Ω-components by the presence of the negatively charged ligand (hydrogen anion), for example, the $^8F_{13/2}$ state is split into Ω-components with $\Omega = 1/2, 3/2, 5/2, 7/2, 9/2, 11/2$ and $13/2$. In total there will be 28 degenerate states arising from the ionic ^8F state with one of the $\Omega = 1/2$ states being the ground state. The first excited configuration of Sm^+ is $4f^56s^2$ with the ^6H term being the lowest arising from this configuration. This state has six J-components with $^6H_{5/2}$ lying lowest in energy. The ligand field splits $^6H_{5/2}$ into $\Omega = 1/2, 3/2$ and $5/2$ components. Kaledin *et al.* [3] calculated that for the SmF molecule the lowest $\Omega = 1/2$ state is located 9800 cm^{-1} above the ground state, which is close to the region where we observe SmH bands. Ren *et al.* [5] calculated the ligand field splittings of the ^6H state for SmF using density functional theory.

The red system appears to have strong R and Q branches, but we were unable to find the P branch because of the great congestion of lines. This intensity pattern points to a $\Delta\Omega = +1$ transition and the excited state could be an $\Omega = 3/2$ state, arising from the $4f^56s^2$ configuration, and the transition could connect to the ground $\Omega = 1/2$ state. The blue system has only an obvious strong P branch with a head, this transition may be from the $\Omega' = 1/2$ state, arising from the $4f^56s^2$ configuration to the first $\Omega'' = 3/2$ state arising from the ground $4f^66s^1$ configuration. Unfortunately we were not able to perform rotational assignment of these bands due to their relatively poor signal to noise ratio.

8.2 Samarium monochloride

The spectrum of SmCl was recorded in the same experimental setup as SmH, but using CH_3Cl gas instead of H_2. The observed bands are so dense that even at an instrumental resolution of 0.04 cm^{-1} the rotational structure was not resolved. In addition the signal to noise ratio of these bands is poor. The bandhead positions are 11 129.6 cm^{-1}, 11 512.7 cm^{-1}, 11 688.0 cm^{-1} and 11710.9 cm^{-1}. The observed bandheads (see Figure 8.2) are in reasonable agreement with the prediction from Ref. [3] for SmCl that an $\Omega' = 1/2$ state of the $4f^56s^2$ configuration lies 12 200 cm^{-1} above the ground state.

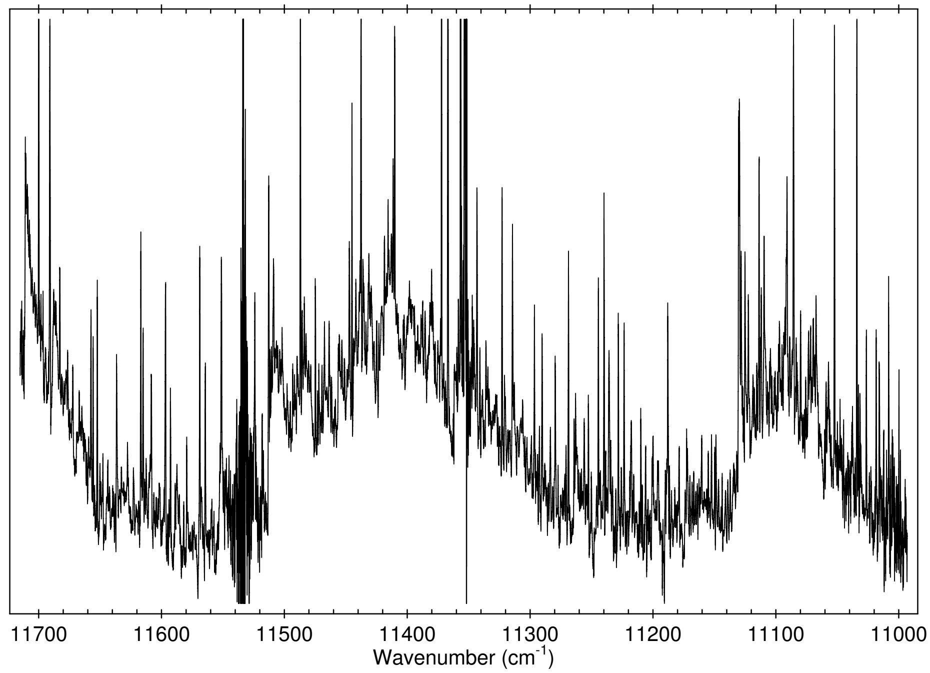

Figure 8.2: Observed bands of SmCl. The bands in this figure are actually recorded at 0.2 cm^{-1} resolution as the bands can be seen more clearly at lower resolution.

8.3 Thulium monohydride

About 20 g of thulium metal was heated in the King furnace (carbon tube furnace), described in the section 3.2.3, to a temperature of ∼2 000°C with a mixture of hydrogen (or deuterium) and helium gases flowing slowly through the system. The inside of the carbon sample holder was wrapped with tantalum and tungsten foils. The total pressure inside the furnace was kept at ∼120 Torr. A BaF_2 lens was employed to image emission from the King furnace onto the entrance aperture of a Bruker IFS 120 HR Fourier transform spectrometer. The TmH emission spectrum was recorded in the $8\,000 - 15\,800$ cm^{-1} region using a silicon photodiode detector, CaF_2 beamsplitter and 640 nm red-pass filter. The TmH bands were found at $14\,000 - 15\,000$ cm^{-1} region (see Figure 8.3). The bands are very weak and have a complicated structure leading to failure of the rotational assignment. Nevertheless one can speculate about the electronic states involved in this spectrum.

In his Dirac-Fock one-center expansion calculations Pyykkö [6] assumed that the ground state electron configuration of TmH is $4f^{14}[(6s + 6p + 6d)\sigma]^2$, but he

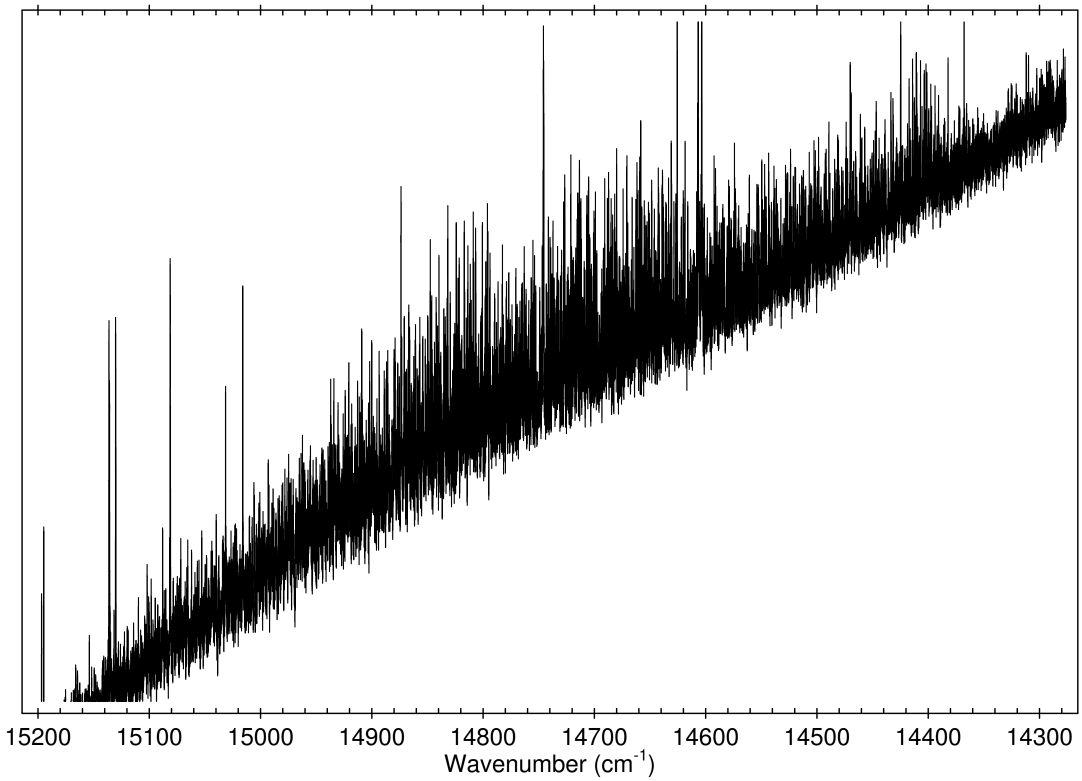

Figure 8.3: TmH electronic transition observed in emission from the King furnace.

admitted that it may not be a realistic choice. The ground configuration of the Er^+ ion is $4f^{12}6s^2$ [3] with the lowest electronic state being $^3H_6$. This $^3H_6$ state is split by the ligand field into 7 spin components with $\Omega = 0^+$ component being the ground state of the TmH. The excited state of the observed transition is probably arising from the $4f^{12}6s^16p^1$ configuration. LFT calculations [3] place the first $\Omega = 0$ component of this configuration for TmF at 16 800 cm^{-1} .

8.4 Erbium monofluoride

The spectrum of ErF was generated in the King furnace (carbon tube furnace) described in the section 3.2.3. The erbium metal sample (about 40 g) was heated in the furnace to a temperature of ~2 200°C with a mixture of SF_6 and helium gases flowing slowly through the system. The inside of the carbon sample holder was wrapped with tantalum and tungsten foils. The total pressure was maintained at ∼150 Torr. Emission from the tube was imaged onto the entrance aperture of a Bruker IFS 120 HR Fourier transform spectrometer. The windows that sealed the furnace and the lens were made from BaF_2. First a survey scan was performed in the visible and the near infrared parts of the spectrum. We have found two ErF bands near 17 500 cm^{-1}. A 550 nm band pass filter was then used to eliminate the contribution of strong black body radiation in order to improve the signal to noise ratio of the molecular lines. One difficulty arose during the experiment in that the emission and absorption lines were "competing" in the spectrum and it was hard to optimize either one. The emission spectrum of ErF is shown in Fig. 8.4. Ten scans were recorded at 0.2 cm^{-1} resolution. Unfortunately at the moment when a higher resolution scan was planned to start, the furnace carbon heating element was permanently damaged by the Er metal, which also destroyed the foils and carbon holder. After that experience we abandoned the experiments with rare earth metals in the King furnace as they proved to be expensive and dangerous.

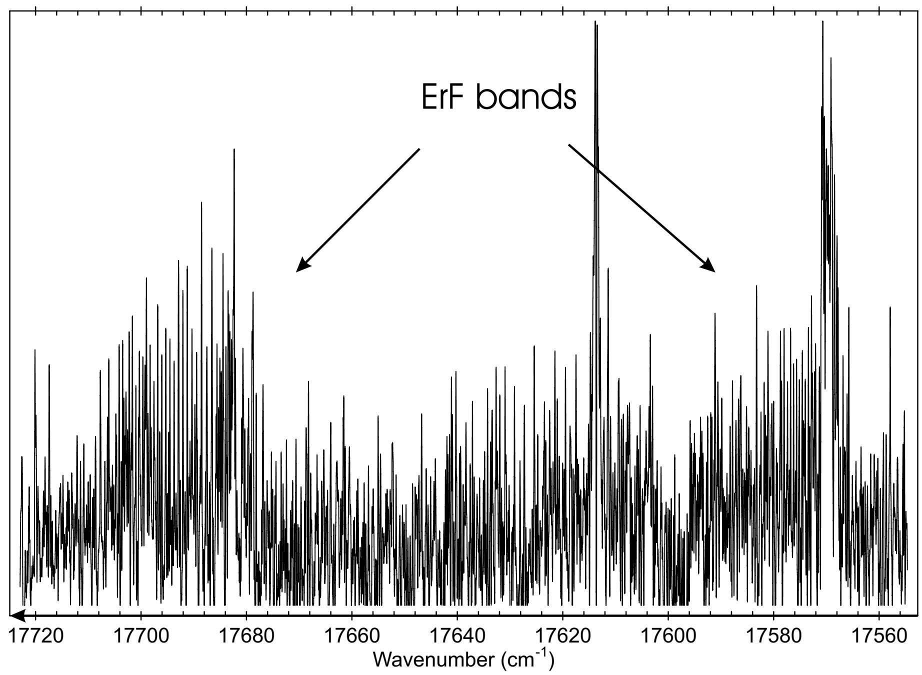

Figure 8.4: ErF electronic transitions.

The two bands of ErF in Fig. 8.4 are therefore recorded at low resolution and poor signal to noise ratio. The bandhead positions are 17 567.8 cm^{-1} and 17 682.3

cm^{-1} . Although a rotational analysis is not possible in these circumstances some conclusions can be made about the nature of the observed transitions. The ground configuration of the Er^+ ion is $4f^{11}6s^2$ [3] with the lowest electronic state being $^4I_{15/2}$. The ligand field splits this state into 8 components with Ω=1/2 to Ω=15/2. The Ω=1/2 component of this state is the ground state of ErF. It is worth noting that in the theoretical work of Lesar *et al.* [7] the authors calculate spectroscopic parameters for erbium and thulium fluorides. They give the ground state of ErF as a $^1\Sigma_g$ state (Table 1 of Ref. [7]), which is probably a typographical error. Kaledin *et al.* [3] predict the Ω=1/2 state of the excited $4f^{11}6s^16p^1$ configuration to be at 16 700 cm^{-1} above the ground electronic state. We observe transitions at 17 550 – 17 720 cm^{-1} region, which is close to that prediction.

As it was mentioned above it is hazardous to resume experiments with ErF in the King furnace, but the observed spectrum can be revisited using the molecular beam apparatus as we did for the EuH molecule at Arizona State University (see Chapter 7). The metal fluorides usually yield stronger signals in laser ablation experiments than hydrides and the probability of a successful experiment is high.

8.5 Conclusions

The emission spectra presented in this chapter represent preliminary observations of transitions of SmH, SmCl, TmH and ErF. These spectra can serve as guides to more detailed spectroscopic studies of these molecules. For example, our spectrum of ErF can be used to plan molecular beam experiments using laser-induced fluorescence detection.

In this thesis spectra of different metal-containing diatomic molecules were studied. Analysis of new high resolution infrared emission spectra of MnH and MnD recorded with a Fourier transform spectrometer have extended earlier data and have given improved spectroscopic constants. Analysis of the electronic emission spectra of CoH and CoD have provided significantly improved spectroscopic constants for the ground and excited electronic states. In addition, a new electronic state of CoD ([13.3]4) has been found in these experiments. Three new near-infrared transitions of YbO are reported in this work, and their rotational analyses were carried out. Extensive work on the EuH molecule has given some insights concerning the electronic structure. Although some spectroscopic parameters were estimated for EuH, there is considerable scope for further work.

Bibliography

[1] B. Elden, Metrologia **2**, 71.

[2] W. Whaling, W. Anderson, M. Carle, J. Brault, and H. Zarem, J. Res. Natl. Inst. Stand. Technol. **107**, 149.

[3] A. L. Kaledin, M. C. Heaven, R. W. Field, and L. A. Kaledin, J. Mol. Spectrosc. **179**, 310 (1996).

[4] W. C. Martin, R. Zalubas, and L. Hagan, *Atomic Energy Levels–The Rare Earth Elements*, US Government Printing Office, Washington, 1978.

[5] J. Ren, M.-H. Whangbo, D. Dai, and L. Li, J. Chem. Phys. **108**, 8479 (1998).

[6] P. Pyykkö, Physica Scripta **20**, 647 (1979).

[7] A. Lesar, G. Muri, and M. Hodoščček, J. Phys. Chem. **102**, 1170 (1998).

APPENDIX

Appendix A

Line lists for MnH and MnD

Line lists for MnH and MnD, together with uncertainties assigned to these lines, calculated lines and differences between calculated and observed wavenumbers. The calculated lines in these tables were obtained from the band constant fits.

A.1 Line list for MnH

Table A.1: Line list for MnH.

N'	v'	J'	N''	v''	J''	Observed	Calculated	Obs-Calc	Uncertainty
1	1	4	0	0	3	1501.6312	1501.6327	-0.0015	0.001
0	1	3	1	0	4	1479.3361	1479.3343	0.0019	0.001
2	1	4	1	0	3	1512.1517	1512.1569	-0.0052	1
2	1	5	1	0	4	1512.1843	1512.1826	0.0018	0.002
1	1	4	2	0	5	1467.8079	1467.8115	-0.0036	10
1	1	3	2	0	4	1467.8476	1467.8408	0.0068	10
1	1	2	2	0	3	1467.9142	1467.9151	-0.0009	0.001
3	1	2	2	0	1	1522.2613	1522.2696	-0.0082	10
3	1	3	2	0	2	1522.2956	1522.3021	-0.0064	10
3	1	4	2	0	3	1522.3343	1522.3376	-0.0033	10
3	1	5	2	0	4	1522.3718	1522.3717	0.0001	0.002
3	1	6	2	0	5	1522.3984	1522.3977	0.0007	0.002
2	1	5	3	0	6	1455.9748	1455.9773	-0.0025	0.005
2	1	4	3	0	5	1456.0077	1456.0091	-0.0014	0.005
2	1	3	3	0	4	1456.0550	1456.0511	0.0039	0.005

N'	v'	J'	N''	v''	J''	Observed	Calculated	Obs-Calc	Uncertainty
2	1	2	3	0	3	1456.0976	1456.0945	0.0031	0.005
2	1	1	3	0	2	1456.1311	1456.1337	-0.0026	0.001
4	1	1	3	0	0	1532.0992	1532.1023	-0.0031	0.005
4	1	2	3	0	1	1532.1235	1532.1275	-0.0040	0.005
4	1	3	3	0	2	1532.1509	1532.1548	-0.0039	0.005
4	1	4	3	0	3	1532.1812	1532.1840	-0.0028	0.005
4	1	5	3	0	4	1532.2148	1532.2141	0.0008	0.001
4	1	6	3	0	5	1532.2437	1532.2432	0.0005	0.001
4	1	7	3	0	6	1532.2691	1532.2688	0.0003	0.001
3	1	6	4	0	7	1443.8396	1443.8414	-0.0018	0.005
3	1	5	4	0	6	1443.8724	1443.8748	-0.0024	0.005
3	1	4	4	0	5	1443.9140	1443.9128	0.0012	0.005
3	1	3	4	0	4	1443.9524	1443.9517	0.0007	0.005
3	1	2	4	0	3	1443.9907	1443.9887	0.0020	0.005
3	1	1	4	0	2	1444.0246	1444.0222	0.0025	0.005
3	1	0	4	0	1	1444.0491	1444.0512	-0.0021	0.005
5	1	2	4	0	1	1541.6338	1541.6296	0.0042	0.001
5	1	3	4	0	2	1541.6512	1541.6551	-0.0039	0.001
5	1	4	4	0	3	1541.6799	1541.6816	-0.0017	0.001
5	1	5	4	0	4	1541.7085	1541.7088	-0.0003	0.001
5	1	6	4	0	5	1541.7374	1541.7364	0.0010	0.001
5	1	7	4	0	6	1541.7636	1541.7632	0.0004	0.001
5	1	8	4	0	7	1541.7877	1541.7881	-0.0004	0.001
4	1	7	5	0	8	1431.4102	1431.4117	-0.0015	0.005
4	1	6	5	0	7	1431.4447	1431.4462	-0.0015	0.005
4	1	5	5	0	6	1431.4830	1431.4833	-0.0003	0.005
4	1	4	5	0	5	1431.5211	1431.5211	0.0001	0.005
4	1	3	5	0	4	1431.5577	1431.5576	0.0001	0.005
4	1	2	5	0	3	1431.5936	1431.5920	0.0016	0.005
4	1	1	5	0	2	1431.6232	1431.6234	-0.0002	0.005
6	1	3	5	0	2	1550.7958	1550.7971	-0.0013	0.001
6	1	4	5	0	3	1550.8210	1550.8221	-0.0011	0.001
6	1	5	5	0	4	1550.8476	1550.8475	0.0001	0.001
6	1	6	5	0	5	1550.8744	1550.8732	0.0012	0.001
6	1	7	5	0	6	1550.9003	1550.8990	0.0013	0.001
6	1	8	5	0	7	1550.9245	1550.9242	0.0003	0.001
6	1	9	5	0	8	1550.9479	1550.9482	-0.0003	0.005
5	1	8	6	0	9	1418.6947	1418.6955	-0.0008	0.005

N'	v'	J'	N''	v''	J''	Observed	Calculated	Obs-Calc	Uncertainty
5	1	7	6	0	8	1418.7301	1418.7310	-0.0009	0.001
5	1	5	6	0	6	1418.8053	1418.8056	-0.0003	0.001
5	1	4	6	0	5	1418.8416	1418.8422	-0.0006	0.001
5	1	3	6	0	4	1418.8772	1418.8772	0.0000	0.001
5	1	2	6	0	3	1418.9103	1418.9100	0.0003	0.001
7	1	4	6	0	3	1559.5977	1559.5981	-0.0004	0.001
7	1	5	6	0	4	1559.6224	1559.6222	0.0002	0.001
7	1	6	6	0	5	1559.6473	1559.6465	0.0008	0.001
7	1	7	6	0	6	1559.6711	1559.6708	0.0003	0.001
7	1	8	6	0	7	1559.6978	1559.6951	0.0027	0.001
7	1	9	6	0	8	1559.7190	1559.7189	0.0001	0.001
7	1	10	6	0	9	1559.7411	1559.7418	-0.0007	0.001
6	1	9	7	0	10	1405.7000	1405.7003	-0.0003	0.002
6	1	8	7	0	9	1405.7361	1405.7366	-0.0005	0.002
6	1	7	7	0	8	1405.7739	1405.7740	-0.0001	0.002
6	1	6	7	0	7	1405.8114	1405.8115	-0.0001	0.002
6	1	5	7	0	6	1405.8473	1405.8484	-0.0011	0.002
6	1	4	7	0	5	1405.8831	1405.8840	-0.0009	0.002
6	1	3	7	0	4	1405.9178	1405.9178	0.0000	0.002
8	1	5	7	0	4	1568.0257	1568.0256	0.0001	0.001
8	1	6	7	0	5	1568.0489	1568.0487	0.0003	0.001
8	1	7	7	0	6	1568.0727	1568.0717	0.0010	0.001
8	1	8	7	0	7	1568.0957	1568.0947	0.0010	0.001
8	1	9	7	0	8	1568.1186	1568.1176	0.0011	0.001
8	1	10	7	0	9	1568.1399	1568.1400	-0.0001	0.001
8	1	11	7	0	10	1568.1609	1568.1618	-0.0009	0.001
7	1	10	8	0	11	1392.4333	1392.4333	0.0000	0.002
7	1	9	8	0	10	1392.4700	1392.4702	-0.0002	0.002
7	1	8	8	0	9	1392.5084	1392.5080	0.0004	0.002
7	1	7	8	0	8	1392.5459	1392.5458	0.0001	0.002
7	1	6	8	0	7	1392.5826	1392.5831	-0.0005	0.002
7	1	5	8	0	6	1392.6189	1392.6192	-0.0003	0.002
7	1	4	8	0	5	1392.6539	1392.6538	0.0001	0.002
9	1	6	8	0	5	1576.0732	1576.0726	0.0007	0.001
9	1	7	8	0	6	1576.0949	1576.0944	0.0005	0.001
9	1	8	8	0	7	1576.1171	1576.1162	0.0009	0.001
9	1	9	8	0	8	1576.1389	1576.1379	0.0011	0.001
9	1	10	8	0	9	1576.1600	1576.1593	0.0007	0.001

N'	v'	J'	N''	v''	J''	Observed	Calculated	Obs-Calc	Uncertainty
9	1	11	8	0	10	1576.1600	1576.1804	-0.0204	1
9	1	12	8	0	11	1576.1998	1576.2010	-0.0012	0.002
8	1	11	9	0	12	1378.9017	1378.9015	0.0002	0.002
8	1	10	9	0	11	1378.9392	1378.9392	0.0000	0.002
8	1	9	9	0	10	1378.9779	1378.9774	0.0005	0.002
8	1	8	9	0	9	1379.0157	1379.0155	0.0002	0.002
8	1	7	9	0	8	1379.0528	1379.0531	-0.0003	0.002
8	1	6	9	0	7	1379.0894	1379.0898	-0.0004	0.002
8	1	5	9	0	6	1379.1251	1379.1251	0.0000	0.002
10	1	7	9	0	6	1583.7323	1583.7319	0.0004	0.001
10	1	8	9	0	7	1583.7528	1583.7525	0.0003	0.001
10	1	9	9	0	8	1583.7735	1583.7729	0.0006	0.001
10	1	10	9	0	9	1583.7941	1583.7932	0.0009	0.001
10	1	11	9	0	10	1583.8138	1583.8132	0.0006	0.001
10	1	12	9	0	11	1583.8326	1583.8330	-0.0004	0.001
10	1	13	9	0	12	1583.8513	1583.8523	-0.0010	0.001
9	1	12	10	0	13	1365.1126	1365.1122	0.0005	0.002
9	1	11	10	0	12	1365.1508	1365.1504	0.0004	0.002
9	1	10	10	0	11	1365.1900	1365.1891	0.0009	0.002
9	1	9	10	0	10	1365.2283	1365.2276	0.0007	0.002
9	1	8	10	0	9	1365.2658	1365.2656	0.0002	0.002
9	1	7	10	0	8	1365.3025	1365.3027	-0.0002	0.002
9	1	6	10	0	7	1365.3387	1365.3387	0.0000	0.002
11	1	8	10	0	7	1590.9965	1590.9965	0.0000	0.001
11	1	9	10	0	8	1591.0158	1591.0158	0.0000	0.001
11	1	10	10	0	9	1591.0353	1591.0349	0.0004	0.001
11	1	11	10	0	10	1591.0543	1591.0537	0.0006	0.001
11	1	12	10	0	11	1591.0725	1591.0723	0.0002	0.001
11	1	13	10	0	12	1591.0904	1591.0906	-0.0002	0.001
11	1	14	10	0	13	1591.1074	1591.1086	-0.0012	0.001
10	1	13	11	0	14	1351.0729	1351.0722	0.0007	0.002
10	1	12	11	0	13	1351.1116	1351.1110	0.0006	0.002
10	1	11	11	0	12	1351.1511	1351.1501	0.0010	0.002
10	1	10	11	0	11	1351.1899	1351.1890	0.0009	0.002
10	1	9	11	0	10	1351.2275	1351.2274	0.0001	0.002
10	1	8	11	0	9	1351.2650	1351.2650	0.0000	0.002
10	1	7	11	0	8	1351.3017	1351.3015	0.0002	0.002
12	1	9	11	0	8	1597.8591	1597.8595	-0.0004	0.001

N'	v'	J'	N''	v''	J''	Observed	Calculated	Obs-Calc	Uncertainty
12	1	10	11	0	9	1597.8772	1597.8774	-0.0002	0.001
12	1	11	11	0	10	1597.8954	1597.8950	0.0004	0.001
12	1	12	11	0	11	1597.9133	1597.9124	0.0009	0.001
12	1	13	11	0	12	1597.9299	1597.9295	0.0004	0.001
12	1	14	11	0	13	1597.9459	1597.9463	-0.0004	0.001
12	1	15	11	0	14	1597.9617	1597.9629	-0.0012	0.002
11	1	14	12	0	15	1336.7892	1336.7884	0.0008	0.001
11	1	13	12	0	14	1336.8283	1336.8278	0.0005	0.001
11	1	12	12	0	13	1336.8686	1336.8673	0.0013	0.001
11	1	11	12	0	12	1336.9069	1336.9066	0.0003	0.001
11	1	10	12	0	11	1336.9448	1336.9454	-0.0006	0.001
11	1	9	12	0	10	1336.9826	1336.9834	-0.0008	0.001
11	1	8	12	0	9	1337.0199	1337.0205	-0.0006	0.001
13	1	10	12	0	9	1604.3139	1604.3139	0.0000	0.001
13	1	11	12	0	10	1604.3298	1604.3303	-0.0005	0.001
13	1	12	12	0	11	1604.3465	1604.3464	0.0001	0.001
13	1	13	12	0	12	1604.3629	1604.3622	0.0007	0.001
13	1	14	12	0	13	1604.3783	1604.3778	0.0005	0.001
13	1	15	12	0	14	1604.3929	1604.3932	-0.0003	0.001
13	1	16	12	0	15	1604.4071	1604.4082	-0.0011	0.001
12	1	15	13	0	16	1322.2684	1322.2677	0.0007	0.001
12	1	14	13	0	15	1322.3082	1322.3076	0.0006	0.001
12	1	13	13	0	14	1322.3487	1322.3476	0.0011	0.001
12	1	12	13	0	13	1322.3883	1322.3872	0.0011	0.001
12	1	11	13	0	12	1322.4265	1322.4264	0.0001	0.001
12	1	10	13	0	11	1322.4648	1322.4648	0.0000	0.001
12	1	9	13	0	10	1322.5027	1322.5023	0.0004	0.001
14	1	11	13	0	10	1610.3523	1610.3527	-0.0004	0.001
14	1	12	13	0	11	1610.3673	1610.3676	-0.0003	0.001
14	1	13	13	0	12	1610.3826	1610.3821	0.0005	0.001
14	1	14	13	0	13	1610.3973	1610.3964	0.0009	0.001
14	1	15	13	0	14	1610.4113	1610.4104	0.0009	0.001
14	1	16	13	0	15	1610.4244	1610.4242	0.0002	0.001
14	1	17	13	0	16	1610.4373	1610.4377	-0.0004	0.001
13	1	16	14	0	17	1307.5173	1307.5166	0.0007	0.001
13	1	15	14	0	16	1307.5575	1307.5570	0.0005	0.001
13	1	14	14	0	15	1307.5983	1307.5974	0.0009	0.001
13	1	13	14	0	14	1307.6381	1307.6374	0.0007	0.001

N'	v'	J'	N''	v''	J''	Observed	Calculated	Obs-Calc	Uncertainty
13	1	12	14	0	13	1307.6772	1307.6770	0.0003	0.001
13	1	11	14	0	12	1307.7156	1307.7158	-0.0002	0.001
13	1	10	14	0	11	1307.7536	1307.7537	-0.0001	0.001
15	1	12	14	0	11	1615.9688	1615.9692	-0.0004	0.001
15	1	13	14	0	12	1615.9824	1615.9825	-0.0001	0.001
15	1	14	14	0	13	1615.9965	1615.9954	0.0011	0.002
15	1	15	14	0	14	1616.0094	1616.0080	0.0014	0.002
15	1	16	14	0	15	1616.0220	1616.0204	0.0016	0.002
15	1	17	14	0	16	1616.0338	1616.0325	0.0013	0.001
15	1	18	14	0	17	1616.0444	1616.0444	0.0000	0.001
14	1	17	15	0	18	1292.5421	1292.5416	0.0005	0.001
14	1	16	15	0	17	1292.5828	1292.5825	0.0003	0.001
14	1	15	15	0	16	1292.6238	1292.6233	0.0005	0.001
14	1	14	15	0	15	1292.6644	1292.6637	0.0007	0.001
14	1	13	15	0	14	1292.7038	1292.7036	0.0002	0.001
14	1	12	15	0	13	1292.7424	1292.7427	-0.0003	0.001
14	1	11	15	0	12	1292.7809	1292.7811	-0.0002	0.001
16	1	13	15	0	12	1621.1569	1621.1566	0.0003	0.002
16	1	14	15	0	13	1621.1693	1621.1682	0.0011	0.002
16	1	15	15	0	14	1621.1813	1621.1794	0.0019	0.002
16	1	16	15	0	15	1621.1927	1621.1903	0.0024	0.003
16	1	17	15	0	16	1621.2037	1621.2010	0.0027	0.003
16	1	18	15	0	17	1621.2138	1621.2114	0.0024	0.003
16	1	19	15	0	18	1621.2226	1621.2217	0.0009	0.001
15	1	18	16	0	19	1277.3491	1277.3491	0.0000	0.001
15	1	17	16	0	18	1277.3902	1277.3904	-0.0002	0.001
15	1	16	16	0	17	1277.4322	1277.4315	0.0007	0.001
15	1	15	16	0	16	1277.4725	1277.4723	0.0002	0.001
15	1	14	16	0	15	1277.5123	1277.5125	-0.0002	0.001
15	1	13	16	0	14	1277.5517	1277.5521	-0.0004	0.001
15	1	12	16	0	13	1277.5906	1277.5908	-0.0002	0.001
17	1	14	16	0	13	1625.9097	1625.9082	0.0015	0.002
17	1	15	16	0	14	1625.9196	1625.9181	0.0016	0.002
17	1	16	16	0	15	1625.9304	1625.9275	0.0029	0.003
17	1	17	16	0	16	1625.9304	1625.9367	-0.0063	0.1
17	1	18	16	0	17	1625.9493	1625.9456	0.0037	0.003
17	1	19	16	0	18	1625.9493	1625.9543	-0.0050	0.003
17	1	20	16	0	19	1625.9630	1625.9627	0.0003	0.001

N'	v'	J'	N''	v''	J''	Observed	Calculated	Obs-Calc	Uncertainty
16	1	19	17	0	20	1261.9449	1261.9451	-0.0002	0.001
16	1	18	17	0	19	1261.9866	1261.9869	-0.0003	0.001
16	1	17	17	0	18	1262.0282	1262.0284	-0.0002	0.001
16	1	16	17	0	17	1262.0694	1262.0695	-0.0001	0.001
16	1	15	17	0	16	1262.1092	1262.1100	-0.0008	0.001
16	1	14	17	0	15	1262.1491	1262.1499	-0.0008	0.001
16	1	13	17	0	14	1262.1884	1262.1890	-0.0006	0.001
18	1	15	17	0	14	1630.2261	1630.2176	0.0086	10
18	1	16	17	0	15	1630.2261	1630.2256	0.0005	0.002
18	1	17	17	0	16	1630.2261	1630.2332	-0.0071	10
18	1	18	17	0	17	1630.2385	1630.2406	-0.0021	0.002
18	1	19	17	0	18	1630.2385	1630.2476	-0.0091	0.1
18	1	20	17	0	19	1630.2607	1630.2545	0.0062	0.1
18	1	21	17	0	20	1630.2607	1630.2611	-0.0004	0.002
17	1	20	18	0	21	1246.3353	1246.3357	-0.0004	0.001
17	1	19	18	0	20	1246.3774	1246.3778	-0.0004	0.001
17	1	18	18	0	19	1246.4193	1246.4197	-0.0004	0.001
17	1	17	18	0	18	1246.4608	1246.4612	-0.0004	0.001
17	1	16	18	0	17	1246.5015	1246.5020	-0.0005	0.001
17	1	15	18	0	16	1246.5410	1246.5422	-0.0012	0.001
17	1	14	18	0	15	1246.5808	1246.5816	-0.0008	0.001
19	1	16	18	0	15	1634.0789	1634.0782	0.0007	0.002
19	1	17	18	0	16	1634.0789	1634.0844	-0.0055	0.005
19	1	18	18	0	17	1634.0906	1634.0901	0.0005	0.002
19	1	19	18	0	18	1634.0906	1634.0956	-0.0050	0.005
19	1	20	18	0	19	1634.1024	1634.1007	0.0017	0.002
19	1	21	18	0	20	1634.1024	1634.1057	-0.0033	0.003
19	1	22	18	0	21	1634.1123	1634.1104	0.0019	0.002
18	1	21	19	0	22	1230.5255	1230.5266	-0.0011	0.001
18	1	20	19	0	21	1230.5684	1230.5691	-0.0007	0.001
18	1	19	19	0	20	1230.6106	1230.6113	-0.0007	0.001
18	1	18	19	0	19	1230.6528	1230.6531	-0.0003	0.001
18	1	17	19	0	18	1230.6931	1230.6943	-0.0012	0.001
18	1	16	19	0	17	1230.7334	1230.7348	-0.0014	0.001
18	1	15	19	0	16	1230.7736	1230.7744	-0.0008	0.001
20	1	17	19	0	16	1637.4862	1637.4841	0.0021	0.005
20	1	18	19	0	17	1637.4862	1637.4882	-0.0020	0.002
20	1	19	19	0	18	1637.4862	1637.4920	-0.0058	0.1

N'	v'	J'	N''	v''	J''	Observed	Calculated	Obs-Calc	Uncertainty
20	1	20	19	0	19	1637.4994	1637.4955	0.0039	0.005
20	1	21	19	0	20	1637.4994	1637.4987	0.0007	0.002
20	1	22	19	0	21	1637.4994	1637.5017	-0.0023	0.003
20	1	23	19	0	22	1637.4994	1637.5045	-0.0051	0.005
19	1	22	20	0	23	1214.5223	1214.5233	-0.0010	0.001
19	1	21	20	0	22	1214.5648	1214.5662	-0.0014	0.001
19	1	20	20	0	21	1214.6077	1214.6088	-0.0011	0.001
19	1	19	20	0	20	1214.6500	1214.6508	-0.0008	0.001
19	1	18	20	0	19	1214.6912	1214.6923	-0.0011	0.002
19	1	17	20	0	18	1214.7313	1214.7331	-0.0018	0.001
19	1	16	20	0	17	1214.7717	1214.7731	-0.0014	0.001
21	1	18	20	0	17	1640.4404	1640.4291	0.0113	1
21	1	19	20	0	18	1640.4404	1640.4312	0.0092	1
21	1	20	20	0	19	1640.4404	1640.4330	0.0074	1
21	1	21	20	0	20	1640.4404	1640.4344	0.0060	1
21	1	22	20	0	21	1640.4404	1640.4356	0.0048	1
21	1	23	20	0	22	1640.4404	1640.4365	0.0039	0.003
21	1	24	20	0	23	1640.4404	1640.4372	0.0032	0.003
20	1	23	21	0	24	1198.3304	1198.3312	-0.0008	0.001
20	1	22	21	0	23	1198.3738	1198.3745	-0.0007	0.001
20	1	21	21	0	22	1198.4173	1198.4174	-0.0001	0.001
20	1	20	21	0	21	1198.4588	1198.4598	-0.0010	0.001
20	1	19	21	0	20	1198.5008	1198.5015	-0.0007	0.001
20	1	18	21	0	19	1198.5413	1198.5426	-0.0013	0.001
20	1	17	21	0	18	1198.5814	1198.5829	-0.0015	0.001
22	1	19	21	0	18	1642.9063	1642.9075	-0.0012	0.001
22	1	20	21	0	19	1642.9063	1642.9076	-0.0013	0.001
22	1	21	21	0	20	1642.9063	1642.9073	-0.0010	0.001
22	1	22	21	0	21	1642.9063	1642.9066	-0.0003	0.001
22	1	23	21	0	22	1642.9063	1642.9056	0.0007	0.001
22	1	24	21	0	23	1642.9063	1642.9044	0.0019	0.001
22	1	25	21	0	24	1642.9063	1642.9031	0.0033	0.001
21	1	24	22	0	25	1181.9552	1181.9556	-0.0004	0.001
21	1	23	22	0	24	1181.9986	1181.9992	-0.0006	0.001
21	1	22	22	0	23	1182.0419	1182.0424	-0.0005	0.001
21	1	21	22	0	22	1182.0851	1182.0851	0.0000	0.001
21	1	20	22	0	21	1182.1269	1182.1271	-0.0002	0.001
21	1	19	22	0	20	1182.1684	1182.1684	0.0000	0.001

N'	v'	J'	N''	v''	J''	Observed	Calculated	Obs-Calc	Uncertainty
21	1	18	22	0	19	1182.2088	1182.2090	-0.0002	0.001
23	1	20	22	0	19	1644.8992	1644.9141	-0.0149	1
23	1	21	22	0	20	1644.8992	1644.9120	-0.0128	1
23	1	22	22	0	21	1644.8992	1644.9095	-0.0103	0.1
23	1	23	22	0	22	1644.8992	1644.9066	-0.0074	0.1
23	1	24	22	0	23	1644.8992	1644.9035	-0.0043	0.003
23	1	25	22	0	24	1644.8992	1644.9001	-0.0009	0.002
23	1	26	22	0	25	1644.8992	1644.8965	0.0027	0.002
22	1	25	23	0	26	1165.4024	1165.4012	0.0012	0.001
22	1	24	23	0	25	1165.4451	1165.4452	-0.0001	0.001
22	1	23	23	0	24	1165.4891	1165.4887	0.0004	0.001
22	1	22	23	0	23	1165.5320	1165.5317	0.0003	0.001
22	1	21	23	0	22	1165.5740	1165.5740	0.0000	0.001
22	1	20	23	0	21	1165.6157	1165.6156	0.0001	0.001
22	1	19	23	0	20	1165.6566	1165.6564	0.0002	0.001
24	1	21	23	0	20	1646.4115	1646.4439	-0.0324	1
24	1	22	23	0	21	1646.4115	1646.4395	-0.0280	1
24	1	23	23	0	22	1646.4115	1646.4347	-0.0232	0.1
24	1	24	23	0	23	1646.4115	1646.4296	-0.0181	0.1
24	1	25	23	0	24	1646.4115	1646.4242	-0.0127	0.1
24	1	26	23	0	25	1646.4115	1646.4185	-0.0070	0.1
24	1	27	23	0	26	1646.4115	1646.4127	-0.0012	0.001
23	1	26	24	0	27	1148.6733	1148.6730	0.0003	0.001
23	1	25	24	0	26	1148.7174	1148.7174	0.0000	0.001
23	1	24	24	0	25	1148.7620	1148.7612	0.0008	0.001
23	1	23	24	0	24	1148.8046	1148.8044	0.0002	0.001
23	1	22	24	0	23	1148.8481	1148.8470	0.0011	0.001
23	1	21	24	0	22	1148.8883	1148.8889	-0.0006	0.001
23	1	20	24	0	21	1148.9317	1148.9299	0.0018	0.001
25	1	22	24	0	21	1647.4427	1647.4922	-0.0495	1
25	1	23	24	0	22	1647.4427	1647.4855	-0.0428	1
25	1	24	24	0	23	1647.4427	1647.4784	-0.0357	0.1
25	1	25	24	0	24	1647.4427	1647.4709	-0.0282	0.1
25	1	26	24	0	25	1647.4427	1647.4632	-0.0205	0.1
25	1	27	24	0	26	1647.4427	1647.4551	-0.0124	0.1
25	1	28	24	0	27	1647.4427	1647.4470	-0.0043	0.1
24	1	27	25	0	28	1131.7746	1131.7756	-0.0010	0.001
24	1	26	25	0	27	1131.8216	1131.8202	0.0014	0.001

N'	v'	J'	N''	v''	J''	Observed	Calculated	Obs-Calc	Uncertainty
24	1	25	25	0	26	1131.8643	1131.8644	-0.0001	0.001
24	1	24	25	0	25	1131.9088	1131.9079	0.0009	0.001
24	1	23	25	0	24	1131.9523	1131.9507	0.0016	0.001
24	1	22	25	0	23	1131.9939	1131.9928	0.0011	0.001
24	1	21	25	0	22	1132.0347	1132.0341	0.0006	0.001
26	1	24	25	0	23	1648.0014	1648.0461	-0.0447	1
26	1	25	25	0	24	1648.0014	1648.0366	-0.0352	1
26	1	27	25	0	26	1648.0014	1648.0165	-0.0151	1
26	1	28	25	0	27	1648.0014	1648.0061	-0.0047	1
26	1	29	25	0	28	1648.0014	1647.9954	0.0060	0.002
25	1	28	26	0	29	1114.7138	1114.7133	0.0005	0.001
25	1	27	26	0	28	1114.7600	1114.7583	0.0017	0.001
25	1	26	26	0	27	1114.8033	1114.8027	0.0006	0.001
25	1	25	26	0	26	1114.8469	1114.8465	0.0004	0.001
25	1	24	26	0	25	1114.8908	1114.8896	0.0012	0.001
25	1	23	26	0	24	1114.9340	1114.9320	0.0020	0.001
25	1	22	26	0	23	1114.9734	1114.9735	-0.0001	0.001
26	1	29	27	0	30	1097.4892	1097.4906	-0.0014	0.001
26	1	28	27	0	29	1097.5344	1097.5359	-0.0015	0.001
26	1	27	27	0	28	1097.5804	1097.5806	-0.0002	0.001
26	1	26	27	0	27	1097.6246	1097.6247	-0.0001	0.001
26	1	25	27	0	26	1097.6676	1097.6681	-0.0005	0.001
26	1	24	27	0	25	1097.7084	1097.7106	-0.0022	0.001
0	1	3	1	0	3	1479.4851	1479.4909	-0.0058	0.004
1	1	4	2	0	4	1467.9990	1467.9961	0.0029	0.003
2	1	5	3	0	5	1456.1830	1456.1913	-0.0083	1
0	1	3	1	0	2	1479.5298	1479.5427	-0.0129	1
1	1	3	2	0	2	1468.0428	1468.0365	0.0063	1
1	1	2	2	0	1	1468.0250	1468.0324	-0.0074	1
1	1	2	2	0	2	1467.9795	1467.9900	-0.0105	1
2	1	3	3	0	3	1456.1585	1456.1656	-0.0071	1
2	1	2	3	0	2	1456.1720	1456.1731	-0.0011	0.001
1	1	3	0	0	3	1501.4732	1501.4774	-0.0042	0.004
2	1	4	1	0	4	1512.0054	1512.0004	0.0050	0.004
2	2	5	1	1	4	1453.5452	1453.5400	0.0052	0.005
1	2	4	2	1	5	1410.4748	1410.4771	-0.0023	0.005
1	2	3	2	1	4	1410.5096	1410.5057	0.0039	0.005
1	2	2	2	1	3	1410.5773	1410.5819	-0.0046	0.005

N'	v'	J'	N''	v''	J''	Observed	Calculated	Obs-Calc	Uncertainty
3	2	2	2	1	1	1463.3151	1463.2895	0.0256	10
3	2	3	2	1	2	1463.3275	1463.3212	0.0063	10
3	2	4	2	1	3	1463.3543	1463.3561	-0.0018	0.005
3	2	5	2	1	4	1463.3890	1463.3895	-0.0005	0.002
3	2	6	2	1	5	1463.4170	1463.4140	0.0030	0.003
2	2	5	3	1	6	1398.9522	1398.9537	-0.0015	0.002
2	2	4	3	1	5	1398.9869	1398.9850	0.0019	0.002
2	2	2	3	1	3	1399.0239	1399.0703	-0.0464	100
2	2	3	3	1	4	1399.0239	1399.0269	-0.0030	0.005
2	2	1	3	1	2	1399.1310	1399.1091	0.0220	100
4	2	1	3	1	0	1472.7755	1472.7785	-0.0029	0.005
4	2	2	3	1	1	1472.7985	1472.8024	-0.0039	0.005
4	2	3	3	1	2	1472.8257	1472.8286	-0.0029	0.005
4	2	4	3	1	3	1472.8557	1472.8568	-0.0011	0.002
4	2	5	3	1	4	1472.8854	1472.8858	-0.0004	0.001
4	2	6	3	1	5	1472.9164	1472.9138	0.0026	0.001
4	2	7	3	1	6	1472.9392	1472.9379	0.0013	0.001
3	2	6	4	1	7	1387.1222	1387.1225	-0.0003	0.001
3	2	5	4	1	6	1387.1544	1387.1554	-0.0010	0.001
3	2	4	4	1	5	1387.1938	1387.1931	0.0007	0.001
3	2	3	4	1	4	1387.2327	1387.2318	0.0009	0.001
3	2	2	4	1	3	1387.2721	1387.2684	0.0037	0.001
3	2	1	4	1	2	1387.3020	1387.3011	0.0009	0.001
3	2	0	4	1	1	1387.3238	1387.3291	-0.0053	0.002
5	2	2	4	1	1	1481.9498	1481.9529	-0.0031	0.002
5	2	3	4	1	2	1481.9778	1481.9771	0.0006	0.002
5	2	4	4	1	3	1481.9993	1482.0024	-0.0031	0.002
5	2	5	4	1	4	1482.0290	1482.0285	0.0005	0.002
5	2	6	4	1	5	1482.0561	1482.0548	0.0013	0.001
5	2	7	4	1	6	1482.0821	1482.0803	0.0018	0.001
5	2	8	4	1	7	1482.1050	1482.1036	0.0014	0.001
4	2	7	5	1	8	1374.9911	1374.9912	-0.0001	0.001
4	2	6	5	1	7	1375.0252	1375.0253	-0.0001	0.001
4	2	5	5	1	6	1375.0623	1375.0622	0.0001	0.001
4	2	4	5	1	5	1375.1001	1375.0996	0.0005	0.001
4	2	3	5	1	4	1375.1368	1375.1358	0.0010	0.001
4	2	2	5	1	3	1375.1703	1375.1695	0.0008	0.002
4	2	1	5	1	2	1375.1703	1375.2000	-0.0297	100

N'	v'	J'	N''	v''	J''	Observed	Calculated	Obs-Calc	Uncertainty
6	2	3	5	1	2	1490.7596	1490.7610	-0.0014	0.001
6	2	4	5	1	3	1490.7850	1490.7847	0.0004	0.001
6	2	5	5	1	4	1490.8086	1490.8088	-0.0002	0.001
6	2	6	5	1	5	1490.8360	1490.8333	0.0028	0.001
6	2	7	5	1	6	1490.8580	1490.8577	0.0004	0.001
6	2	8	5	1	7	1490.8822	1490.8814	0.0008	0.001
6	2	9	5	1	8	1490.9037	1490.9037	0.0000	0.001
5	2	8	6	1	9	1362.5670	1362.5671	-0.0001	0.001
5	2	7	6	1	8	1362.6026	1362.6023	0.0003	0.001
5	2	6	6	1	7	1362.6391	1362.6392	-0.0001	0.001
5	2	5	6	1	6	1362.6774	1362.6763	0.0011	0.001
5	2	4	6	1	5	1362.7121	1362.7126	-0.0005	0.001
5	2	3	6	1	4	1362.7461	1362.7470	-0.0009	0.001
5	2	2	6	1	3	1362.7793	1362.7791	0.0002	0.001
7	2	4	6	1	3	1499.1958	1499.1958	0.0000	0.001
7	2	5	6	1	4	1499.2187	1499.2185	0.0002	0.001
7	2	6	6	1	5	1499.2417	1499.2414	0.0003	0.001
7	2	7	6	1	6	1499.2653	1499.2644	0.0009	0.001
7	2	8	6	1	7	1499.2873	1499.2872	0.0001	0.001
7	2	9	6	1	8	1499.3094	1499.3094	0.0000	0.001
7	2	10	6	1	9	1499.3304	1499.3306	-0.0002	0.001
6	2	9	7	1	10	1349.8571	1349.8574	-0.0003	0.001
6	2	8	7	1	9	1349.8930	1349.8935	-0.0005	0.001
6	2	7	7	1	8	1349.9303	1349.9307	-0.0004	0.001
6	2	6	7	1	7	1349.9676	1349.9680	-0.0004	0.001
6	2	5	7	1	6	1350.0044	1350.0045	-0.0001	0.001
6	2	4	7	1	5	1350.0411	1350.0396	0.0015	0.001
6	2	3	7	1	4	1350.0718	1350.0729	-0.0011	0.001
8	2	5	7	1	4	1507.2500	1507.2501	-0.0001	0.001
8	2	6	7	1	5	1507.2733	1507.2717	0.0016	0.001
8	2	7	7	1	6	1507.2941	1507.2933	0.0008	0.001
8	2	8	7	1	7	1507.3150	1507.3148	0.0002	0.001
8	2	9	7	1	8	1507.3359	1507.3360	-0.0001	0.001
8	2	10	7	1	9	1507.3566	1507.3568	-0.0002	0.001
8	2	11	7	1	10	1507.3765	1507.3768	-0.0003	0.001
7	2	10	8	1	11	1336.8686	1336.8691	-0.0005	0.001
9	2	6	8	1	5	1514.9168	1514.9164	0.0004	0.001
9	2	7	8	1	6	1514.9375	1514.9368	0.0007	0.001

N'	v'	J'	N''	v''	J''	Observed	Calculated	Obs-Calc	Uncertainty
9	2	8	8	1	7	1514.9576	1514.9570	0.0006	0.001
9	2	9	8	1	8	1514.9754	1514.9770	-0.0016	0.001
9	2	10	8	1	9	1514.9969	1514.9968	0.0001	0.001
9	2	11	8	1	10	1515.0157	1515.0161	-0.0004	0.001
9	2	12	8	1	11	1515.0338	1515.0348	-0.0010	0.001
8	2	11	9	1	12	1323.6088	1323.6090	-0.0002	0.001
8	2	10	9	1	11	1323.6467	1323.6466	0.0001	0.001
8	2	9	9	1	10	1323.6844	1323.6848	-0.0004	0.001
8	2	8	9	1	9	1323.7225	1323.7228	-0.0003	0.001
8	2	7	9	1	8	1323.7593	1323.7601	-0.0008	0.001
8	2	6	9	1	7	1323.7965	1323.7965	0.0001	0.001
8	2	5	9	1	6	1323.8310	1323.8314	-0.0004	0.001
10	2	7	9	1	6	1522.1877	1522.1874	0.0003	0.001
10	2	8	9	1	7	1522.2059	1522.2064	-0.0005	0.001
10	2	9	9	1	8	1522.2241	1522.2252	-0.0011	0.001
10	2	10	9	1	9	1522.2428	1522.2437	-0.0009	0.001
10	2	11	9	1	10	1522.2613	1522.2620	-0.0007	0.001
10	2	12	9	1	11	1522.2789	1522.2798	-0.0009	0.001
10	2	13	9	1	12	1522.2956	1522.2971	-0.0015	0.001
9	2	12	10	1	13	1310.0839	1310.0840	-0.0001	0.001
9	2	11	10	1	12	1310.1224	1310.1223	0.0001	0.001
9	2	10	10	1	11	1310.1607	1310.1609	-0.0002	0.001
9	2	9	10	1	10	1310.1989	1310.1994	-0.0005	0.001
9	2	8	10	1	9	1310.2372	1310.2372	0.0000	0.001
9	2	7	10	1	8	1310.2745	1310.2741	0.0005	0.001
9	2	6	10	1	7	1310.3091	1310.3097	-0.0006	0.001
11	2	8	10	1	7	1529.0548	1529.0555	-0.0007	0.001
11	2	9	10	1	8	1529.0735	1529.0731	0.0004	0.001
11	2	10	10	1	9	1529.0899	1529.0904	-0.0005	0.001
11	2	11	10	1	10	1529.1068	1529.1074	-0.0006	0.001
11	2	12	10	1	11	1529.1234	1529.1241	-0.0007	0.001
11	2	13	10	1	12	1529.1393	1529.1404	-0.0011	0.001
11	2	14	10	1	13	1529.1546	1529.1563	-0.0017	0.001
10	2	13	11	1	14	1296.3009	1296.3007	0.0002	0.001
10	2	12	11	1	13	1296.3392	1296.3396	-0.0004	0.001
10	2	11	11	1	12	1296.3781	1296.3787	-0.0006	0.001
10	2	10	11	1	11	1296.4177	1296.4176	0.0001	0.001
10	2	9	11	1	10	1296.4558	1296.4559	-0.0001	0.001

N'	v'	J'	N''	v''	J''	Observed	Calculated	Obs-Calc	Uncertainty
10	2	8	11	1	9	1296.4927	1296.4933	-0.0006	0.001
10	2	7	11	1	8	1296.5293	1296.5295	-0.0002	0.001
12	2	9	11	1	8	1535.5130	1535.5133	-0.0003	0.001
12	2	10	11	1	9	1535.5296	1535.5294	0.0002	0.001
12	2	11	11	1	10	1535.5445	1535.5452	-0.0007	0.001
12	2	12	11	1	11	1535.5603	1535.5606	-0.0003	0.001
12	2	13	11	1	12	1535.5750	1535.5757	-0.0007	0.001
12	2	14	11	1	13	1535.5900	1535.5905	-0.0005	0.001
12	2	15	11	1	14	1535.6032	1535.6048	-0.0016	0.001
11	2	14	12	1	15	1282.2661	1282.2655	0.0006	0.001
11	2	13	12	1	14	1282.3053	1282.3051	0.0002	0.001
11	2	12	12	1	13	1282.3439	1282.3447	-0.0008	0.001
11	2	11	12	1	12	1282.3840	1282.3841	-0.0001	0.001
11	2	10	12	1	11	1282.4224	1282.4228	-0.0004	0.001
11	2	9	12	1	10	1282.4610	1282.4607	0.0003	0.001
11	2	8	12	1	9	1282.4974	1282.4975	-0.0001	0.001
13	2	10	12	1	9	1541.5524	1541.5533	-0.0009	0.001
13	2	11	12	1	10	1541.5681	1541.5678	0.0003	0.001
13	2	12	12	1	11	1541.5824	1541.5820	0.0004	0.001
13	2	13	12	1	12	1541.5954	1541.5958	-0.0004	0.001
13	2	14	12	1	13	1541.6093	1541.6093	0.0000	0.001
13	2	15	12	1	14	1541.6227	1541.6224	0.0003	0.001
13	2	16	12	1	15	1541.6338	1541.6352	-0.0014	0.001
12	2	15	13	1	16	1267.9854	1267.9850	0.0004	0.001
12	2	14	13	1	15	1268.0254	1268.0251	0.0003	0.001
12	2	13	13	1	14	1268.0654	1268.0652	0.0002	0.001
12	2	12	13	1	13	1268.1052	1268.1050	0.0002	0.001
12	2	11	13	1	12	1268.1446	1268.1442	0.0004	0.001
12	2	10	13	1	11	1268.1822	1268.1825	-0.0003	0.001
12	2	9	13	1	10	1268.2204	1268.2199	0.0005	0.001
14	2	11	13	1	10	1547.1685	1547.1681	0.0005	0.001
14	2	12	13	1	11	1547.1815	1547.1809	0.0006	0.001
14	2	13	13	1	12	1547.1940	1547.1934	0.0006	0.001
14	2	14	13	1	13	1547.2058	1547.2056	0.0002	0.001
14	2	15	13	1	14	1547.2186	1547.2173	0.0013	0.001
14	2	16	13	1	15	1547.2295	1547.2288	0.0007	0.001
14	2	17	13	1	16	1547.2401	1547.2399	0.0002	0.001
13	2	16	14	1	17	1253.4654	1253.4652	0.0002	0.003

N'	v'	J'	N''	v''	J''	Observed	Calculated	Obs-Calc	Uncertainty
13	2	15	14	1	16	1253.5062	1253.5059	0.0004	0.003
13	2	14	14	1	15	1253.5460	1253.5464	-0.0004	0.003
13	2	13	14	1	14	1253.5869	1253.5866	0.0003	0.003
13	2	12	14	1	13	1253.6266	1253.6262	0.0004	0.003
13	2	11	14	1	12	1253.6649	1253.6651	-0.0002	0.003
13	2	10	14	1	11	1253.7028	1253.7029	-0.0001	0.003
15	2	12	14	1	11	1552.3511	1552.3501	0.0010	0.003
15	2	13	14	1	12	1552.3629	1552.3613	0.0016	0.003
15	2	14	14	1	13	1552.3744	1552.3721	0.0024	0.003
15	2	15	14	1	14	1552.3841	1552.3824	0.0017	0.003
15	2	16	14	1	15	1552.3936	1552.3925	0.0011	0.003
15	2	17	14	1	16	1552.4047	1552.4022	0.0025	0.003
15	2	18	14	1	17	1552.4131	1552.4116	0.0015	0.003
14	2	17	15	1	18	1238.7124	1238.7121	0.0003	0.003
14	2	16	15	1	17	1238.7536	1238.7533	0.0003	0.003
14	2	15	15	1	16	1238.7946	1238.7943	0.0003	0.003
14	2	14	15	1	15	1238.8348	1238.8350	-0.0002	0.003
14	2	13	15	1	14	1238.8750	1238.8750	0.0000	0.003
14	2	12	15	1	13	1238.9145	1238.9142	0.0003	0.003
14	2	11	15	1	12	1238.9521	1238.9525	-0.0004	0.003
16	2	13	15	1	12	1557.0939	1557.0921	0.0018	0.002
16	2	14	15	1	13	1557.1040	1557.1015	0.0025	0.002
16	2	15	15	1	14	1557.1040	1557.1105	-0.0065	0.003
16	2	16	15	1	15	1557.1130	1557.1191	-0.0061	0.003
16	2	17	15	1	16	1557.1224	1557.1273	-0.0049	0.002
16	2	18	15	1	17	1557.1312	1557.1352	-0.0040	0.003
16	2	19	15	1	18	1557.1423	1557.1428	-0.0005	0.002
15	2	18	16	1	19	1223.7317	1223.7316	0.0002	0.001
15	2	17	16	1	18	1223.7738	1223.7733	0.0005	0.001
15	2	16	16	1	17	1223.8145	1223.8148	-0.0003	0.001
15	2	15	16	1	16	1223.8558	1223.8558	0.0000	0.001
15	2	14	16	1	15	1223.8956	1223.8962	-0.0006	0.001
15	2	13	16	1	14	1223.9358	1223.9359	-0.0001	0.001
15	2	12	16	1	13	1223.9750	1223.9746	0.0004	0.001
17	2	14	16	1	13	1561.3972	1561.3867	0.0105	1
17	2	15	16	1	14	1561.3972	1561.3943	0.0030	0.003
17	2	16	16	1	15	1561.3972	1561.4014	-0.0042	0.002
17	2	17	16	1	16	1561.4081	1561.4081	0.0001	0.003

N'	v'	J'	N''	v''	J''	Observed	Calculated	Obs-Calc	Uncertainty
17	2	18	16	1	17	1561.4168	1561.4144	0.0024	0.003
17	2	19	16	1	18	1561.4168	1561.4205	-0.0037	0.003
17	2	20	16	1	19	1561.4287	1561.4262	0.0025	0.001
16	2	19	17	1	20	1208.5299	1208.5291	0.0008	0.001
16	2	18	17	1	19	1208.5722	1208.5713	0.0009	0.001
16	2	17	17	1	18	1208.6130	1208.6132	-0.0002	0.001
16	2	16	17	1	17	1208.6545	1208.6547	-0.0002	0.001
16	2	15	17	1	16	1208.6958	1208.6955	0.0003	0.001
16	2	14	17	1	15	1208.7358	1208.7355	0.0003	0.001
16	2	13	17	1	14	1208.7747	1208.7747	0.0000	0.001
18	2	15	17	1	14	1565.2287	1565.2267	0.0020	0.001
18	2	16	17	1	15	1565.2287	1565.2323	-0.0036	0.003
18	2	17	17	1	16	1565.2287	1565.2375	-0.0088	10
18	2	18	17	1	17	1565.2460	1565.2422	0.0038	0.003
18	2	19	17	1	18	1565.2460	1565.2467	-0.0007	0.002
18	2	20	17	1	19	1565.2460	1565.2507	-0.0047	0.004
18	2	21	17	1	20	1565.2581	1565.2546	0.0036	0.002
17	2	20	18	1	21	1193.1114	1193.1102	0.0012	0.001
17	2	19	18	1	20	1193.1526	1193.1529	-0.0003	0.001
17	2	18	18	1	19	1193.1955	1193.1952	0.0003	0.001
17	2	17	18	1	18	1193.2366	1193.2370	-0.0004	0.001
17	2	16	18	1	17	1193.2787	1193.2782	0.0005	0.001
17	2	15	18	1	16	1193.3184	1193.3186	-0.0002	0.001
17	2	14	18	1	15	1193.3589	1193.3581	0.0008	0.001
19	2	16	18	1	15	1568.6086	1568.6049	0.0037	0.003
19	2	17	18	1	16	1568.6086	1568.6085	0.0001	0.002
19	2	18	18	1	17	1568.6086	1568.6117	-0.0031	0.002
19	2	19	18	1	18	1568.6086	1568.6144	-0.0058	0.003
19	2	20	18	1	19	1568.6259	1568.6169	0.0091	1
19	2	21	18	1	20	1568.6259	1568.6189	0.0070	0.003
19	2	22	18	1	21	1568.6259	1568.6207	0.0052	0.002
18	2	21	19	1	22	1177.4808	1177.4798	0.0010	0.001
18	2	20	19	1	21	1177.5238	1177.5229	0.0009	0.001
18	2	19	19	1	20	1177.5644	1177.5656	-0.0012	0.001
18	2	18	19	1	19	1177.6073	1177.6078	-0.0005	0.001
18	2	17	19	1	18	1177.6493	1177.6494	-0.0001	0.001
18	2	16	19	1	17	1177.6905	1177.6901	0.0004	0.001
18	2	15	19	1	16	1177.7305	1177.7300	0.0005	0.001

N'	v'	J'	N''	v''	J''	Observed	Calculated	Obs-Calc	Uncertainty
20	2	17	19	1	16	1571.5233	1571.5144	0.0089	0.01
20	2	18	19	1	17	1571.5233	1571.5160	0.0074	0.01
20	2	19	19	1	18	1571.5233	1571.5171	0.0063	0.01
20	2	20	19	1	19	1571.5233	1571.5177	0.0056	0.01
20	2	21	19	1	20	1571.5233	1571.5181	0.0052	0.01
20	2	22	19	1	21	1571.5233	1571.5181	0.0053	0.005
20	2	23	19	1	22	1571.5233	1571.5178	0.0055	0.005
19	2	22	20	1	23	1161.6438	1161.6428	0.0010	0.001
19	2	21	20	1	22	1161.6867	1161.6863	0.0004	0.001
19	2	20	20	1	21	1161.7291	1161.7295	-0.0004	0.001
19	2	19	20	1	20	1161.7732	1161.7720	0.0012	0.001
19	2	18	20	1	19	1161.8144	1161.8139	0.0005	0.001
19	2	17	20	1	18	1161.8557	1161.8550	0.0007	0.001
19	2	16	20	1	17	1161.8943	1161.8953	-0.0010	0.001
21	2	18	20	1	17	1573.9457	1573.9485	-0.0028	0.003
21	2	19	20	1	18	1573.9457	1573.9479	-0.0022	0.002
21	2	20	20	1	19	1573.9457	1573.9468	-0.0011	0.002
21	2	21	20	1	20	1573.9457	1573.9454	0.0003	0.002
21	2	22	20	1	21	1573.9457	1573.9435	0.0022	0.002
21	2	23	20	1	22	1573.9457	1573.9414	0.0043	0.002
21	2	24	20	1	23	1573.9457	1573.9389	0.0068	0.003
20	2	23	21	1	24	1145.6039	1145.6038	0.0001	0.001
20	2	22	21	1	23	1145.6486	1145.6478	0.0008	0.001
20	2	21	21	1	22	1145.6923	1145.6912	0.0011	0.001
20	2	20	21	1	21	1145.7346	1145.7342	0.0005	0.001
20	2	19	21	1	20	1145.7776	1145.7764	0.0012	0.001
20	2	18	21	1	19	1145.8187	1145.8178	0.0009	0.001
20	2	17	21	1	18	1145.8601	1145.8584	0.0017	0.001
22	2	19	21	1	18	1575.8844	1575.9006	-0.0162	10
22	2	20	21	1	19	1575.8844	1575.8978	-0.0134	10
22	2	21	21	1	20	1575.8844	1575.8945	-0.0101	10
22	2	22	21	1	21	1575.8844	1575.8908	-0.0064	10
22	2	23	21	1	22	1575.8844	1575.8868	-0.0024	0.003
22	2	25	21	1	24	1575.8844	1575.8777	0.0067	0.003
21	2	24	22	1	25	1129.3676	1129.3671	0.0005	0.001
21	2	23	22	1	24	1129.4121	1129.4115	0.0006	0.001
21	2	22	22	1	23	1129.4563	1129.4553	0.0010	0.001
21	2	21	22	1	22	1129.4995	1129.4986	0.0009	0.001

N'	v'	J'	N''	v''	J''	Observed	Calculated	Obs-Calc	Uncertainty
21	2	20	22	1	21	1129.5422	1129.5411	0.0011	0.001
21	2	19	22	1	20	1129.5828	1129.5829	-0.0001	0.001
21	2	18	22	1	19	1129.6248	1129.6238	0.0010	0.001
23	2	20	22	1	19	1577.3280	1577.3646	-0.0366	100
23	2	21	22	1	20	1577.3280	1577.3595	-0.0315	100
23	2	22	22	1	21	1577.3280	1577.3540	-0.0260	100
23	2	23	22	1	22	1577.3280	1577.3480	-0.0200	100
23	2	24	22	1	23	1577.3280	1577.3416	-0.0136	100
23	2	25	22	1	24	1577.3280	1577.3349	-0.0069	100
23	2	26	22	1	25	1577.3280	1577.3279	0.0001	0.002
22	2	25	23	1	26	1112.9360	1112.9367	-0.0007	0.001
22	2	24	23	1	25	1112.9819	1112.9815	0.0004	0.001
22	2	23	23	1	24	1113.0252	1113.0257	-0.0005	0.001
22	2	22	23	1	23	1113.0701	1113.0693	0.0008	0.001
22	2	21	23	1	22	1113.1095	1113.1122	-0.0027	0.001
22	2	20	23	1	21	1113.1540	1113.1542	-0.0002	0.001
22	2	19	23	1	20	1113.1945	1113.1954	-0.0009	0.001
24	2	24	23	1	23	1578.3087	1578.3110	-0.0023	0.002
24	2	25	23	1	24	1578.2622	1578.3022	-0.0400	10
24	2	26	23	1	25	1578.2898	1578.2931	-0.0033	0.002
24	2	27	23	1	26	1578.2898	1578.2838	0.0061	0.003
24	2	22	23	1	21	1578.3186	1578.3273	-0.0087	1
24	2	23	23	1	22	1578.3186	1578.3194	-0.0008	0.001
23	2	26	24	1	27	1096.3149	1096.3165	-0.0016	0.001
23	2	25	24	1	26	1096.3611	1096.3616	-0.0005	0.001
23	2	24	24	1	25	1096.4043	1096.4062	-0.0019	0.001
23	2	23	24	1	24	1096.4503	1096.4501	0.0002	0.001
23	2	22	24	1	23	1096.4920	1096.4933	-0.0013	0.001
23	2	21	24	1	22	1096.5784	1096.5356	0.0428	10
4	3	7	3	2	6	1411.6947	1411.6917	0.0030	0.003
3	3	6	4	2	7	1328.5533	1328.5519	0.0015	0.003
3	3	5	4	2	6	1328.5881	1328.5842	0.0039	0.003
5	3	6	4	2	5	1420.4347	1420.4334	0.0013	0.003
5	3	7	4	2	6	1420.4599	1420.4575	0.0024	0.003
5	3	8	4	2	7	1420.4798	1420.4791	0.0007	0.003
4	3	7	5	2	8	1316.7117	1316.7106	0.0011	0.001
4	3	6	5	2	7	1316.7443	1316.7443	0.0000	0.001
4	3	5	5	2	6	1316.7818	1316.7808	0.0010	0.001

N'	v'	J'	N''	v''	J''	Observed	Calculated	Obs-Calc	Uncertainty
4	3	4	5	2	5	1316.8353	1316.8178	0.0175	10
4	3	3	5	2	4	1316.8569	1316.8535	0.0035	0.002
6	3	3	5	2	2	1428.7801	1428.7564	0.0238	10
6	3	4	5	2	3	1428.7801	1428.7787	0.0014	0.003
6	3	5	5	2	4	1428.8039	1428.8014	0.0025	0.003
6	3	6	5	2	5	1428.8245	1428.8245	0.0000	0.003
6	3	7	5	2	6	1428.8478	1428.8475	0.0003	0.003
6	3	8	5	2	7	1428.8713	1428.8697	0.0016	0.003
6	3	9	5	2	8	1428.8910	1428.8902	0.0008	0.003
5	3	8	6	2	9	1304.5668	1304.5666	0.0002	0.001
5	3	7	6	2	8	1304.6027	1304.6014	0.0013	0.001
5	3	6	6	2	7	1304.6397	1304.6380	0.0017	0.001
5	3	5	6	2	6	1304.6735	1304.6748	-0.0013	0.001
5	3	4	6	2	5	1304.7104	1304.7105	-0.0001	0.001
5	3	3	6	2	4	1304.7469	1304.7444	0.0025	0.001
5	3	2	6	2	3	1304.7770	1304.7757	0.0013	0.001
7	3	6	6	2	5	1436.8347	1436.8346	0.0001	0.001
7	3	5	6	2	4	1436.8347	1436.8131	0.0216	10
7	3	7	6	2	6	1436.8563	1436.8560	0.0003	0.001
7	3	8	6	2	7	1436.8759	1436.8772	-0.0013	0.001
7	3	9	6	2	8	1436.8984	1436.8978	0.0006	0.001
7	3	10	6	2	9	1436.9167	1436.9172	-0.0005	0.001
6	3	9	7	2	10	1292.1283	1292.1268	0.0015	0.003
6	3	8	7	2	9	1292.1630	1292.1626	0.0004	0.003
6	3	7	7	2	8	1292.1998	1292.1995	0.0003	0.003
6	3	6	7	2	7	1292.2362	1292.2365	-0.0003	0.003
6	3	5	7	2	6	1292.2721	1292.2726	-0.0005	0.003
6	3	4	7	2	5	1292.3090	1292.3072	0.0019	0.003
6	3	3	7	2	4	1292.3395	1292.3397	-0.0002	0.001
8	3	5	7	2	4	1444.4353	1444.4353	0.0001	0.001
8	3	6	7	2	5	1444.4561	1444.4554	0.0007	0.001
8	3	7	7	2	6	1444.4763	1444.4754	0.0009	0.001
8	3	8	7	2	7	1444.4951	1444.4953	-0.0002	0.001
8	3	9	7	2	8	1444.5142	1444.5149	-0.0007	0.001
8	3	10	7	2	9	1444.5330	1444.5339	-0.0009	0.001
8	3	11	7	2	10	1444.5516	1444.5519	-0.0003	0.001
7	3	10	8	2	11	1279.3985	1279.3978	0.0007	0.003
7	3	9	8	2	10	1279.4348	1279.4345	0.0003	0.003

N'	v'	J'	N''	v''	J''	Observed	Calculated	Obs-Calc	Uncertainty
7	3	8	8	2	9	1279.4717	1279.4719	-0.0002	0.003
7	3	7	8	2	8	1279.5091	1279.5092	-0.0001	0.003
7	3	6	8	2	7	1279.5450	1279.5458	-0.0008	0.003
7	3	5	8	2	6	1279.5823	1279.5811	0.0012	0.003
7	3	4	8	2	5	1279.6149	1279.6146	0.0003	0.003
9	3	6	8	2	5	1451.6790	1451.6788	0.0002	0.001
9	3	7	8	2	6	1451.6974	1451.6976	-0.0002	0.001
9	3	8	8	2	7	1451.7159	1451.7162	-0.0003	0.001
9	3	9	8	2	8	1451.7340	1451.7345	-0.0005	0.001
9	3	10	8	2	9	1451.7519	1451.7525	-0.0006	0.001
9	3	11	8	2	10	1451.7695	1451.7699	-0.0004	0.001
9	3	12	8	2	11	1451.7858	1451.7866	-0.0008	0.001
8	3	11	9	2	12	1266.3870	1266.3863	0.0008	0.001
8	3	10	9	2	11	1266.4232	1266.4237	-0.0005	0.001
8	3	9	9	2	10	1266.4610	1266.4617	-0.0007	0.001
8	3	8	9	2	9	1266.4995	1266.4995	0.0000	0.001
8	3	7	9	2	8	1266.5362	1266.5366	-0.0004	0.001
8	3	6	9	2	7	1266.5709	1266.5725	-0.0016	0.001
8	3	5	9	2	6	1266.6078	1266.6069	0.0010	0.001
10	3	7	9	2	6	1458.5142	1458.5144	-0.0002	0.001
10	3	8	9	2	7	1458.5341	1458.5318	0.0023	0.001
10	3	9	9	2	8	1458.5491	1458.5488	0.0003	0.001
10	3	10	9	2	9	1458.5645	1458.5656	-0.0011	0.001
10	3	11	9	2	10	1458.5803	1458.5819	-0.0016	0.001
10	3	12	9	2	11	1458.5970	1458.5978	-0.0008	0.001
10	3	13	9	2	12	1458.6124	1458.6130	-0.0006	0.001
9	3	12	10	2	13	1253.0999	1253.0985	0.0014	0.003
9	3	11	10	2	12	1253.1369	1253.1367	0.0002	0.003
9	3	10	10	2	11	1253.1749	1253.1752	-0.0003	0.003
9	3	9	10	2	10	1253.2125	1253.2135	-0.0010	0.003
9	3	8	10	2	9	1253.2515	1253.2511	0.0004	0.003
9	3	7	10	2	8	1253.2860	1253.2876	-0.0016	0.003
9	3	6	10	2	7	1253.3216	1253.3228	-0.0012	0.003
11	3	8	10	2	7	1464.9343	1464.9340	0.0003	0.001
11	3	9	10	2	8	1464.9501	1464.9499	0.0002	0.001
11	3	10	10	2	9	1464.9632	1464.9653	-0.0021	0.001
11	3	11	10	2	10	1464.9795	1464.9805	-0.0010	0.001
11	3	12	10	2	11	1464.9937	1464.9952	-0.0015	0.001

N'	v'	J'	N''	v''	J''	Observed	Calculated	Obs-Calc	Uncertainty
11	3	13	10	2	12	1465.0095	1465.0094	0.0001	0.001
11	3	14	10	2	13	1465.0224	1465.0230	-0.0006	0.001
10	3	13	11	2	14	1239.5408	1239.5407	0.0001	0.003
10	3	12	11	2	13	1239.5794	1239.5797	-0.0003	0.003
10	3	11	11	2	12	1239.6186	1239.6187	-0.0001	0.003
10	3	10	11	2	11	1239.6557	1239.6575	-0.0018	0.003
10	3	9	11	2	10	1239.6946	1239.6956	-0.0010	0.003
10	3	8	11	2	9	1239.7328	1239.7327	0.0001	0.003
10	3	7	11	2	8	1239.7685	1239.7686	-0.0001	0.003
12	3	9	11	2	8	1470.9285	1470.9294	-0.0009	0.001
12	3	10	11	2	9	1470.9433	1470.9437	-0.0004	0.001
12	3	11	11	2	10	1470.9589	1470.9575	0.0014	0.001
12	3	12	11	2	11	1470.9709	1470.9709	0.0000	0.001
12	3	13	11	2	12	1470.9837	1470.9839	-0.0002	0.001
12	3	14	11	2	13	1470.9959	1470.9965	-0.0006	0.001
12	3	15	11	2	14	1471.0079	1471.0085	-0.0006	0.001
11	3	14	12	2	15	1225.7198	1225.7189	0.0009	0.001
11	3	13	12	2	14	1225.7581	1225.7585	-0.0004	0.001
11	3	12	12	2	13	1225.7969	1225.7982	-0.0013	0.001
11	3	11	12	2	12	1225.8376	1225.8375	0.0001	0.001
11	3	10	12	2	11	1225.8752	1225.8761	-0.0009	0.001
11	3	9	12	2	10	1225.9137	1225.9138	-0.0001	0.001
11	3	8	12	2	9	1225.9497	1225.9503	-0.0006	0.001
13	3	10	12	2	9	1476.4901	1476.4924	-0.0023	0.002
13	3	11	12	2	10	1476.5053	1476.5049	0.0004	0.001
13	3	12	12	2	11	1476.5171	1476.5170	0.0001	0.001
13	3	13	12	2	12	1476.5281	1476.5288	-0.0007	0.001
13	3	14	12	2	13	1476.5410	1476.5400	0.0010	0.001
13	3	15	12	2	14	1476.5509	1476.5509	0.0000	0.001
13	3	16	12	2	15	1476.5617	1476.5612	0.0005	0.001
12	3	15	13	2	16	1211.6411	1211.6389	0.0022	0.001
12	3	14	13	2	15	1211.6804	1211.6792	0.0012	0.001
12	3	13	13	2	14	1211.7199	1211.7194	0.0005	0.001
12	3	12	13	2	13	1211.7591	1211.7592	-0.0001	0.001
12	3	11	13	2	12	1211.7981	1211.7983	-0.0002	0.001
12	3	10	13	2	11	1211.8366	1211.8365	0.0001	0.001
12	3	9	13	2	10	1211.8754	1211.8736	0.0018	0.001
14	3	11	13	2	10	1481.6178	1481.6145	0.0033	0.002

N'	v'	J'	N''	v''	J''	Observed	Calculated	Obs-Calc	Uncertainty
14	3	12	13	2	11	1481.6286	1481.6254	0.0032	0.002
14	3	13	13	2	12	1481.6359	1481.6357	0.0002	0.002
14	3	14	13	2	13	1481.6481	1481.6456	0.0025	0.002
14	3	15	13	2	14	1481.6563	1481.6551	0.0012	0.002
14	3	16	13	2	15	1481.6676	1481.6642	0.0034	0.002
14	3	17	13	2	16	1481.6762	1481.6728	0.0034	0.002
13	3	16	14	2	17	1197.3078	1197.3063	0.0015	0.001
13	3	15	14	2	16	1197.3473	1197.3472	0.0001	0.001
13	3	14	14	2	15	1197.3865	1197.3879	-0.0014	0.001
13	3	13	14	2	14	1197.4279	1197.4282	-0.0003	0.001
13	3	12	14	2	13	1197.4679	1197.4678	0.0001	0.001
13	3	11	14	2	12	1197.5063	1197.5065	-0.0002	0.001
13	3	10	14	2	11	1197.5432	1197.5442	-0.0010	0.001
15	3	12	14	2	11	1486.2899	1486.2877	0.0022	0.002
15	3	13	14	2	12	1486.2899	1486.2967	-0.0068	0.1
15	3	14	14	2	13	1486.3094	1486.3052	0.0042	0.003
15	3	15	14	2	14	1486.3094	1486.3133	-0.0039	0.003
15	3	16	14	2	15	1486.3200	1486.3209	-0.0009	0.001
15	3	17	14	2	16	1486.3266	1486.3281	-0.0015	0.001
15	3	18	14	2	17	1486.3353	1486.3349	0.0004	0.001
14	3	17	15	2	18	1182.7270	1182.7264	0.0006	0.001
14	3	16	15	2	17	1182.7681	1182.7678	0.0003	0.001
14	3	15	15	2	16	1182.8087	1182.8091	-0.0004	0.001
14	3	14	15	2	15	1182.8492	1182.8498	-0.0006	0.001
14	3	13	15	2	14	1182.8881	1182.8899	-0.0018	0.001
14	3	12	15	2	13	1182.9279	1182.9291	-0.0012	0.001
14	3	11	15	2	12	1182.9683	1182.9673	0.0010	0.001
16	3	13	15	2	12	1490.5116	1490.5034	0.0082	1
16	3	14	15	2	13	1490.5116	1490.5106	0.0011	0.002
16	3	15	15	2	14	1490.5116	1490.5172	-0.0056	0.004
16	3	16	15	2	15	1490.5281	1490.5233	0.0048	0.004
16	3	17	15	2	16	1490.5281	1490.5290	-0.0009	0.002
16	3	18	15	2	17	1490.5382	1490.5343	0.0039	0.002
16	3	19	15	2	18	1490.5382	1490.5392	-0.0010	0.001
15	3	18	16	2	19	1167.9043	1167.9042	0.0001	0.001
15	3	17	16	2	18	1167.9459	1167.9462	-0.0003	0.001
15	3	16	16	2	17	1167.9885	1167.9880	0.0005	0.001
15	3	15	16	2	16	1168.0314	1168.0292	0.0022	0.001

N'	v'	J'	N''	v''	J''	Observed	Calculated	Obs-Calc	Uncertainty
15	3	14	16	2	15	1168.0702	1168.0697	0.0005	0.001
15	3	13	16	2	14	1168.1086	1168.1094	-0.0008	0.001
15	3	12	16	2	13	1168.1482	1168.1481	0.0001	0.001
17	3	14	16	2	13	1494.2567	1494.2535	0.0033	0.002
17	3	15	16	2	14	1494.2567	1494.2586	-0.0019	0.002
17	3	16	16	2	15	1494.2658	1494.2633	0.0025	0.002
17	3	17	16	2	16	1494.2658	1494.2675	-0.0017	0.002
17	3	18	16	2	17	1494.2658	1494.2712	-0.0054	0.003
17	3	19	16	2	18	1494.2800	1494.2745	0.0055	0.1
17	3	20	16	2	19	1494.2800	1494.2774	0.0026	0.002
16	3	19	17	2	20	1152.8442	1152.8446	-0.0004	0.001
16	3	18	17	2	19	1152.8875	1152.8872	0.0004	0.001
16	3	17	17	2	18	1152.9306	1152.9294	0.0012	0.001
16	3	16	17	2	17	1152.9712	1152.9711	0.0002	0.001
16	3	15	17	2	16	1153.0111	1153.0120	-0.0009	0.001
16	3	14	17	2	15	1153.0529	1153.0522	0.0007	0.001
16	3	13	17	2	14	1153.0907	1153.0913	-0.0006	0.001
18	3	17	17	2	16	1497.5296	1497.5352	-0.0056	0.002
18	3	15	17	2	14	1497.5296	1497.5295	0.0001	0.001
18	3	16	17	2	15	1497.5296	1497.5326	-0.0030	0.002
18	3	18	17	2	17	1497.5440	1497.5374	0.0066	1
18	3	19	17	2	18	1497.5440	1497.5390	0.0050	1
18	3	20	17	2	19	1497.5440	1497.5403	0.0037	0.003
18	3	21	17	2	20	1497.5440	1497.5412	0.0028	0.002
17	3	20	18	2	21	1137.5515	1137.5520	-0.0005	0.001
17	3	19	18	2	20	1137.5942	1137.5951	-0.0009	0.001
17	3	18	18	2	19	1137.6367	1137.6378	-0.0011	0.001
17	3	17	18	2	18	1137.6818	1137.6799	0.0019	0.001
17	3	16	18	2	17	1137.7226	1137.7213	0.0013	0.001
17	3	15	18	2	16	1137.7627	1137.7619	0.0008	0.001
17	3	14	18	2	15	1137.8036	1137.8015	0.0021	0.001
19	3	18	18	2	17	1500.3252	1500.3248	0.0004	0.001
19	3	19	18	2	18	1500.3252	1500.3249	0.0004	0.002
19	3	20	18	2	19	1500.3252	1500.3244	0.0008	0.001
19	3	21	18	2	20	1500.3252	1500.3236	0.0017	0.001
19	3	22	18	2	21	1500.3252	1500.3223	0.0029	0.001
19	3	16	18	2	15	1500.3252	1500.3233	0.0019	0.001
19	3	17	18	2	16	1500.3252	1500.3243	0.0009	0.001

N'	v'	J'	N''	v''	J''	Observed	Calculated	Obs-Calc	Uncertainty
20	3	19	19	2	18	1502.6154	1502.6240	-0.0086	1
20	3	20	19	2	19	1502.6154	1502.6218	-0.0064	0.003
20	3	21	19	2	20	1502.6154	1502.6192	-0.0038	0.003
20	3	22	19	2	21	1502.6154	1502.6161	-0.0007	0.001
20	3	23	19	2	22	1502.6154	1502.6127	0.0027	0.003
20	3	17	19	2	16	1502.6154	1502.6268	-0.0114	0.1
20	3	18	19	2	17	1502.6154	1502.6257	-0.0103	1
21	3	20	20	2	19	1504.4007	1504.4248	-0.0241	1
21	3	21	20	2	20	1504.4007	1504.4204	-0.0197	0.1
21	3	22	20	2	21	1504.4007	1504.4155	-0.0148	1
21	3	23	20	2	22	1504.4007	1504.4101	-0.0094	1
21	3	24	20	2	23	1504.4007	1504.4044	-0.0037	0.003
21	3	18	20	2	17	1504.4007	1504.4321	-0.0314	1
21	3	19	20	2	18	1504.4007	1504.4288	-0.0281	1
22	3	19	21	2	18	1505.6792	1505.7316	-0.0524	1
22	3	20	21	2	19	1505.6792	1505.7259	-0.0467	1
22	3	21	21	2	20	1505.6965	1505.7196	-0.0231	1
22	3	22	21	2	21	1505.6965	1505.7128	-0.0163	1
22	3	23	21	2	22	1505.6965	1505.7055	-0.0090	1
22	3	24	21	2	23	1505.6965	1505.6979	-0.0014	0.001
22	3	25	21	2	24	1505.6965	1505.6898	0.0067	1

Lines from R.-D. Urban and H. Jones, Chem. Phys. Lett. 163 (1989) 34-40

1	1	4	2	0	5	1467.8086	1467.8115	-0.0029	0.001
1	1	3	2	0	4	1467.8456	1467.8408	0.0048	0.004
1	1	2	2	0	3	1467.9094	1467.9151	-0.0057	0.004
2	1	5	3	0	6	1455.9754	1455.9773	-0.0019	0.001
2	1	4	3	0	5	1456.0095	1456.0091	0.0004	0.001
3	1	6	4	0	7	1443.8375	1443.8414	-0.0039	0.001
3	1	5	4	0	6	1443.8720	1443.8748	-0.0028	0.001
3	1	4	4	0	5	1443.9126	1443.9128	-0.0002	0.001
3	1	3	4	0	4	1443.9517	1443.9517	0.0000	0.001
3	1	2	4	0	3	1443.9895	1443.9887	0.0008	0.001
3	1	1	4	0	2	1444.0233	1444.0222	0.0012	0.001
4	1	7	5	0	8	1431.4098	1431.4117	-0.0019	0.001
4	1	6	5	0	7	1431.4450	1431.4462	-0.0012	0.001
4	1	5	5	0	6	1431.4831	1431.4833	-0.0002	0.001

N'	v'	J'	N''	v''	J''	Observed	Calculated	Obs-Calc	Uncertainty
4	1	4	5	0	5	1431.5221	1431.5211	0.0011	0.001
4	1	3	5	0	4	1431.5581	1431.5576	0.0005	0.001
4	1	2	5	0	3	1431.5931	1431.5920	0.0011	0.001
4	1	1	5	0	2	1431.6244	1431.6234	0.0011	0.001
5	1	8	6	0	9	1418.6955	1418.6955	0.0000	0.001
5	1	7	6	0	8	1418.7303	1418.7310	-0.0007	0.001
6	1	9	7	0	10	1405.6994	1405.7003	-0.0009	0.001
6	1	8	7	0	9	1405.7353	1405.7366	-0.0013	0.001
6	1	7	7	0	8	1405.7729	1405.7740	-0.0011	0.001
6	1	6	7	0	7	1405.8107	1405.8115	-0.0008	0.001
6	1	5	7	0	6	1405.8475	1405.8484	-0.0009	0.001
6	1	4	7	0	5	1405.8841	1405.8840	0.0001	0.001
6	1	3	7	0	4	1405.9167	1405.9178	-0.0011	0.001
7	1	10	8	0	11	1392.4321	1392.4333	-0.0012	0.001
7	1	9	8	0	10	1392.4701	1392.4702	-0.0001	0.001
7	1	8	8	0	9	1392.5072	1392.5080	-0.0008	0.001
7	1	7	8	0	8	1392.5457	1392.5458	-0.0001	0.001
7	1	6	8	0	7	1392.5816	1392.5831	-0.0015	0.001
7	1	5	8	0	6	1392.6184	1392.6192	-0.0008	0.001
7	1	4	8	0	5	1392.6532	1392.6538	-0.0006	0.001
8	1	11	9	0	12	1378.9013	1378.9015	-0.0002	0.001
8	1	10	9	0	11	1378.9390	1378.9392	-0.0002	0.001
8	1	9	9	0	10	1378.9768	1378.9774	-0.0006	0.001
8	1	8	9	0	9	1379.0148	1379.0155	-0.0007	0.001
8	1	7	9	0	8	1379.0524	1379.0531	-0.0007	0.001
8	1	6	9	0	7	1379.0903	1379.0898	0.0006	0.001
8	1	5	9	0	6	1379.1244	1379.1251	-0.0007	0.001
9	1	12	10	0	13	1365.1130	1365.1122	0.0009	0.001
9	1	11	10	0	12	1365.1512	1365.1504	0.0008	0.001
9	1	10	10	0	11	1365.1904	1365.1891	0.0013	0.001
9	1	9	10	0	10	1365.2277	1365.2276	0.0001	0.001
9	1	8	10	0	9	1365.2681	1365.2656	0.0025	0.001
9	1	7	10	0	8	1365.3037	1365.3027	0.0010	0.001
9	1	6	10	0	7	1365.3414	1365.3387	0.0027	0.001
10	1	13	11	0	14	1351.0738	1351.0722	0.0016	0.001
10	1	12	11	0	13	1351.1130	1351.1110	0.0020	0.001
10	1	11	11	0	12	1351.1514	1351.1501	0.0013	0.001
10	1	10	11	0	11	1351.1907	1351.1890	0.0017	0.001

N'	v'	J'	N''	v''	J''	Observed	Calculated	Obs-Calc	Uncertainty
10	1	9	11	0	10	1351.2284	1351.2274	0.0010	0.001
10	1	8	11	0	9	1351.2656	1351.2650	0.0006	0.001
10	1	7	11	0	8	1351.3027	1351.3015	0.0012	0.001
16	1	19	17	0	20	1261.9857	1261.9451	0.0406	1
16	1	18	17	0	19	1262.0271	1261.9869	0.0402	1
16	1	17	17	0	18	1262.0679	1262.0284	0.0395	1
16	1	16	17	0	17	1262.1085	1262.0695	0.0390	1
16	1	15	17	0	16	1262.1483	1262.1100	0.0383	1
16	1	14	17	0	15	1262.1874	1262.1499	0.0375	1
16	1	13	17	0	14	1262.2289	1262.1890	0.0399	1
12	2	9	11	1	8	1535.5121	1535.5133	-0.0012	0.001
12	2	10	11	1	9	1535.5289	1535.5294	-0.0005	0.001
12	2	11	11	1	10	1535.5447	1535.5452	-0.0005	0.001
12	2	12	11	1	11	1535.5598	1535.5606	-0.0008	0.001
12	2	13	11	1	12	1535.5747	1535.5757	-0.0010	0.001
12	2	14	11	1	13	1535.5898	1535.5905	-0.0007	0.001
12	2	15	11	1	14	1535.6031	1535.6048	-0.0017	0.001
13	2	16	14	1	17	1253.4648	1253.4652	-0.0004	0.001
13	2	15	14	1	16	1253.5054	1253.5059	-0.0005	0.001
13	2	14	14	1	15	1253.5450	1253.5464	-0.0014	0.001
13	2	13	14	1	14	1253.5861	1253.5866	-0.0005	0.001
13	2	12	14	1	13	1253.6255	1253.6262	-0.0007	0.001
13	2	11	14	1	12	1253.6629	1253.6651	-0.0022	0.001
13	2	10	14	1	11	1253.7035	1253.7029	0.0006	0.001
15	2	12	14	1	11	1552.3491	1552.3501	-0.0010	0.001
15	2	13	14	1	12	1552.3607	1552.3613	-0.0006	0.001
15	2	14	14	1	13	1552.3719	1552.3721	-0.0002	0.001
15	2	15	14	1	14	1552.3819	1552.3824	-0.0005	0.001
15	2	16	14	1	15	1552.3922	1552.3925	-0.0003	0.001
15	2	17	14	1	16	1552.4025	1552.4022	0.0003	0.001
15	2	18	14	1	17	1552.4117	1552.4116	0.0001	0.001
14	2	17	15	1	18	1238.7118	1238.7121	-0.0003	0.001
14	2	16	15	1	17	1238.7534	1238.7533	0.0001	0.001
14	2	15	15	1	16	1238.7941	1238.7943	-0.0002	0.001
14	2	14	15	1	15	1238.8351	1238.8350	0.0001	0.001
14	2	13	15	1	14	1238.8749	1238.8750	-0.0001	0.001
14	2	12	15	1	13	1238.9138	1238.9142	-0.0004	0.001
14	2	11	15	1	12	1238.9525	1238.9525	0.0000	0.001

N'	v'	J'	N''	v''	J''	Observed	Calculated	Obs-Calc	Uncertainty
5	3	3	4	2	2	1420.3590	1420.3595	-0.0005	0.001
5	3	4	4	2	3	1420.3850	1420.3836	0.0014	0.001
5	3	5	4	2	4	1420.4086	1420.4084	0.0002	0.001
5	3	6	4	2	5	1420.4334	1420.4334	0.0000	0.001
5	3	7	4	2	6	1420.4587	1420.4575	0.0012	0.001
5	3	8	4	2	7	1420.4808	1420.4791	0.0017	0.001
6	3	3	5	2	2	1428.7556	1428.7564	-0.0008	0.001
6	3	4	5	2	3	1428.7782	1428.7787	-0.0005	0.001
6	3	5	5	2	4	1428.8009	1428.8014	-0.0005	0.001
6	3	6	5	2	5	1428.8234	1428.8245	-0.0011	0.001
6	3	7	5	2	6	1428.8475	1428.8475	0.0000	0.001
6	3	8	5	2	7	1428.8693	1428.8697	-0.0004	0.001
6	3	9	5	2	8	1428.8901	1428.8902	-0.0001	0.001
6	3	9	7	2	10	1292.1273	1292.1268	0.0005	0.001
6	3	8	7	2	9	1292.1620	1292.1626	-0.0006	0.001
6	3	7	7	2	8	1292.1986	1292.1995	-0.0009	0.001
6	3	6	7	2	7	1292.2358	1292.2365	-0.0007	0.001
6	3	5	7	2	6	1292.2717	1292.2726	-0.0009	0.001
6	3	4	7	2	5	1292.3069	1292.3072	-0.0003	0.001
7	3	10	8	2	11	1279.3979	1279.3978	0.0001	0.001
7	3	9	8	2	10	1279.4342	1279.4345	-0.0003	0.001
7	3	8	8	2	9	1279.4711	1279.4719	-0.0008	0.001
7	3	7	8	2	8	1279.5089	1279.5092	-0.0003	0.001
7	3	6	8	2	7	1279.5461	1279.5458	0.0003	0.001
7	3	5	8	2	6	1279.5817	1279.5811	0.0006	0.001
7	3	4	8	2	5	1279.6148	1279.6146	0.0002	0.001
9	3	12	10	2	13	1253.0974	1253.0985	-0.0011	0.001
9	3	11	10	2	12	1253.1356	1253.1367	-0.0011	0.001
9	3	10	10	2	11	1253.1757	1253.1752	0.0005	0.001
9	3	9	10	2	10	1253.2121	1253.2135	-0.0014	0.001
9	3	8	10	2	9	1253.2494	1253.2511	-0.0017	0.001
9	3	7	10	2	8	1253.2863	1253.2876	-0.0013	0.001
9	3	6	10	2	7	1253.3219	1253.3228	-0.0009	0.001
10	3	13	11	2	14	1239.5417	1239.5407	0.0010	0.001
10	3	12	11	2	13	1239.5803	1239.5797	0.0007	0.001
10	3	11	11	2	12	1239.6193	1239.6187	0.0006	0.001
10	3	10	11	2	11	1239.6576	1239.6575	0.0001	0.001
10	3	9	11	2	10	1239.6954	1239.6956	-0.0002	0.001

N'	v'	J'	N''	v''	J''	Observed	Calculated	Obs-Calc	Uncertainty
10	3	8	11	2	9	1239.7330	1239.7327	0.0003	0.001
10	3	7	11	2	8	1239.7694	1239.7686	0.0008	0.001
19	3	19	18	2	18	1500.3247	1500.3249	-0.0002	0.001

A.2 Line list for MnD

Table A.2: Line list for MnD.

N'	v'	J'	N''	v''	J''	Observed	Calculated	Obs-Calc	Uncertainty
2	1	5	3	0	6	1058.3052	1058.3104	-0.00519	0.005
2	1	4	3	0	5	1058.33	1058.3263	0.00375	0.005
2	1	3	3	0	4	1058.3519	1058.3471	0.00481	0.005
2	1	2	3	0	3	1058.3678	1058.3688	-0.00095	0.001
2	1	1	3	0	2	1058.3843	1058.3884	-0.00413	0.004
2	1	5	1	0	4	1087.1005	1087.0944	0.00607	0.01
3	1	6	4	0	7	1052.2299	1052.2317	-0.00177	0.003
3	1	5	4	0	6	1052.2485	1052.2482	0.00032	0.003
3	1	4	4	0	5	1052.2657	1052.2671	-0.00135	0.003
3	1	3	4	0	4	1052.2894	1052.2865	0.00294	0.003
3	1	2	4	0	3	1052.3067	1052.3051	0.00162	0.003
3	1	1	4	0	2	1052.3193	1052.3221	-0.00276	0.003
3	1	0	4	0	1	1052.3323	1052.337	-0.00473	0.1
3	1	2	2	0	1	1092.4103	1092.4078	0.00254	0.003
3	1	3	2	0	2	1092.4218	1092.4248	-0.00298	0.003
3	1	4	2	0	3	1092.4344	1092.4433	-0.00893	1
3	1	5	2	0	4	1092.4617	1092.4612	0.00047	0.001
3	1	6	2	0	5	1092.4774	1092.4752	0.0022	0.003
4	1	7	5	0	8	1046.0428	1046.0435	-0.00074	0.003
4	1	6	5	0	7	1046.0587	1046.0605	-0.00181	0.003
4	1	5	5	0	6	1046.0801	1046.0789	0.00119	0.003
4	1	4	5	0	5	1046.1003	1046.0977	0.00262	0.003
4	1	3	5	0	4	1046.1187	1046.116	0.00267	0.003
4	1	2	5	0	3	1046.134	1046.1334	0.0006	0.003
4	1	1	5	0	2	1046.1468	1046.1495	-0.00266	0.003

N'	v'	J'	N''	v''	J''	Observed	Calculated	Obs-Calc	Uncertainty
4	1	1	3	0	0	1097.6434	1097.6446	-0.0012	0.001
4	1	2	3	0	1	1097.6562	1097.658	-0.00184	0.001
4	1	3	3	0	2	1097.6703	1097.6726	-0.0023	0.003
4	1	4	3	0	3	1097.6829	1097.6882	-0.00526	0.1
4	1	5	3	0	4	1097.7013	1097.7042	-0.00288	0.003
4	1	6	3	0	5	1097.7195	1097.7198	-0.00028	0.003
4	1	7	3	0	6	1097.734	1097.7337	0.00033	0.003
5	1	8	6	0	9	1039.7474	1039.748	-0.00058	0.001
5	1	6	6	0	7	1039.7841	1039.7837	0.00045	0.001
5	1	5	6	0	6	1039.8011	1039.8022	-0.00114	0.001
5	1	4	6	0	5	1039.8211	1039.8206	0.00054	0.001
5	1	3	6	0	4	1039.8384	1039.8382	0.00018	0.001
5	1	2	6	0	3	1039.854	1039.8549	-0.00092	0.001
5	1	2	4	0	1	1102.7833	1102.7817	0.0016	0.003
5	1	3	4	0	2	1102.7927	1102.7954	-0.00274	0.003
5	1	4	4	0	3	1102.8069	1102.8098	-0.00285	0.003
5	1	5	4	0	4	1102.8216	1102.8245	-0.00292	0.003
5	1	6	4	0	5	1102.837	1102.8395	-0.00245	0.003
5	1	7	4	0	6	1102.8553	1102.8541	0.00123	0.003
5	1	8	4	0	7	1102.8699	1102.8677	0.00218	0.003
6	1	9	7	0	10	1033.3474	1033.347	0.00044	0.003
6	1	8	7	0	9	1033.3643	1033.3646	-0.00033	0.003
6	1	7	7	0	8	1033.383	1033.383	0	0.003
6	1	6	7	0	7	1033.401	1033.4016	-0.00059	0.003
6	1	5	7	0	6	1033.4201	1033.42	0.00011	0.003
6	1	4	7	0	5	1033.4368	1033.4379	-0.00109	0.003
6	1	3	7	0	4	1033.4545	1033.4551	-0.00056	0.003
6	1	3	5	0	2	1107.7913	1107.7921	-0.00075	0.002
6	1	4	5	0	3	1107.8057	1107.8057	-0.00001	0.002
6	1	5	5	0	4	1107.8181	1107.8197	-0.00157	0.002
6	1	6	5	0	5	1107.8329	1107.8339	-0.00095	0.002
6	1	7	5	0	6	1107.8484	1107.8481	0.00033	0.002
6	1	8	5	0	7	1107.8628	1107.8621	0.00075	0.001
6	1	9	5	0	8	1107.8768	1107.8754	0.0014	0.002
7	1	10	8	0	11	1026.8427	1026.8424	0.00031	0.002
7	1	9	8	0	10	1026.8604	1026.8603	0.00006	0.002
7	1	8	8	0	9	1026.8795	1026.8788	0.00067	0.002
7	1	7	8	0	8	1026.898	1026.8975	0.00051	0.002

N'	v'	J'	N''	v''	J''	Observed	Calculated	Obs-Calc	Uncertainty
7	1	6	8	0	7	1026.9168	1026.916	0.00079	0.002
7	1	5	8	0	6	1026.9328	1026.9341	-0.00134	0.002
7	1	4	8	0	5	1026.9499	1026.9517	-0.00178	0.002
7	1	4	6	0	3	1112.6743	1112.674	0.00028	0.001
7	1	5	6	0	4	1112.6865	1112.6874	-0.00094	0.001
7	1	6	6	0	5	1112.7006	1112.701	-0.00042	0.001
7	1	7	6	0	6	1112.7139	1112.7147	-0.00079	0.001
7	1	8	6	0	7	1112.7275	1112.7283	-0.00084	0.001
7	1	9	6	0	8	1112.7418	1112.7418	0.00002	0.001
7	1	10	6	0	9	1112.7553	1112.7548	0.00052	0.001
8	1	11	9	0	12	1020.2352	1020.2362	-0.00097	0.002
8	1	10	9	0	11	1020.2544	1020.2544	0.00003	0.002
8	1	9	9	0	10	1020.2731	1020.273	0.00009	0.002
8	1	8	9	0	9	1020.2926	1020.2918	0.00082	0.002
8	1	7	9	0	8	1020.311	1020.3104	0.00056	0.002
8	1	6	9	0	7	1020.329	1020.3288	0.00022	0.001
8	1	5	9	0	6	1020.3466	1020.3466	-0.00004	0.001
8	1	5	7	0	4	1117.427	1117.4258	0.0012	0.001
8	1	6	7	0	5	1117.4384	1117.4389	-0.0005	0.001
8	1	7	7	0	6	1117.4521	1117.4521	0.00002	0.001
8	1	8	7	0	7	1117.465	1117.4653	-0.00028	0.001
8	1	9	7	0	8	1117.4779	1117.4784	-0.00052	0.001
8	1	10	7	0	9	1117.4918	1117.4914	0.00043	0.001
8	1	11	7	0	10	1117.5049	1117.504	0.00091	0.001
9	1	12	10	0	13	1013.5313	1013.5302	0.00111	0.002
9	1	11	10	0	12	1013.5493	1013.5486	0.00067	0.002
9	1	10	10	0	11	1013.5686	1013.5674	0.00118	0.002
9	1	9	10	0	10	1013.5864	1013.5863	0.00008	0.002
9	1	8	10	0	9	1013.6045	1013.6051	-0.00063	0.002
9	1	7	10	0	8	1013.6231	1013.6237	-0.00058	0.002
9	1	6	10	0	7	1013.6407	1013.6418	-0.00111	0.002
9	1	6	8	0	5	1122.0448	1122.0456	-0.00076	0.002
9	1	7	8	0	6	1122.0575	1122.0583	-0.00081	0.002
9	1	8	8	0	7	1122.0704	1122.0711	-0.00067	0.002
9	1	9	8	0	8	1122.0831	1122.0838	-0.00071	0.002
9	1	10	8	0	9	1122.0965	1122.0965	0.00004	0.002
9	1	11	8	0	10	1122.1108	1122.1089	0.00186	0.002
9	1	12	8	0	11	1122.1231	1122.1212	0.00194	0.002

N'	v'	J'	N''	v''	J''	Observed	Calculated	Obs-Calc	Uncertainty
10	1	13	11	0	14	1006.7269	1006.7263	0.00056	0.001
10	1	12	11	0	13	1006.7451	1006.745	0.00011	0.001
10	1	11	11	0	12	1006.7647	1006.7639	0.00076	0.001
10	1	10	11	0	11	1006.7835	1006.783	0.00052	0.001
10	1	9	11	0	10	1006.8021	1006.802	0.00015	0.001
10	1	8	11	0	9	1006.8207	1006.8207	0.00002	0.001
10	1	7	11	0	8	1006.8383	1006.8391	-0.00077	0.001
10	1	7	9	0	6	1126.5351	1126.5315	0.00363	0.002
10	1	8	9	0	7	1126.5445	1126.5438	0.00066	0.001
10	1	9	9	0	8	1126.5575	1126.5562	0.00133	0.001
10	1	10	9	0	9	1126.5691	1126.5684	0.00066	0.001
10	1	11	9	0	10	1126.5814	1126.5806	0.00078	0.001
10	1	12	9	0	11	1126.5939	1126.5926	0.00126	0.001
10	1	13	9	0	12	1126.6064	1126.6044	0.00198	0.001
11	1	14	12	0	15	999.82742	999.82649	0.00093	0.002
11	1	13	12	0	14	999.84556	999.84534	0.00022	0.002
11	1	12	12	0	13	999.86446	999.86443	0.00003	0.002
11	1	11	12	0	12	999.88324	999.88362	-0.00038	0.002
11	1	10	12	0	11	999.90242	999.90273	-0.00031	0.002
11	1	9	12	0	10	999.9222	999.92165	0.00055	0.002
11	1	8	12	0	9	999.93968	999.94026	-0.00058	0.002
11	1	8	10	0	7	1130.8794	1130.8817	-0.00229	0.003
11	1	9	10	0	8	1130.8907	1130.8937	-0.00295	0.003
11	1	10	10	0	9	1130.9033	1130.9055	-0.00224	0.003
11	1	11	10	0	10	1130.9159	1130.9174	-0.00145	0.003
11	1	12	10	0	11	1130.9284	1130.9291	-0.00065	0.003
11	1	13	10	0	12	1130.9409	1130.9406	0.0003	0.003
11	1	14	10	0	13	1130.9534	1130.952	0.00145	0.003
12	1	15	13	0	16	992.83255	992.8325	0.00005	0.002
12	1	14	13	0	15	992.85059	992.85152	-0.00093	0.002
12	1	13	13	0	14	992.87189	992.87076	0.00113	0.002
12	1	12	13	0	13	992.89081	992.89008	0.00073	0.002
12	1	11	13	0	12	992.90986	992.90935	0.00051	0.002
12	1	10	13	0	11	992.92851	992.92844	0.00007	0.001
12	1	9	13	0	10	992.9458	992.94725	-0.00145	0.002
12	1	9	11	0	8	1135.0917	1135.0944	-0.00269	0.002
12	1	10	11	0	9	1135.103	1135.1059	-0.00292	0.002
12	1	11	11	0	10	1135.1157	1135.1174	-0.00166	0.001

N'	v'	J'	N''	v''	J''	Observed	Calculated	Obs-Calc	Uncertainty
12	1	12	11	0	11	1135.1284	1135.1287	-0.0003	0.001
12	1	13	11	0	12	1135.1415	1135.1399	0.00158	0.001
12	1	14	11	0	13	1135.1543	1135.151	0.0033	0.002
12	1	15	11	0	14	1135.1645	1135.1619	0.00261	0.002
13	1	16	14	0	17	985.74577	985.74619	-0.00042	0.001
13	1	15	14	0	16	985.76517	985.76538	-0.00021	0.001
13	1	14	14	0	15	985.78601	985.78476	0.00125	0.001
13	1	13	14	0	14	985.80478	985.80421	0.00057	0.001
13	1	12	14	0	13	985.82351	985.82361	-0.0001	0.001
13	1	11	14	0	12	985.84226	985.84287	-0.00061	0.001
13	1	10	14	0	11	985.86059	985.86187	-0.00128	0.001
13	1	10	12	0	9	1139.1669	1139.1678	-0.00086	0.002
13	1	11	12	0	10	1139.1788	1139.1788	-0.00004	0.002
13	1	12	12	0	11	1139.1922	1139.1898	0.00238	0.003
13	1	13	12	0	12	1139.2058	1139.2007	0.00512	0.01
13	1	14	12	0	13	1139.2192	1139.2114	0.00778	0.01
13	1	15	12	0	14	1139.2192	1139.222	-0.00281	0.003
13	1	16	12	0	15	1139.2325	1139.2324	0.00006	0.002
14	1	17	15	0	18	978.56811	978.5694	-0.00129	0.001
14	1	16	15	0	17	978.59026	978.58874	0.00152	0.001
14	1	15	15	0	16	978.60822	978.60825	-0.00003	0.001
14	1	14	15	0	15	978.62755	978.62782	-0.00027	0.001
14	1	13	15	0	14	978.64646	978.64736	-0.0009	0.001
14	1	12	15	0	13	978.66682	978.66676	0.00006	0.001
14	1	11	15	0	12	978.68641	978.68594	0.00047	0.001
14	1	11	13	0	10	1143.1034	1143.1	0.00343	0.05
14	1	12	13	0	11	1143.1034	1143.1106	-0.0072	0.05
14	1	13	13	0	12	1143.1186	1143.1211	-0.0025	0.05
14	1	14	13	0	13	1143.133	1143.1315	0.00152	0.05
14	1	15	13	0	14	1143.1478	1143.1417	0.00608	0.05
14	1	16	13	0	15	1143.1478	1143.1518	-0.00403	0.05
14	1	17	13	0	16	1143.1611	1143.1618	-0.00067	0.05
15	1	18	16	0	19	971.30483	971.30393	0.0009	0.002
15	1	17	16	0	18	971.32298	971.3234	-0.00042	0.002
15	1	16	16	0	17	971.34223	971.34303	-0.0008	0.002
15	1	15	16	0	16	971.36504	971.36273	0.00231	0.002
15	1	14	16	0	15	971.38294	971.38239	0.00055	0.002
15	1	13	16	0	14	971.40263	971.40193	0.0007	0.002

N'	v'	J'	N''	v''	J''	Observed	Calculated	Obs-Calc	Uncertainty
15	1	12	16	0	13	971.42007	971.42127	-0.0012	0.002
15	1	12	14	0	11	1146.887	1146.8892	-0.00224	0.03
15	1	13	14	0	12	1146.898	1146.8994	-0.00139	0.03
15	1	14	14	0	13	1146.9128	1146.9094	0.00339	0.03
15	1	15	14	0	14	1146.9128	1146.9193	-0.00649	0.03
15	1	16	14	0	15	1146.928	1146.929	-0.00104	0.03
15	1	17	14	0	16	1146.9438	1146.9386	0.00516	0.03
15	1	18	14	0	17	1146.9438	1146.9481	-0.00428	0.03
16	1	19	17	0	20	963.95258	963.95157	0.00101	0.001
16	1	18	17	0	19	963.97018	963.97116	-0.00098	0.001
16	1	17	17	0	18	963.98978	963.9909	-0.00112	0.001
16	1	16	17	0	17	964.01241	964.0107	0.00171	0.001
16	1	15	17	0	16	964.03108	964.03047	0.00061	0.001
16	1	14	17	0	15	964.04951	964.05014	-0.00063	0.001
16	1	13	17	0	14	964.06848	964.06963	-0.00115	0.001
16	1	13	15	0	12	1150.535	1150.5338	0.00122	0.001
16	1	14	15	0	13	1150.5469	1150.5434	0.00346	0.003
16	1	15	15	0	14	1150.5469	1150.553	-0.00606	0.006
16	1	16	15	0	15	1150.5642	1150.5623	0.00186	0.002
16	1	17	15	0	16	1150.5643	1150.5716	-0.00727	0.01
16	1	19	15	0	18	1150.5923	1150.5896	0.00271	0.003
17	1	20	18	0	21	956.51467	956.51406	0.00061	0.001
17	1	19	18	0	20	956.53382	956.53377	0.00005	0.001
17	1	18	18	0	19	956.5524	956.55361	-0.00121	0.001
17	1	17	18	0	18	956.57444	956.57351	0.00093	0.001
17	1	16	18	0	17	956.59337	956.59338	-0.00001	0.001
17	1	15	18	0	16	956.61264	956.61316	-0.00052	0.001
17	1	14	18	0	15	956.6311	956.63278	-0.00168	0.001
17	1	14	16	0	13	1154.033	1154.0318	0.0012	0.003
17	1	15	16	0	14	1154.0479	1154.041	0.00694	0.007
17	1	16	16	0	15	1154.0479	1154.05	-0.00207	0.003
17	1	17	16	0	16	1154.0588	1154.0588	-0.00003	0.003
17	1	18	16	0	17	1154.0676	1154.0675	0.00006	0.003
17	1	19	16	0	18	1154.0762	1154.0761	0.00009	0.003
17	1	20	16	0	19	1154.0857	1154.0845	0.00118	0.003
18	1	21	19	0	22	948.99257	948.99316	-0.00059	0.001
18	1	20	19	0	21	949.01316	949.01296	0.0002	0.001
18	1	19	19	0	20	949.03159	949.03289	-0.0013	0.001

N'	v'	J'	N''	v''	J''	Observed	Calculated	Obs-Calc	Uncertainty
18	1	18	19	0	19	949.05525	949.05288	0.00237	0.001
18	1	17	19	0	18	949.07405	949.07285	0.0012	0.001
18	1	16	19	0	17	949.09194	949.09273	-0.00079	0.001
18	1	15	19	0	16	949.11247	949.11247	0	0.001
18	1	15	17	0	14	1157.3831	1157.3815	0.00157	0.008
18	1	16	17	0	15	1157.394	1157.3902	0.00381	0.008
18	1	17	17	0	16	1157.394	1157.3987	-0.00468	0.008
18	1	18	17	0	17	1157.4055	1157.407	-0.00151	0.008
18	1	19	17	0	18	1157.4178	1157.4152	0.00261	0.008
18	1	20	17	0	19	1157.4292	1157.4232	0.00598	0.008
18	1	21	17	0	20	1157.4292	1157.4311	-0.0019	0.008
19	1	22	20	0	23	941.38978	941.39056	-0.00078	0.001
19	1	21	20	0	22	941.40829	941.41045	-0.00216	0.001
19	1	20	20	0	21	941.4316	941.43046	0.00114	0.001
19	1	19	20	0	20	941.45041	941.45052	-0.00011	0.001
19	1	18	20	0	19	941.47102	941.47057	0.00045	0.001
19	1	17	20	0	18	941.49196	941.49055	0.00141	0.001
19	1	16	20	0	17	941.51079	941.51039	0.0004	0.001
19	1	16	18	0	15	1160.5885	1160.5812	0.00726	0.008
19	1	17	18	0	16	1160.5885	1160.5894	-0.00086	0.002
19	1	18	18	0	17	1160.6028	1160.5973	0.00548	0.006
19	1	19	18	0	18	1160.6028	1160.6051	-0.00232	0.002
19	1	20	18	0	19	1160.6129	1160.6128	0.00015	0.002
19	1	21	18	0	20	1160.6239	1160.6202	0.00366	0.005
19	1	22	18	0	21	1160.6239	1160.6276	-0.00367	0.005
20	1	23	21	0	24	933.70587	933.70795	-0.00208	0.001
20	1	22	21	0	23	933.72788	933.7279	-0.00002	0.001
20	1	21	21	0	22	933.7476	933.74798	-0.00038	0.001
20	1	20	21	0	21	933.76473	933.76811	-0.00338	0.001
20	1	19	21	0	20	933.79142	933.78824	0.00318	0.001
20	1	18	21	0	19	933.80892	933.80829	0.00063	0.001
20	1	17	21	0	18	933.82519	933.82823	-0.00304	0.001
20	1	17	19	0	16	1163.6301	1163.6292	0.00095	0.003
20	1	18	19	0	17	1163.6301	1163.6367	-0.00664	0.007
20	1	19	19	0	18	1163.6437	1163.6442	-0.00046	0.007
20	1	20	19	0	19	1163.6437	1163.6514	-0.0077	0.008
20	1	21	19	0	20	1163.6595	1163.6585	0.00101	0.007
20	1	22	19	0	21	1163.6679	1163.6654	0.00249	0.007

N'	v'	J'	N''	v''	J''	Observed	Calculated	Obs-Calc	Uncertainty
20	1	23	19	0	22	1163.6679	1163.6722	-0.00429	0.007
21	1	24	22	0	25	925.94513	925.94697	-0.00184	0.001
21	1	23	22	0	24	925.96926	925.96698	0.00228	0.001
21	1	22	22	0	23	925.98687	925.98711	-0.00024	0.001
21	1	21	22	0	22	926.01054	926.0073	0.00324	0.001
21	1	20	22	0	21	926.02894	926.02749	0.00145	0.001
21	1	19	22	0	20	926.04587	926.04761	-0.00174	0.001
21	1	18	22	0	19	926.07019	926.06763	0.00256	0.001
21	1	18	20	0	17	1166.5234	1166.5236	-0.00016	0.003
21	1	19	20	0	18	1166.5295	1166.5306	-0.0011	0.004
21	1	20	20	0	19	1166.536	1166.5375	-0.00145	0.003
21	1	21	20	0	20	1166.5436	1166.5441	-0.00054	0.003
21	1	22	20	0	21	1166.5492	1166.5507	-0.00146	0.003
21	1	23	20	0	22	1166.5578	1166.557	0.00078	0.003
21	1	24	20	0	23	1166.5578	1166.5632	-0.00542	0.003
22	1	25	23	0	26	918.107	918.10922	-0.00222	0.001
22	1	24	23	0	25	918.12718	918.12929	-0.00211	0.001
22	1	23	23	0	24	918.15238	918.14947	0.00291	0.001
22	1	22	23	0	23	918.17079	918.1697	0.00109	0.001
22	1	21	23	0	22	918.1899	918.18993	-0.00003	0.001
22	1	20	23	0	21	918.21243	918.21012	0.00231	0.001
22	1	19	21	0	18	1169.2664	1169.2627	0.00368	0.004
22	1	20	21	0	19	1169.2664	1169.2692	-0.00279	0.004
22	1	21	21	0	20	1169.2778	1169.2755	0.00232	0.003
22	1	22	21	0	21	1169.2778	1169.2816	-0.0038	0.004
22	1	23	21	0	22	1169.2891	1169.2875	0.00156	0.002
22	1	24	21	0	23	1169.2891	1169.2933	-0.00422	0.004
22	1	25	21	0	24	1169.2891	1169.2989	-0.00984	1
23	1	26	24	0	27	910.1955	910.1963	-0.0008	0.001
23	1	20	22	0	19	1171.8567	1171.8449	0.01178	1
23	1	21	22	0	20	1171.8567	1171.8508	0.00587	0.006
23	1	22	22	0	21	1171.8567	1171.8565	0.00016	0.002
23	1	23	22	0	22	1171.8567	1171.8621	-0.00536	0.006
23	1	24	22	0	23	1171.8712	1171.8674	0.00378	0.004
23	1	25	22	0	24	1171.8712	1171.8726	-0.00141	0.002
23	1	26	22	0	25	1171.8712	1171.8776	-0.00644	0.007
24	1	26	25	0	27	902.22849	902.22985	-0.00136	0.001
24	1	27	25	0	28	902.22849	902.20972	0.01877	1

N'	v'	J'	N''	v''	J''	Observed	Calculated	Obs-Calc	Uncertainty
24	1	25	25	0	26	902.25265	902.25008	0.00257	0.002
24	1	24	25	0	25	902.27025	902.27037	-0.00012	0.001
24	1	23	25	0	24	902.29534	902.29067	0.00467	1
24	1	22	25	0	23	902.3121	902.31093	0.00117	0.002
24	1	21	23	0	20	1174.2683	1174.2685	-0.00017	0.002
24	1	22	23	0	21	1174.2683	1174.2738	-0.00548	0.007
24	1	23	23	0	22	1174.2818	1174.2789	0.0029	0.003
24	1	24	23	0	23	1174.2818	1174.2838	-0.00203	0.002
24	1	25	23	0	24	1174.2918	1174.2886	0.00321	0.004
24	1	26	23	0	25	1174.2918	1174.2932	-0.00137	0.002
24	1	27	23	0	26	1174.2918	1174.2976	-0.0058	1
25	1	22	24	0	21	1176.5428	1176.5317	0.01115	1
25	1	23	24	0	22	1176.5428	1176.5364	0.00643	0.008
25	1	24	24	0	23	1176.5428	1176.5409	0.00191	0.002
25	1	25	24	0	24	1176.5428	1176.5452	-0.00241	0.002
25	1	26	24	0	25	1176.5428	1176.5494	-0.00656	0.008
25	1	27	24	0	26	1176.5536	1176.5533	0.00027	0.002
25	1	28	24	0	27	1176.5536	1176.5571	-0.00353	0.004
26	1	23	25	0	22	1178.6368	1178.6328	0.004	0.004
26	1	24	25	0	23	1178.6368	1178.6369	-0.00011	0.002
26	1	25	25	0	24	1178.6368	1178.6408	-0.00401	0.004
26	1	26	25	0	25	1178.6368	1178.6445	-0.00771	0.01
26	1	27	25	0	26	1178.6485	1178.648	0.00047	0.002
26	1	28	25	0	27	1178.6485	1178.6514	-0.00288	0.003
26	1	29	25	0	28	1178.6485	1178.6546	-0.00605	0.008
27	1	24	26	0	23	1180.5706	1180.5702	0.00038	0.002
27	1	25	26	0	24	1180.5706	1180.5737	-0.0031	0.003
27	1	26	26	0	25	1180.5807	1180.577	0.00372	0.004
27	1	27	26	0	26	1180.5807	1180.5801	0.00064	0.002
27	1	28	26	0	27	1180.5807	1180.5829	-0.00224	0.002
27	1	29	26	0	28	1180.5807	1180.5857	-0.00495	0.006
27	1	30	26	0	29	1180.5807	1180.5882	-0.00748	0.1
28	1	25	27	0	24	1182.349	1182.3422	0.00676	0.009
28	1	26	27	0	25	1182.349	1182.3451	0.0039	0.006
28	1	27	27	0	26	1182.349	1182.3477	0.00127	0.002
28	1	28	27	0	27	1182.349	1182.3502	-0.00117	0.002
28	1	29	27	0	28	1182.349	1182.3524	-0.00341	0.003
28	1	30	27	0	29	1182.349	1182.3545	-0.00546	0.008

N'	v'	J'	N''	v''	J''	Observed	Calculated	Obs-Calc	Uncertainty
28	1	31	27	0	30	1182.349	1182.3563	-0.00734	0.008
29	1	26	28	0	25	1183.9515	1183.9472	0.00429	0.005
29	1	27	28	0	26	1183.9515	1183.9494	0.00209	0.002
29	1	28	28	0	27	1183.9515	1183.9514	0.0001	0.002
29	1	29	28	0	28	1183.9515	1183.9532	-0.00168	0.002
29	1	30	28	0	29	1183.9515	1183.9548	-0.00326	0.005
29	1	31	28	0	30	1183.9515	1183.9562	-0.00466	0.005
29	1	32	28	0	31	1183.9515	1183.9574	-0.00587	0.008
30	1	27	29	0	26	1185.3851	1185.3835	0.00165	0.002
30	1	28	29	0	27	1185.3851	1185.385	0.0001	0.002
30	1	29	29	0	28	1185.3851	1185.3863	-0.00123	0.002
30	1	30	29	0	29	1185.3851	1185.3874	-0.00234	0.003
30	1	31	29	0	30	1185.3851	1185.3884	-0.00325	0.004
30	1	32	29	0	31	1185.3851	1185.3891	-0.00397	0.005
30	1	33	29	0	32	1185.3851	1185.3896	-0.00451	0.009
31	1	28	30	0	27	1186.6496	1186.6493	0.00028	0.002
31	1	29	30	0	28	1186.6496	1186.6502	-0.0006	0.002
31	1	30	30	0	29	1186.6496	1186.6509	-0.00126	0.002
31	1	31	30	0	30	1186.6496	1186.6513	-0.00169	0.002
31	1	32	30	0	31	1186.6496	1186.6515	-0.00192	0.002
31	1	33	30	0	32	1186.6496	1186.6516	-0.00196	0.002
31	1	34	30	0	33	1186.6496	1186.6514	-0.0018	0.002
32	1	29	31	0	28	1187.7413	1187.7432	-0.00186	0.002
32	1	30	31	0	29	1187.7413	1187.7434	-0.00206	0.002
32	1	31	31	0	30	1187.7413	1187.7433	-0.00203	0.002
32	1	32	31	0	31	1187.7413	1187.7431	-0.00178	0.002
32	1	33	31	0	32	1187.7413	1187.7426	-0.00131	0.002
32	1	34	31	0	33	1187.7413	1187.742	-0.00065	0.002
32	1	35	31	0	34	1187.7413	1187.7411	0.0002	0.002
33	1	30	32	0	29	1188.6607	1188.6633	-0.00263	0.003
33	1	31	32	0	30	1188.6607	1188.6628	-0.00214	0.003
33	1	32	32	0	31	1188.6607	1188.6621	-0.00141	0.002
33	1	33	32	0	32	1188.6607	1188.6612	-0.00045	0.002
33	1	34	32	0	33	1188.6607	1188.66	0.00072	0.002
33	1	35	32	0	34	1188.6607	1188.6586	0.00209	0.002
33	1	36	32	0	35	1188.6607	1188.6571	0.00365	0.003
34	1	31	33	0	30	1189.4042	1189.4082	-0.00397	0.005
34	1	32	33	0	31	1189.4042	1189.407	-0.00277	0.003

N'	v'	J'	N''	v''	J''	Observed	Calculated	Obs-Calc	Uncertainty
34	1	33	33	0	32	1189.4042	1189.4055	-0.00134	0.003
34	1	34	33	0	33	1189.4042	1189.4039	0.00033	0.002
34	1	35	33	0	34	1189.4042	1189.402	0.00222	0.002
34	1	36	33	0	35	1189.4042	1189.3999	0.00431	0.003
34	1	37	33	0	36	1189.4042	1189.3976	0.0066	0.01
35	1	32	34	0	31	1189.9714	1189.9761	-0.00465	0.005
35	1	33	34	0	32	1189.9714	1189.9741	-0.00273	0.003
35	1	34	34	0	33	1189.9714	1189.972	-0.00057	0.002
35	1	36	34	0	35	1189.9714	1189.967	0.00443	0.005
35	1	37	34	0	36	1189.9714	1189.9641	0.00726	0.01
35	1	38	34	0	37	1189.9714	1189.9611	0.01028	0.01
36	1	33	35	0	32	1190.3588	1190.3653	-0.0065	0.01
36	1	34	35	0	33	1190.3588	1190.3627	-0.00386	0.01
36	1	35	35	0	34	1190.3588	1190.3598	-0.00097	0.002
36	1	36	35	0	35	1190.3588	1190.3566	0.00216	0.003
36	1	37	35	0	36	1190.3588	1190.3533	0.00551	0.01
36	1	38	35	0	37	1190.3588	1190.3497	0.00908	0.01
36	1	39	35	0	38	1190.3588	1190.3459	0.01286	1
37	1	34	36	0	33	1190.5726	1190.5743	-0.00169	0.002
37	1	35	36	0	34	1190.5726	1190.5709	0.00169	0.002
37	1	36	36	0	35	1190.5726	1190.5673	0.00533	0.005
37	1	37	36	0	36	1190.561	1190.5634	-0.0024	0.003
37	1	38	36	0	37	1190.561	1190.5593	0.00171	0.002
37	1	39	36	0	38	1190.561	1190.555	0.00603	0.01
37	1	40	36	0	39	1190.561	1190.5504	0.01057	0.01
38	1	35	37	0	34	1190.6033	1190.6014	0.00194	0.002
38	1	36	37	0	35	1190.6033	1190.5972	0.00607	0.01
38	1	37	37	0	36	1190.6033	1190.5928	0.01046	1
0	1	3	1	0	2	1070.2317	1070.2373	-0.00558	0.005
1	1	2	2	0	1	1064.382	1064.3903	-0.00826	1
1	1	4	2	0	4	1064.3709	1064.3713	-0.00041	0.001
1	1	3	0	0	3	1081.5099	1081.5153	-0.00536	0.003
3	1	5	2	0	5	1092.3669	1092.3674	-0.00054	0.001
1	1	2	0	0	3	1081.4949	1081.4896	0.00532	0.005
3	1	4	2	0	4	1092.3801	1092.3812	-0.00111	0.003
2	1	1	3	0	0	1058.4212	1058.4263	-0.00512	0.005
2	1	2	3	0	1	1058.4357	1058.4352	0.00046	0.001
0	1	3	1	0	4	1070.1269	1070.13	-0.00312	0.003

N'	v'	J'	N''	v''	J''	Observed	Calculated	Obs-Calc	Uncertainty
1	1	4	2	0	5	1064.269	1064.2775	-0.00852	1
1	1	4	0	0	3	1081.5961	1081.5943	0.00182	0.002
1	1	3	2	0	4	1064.2928	1064.2923	0.00051	0.001
1	1	3	2	0	3	1064.3574	1064.3544	0.003	0.003
3	1	1	2	0	1	1092.3801	1092.3832	-0.00311	0.003
2	1	2	1	0	3	1086.978	1086.9825	-0.00451	0.005
0	2	3	1	1	4	1041.0227	1041.0219	0.00082	0.001
2	2	4	1	1	3	1057.6118	1057.617	-0.00517	0.005
2	2	5	1	1	4	1057.6351	1057.6301	0.00497	0.005
1	2	4	2	1	5	1035.2794	1035.2852	-0.00576	0.005
3	2	4	2	1	3	1062.8567	1062.859	-0.00226	0.003
3	2	5	2	1	4	1062.8758	1062.8767	-0.00087	0.001
3	2	6	2	1	5	1062.8943	1062.8902	0.00414	0.003
2	2	5	3	1	6	1029.4302	1029.4325	-0.00226	0.003
2	2	4	3	1	5	1029.4496	1029.448	0.00157	0.002
2	2	3	3	1	4	1029.4668	1029.4688	-0.00202	0.002
4	2	1	3	1	0	1067.9206	1067.9398	-0.01923	1
4	2	2	3	1	1	1067.9474	1067.9528	-0.00541	0.006
4	2	3	3	1	2	1067.9664	1067.967	-0.00061	0.001
4	2	4	3	1	3	1067.9767	1067.9823	-0.00555	0.006
4	2	5	3	1	4	1067.9962	1067.998	-0.00179	0.002
4	2	6	3	1	5	1068.016	1068.0133	0.00275	0.003
4	2	7	3	1	6	1068.03	1068.0267	0.00333	0.003
3	2	6	4	1	7	1023.4656	1023.4669	-0.00129	0.001
5	2	2	4	1	1	1072.9533	1072.9539	-0.00055	0.001
5	2	3	4	1	2	1072.9663	1072.9672	-0.00087	0.001
5	2	4	4	1	3	1072.9809	1072.9811	-0.0002	0.001
5	2	5	4	1	4	1072.9931	1072.9955	-0.00241	0.001
5	2	6	4	1	5	1073.007	1073.0101	-0.00308	0.001
5	2	7	4	1	6	1073.0248	1073.0243	0.00049	0.001
5	2	8	4	1	7	1073.0389	1073.0375	0.00141	0.001
4	2	7	5	1	8	1017.3898	1017.3906	-0.00082	0.001
4	2	6	5	1	7	1017.4073	1017.4074	-0.00007	0.001
4	2	5	5	1	6	1017.4259	1017.4256	0.00031	0.001
4	2	4	5	1	5	1017.4441	1017.4442	-0.00009	0.001
6	2	3	5	1	2	1077.841	1077.8398	0.00118	0.003
6	2	4	5	1	3	1077.8545	1077.8531	0.00145	0.003
6	2	5	5	1	4	1077.8662	1077.8666	-0.00042	0.003

N'	v'	J'	N''	v''	J''	Observed	Calculated	Obs-Calc	Uncertainty
6	2	6	5	1	5	1077.8793	1077.8804	-0.00112	0.003
6	2	7	5	1	6	1077.8936	1077.8942	-0.00064	0.003
6	2	8	5	1	7	1077.9079	1077.9078	0.00011	0.003
6	2	9	5	1	8	1077.9206	1077.9207	-0.00005	0.003
5	2	8	6	1	9	1011.2059	1011.2056	0.00027	0.003
5	2	7	6	1	8	1011.2227	1011.2228	-0.00008	0.003
5	2	6	6	1	7	1011.2421	1011.2409	0.00118	0.003
5	2	5	6	1	6	1011.2596	1011.2593	0.00027	0.003
5	2	4	6	1	5	1011.2806	1011.2775	0.00315	0.003
5	2	3	6	1	4	1011.2947	1011.2949	-0.00016	0.003
5	2	2	6	1	3	1011.3097	1011.3113	-0.00156	0.003
7	2	4	6	1	3	1082.5953	1082.5961	-0.00078	0.001
7	2	5	6	1	4	1082.6088	1082.6091	-0.00027	0.001
7	2	6	6	1	5	1082.6218	1082.6222	-0.00043	0.001
7	2	7	6	1	6	1082.6349	1082.6355	-0.00059	0.001
7	2	8	6	1	7	1082.6479	1082.6487	-0.00082	0.001
7	2	9	6	1	8	1082.6617	1082.6617	-0.00001	0.001
7	2	10	6	1	9	1082.6749	1082.6742	0.00069	0.001
6	2	9	7	1	10	1004.9151	1004.9139	0.00124	0.003
6	2	8	7	1	9	1004.9307	1004.9314	-0.00065	0.003
6	2	7	7	1	8	1004.9513	1004.9496	0.00175	0.003
6	2	6	7	1	7	1004.9687	1004.968	0.00074	0.003
6	2	5	7	1	6	1004.9865	1004.9862	0.00033	0.003
6	2	4	7	1	5	1005.0034	1005.0038	-0.00043	0.003
6	2	3	7	1	4	1005.0187	1005.0207	-0.00202	0.003
8	2	5	7	1	4	1087.222	1087.2208	0.0012	0.001
8	2	6	7	1	5	1087.2332	1087.2335	-0.00027	0.001
8	2	7	7	1	6	1087.2461	1087.2462	-0.00011	0.001
8	2	8	7	1	7	1087.2584	1087.259	-0.00058	0.001
8	2	9	7	1	8	1087.2717	1087.2717	0.00003	0.001
8	2	10	7	1	9	1087.2846	1087.2842	0.00045	0.001
8	2	11	7	1	10	1087.2976	1087.2963	0.00134	0.001
7	2	10	8	1	11	998.51709	998.51719	-0.0001	0.001
7	2	9	8	1	10	998.53445	998.53497	-0.00052	0.001
7	2	8	8	1	9	998.55282	998.55331	-0.00049	0.001
7	2	7	8	1	8	998.57185	998.5718	0.00005	0.001
7	2	6	8	1	7	998.58906	998.59014	-0.00108	0.001
7	2	5	8	1	6	998.60801	998.60805	-0.00004	0.001

N'	v'	J'	N''	v''	J''	Observed	Calculated	Obs-Calc	Uncertainty
7	2	4	8	1	5	998.62345	998.62534	-0.00189	0.001
9	2	6	8	1	5	1091.713	1091.7121	0.00088	0.003
9	2	7	8	1	6	1091.7255	1091.7244	0.00107	0.003
9	2	8	8	1	7	1091.7384	1091.7367	0.00166	0.003
9	2	9	8	1	8	1091.7494	1091.749	0.00038	0.003
9	2	10	8	1	9	1091.762	1091.7612	0.0008	0.003
9	2	11	8	1	10	1091.7746	1091.7732	0.00141	0.003
9	2	12	8	1	11	1091.787	1091.7849	0.00212	0.003
8	2	11	9	1	12	992.01876	992.01749	0.00127	0.003
8	2	10	9	1	11	992.03575	992.03555	0.0002	0.003
8	2	9	9	1	10	992.05398	992.05404	-0.00006	0.003
8	2	8	9	1	9	992.07173	992.07266	-0.00093	0.003
8	2	7	9	1	8	992.09103	992.09115	-0.00012	0.003
8	2	6	9	1	7	992.10828	992.10929	-0.00101	0.003
8	2	5	9	1	6	992.12689	992.12691	-0.00002	0.003
10	2	7	9	1	6	1096.0679	1096.0682	-0.00028	0.003
10	2	8	9	1	7	1096.0753	1096.0801	-0.00478	0.01
10	2	9	9	1	8	1096.088	1096.092	-0.00395	0.01
10	2	10	9	1	9	1096.102	1096.1038	-0.00175	0.003
10	2	11	9	1	10	1096.1132	1096.1154	-0.00223	0.003
10	2	12	9	1	11	1096.1257	1096.1269	-0.00124	0.003
10	2	13	9	1	12	1096.1382	1096.1382	0.00001	0.003
9	2	12	10	1	13	985.41709	985.41662	0.00047	0.003
9	2	11	10	1	12	985.43548	985.43493	0.00055	0.003
9	2	10	10	1	11	985.45419	985.45359	0.0006	0.003
9	2	9	10	1	10	985.47243	985.47236	0.00007	0.003
9	2	8	10	1	9	985.49066	985.49101	-0.00035	0.003
9	2	7	10	1	8	985.50926	985.50937	-0.00011	0.003
9	2	6	10	1	7	985.52676	985.52729	-0.00053	0.003
11	2	8	10	1	7	1100.2815	1100.2871	-0.00558	0.004
11	2	9	10	1	8	1100.292	1100.2986	-0.00656	0.004
11	2	10	10	1	9	1100.3058	1100.31	-0.00417	0.003
11	2	11	10	1	10	1100.3189	1100.3213	-0.00239	0.001
11	2	12	10	1	11	1100.3314	1100.3325	-0.00108	0.001
11	2	13	10	1	12	1100.3444	1100.3435	0.0009	0.001
11	2	14	10	1	13	1100.3562	1100.3543	0.00191	0.001
10	2	13	11	1	14	978.7167	978.71643	0.00027	0.001
10	2	12	11	1	13	978.73426	978.73497	-0.00071	0.001

N'	v'	J'	N''	v''	J''	Observed	Calculated	Obs-Calc	Uncertainty
10	2	11	11	1	12	978.75347	978.7538	-0.00033	0.001
10	2	10	11	1	11	978.77175	978.77272	-0.00097	0.001
10	2	9	11	1	10	978.79112	978.79154	-0.00042	0.001
10	2	8	11	1	9	978.80917	978.81011	-0.00094	0.001
10	2	7	11	1	8	978.8269	978.8283	-0.0014	0.001
12	2	9	11	1	8	1104.3625	1104.367	-0.00446	0.003
12	2	10	11	1	9	1104.3722	1104.378	-0.00579	0.003
12	2	11	11	1	10	1104.3859	1104.3889	-0.00303	0.003
12	2	12	11	1	11	1104.3996	1104.3998	-0.00017	0.003
12	2	13	11	1	12	1104.4139	1104.4105	0.00344	0.003
12	2	14	11	1	13	1104.4139	1104.421	-0.00709	0.003
12	2	15	11	1	14	1104.4277	1104.4313	-0.00361	0.003
11	2	14	12	1	15	971.91991	971.91875	0.00116	0.001
11	2	13	12	1	14	971.9372	971.93749	-0.00029	0.001
11	2	12	12	1	13	971.95547	971.95649	-0.00102	0.001
11	2	11	12	1	12	971.97441	971.97557	-0.00116	0.001
11	2	10	12	1	11	971.99364	971.99456	-0.00092	0.001
11	2	9	12	1	10	972.0132	972.01333	-0.00013	0.001
11	2	8	12	1	9	972.03052	972.03176	-0.00124	0.001
13	2	10	12	1	9	1108.3063	1108.3059	0.00037	0.001
13	2	11	12	1	10	1108.3189	1108.3165	0.00239	0.002
13	2	12	12	1	11	1108.3328	1108.327	0.00583	0.006
13	2	13	12	1	12	1108.3328	1108.3373	-0.00451	0.004
13	2	14	12	1	13	1108.3461	1108.3475	-0.0014	0.002
13	2	15	12	1	14	1108.3606	1108.3575	0.00307	0.003
13	2	16	12	1	15	1108.3606	1108.3674	-0.00676	0.009
12	2	15	13	1	16	965.02592	965.02537	0.00055	0.001
12	2	14	13	1	15	965.04331	965.04431	-0.001	0.001
12	2	13	13	1	14	965.0618	965.06348	-0.00168	0.001
12	2	12	13	1	13	965.08082	965.0827	-0.00188	0.001
12	2	11	13	1	12	965.1026	965.10185	0.00075	0.001
12	2	10	13	1	11	965.1225	965.12081	0.00169	0.001
12	2	9	13	1	10	965.13938	965.13947	-0.00009	0.001
14	2	11	13	1	10	1112.1028	1112.1021	0.00066	0.003
14	2	12	13	1	11	1112.1171	1112.1122	0.00486	0.01
14	2	13	13	1	12	1112.1171	1112.1222	-0.00511	0.003
14	2	14	13	1	13	1112.1324	1112.132	0.00036	0.003
14	2	15	13	1	14	1112.1481	1112.1417	0.00638	0.01

N'	v'	J'	N''	v''	J''	Observed	Calculated	Obs-Calc	Uncertainty
14	2	16	13	1	15	1112.1481	1112.1512	-0.00314	0.003
14	2	17	13	1	16	1112.1599	1112.1606	-0.00068	0.003
13	2	16	14	1	17	958.03896	958.03809	0.00087	0.001
13	2	15	14	1	16	958.05777	958.05722	0.00055	0.001
13	2	14	14	1	15	958.07674	958.07654	0.0002	0.001
13	2	13	14	1	14	958.09484	958.09591	-0.00107	0.001
13	2	12	14	1	13	958.11374	958.11521	-0.00147	0.001
13	2	11	14	1	12	958.13363	958.13435	-0.00072	0.001
13	2	10	14	1	11	958.15254	958.15321	-0.00067	0.001
15	2	12	14	1	11	1115.7546	1115.7537	0.0009	0.003
15	2	13	14	1	12	1115.7688	1115.7633	0.00548	0.003
15	2	14	14	1	13	1115.7688	1115.7728	-0.00398	0.003
15	2	15	14	1	14	1115.7787	1115.7821	-0.0034	0.003
15	2	16	14	1	15	1115.7884	1115.7913	-0.00287	0.003
15	2	17	14	1	16	1115.8055	1115.8003	0.00523	0.003
15	2	18	14	1	17	1115.8055	1115.8091	-0.00359	0.003
14	2	17	15	1	18	950.95949	950.95869	0.0008	0.001
14	2	16	15	1	17	950.97789	950.97798	-0.00009	0.001
14	2	15	15	1	16	950.99639	950.99744	-0.00105	0.001
14	2	14	15	1	15	951.01635	951.01696	-0.00061	0.001
14	2	13	15	1	14	951.03798	951.03641	0.00157	0.001
14	2	12	15	1	13	951.05629	951.05571	0.00058	0.001
14	2	11	15	1	12	951.07432	951.07477	-0.00045	0.001
16	2	13	15	1	12	1119.2591	1119.2588	0.00032	0.003
16	2	14	15	1	13	1119.2698	1119.2679	0.00191	0.003
16	2	15	15	1	14	1119.2698	1119.2768	-0.00704	0.01
16	2	16	15	1	15	1119.2874	1119.2856	0.00176	0.003
16	2	17	15	1	16	1119.2874	1119.2943	-0.00687	0.01
16	2	18	15	1	17	1119.3021	1119.3028	-0.00065	0.003
16	2	19	15	1	18	1119.314	1119.311	0.00296	0.003
15	2	18	16	1	19	943.78887	943.7889	-0.00003	0.001
15	2	17	16	1	18	943.80846	943.80835	0.00011	0.001
15	2	16	16	1	17	943.82741	943.82795	-0.00054	0.001
15	2	15	16	1	16	943.84852	943.84759	0.00093	0.001
15	2	14	16	1	15	943.86584	943.86718	-0.00134	0.001
15	2	13	16	1	14	943.88825	943.88664	0.00161	0.001
15	2	12	16	1	13	943.90497	943.90587	-0.0009	0.001
17	2	14	16	1	13	1122.6143	1122.6155	-0.00121	0.003

N'	v'	J'	N''	v''	J''	Observed	Calculated	Obs-Calc	Uncertainty
17	2	15	16	1	14	1122.6265	1122.6241	0.0024	0.003
17	2	16	16	1	15	1122.6265	1122.6325	-0.00603	0.003
17	2	17	16	1	16	1122.6415	1122.6408	0.00071	0.003
17	2	18	16	1	17	1122.6497	1122.6489	0.00081	0.003
17	2	19	16	1	18	1122.6497	1122.6568	-0.00712	0.003
17	2	20	16	1	19	1122.6639	1122.6646	-0.00068	0.003
16	2	19	17	1	20	936.53135	936.53045	0.0009	0.001
16	2	18	17	1	19	936.54954	936.55004	-0.0005	0.001
16	2	17	17	1	18	936.56732	936.56977	-0.00245	0.001
16	2	16	17	1	17	936.58806	936.58953	-0.00147	0.001
16	2	15	17	1	16	936.60967	936.60926	0.00041	0.001
16	2	14	17	1	15	936.62887	936.62885	0.00002	0.001
16	2	13	17	1	14	936.64779	936.64825	-0.00046	0.001
18	2	15	17	1	14	1125.8254	1125.822	0.00336	0.01
18	2	16	17	1	15	1125.8254	1125.8301	-0.0047	0.01
18	2	17	17	1	16	1125.8353	1125.838	-0.00269	0.01
18	2	18	17	1	17	1125.8509	1125.8457	0.00519	0.01
18	2	19	17	1	18	1125.8509	1125.8533	-0.00236	0.01
18	2	20	17	1	19	1125.8509	1125.8606	-0.00974	0.01
18	2	21	17	1	20	1125.8635	1125.8679	-0.00435	0.01
17	2	20	18	1	21	929.18647	929.18504	0.00143	0.001
17	2	19	18	1	20	929.2087	929.20476	0.00394	0.001
17	2	18	18	1	19	929.22664	929.2246	0.00204	0.001
17	2	17	18	1	18	929.24548	929.24448	0.001	0.001
17	2	16	18	1	17	929.2643	929.26432	-0.00002	0.001
17	2	15	18	1	16	929.28297	929.28405	-0.00108	0.001
17	2	14	18	1	15	929.30335	929.3036	-0.00025	0.001
19	2	16	18	1	15	1128.8826	1128.8765	0.00607	0.006
19	2	17	18	1	16	1128.8826	1128.8841	-0.00145	0.002
19	2	18	18	1	17	1128.8826	1128.8914	-0.00879	0.01
19	2	19	18	1	18	1128.898	1128.8986	-0.00056	0.002
19	2	20	18	1	19	1128.898	1128.9056	-0.00755	0.01
19	2	21	18	1	20	1128.9135	1128.9124	0.00113	0.002
19	2	22	18	1	21	1128.9135	1128.919	-0.00551	0.008
18	2	21	19	1	22	921.74752	921.75434	-0.00682	0.01
18	2	20	19	1	21	921.77298	921.77417	-0.00119	0.001
18	2	19	19	1	20	921.79499	921.79412	0.00087	0.001
18	2	18	19	1	19	921.81629	921.8141	0.00219	0.001

N'	v'	J'	N''	v''	J''	Observed	Calculated	Obs-Calc	Uncertainty
18	2	17	19	1	18	921.83324	921.83405	-0.00081	0.001
18	2	16	19	1	17	921.85431	921.8539	0.00041	0.001
20	2	17	19	1	16	1131.781	1131.7772	0.00385	0.004
20	2	18	19	1	17	1131.781	1131.7841	-0.00312	0.003
20	2	19	19	1	18	1131.7928	1131.7909	0.0019	0.002
20	2	20	19	1	19	1131.7928	1131.7975	-0.00469	0.006
20	2	21	19	1	20	1131.8119	1131.8039	0.00799	0.008
20	2	22	19	1	21	1131.8119	1131.8102	0.00174	0.002
20	2	23	19	1	22	1131.8119	1131.8162	-0.00433	0.006
19	2	22	20	1	23	914.24141	914.23998	0.00143	0.001
19	2	21	20	1	22	914.25873	914.25991	-0.00118	0.001
19	2	19	20	1	20	914.29788	914.30003	-0.00215	0.001
19	2	18	20	1	19	914.31517	914.32008	-0.00491	0.005
19	2	17	20	1	18	914.34063	914.34004	0.00059	0.001
19	2	16	20	1	17	914.35739	914.35985	-0.00246	0.001
21	2	18	20	1	17	1134.5283	1134.5221	0.00624	0.01
21	2	19	20	1	18	1134.5283	1134.5285	-0.00016	0.01
21	2	20	20	1	19	1134.5283	1134.5347	-0.00637	0.01
21	2	21	20	1	20	1134.5438	1134.5407	0.00311	0.01
21	2	22	20	1	21	1134.5541	1134.5465	0.00758	0.01
21	2	23	20	1	22	1134.5541	1134.5522	0.00192	0.01
21	2	24	20	1	23	1134.5541	1134.5577	-0.00357	0.01
22	2	19	21	1	18	1137.116	1137.1094	0.00657	0.01
22	2	20	21	1	19	1137.116	1137.1153	0.00074	0.002
22	2	21	21	1	20	1137.1259	1137.1209	0.00502	0.005
22	2	22	21	1	21	1137.1259	1137.1263	-0.00041	0.002
22	2	23	21	1	22	1137.1371	1137.1316	0.00555	0.006
22	2	24	21	1	23	1137.1371	1137.1366	0.00048	0.002
22	2	25	21	1	24	1137.1371	1137.1415	-0.0044	0.005
21	2	24	22	1	25	898.96635	898.96668	-0.00033	0.001
21	2	23	22	1	24	898.98662	898.98677	-0.00015	0.001
21	2	22	22	1	23	899.00556	899.00697	-0.00141	0.001
21	2	21	22	1	22	899.02822	899.0272	0.00102	0.001
21	2	20	22	1	21	899.04671	899.04742	-0.00071	0.001
21	2	19	22	1	20	899.07019	899.06756	0.00263	0.002
21	2	18	22	1	19	899.08969	899.08757	0.00212	0.002
23	2	20	22	1	19	1139.5446	1139.5375	0.00715	0.008
23	2	21	22	1	20	1139.5446	1139.5427	0.00192	0.002

N'	v'	J'	N''	v''	J''	Observed	Calculated	Obs-Calc	Uncertainty
23	2	22	22	1	21	1139.5446	1139.5477	-0.00311	0.003
23	2	23	22	1	22	1139.5527	1139.5525	0.00016	0.002
23	2	24	22	1	23	1139.5609	1139.5572	0.00373	0.005
23	2	25	22	1	24	1139.5609	1139.5616	-0.00073	0.005
23	2	26	22	1	25	1139.5609	1139.5659	-0.00501	0.006
24	2	21	23	1	20	1141.8068	1141.8043	0.00252	0.003
24	2	22	23	1	21	1141.8068	1141.8089	-0.00211	0.003
24	2	23	23	1	22	1141.8068	1141.8133	-0.00653	0.008
24	2	24	23	1	23	1141.8205	1141.8176	0.00295	0.003
24	2	25	23	1	24	1141.8205	1141.8216	-0.00107	0.002
24	2	26	23	1	25	1141.8205	1141.8254	-0.0049	0.005
24	2	27	23	1	26	1141.8205	1141.8291	-0.00856	0.01
25	2	22	24	1	21	1143.914	1143.9081	0.00588	0.01
25	2	23	24	1	22	1143.914	1143.9121	0.00187	0.002
25	2	24	24	1	23	1143.914	1143.9159	-0.00193	0.002
25	2	25	24	1	24	1143.9244	1143.9195	0.00487	0.006
25	2	26	24	1	25	1143.9244	1143.9229	0.00148	0.002
25	2	27	24	1	26	1143.9244	1143.9261	-0.00172	0.002
25	2	28	24	1	27	1143.9244	1143.9291	-0.00474	0.005
26	2	23	25	1	22	1145.8503	1145.8471	0.00316	0.003
26	2	24	25	1	23	1145.8503	1145.8505	-0.00023	0.002
26	2	25	25	1	24	1145.8503	1145.8537	-0.0034	0.005
26	2	26	25	1	25	1145.8603	1145.8567	0.00364	0.005
26	2	27	25	1	26	1145.8603	1145.8594	0.00089	0.002
26	2	28	25	1	27	1145.8603	1145.862	-0.00167	0.002
26	2	29	25	1	28	1145.8603	1145.8644	-0.00405	0.004
27	2	24	26	1	23	1147.6211	1147.6195	0.00156	0.002
27	2	25	26	1	24	1147.6211	1147.6223	-0.0012	0.002
27	2	26	26	1	25	1147.6211	1147.6248	-0.00372	0.004
27	2	27	26	1	26	1147.6316	1147.6271	0.00447	0.004
27	2	28	26	1	27	1147.6317	1147.6292	0.00247	0.002
27	2	29	26	1	28	1147.6317	1147.6311	0.00056	0.002
27	2	30	26	1	29	1147.6317	1147.6329	-0.00115	0.002
28	2	25	27	1	24	1149.233	1149.2235	0.00949	0.01
28	2	26	27	1	25	1149.233	1149.2256	0.00739	0.01
28	2	27	27	1	26	1149.233	1149.2275	0.00552	0.01
28	2	28	27	1	27	1149.233	1149.2291	0.00387	0.003
28	2	29	27	1	28	1149.233	1149.2306	0.00243	0.002

N'	v'	J'	N''	v''	J''	Observed	Calculated	Obs-Calc	Uncertainty
28	2	30	27	1	29	1149.233	1149.2318	0.00119	0.002
28	2	31	27	1	30	1149.233	1149.2329	0.00015	0.002
29	2	26	28	1	25	1150.6601	1150.6572	0.00287	0.003
29	2	27	28	1	26	1150.6601	1150.6587	0.00144	0.002
29	2	28	28	1	27	1150.6601	1150.6599	0.00023	0.002
29	2	29	28	1	28	1150.6601	1150.6609	-0.00075	0.002
29	2	30	28	1	29	1150.6601	1150.6616	-0.00151	0.002
29	2	31	28	1	30	1150.6601	1150.6622	-0.00207	0.003
29	2	32	28	1	31	1150.6601	1150.6625	-0.00244	0.003
30	2	27	29	1	26	1151.9218	1151.9189	0.00292	0.003
30	2	28	29	1	27	1151.9218	1151.9197	0.00215	0.002
30	2	29	29	1	28	1151.9218	1151.9202	0.00163	0.002
30	2	30	29	1	29	1151.9218	1151.9205	0.00133	0.002
30	2	31	29	1	30	1151.9218	1151.9206	0.00125	0.002
30	2	32	29	1	31	1151.9218	1151.9204	0.00138	0.002
30	2	33	29	1	32	1151.9218	1151.9201	0.00171	0.002
31	2	28	30	1	27	1153.008	1153.0067	0.00133	0.002
31	2	29	30	1	28	1153.008	1153.0068	0.00125	0.002
31	2	30	30	1	29	1153.008	1153.0066	0.00142	0.002
31	2	31	30	1	30	1153.008	1153.0062	0.00181	0.002
31	2	32	30	1	31	1153.008	1153.0056	0.00243	0.002
31	2	33	30	1	32	1153.008	1153.0047	0.00327	0.003
31	2	34	30	1	33	1153.008	1153.0037	0.0043	0.004
32	2	29	31	1	28	1153.918	1153.9188	-0.00076	0.001
32	2	30	31	1	29	1153.918	1153.9181	-0.00014	0.001
32	2	31	31	1	30	1153.918	1153.9173	0.00072	0.001
32	2	32	31	1	31	1153.918	1153.9162	0.00183	0.002
32	2	33	31	1	32	1153.918	1153.9148	0.00316	0.003
32	2	34	31	1	33	1153.918	1153.9133	0.0047	0.005
32	2	35	31	1	34	1153.918	1153.9115	0.00646	0.007
33	2	30	32	1	29	1154.6496	1154.6534	-0.00375	0.003
33	2	31	32	1	30	1154.6496	1154.652	-0.00242	0.002
33	2	32	32	1	31	1154.6496	1154.6504	-0.00084	0.002
33	2	33	32	1	32	1154.6496	1154.6486	0.00098	0.002
33	2	34	32	1	33	1154.6496	1154.6466	0.00303	0.003
33	2	35	32	1	34	1154.6496	1154.6443	0.00531	0.01
33	2	36	32	1	35	1154.6496	1154.6418	0.00779	0.01
34	2	33	33	1	32	1155.2007	1155.2042	-0.00354	0.01

N'	v'	J'	N''	v''	J''	Observed	Calculated	Obs-Calc	Uncertainty
34	2	31	33	1	30	1155.2007	1155.2086	-0.0079	0.01
34	2	32	33	1	31	1155.2007	1155.2066	-0.00585	0.01
34	2	34	33	1	33	1155.2007	1155.2017	-0.00099	0.002
34	2	35	33	1	34	1155.2007	1155.1989	0.00179	0.002
34	2	36	33	1	35	1155.2007	1155.1959	0.0048	0.01
34	2	37	33	1	36	1155.2007	1155.1927	0.00803	0.01
35	2	32	34	1	31	1155.5817	1155.5827	-0.00098	0.002
35	2	33	34	1	32	1155.5687	1155.5799	-0.0112	1
35	2	34	34	1	33	1155.5687	1155.5769	-0.00815	1
35	2	35	34	1	34	1155.5687	1155.5736	-0.00486	1
35	2	36	34	1	35	1155.5687	1155.57	-0.00133	0.002
35	2	37	34	1	36	1155.5687	1155.5663	0.00243	0.003
35	2	38	34	1	37	1155.5687	1155.5623	0.00641	1
36	2	34	35	1	33	1155.7699	1155.7702	-0.00033	0.002
36	2	35	35	1	34	1155.7699	1155.7664	0.00346	1
36	2	36	35	1	35	1155.7556	1155.7624	-0.00679	1
36	2	37	35	1	36	1155.7556	1155.7581	-0.0025	0.002
36	2	33	35	1	32	1155.7699	1155.7738	-0.00386	0.003
36	2	38	35	1	37	1155.7556	1155.7536	0.00202	0.003
36	2	39	35	1	38	1155.7556	1155.7488	0.00676	1
37	2	34	36	1	33	1155.7699	1155.78	-0.01008	1
37	2	35	36	1	34	1155.7699	1155.7757	-0.00579	0.005
37	2	36	36	1	35	1155.7699	1155.7711	-0.00124	0.002
3	3	6	4	2	7	994.18893	994.18881	0.00012	0.001
3	3	5	4	2	6	994.2047	994.20479	-0.00009	0.001
3	3	4	4	2	5	994.22946	994.22334	0.00612	0.005
3	3	3	4	2	4	994.24777	994.24246	0.00531	0.005
3	3	2	4	2	3	994.2597	994.26067	-0.00097	0.001
3	3	1	4	2	2	994.2793	994.27706	0.00224	0.003
3	3	0	4	2	1	994.29682	994.2912	0.00562	0.005
5	3	2	4	2	1	1042.5966	1042.5966	0.00005	0.001
5	3	3	4	2	2	1042.6104	1042.6094	0.00098	0.001
5	3	4	4	2	3	1042.6239	1042.623	0.00095	0.001
5	3	5	4	2	4	1042.637	1042.637	0.00001	0.001
5	3	6	4	2	5	1042.649	1042.6512	-0.00219	0.001
5	3	7	4	2	6	1042.6631	1042.665	-0.00192	0.001
5	3	8	4	2	7	1042.678	1042.6777	0.0003	0.001
4	3	7	5	2	8	988.22415	988.22351	0.00064	0.003

N'	v'	J'	N''	v''	J''	Observed	Calculated	Obs-Calc	Uncertainty
4	3	6	5	2	7	988.23952	988.24001	-0.00049	0.003
4	3	5	5	2	6	988.25748	988.25805	-0.00057	0.003
4	3	4	5	2	5	988.28042	988.27646	0.00396	0.001
4	3	3	5	2	4	988.2958	988.29438	0.00142	0.001
4	3	2	5	2	3	988.30849	988.3112	-0.00271	0.001
4	3	1	5	2	2	988.32377	988.32656	-0.00279	0.001
6	3	5	5	2	4	1047.3794	1047.3795	-0.00008	0.001
6	3	6	5	2	5	1047.3927	1047.3929	-0.00018	0.001
6	3	7	5	2	6	1047.4066	1047.4063	0.00031	0.001
6	3	8	5	2	7	1047.4197	1047.4194	0.0003	0.001
6	3	9	5	2	8	1047.4333	1047.4318	0.00154	0.001
5	3	8	6	2	9	982.1472	982.14767	-0.00047	0.003
5	3	7	6	2	8	982.16537	982.16459	0.00078	0.003
7	3	4	6	2	3	1051.9812	1051.9789	0.0023	0.003
7	3	5	6	2	4	1051.9934	1051.9915	0.00195	0.003
7	3	6	6	2	5	1052.0054	1052.0042	0.00122	0.003
7	3	7	6	2	6	1052.0159	1052.017	-0.00112	0.003
7	3	8	6	2	7	1052.0308	1052.0298	0.00099	0.003
7	3	9	6	2	8	1052.0441	1052.0423	0.00177	0.003
7	3	10	6	2	9	1052.0549	1052.0543	0.00058	0.003
6	3	9	7	2	10	975.96444	975.96318	0.00126	0.003
6	3	8	7	2	9	975.98038	975.98047	-0.00009	0.003
6	3	7	7	2	8	976.00176	975.99849	0.00327	0.003
6	3	6	7	2	7	976.01901	976.01672	0.00229	0.003
6	3	5	7	2	6	976.03629	976.03471	0.00158	0.003
6	3	4	7	2	5	976.05318	976.05212	0.00106	0.003
6	3	3	7	2	4	976.06624	976.06872	-0.00248	0.003
8	3	5	7	2	4	1056.4702	1056.4708	-0.00058	0.003
8	3	6	7	2	5	1056.4826	1056.483	-0.0004	0.003
8	3	7	7	2	6	1056.4954	1056.4953	0.00011	0.003
8	3	8	7	2	7	1056.5073	1056.5076	-0.00031	0.003
8	3	9	7	2	8	1056.5195	1056.5198	-0.00033	0.003
8	3	10	7	2	9	1056.5328	1056.5318	0.00097	0.003
8	3	11	7	2	10	1056.5447	1056.5434	0.0013	0.003
7	3	10	8	2	11	969.67406	969.67192	0.00214	0.001
7	3	9	8	2	10	969.68993	969.68953	0.0004	0.001
7	3	8	8	2	9	969.70668	969.70769	-0.00101	0.001
7	3	7	8	2	8	969.72567	969.726	-0.00033	0.001

N'	v'	J'	N''	v''	J''	Observed	Calculated	Obs-Calc	Uncertainty
7	3	6	8	2	7	969.74527	969.74414	0.00113	0.001
7	3	5	8	2	6	969.76395	969.76182	0.00213	0.001
7	3	4	8	2	5	969.77845	969.77883	-0.00038	0.001
9	3	6	8	2	5	1060.8277	1060.8273	0.00044	0.003
9	3	7	8	2	6	1060.8405	1060.8391	0.0014	0.003
9	3	8	8	2	7	1060.8557	1060.8509	0.00476	0.003
9	3	9	8	2	8	1060.8663	1060.8628	0.00355	0.003
9	3	10	8	2	9	1060.8774	1060.8745	0.00295	0.003
9	3	11	8	2	10	1060.8891	1060.8859	0.00316	0.003
9	3	12	8	2	11	1060.9007	1060.8971	0.00362	0.003
10	3	7	9	2	6	1065.0481	1065.0464	0.00168	0.003
10	3	8	9	2	7	1065.0596	1065.0578	0.00176	0.003
10	3	9	9	2	8	1065.0742	1065.0692	0.00497	0.003
10	3	10	9	2	9	1065.0837	1065.0805	0.00317	0.003
10	3	12	9	2	11	1065.101	1065.1027	-0.0017	0.003
10	3	13	9	2	12	1065.114	1065.1134	0.00062	0.003
9	3	12	10	2	13	956.77601	956.77638	-0.00037	0.001
11	3	8	10	2	7	1069.1291	1069.1263	0.00279	0.003
11	3	9	10	2	8	1069.1425	1069.1373	0.0052	0.006
11	3	10	10	2	9	1069.1425	1069.1482	-0.0057	0.006
11	3	11	10	2	10	1069.1545	1069.159	-0.00451	0.006
11	3	12	10	2	11	1069.1677	1069.1697	-0.00198	0.003
11	3	13	10	2	12	1069.1816	1069.1802	0.00144	0.003
11	3	14	10	2	13	1069.1933	1069.1904	0.00293	0.003
10	3	13	11	2	14	950.17507	950.17571	-0.00064	0.001
10	3	12	11	2	13	950.19409	950.19413	-0.00004	0.001
10	3	11	11	2	12	950.21159	950.21283	-0.00124	0.001
10	3	10	11	2	11	950.22793	950.2316	-0.00367	0.001
10	3	9	11	2	10	950.24845	950.25027	-0.00182	0.001
10	3	8	11	2	9	950.26724	950.26865	-0.00141	0.001
10	3	7	11	2	8	950.28493	950.28663	-0.0017	0.001
12	3	9	11	2	8	1073.0707	1073.065	0.00571	0.006
12	3	10	11	2	9	1073.0707	1073.0755	-0.00482	0.005
12	3	11	11	2	10	1073.0866	1073.0859	0.00066	0.002
12	3	13	11	2	12	1073.1003	1073.1064	-0.0061	0.008
12	3	12	11	2	11	1073.10034	1073.0963	0.00409	0.005
12	3	14	11	2	13	1073.1141	1073.1164	-0.00227	0.003
12	3	15	11	2	14	1073.1271	1073.1261	0.00101	0.002

N'	v'	J'	N''	v''	J''	Observed	Calculated	Obs-Calc	Uncertainty
11	3	14	12	2	15	943.47791	943.4755	0.00241	0.001
11	3	13	12	2	14	943.49576	943.49414	0.00162	0.001
11	3	12	12	2	13	943.51381	943.51302	0.00079	0.001
11	3	11	12	2	12	943.53336	943.53197	0.00139	0.001
11	3	10	12	2	11	943.55122	943.55081	0.00041	0.001
11	3	9	12	2	10	943.57112	943.56941	0.00171	0.001
13	3	10	12	2	9	1076.862	1076.8605	0.00148	0.001
13	3	11	12	2	10	1076.8715	1076.8706	0.00093	0.001
13	3	12	12	2	11	1076.8862	1076.8805	0.0057	0.005
13	3	13	12	2	12	1076.8862	1076.8903	-0.00409	0.003
13	3	14	12	2	13	1076.8993	1076.8999	-0.00062	0.002
13	3	15	12	2	14	1076.9138	1076.9094	0.00443	0.005
13	3	16	12	2	15	1076.9138	1076.9186	-0.0048	0.005
14	3	11	13	2	10	1080.5212	1080.5109	0.01026	1
14	3	12	13	2	11	1080.5212	1080.5205	0.0007	0.002
14	3	13	13	2	12	1080.5212	1080.5299	-0.00872	1
14	3	17	13	2	16	1080.5667	1080.5659	0.00077	0.002
15	3	12	14	2	11	1084.0232	1084.0143	0.00889	1
15	3	13	14	2	12	1084.0232	1084.0234	-0.00016	0.003
15	3	14	14	2	13	1084.0365	1084.0323	0.00424	0.005
15	3	15	14	2	14	1084.0365	1084.041	-0.0045	0.005
15	3	16	14	2	15	1084.0503	1084.0496	0.00073	0.003
15	3	17	14	2	16	1084.0503	1084.058	-0.00766	1
15	3	18	14	2	17	1084.0636	1084.0661	-0.00254	0.003
14	3	11	15	2	12	922.90984	922.91045	-0.00061	0.001
16	3	13	15	2	12	1087.3732	1087.3687	0.00454	0.005
16	3	14	15	2	13	1087.3732	1087.3772	-0.004	0.005
16	3	15	15	2	14	1087.3829	1087.3856	-0.00267	0.005
16	3	16	15	2	15	1087.3964	1087.3938	0.00263	0.005
16	3	17	15	2	16	1087.3964	1087.4018	-0.00539	0.005
16	3	18	15	2	17	1087.4089	1087.4096	-0.00073	0.005
16	3	19	15	2	18	1087.4185	1087.4173	0.00123	0.005
15	3	18	16	2	19	915.70969	915.71378	-0.00409	0.005
15	3	17	16	2	18	915.72888	915.73319	-0.00431	0.005
15	3	16	16	2	17	915.74558	915.75274	-0.00716	1
15	3	15	16	2	16	915.77199	915.77232	-0.00033	0.002
15	3	14	16	2	15	915.79541	915.79183	0.00358	0.003
15	3	13	16	2	14	915.81326	915.81118	0.00208	0.002

N'	v'	J'	N''	v''	J''	Observed	Calculated	Obs-Calc	Uncertainty
17	3	14	16	2	13	1090.5784	1090.5721	0.00634	0.01
17	3	15	16	2	14	1090.5784	1090.5801	-0.00166	0.002
17	3	16	16	2	15	1090.5924	1090.5879	0.00451	0.005
17	3	17	16	2	16	1090.5924	1090.5955	-0.00314	0.003
17	3	18	16	2	17	1090.6025	1090.603	-0.0005	0.002
17	3	19	16	2	18	1090.6025	1090.6103	-0.00779	0.01
17	3	20	16	2	19	1090.6134	1090.6174	-0.00397	0.004
16	3	19	17	2	20	908.5393	908.54159	-0.00229	0.003
16	3	18	17	2	19	908.5565	908.56116	-0.00466	0.005
16	3	17	17	2	18	908.57535	908.58085	-0.0055	0.005
16	3	16	17	2	17	908.59605	908.60057	-0.00452	0.005
16	3	15	17	2	16	908.61314	908.62022	-0.00708	0.01
16	3	14	17	2	15	908.64275	908.63974	0.00301	0.003
18	3	15	17	2	14	1093.6273	1093.6225	0.00477	0.005
18	3	16	17	2	15	1093.6273	1093.63	-0.00269	0.003
18	3	17	17	2	16	1093.6445	1093.6373	0.00723	0.01
18	3	18	17	2	17	1093.6445	1093.6444	0.00015	0.002
18	3	19	17	2	18	1093.6445	1093.6513	-0.00676	0.01
18	3	20	17	2	19	1093.6568	1093.658	-0.00117	0.002
18	3	21	17	2	20	1093.6568	1093.6645	-0.00769	1
19	3	16	18	2	15	1096.5223	1096.5181	0.00416	0.004
19	3	17	18	2	16	1096.5223	1096.525	-0.00274	0.003
19	3	18	18	2	17	1096.5364	1096.5318	0.00465	0.005
19	3	19	18	2	18	1096.5364	1096.5383	-0.00186	0.002
19	3	20	18	2	19	1096.5364	1096.5446	-0.00819	1
19	3	21	18	2	20	1096.5579	1096.5507	0.00718	1
19	3	22	18	2	21	1096.5579	1096.5567	0.00123	0.002
20	3	17	19	2	16	1099.2634	1099.2569	0.00648	1
20	3	18	19	2	17	1099.2634	1099.2633	0.00015	0.002
20	3	19	19	2	18	1099.2634	1099.2694	-0.00598	1
20	3	20	19	2	19	1099.2755	1099.2753	0.00019	0.002
20	3	21	19	2	20	1099.2755	1099.281	-0.00554	1
20	3	22	19	2	21	1099.2875	1099.2866	0.00091	0.002
20	3	23	19	2	22	1099.2875	1099.2919	-0.00444	0.003
21	3	18	20	2	17	1101.8474	1101.8369	0.0105	1
21	3	19	20	2	18	1101.8474	1101.8427	0.00475	0.005
21	3	20	20	2	19	1101.8474	1101.8482	-0.00079	0.003
21	3	21	20	2	20	1101.8474	1101.8535	-0.00613	1

N'	v'	J'	N''	v''	J''	Observed	Calculated	Obs-Calc	Uncertainty
21	3	22	20	2	21	1101.8667	1101.8587	0.00804	1
21	3	23	20	2	22	1101.8667	1101.8636	0.00309	0.003
21	3	24	20	2	23	1101.8667	1101.8684	-0.00166	0.003
22	3	19	21	2	18	1104.2637	1104.2561	0.00757	1
22	3	20	21	2	19	1104.2637	1104.2613	0.00241	0.003
22	3	21	21	2	20	1104.2637	1104.2662	-0.00253	0.003
22	3	22	21	2	21	1104.2637	1104.271	-0.00726	1
22	3	23	21	2	22	1104.2833	1104.2755	0.00782	1
22	3	24	21	2	23	1104.2833	1104.2798	0.00349	0.003
22	3	25	21	2	24	1104.2833	1104.284	-0.00065	0.003
23	3	20	22	2	19	1106.5148	1106.5127	0.00215	0.003
23	3	21	22	2	20	1106.5148	1106.5172	-0.00239	0.003
23	3	22	22	2	21	1106.5248	1106.5215	0.00328	0.003
23	3	23	22	2	22	1106.5248	1106.5256	-0.00083	0.003
23	3	24	22	2	23	1106.538	1106.5295	0.00846	1
23	3	25	22	2	24	1106.538	1106.5332	0.00476	0.003
23	3	26	22	2	25	1106.538	1106.5368	0.00125	0.003
24	3	21	23	2	20	1108.613	1108.6045	0.00852	1
24	3	22	23	2	21	1108.613	1108.6084	0.0046	0.005
24	3	23	23	2	22	1108.613	1108.6121	0.00089	0.003
24	3	24	23	2	23	1108.613	1108.6156	-0.00259	0.003
24	3	25	23	2	24	1108.6286	1108.6189	0.00974	1
24	3	26	23	2	25	1108.6286	1108.6219	0.00667	1
24	3	27	23	2	26	1108.6286	1108.6248	0.0038	0.004
25	3	22	24	2	21	1110.5352	1110.5297	0.00555	1
25	3	23	24	2	22	1110.5352	1110.5329	0.00226	0.002
25	3	24	24	2	23	1110.5352	1110.536	-0.00081	0.002
25	3	25	24	2	24	1110.5352	1110.5389	-0.00365	0.003
25	3	26	24	2	25	1110.5352	1110.5415	-0.00628	1
25	3	27	24	2	26	1110.5352	1110.5439	-0.0087	1
25	3	28	24	2	27	1110.5352	1110.5461	-0.01091	1
26	3	23	25	2	22	1112.2944	1112.2862	0.00822	1
26	3	24	25	2	23	1112.2944	1112.2888	0.00557	1
26	3	25	25	2	24	1112.2944	1112.2913	0.00315	1
26	3	26	25	2	25	1112.2944	1112.2934	0.00096	0.002
26	3	27	25	2	26	1112.2944	1112.2954	-0.00101	0.002
26	3	28	25	2	27	1112.2944	1112.2972	-0.00277	0.002
26	3	29	25	2	28	1112.2944	1112.2987	-0.00432	1

N'	v'	J'	N''	v''	J''	Observed	Calculated	Obs-Calc	Uncertainty
27	3	24	26	2	23	1113.8793	1113.8721	0.00721	1
27	3	25	26	2	24	1113.8793	1113.8741	0.00521	1
27	3	26	26	2	25	1113.8793	1113.8759	0.00345	0.004
27	3	27	26	2	26	1113.8793	1113.8774	0.00193	0.003
27	3	28	26	2	27	1113.8793	1113.8787	0.00062	0.001
27	3	29	26	2	28	1113.8793	1113.8798	-0.00046	0.001
27	3	30	26	2	29	1113.8793	1113.8806	-0.00134	0.001
28	3	25	27	2	24	1115.29	1115.2854	0.00461	0.01
28	3	26	27	2	25	1115.29	1115.2867	0.00328	0.004
28	3	27	27	2	26	1115.29	1115.2878	0.00219	0.003
28	3	28	27	2	27	1115.29	1115.2887	0.00134	0.001
28	3	29	27	2	28	1115.29	1115.2893	0.00072	0.001
28	3	30	27	2	29	1115.29	1115.2897	0.00031	0.001
28	3	31	27	2	30	1115.29	1115.2899	0.00012	0.001
29	3	26	28	2	25	1116.5253	1116.5241	0.00121	0.001
29	3	27	28	2	26	1116.5253	1116.5247	0.00056	0.001
29	3	28	28	2	27	1116.5253	1116.5251	0.00016	0.001
29	3	29	28	2	28	1116.5253	1116.5253	-0.00001	0.001
29	3	30	28	2	29	1116.5253	1116.5252	0.00006	0.001
29	3	31	28	2	30	1116.5253	1116.525	0.00035	0.001
29	3	32	28	2	31	1116.5253	1116.5244	0.00086	0.001
30	3	27	29	2	26	1117.5873	1117.5862	0.00113	0.001
30	3	28	29	2	27	1117.5873	1117.5861	0.00117	0.001
30	3	29	29	2	28	1117.5873	1117.5858	0.00146	0.003
30	3	30	29	2	29	1117.5873	1117.5853	0.00199	0.003
30	3	31	29	2	30	1117.5873	1117.5845	0.00276	0.004
30	3	32	29	2	31	1117.5873	1117.5835	0.00376	1
30	3	33	29	2	32	1117.5873	1117.5823	0.00498	1
31	3	28	30	2	27	1118.466	1118.4696	-0.00363	0.002
31	3	29	30	2	28	1118.466	1118.4689	-0.00289	0.002
31	3	30	30	2	29	1118.466	1118.4679	-0.00189	0.002
31	3	31	30	2	30	1118.466	1118.4667	-0.00065	0.002
31	3	32	30	2	31	1118.466	1118.4652	0.00084	0.002
31	3	33	30	2	32	1118.466	1118.4634	0.00256	0.004
31	3	34	30	2	33	1118.466	1118.4615	0.0045	1
32	3	29	31	2	28	1119.1619	1119.1724	-0.01054	1
32	3	30	31	2	29	1119.1619	1119.171	-0.00909	1
32	3	31	31	2	30	1119.1619	1119.1693	-0.00737	1

N'	v'	J'	N''	v''	J''	Observed	Calculated	Obs-Calc	Uncertainty
32	3	32	31	2	31	1119.1619	1119.1673	-0.0054	0.003
32	3	33	31	2	32	1119.1619	1119.1651	-0.00319	0.002
32	3	34	31	2	33	1119.1619	1119.1626	-0.00074	0.002
32	3	35	31	2	34	1119.1619	1119.16	0.00193	0.003
33	3	30	32	2	29	1119.6762	1119.6926	-0.01636	1
33	3	31	32	2	30	1119.6762	1119.6904	-0.01418	1
33	3	32	32	2	31	1119.6762	1119.6879	-0.01173	1
33	3	33	32	2	32	1119.6762	1119.6852	-0.00903	1
33	3	34	32	2	33	1119.6762	1119.6823	-0.00608	1
33	3	35	32	2	34	1119.6762	1119.6791	-0.00289	0.002
33	3	36	32	2	35	1119.6762	1119.6757	0.00053	0.002
34	3	31	33	2	30	1120.0112	1120.028	-0.01675	1
34	3	32	33	2	31	1120.0112	1120.025	-0.01383	1
34	3	33	33	2	32	1120.0112	1120.0218	-0.01064	1
34	3	34	33	2	33	1120.0112	1120.0184	-0.00719	1
34	3	35	33	2	34	1120.0112	1120.0147	-0.00349	0.002
34	3	36	33	2	35	1120.0112	1120.0108	0.00045	0.002
34	3	37	33	2	36	1120.0112	1120.0066	0.00463	1
Lines from R.-D. Urban and H. Jones, Chem. Phys. Lett. 178 (1991) 295-300									
3	1	6	4	0	7	1052.2295	1052.2317	-0.00217	0.001
3	1	5	4	0	6	1052.2472	1052.2482	-0.00098	0.001
3	1	4	4	0	5	1052.2681	1052.2671	0.00105	0.001
3	1	3	4	0	4	1052.2881	1052.2865	0.00164	0.001
3	1	2	4	0	3	1052.3038	1052.3051	-0.00128	0.001
3	1	1	4	0	2	1052.3193	1052.3221	-0.00276	0.001
3	1	0	4	0	1	1052.3361	1052.337	-0.00093	0.001
3	1	6	2	0	5	1092.4761	1092.4752	0.0009	0.001
4	1	7	5	0	8	1046.0431	1046.0435	-0.00044	0.001
4	1	6	5	0	7	1046.0602	1046.0605	-0.00031	0.001
4	1	5	5	0	6	1046.0797	1046.0789	0.00079	0.001
4	1	4	5	0	5	1046.0995	1046.0977	0.00182	0.001
4	1	3	5	0	4	1046.1189	1046.116	0.00287	0.001
4	1	2	5	0	3	1046.1313	1046.1334	-0.0021	0.001
4	1	1	5	0	2	1046.1468	1046.1495	-0.00266	0.001
4	1	3	3	0	2	1097.6693	1097.6726	-0.0033	0.001
4	1	4	3	0	3	1097.6842	1097.6882	-0.00396	0.001

N'	v'	J'	N''	v''	J''	Observed	Calculated	Obs-Calc	Uncertainty
4	1	5	3	0	4	1097.7008	1097.7042	-0.00338	0.001
4	1	6	3	0	5	1097.7214	1097.7198	0.00162	0.001
4	1	7	3	0	6	1097.7351	1097.7337	0.00143	0.001
5	1	2	4	0	1	1102.7808	1102.7817	-0.0009	0.001
5	1	3	4	0	2	1102.7931	1102.7954	-0.00234	0.001
5	1	4	4	0	3	1102.8065	1102.8098	-0.00325	0.001
5	1	5	4	0	4	1102.8226	1102.8245	-0.00192	0.001
5	1	6	4	0	5	1102.8376	1102.8395	-0.00185	0.001
5	1	7	4	0	6	1102.855	1102.8541	0.00093	0.001
5	1	8	4	0	7	1102.8683	1102.8677	0.00058	0.001
6	1	9	7	0	10	1033.3477	1033.347	0.00074	0.001
6	1	8	7	0	9	1033.3654	1033.3646	0.00077	0.001
6	1	7	7	0	8	1033.3838	1033.383	0.0008	0.001
6	1	6	7	0	7	1033.4032	1033.4016	0.00161	0.001
6	1	5	7	0	6	1033.4214	1033.42	0.00141	0.001
6	1	4	7	0	5	1033.4384	1033.4379	0.00051	0.001
6	1	3	7	0	4	1033.4539	1033.4551	-0.00116	0.001
6	1	3	5	0	2	1107.7936	1107.7921	0.00155	0.001
6	1	4	5	0	3	1107.8063	1107.8057	0.00059	0.001
6	1	5	5	0	4	1107.8199	1107.8197	0.00023	0.001
6	1	6	5	0	5	1107.8345	1107.8339	0.00065	0.001
6	1	7	5	0	6	1107.85	1107.8481	0.00193	0.001
6	1	9	5	0	8	1107.8784	1107.8754	0.00300 0.001	
7	1	10	8	0	11	1026.8409	1026.8424	-0.00149	0.001
7	1	9	8	0	10	1026.8597	1026.8603	-0.00064	0.001
7	1	8	8	0	9	1026.8783	1026.8788	-0.00053	0.001
7	1	7	8	0	8	1026.8969	1026.8975	-0.00059	0.001
7	1	6	8	0	7	1026.9161	1026.916	0.00009	0.001
7	1	5	8	0	6	1026.934	1026.9341	-0.00014	0.001
7	1	4	8	0	5	1026.9504	1026.9517	-0.00128	0.001
8	1	11	9	0	12	1020.2361	1020.2362	-0.00007	0.001
8	1	10	9	0	11	1020.2545	1020.2544	0.00013	0.001
8	1	9	9	0	10	1020.2735	1020.273	0.00049	0.001
8	1	8	9	0	9	1020.2916	1020.2918	-0.00018	0.001
8	1	7	9	0	8	1020.3117	1020.3104	0.00126	0.001
9	1	12	10	0	13	1013.53	1013.5302	-0.00019	0.001
9	1	11	10	0	12	1013.5485	1013.5486	-0.00013	0.001
9	1	10	10	0	11	1013.5677	1013.5674	0.00028	0.001

N'	v'	J'	N''	v''	J''	Observed	Calculated	Obs-Calc	Uncertainty
9	1	9	10	0	10	1013.5864	1013.5863	0.00008	0.001
9	1	8	10	0	9	1013.6055	1013.6051	0.00037	0.001
9	1	7	10	0	8	1013.624	1013.6237	0.00032	0.001
9	1	6	10	0	7	1013.6433	1013.6418	0.00149	0.001
9	1	6	8	0	5	1122.0472	1122.0456	0.00164	0.001
9	1	7	8	0	6	1122.0587	1122.0583	0.00039	0.001
9	1	8	8	0	7	1122.0713	1122.0711	0.00023	0.001
9	1	9	8	0	8	1122.0838	1122.0838	-0.00001	0.001
9	1	10	8	0	9	1122.0972	1122.0965	0.00074	0.001
9	1	11	8	0	10	1122.1097	1122.1089	0.00076	0.001
9	1	12	8	0	11	1122.1219	1122.1212	0.00074	0.001
11	1	14	12	0	15	999.8268	999.82649	0.00031	0.001
11	1	13	12	0	14	999.8451	999.84534	-0.00024	0.001
11	1	12	12	0	13	999.8645	999.86443	0.00007	0.001
11	1	11	12	0	12	999.8838	999.88362	0.00018	0.001
11	1	10	12	0	11	999.9028	999.90273	0.00007	0.001
11	1	9	12	0	10	999.9218	999.92165	0.00015	0.001
11	1	8	12	0	9	999.9393	999.94026	-0.00096	0.001
11	1	8	10	0	7	1130.8839	1130.8817	0.00221	0.001
11	1	9	10	0	8	1130.894	1130.8937	0.00035	0.001
11	1	10	10	0	9	1130.9061	1130.9055	0.00056	0.001
11	1	11	10	0	10	1130.918	1130.9174	0.00065	0.001
11	1	12	10	0	11	1130.9301	1130.9291	0.00105	0.001
11	1	13	10	0	12	1130.9412	1130.9406	0.0006	0.001
11	1	14	10	0	13	1130.9529	1130.952	0.00095	0.001
12	1	15	13	0	16	992.8329	992.8325	0.0004	0.001
12	1	14	13	0	15	992.8512	992.85152	-0.00032	0.001
12	1	13	13	0	14	992.8708	992.87076	0.00004	0.001
12	1	12	13	0	13	992.8909	992.89008	0.00082	0.001
12	1	11	13	0	12	992.9101	992.90935	0.00075	0.001
12	1	9	13	0	10	992.9473	992.94725	0.00005	0.001
13	1	10	12	0	9	1139.1682	1139.1678	0.00044	0.001
13	1	11	12	0	10	1139.1801	1139.1788	0.00126	0.001
13	1	12	12	0	11	1139.1902	1139.1898	0.00038	0.001
13	1	13	12	0	12	1139.2008	1139.2007	0.00012	0.001
13	1	14	12	0	13	1139.2113	1139.2114	-0.00012	0.001
13	1	15	12	0	14	1139.2222	1139.222	0.00019	0.001
13	1	16	12	0	15	1139.2327	1139.2324	0.00026	0.001

N'	v'	J'	N''	v''	J''	Observed	Calculated	Obs-Calc	Uncertainty
14	1	11	13	0	10	1143.1007	1143.1	0.00073	0.001
14	1	12	13	0	11	1143.1105	1143.1106	-0.0001	0.001
14	1	13	13	0	12	1143.1208	1143.1211	-0.0003	0.001
14	1	14	13	0	13	1143.1311	1143.1315	-0.00038	0.001
14	1	15	13	0	14	1143.1414	1143.1417	-0.00032	0.001
14	1	16	13	0	15	1143.1519	1143.1518	0.00007	0.001
14	1	17	13	0	16	1143.1619	1143.1618	0.00013	0.001
15	1	18	16	0	19	971.3024	971.30393	-0.00153	0.001
15	1	17	16	0	18	971.3212	971.3234	-0.0022	0.001
15	1	16	16	0	17	971.3425	971.34303	-0.00053	0.001
15	1	15	16	0	16	971.3633	971.36273	0.00057	0.001
15	1	14	16	0	15	971.3831	971.38239	0.00071	0.001
15	1	13	16	0	14	971.4019	971.40193	-0.00003	0.001
15	1	12	16	0	13	971.4203	971.42127	-0.00097	0.001
15	1	12	14	0	11	1146.8901	1146.8892	0.00086	0.001
15	1	13	14	0	12	1146.899	1146.8994	-0.00039	0.001
15	1	14	14	0	13	1146.9097	1146.9094	0.00029	0.001
15	1	15	14	0	14	1146.9196	1146.9193	0.00031	0.001
15	1	16	14	0	15	1146.9293	1146.929	0.00026	0.001
15	1	17	14	0	16	1146.9388	1146.9386	0.00016	0.001
15	1	18	14	0	17	1146.9481	1146.9481	0.00002	0.001
17	1	14	16	0	13	1154.033	1154.0318	0.0012	0.001
17	1	15	16	0	14	1154.0416	1154.041	0.00064	0.001
17	1	16	16	0	15	1154.0508	1154.05	0.00083	0.001
17	1	17	16	0	16	1154.0588	1154.0588	-0.00003	0.001
17	1	18	16	0	17	1154.0676	1154.0675	0.00006	0.001
17	1	19	16	0	18	1154.0762	1154.0761	0.00009	0.001
17	1	20	16	0	19	1154.0857	1154.0845	0.00118	0.001
18	1	15	17	0	14	1157.3818	1157.3815	0.00027	0.001
18	1	16	17	0	15	1157.3904	1157.3902	0.00021	0.001
18	1	17	17	0	16	1157.3986	1157.3987	-0.00008	0.001
18	1	18	17	0	17	1157.4067	1157.407	-0.00031	0.001
18	1	19	17	0	18	1157.4144	1157.4152	-0.00079	0.001
18	1	20	17	0	19	1157.423	1157.4232	-0.00022	0.001
18	1	21	17	0	20	1157.4312	1157.4311	0.0001	0.001
20	1	17	19	0	16	1163.6296	1163.6292	0.00045	0.001
20	1	18	19	0	17	1163.6364	1163.6367	-0.00034	0.001
20	1	19	19	0	18	1163.6436	1163.6442	-0.00056	0.001

N'	v'	J'	N''	v''	J''	Observed	Calculated	Obs-Calc	Uncertainty
20	1	20	19	0	19	1163.6515	1163.6514	0.0001	0.001
20	1	21	19	0	20	1163.6577	1163.6585	-0.00079	0.001
20	1	22	19	0	21	1163.6653	1163.6654	-0.00011	0.001
20	1	23	19	0	22	1163.6727	1163.6722	0.00051	0.001
21	1	18	20	0	17	1166.5231	1166.5236	-0.00046	0.001
21	1	19	20	0	18	1166.5295	1166.5306	-0.0011	0.001
21	1	20	20	0	19	1166.5367	1166.5375	-0.00075	0.001
21	1	21	20	0	20	1166.5436	1166.5441	-0.00054	0.001
21	1	22	20	0	21	1166.5492	1166.5507	-0.00146	0.001
21	1	23	20	0	22	1166.5565	1166.557	-0.00052	0.001
21	1	24	20	0	23	1166.5631	1166.5632	-0.00012	0.001
6	2	3	5	1	2	1077.8402	1077.8398	0.00038	0.001
6	2	4	5	1	3	1077.8521	1077.8531	-0.00095	0.001
6	2	5	5	1	4	1077.8647	1077.8666	-0.00192	0.001
6	2	6	5	1	5	1077.8793	1077.8804	-0.00112	0.001
6	2	7	5	1	6	1077.8933	1077.8942	-0.00094	0.001
6	2	8	5	1	7	1077.9089	1077.9078	0.00111	0.001
6	2	9	5	1	8	1077.9216	1077.9207	0.00095	0.001
5	2	8	6	1	9	1011.2045	1011.2056	-0.00113	0.001
5	2	7	6	1	8	1011.222	1011.2228	-0.00078	0.001
5	2	6	6	1	7	1011.2407	1011.2409	-0.00022	0.001
5	2	5	6	1	6	1011.2605	1011.2593	0.00117	0.001
5	2	4	6	1	5	1011.2785	1011.2775	0.00105	0.001
5	2	3	6	1	4	1011.294	1011.2949	-0.00086	0.001
5	2	2	6	1	3	1011.3098	1011.3113	-0.00146	0.001
6	2	9	7	1	10	1004.9167	1004.9139	0.00284	0.001
6	2	8	7	1	9	1004.9337	1004.9314	0.00235	0.001
6	2	7	7	1	8	1004.9525	1004.9496	0.00295	0.001
6	2	6	7	1	7	1004.9712	1004.968	0.00324	0.001
6	2	5	7	1	6	1004.9895	1004.9862	0.00333	0.001
6	2	4	7	1	5	1005.0056	1005.0038	0.00177	0.001
6	2	3	7	1	4	1005.0212	1005.0207	0.00048	0.001
9	2	6	8	1	5	1091.7133	1091.7121	0.00118	0.001
9	2	7	8	1	6	1091.7247	1091.7244	0.00027	0.001
9	2	8	8	1	7	1091.7368	1091.7367	0.00006	0.001
9	2	9	8	1	8	1091.7493	1091.749	0.00028	0.001
9	2	10	8	1	9	1091.7615	1091.7612	0.0003	0.001
9	2	11	8	1	10	1091.7742	1091.7732	0.00101	0.001

N'	v'	J'	N''	v''	J''	Observed	Calculated	Obs-Calc	Uncertainty
9	2	12	8	1	11	1091.7861	1091.7849	0.00122	0.001
8	2	11	9	1	12	992.0181	992.01749	0.00061	0.001
8	2	10	9	1	11	992.0354	992.03555	-0.00015	0.001
8	2	9	9	1	10	992.0547	992.05404	0.00066	0.001
8	2	8	9	1	9	992.0737	992.07266	0.00104	0.001
8	2	7	9	1	8	992.0917	992.09115	0.00055	0.001
8	2	6	9	1	7	992.1103	992.10929	0.00101	0.001
8	2	5	9	1	6	992.1272	992.12691	0.00029	0.001
10	2	7	9	1	6	1096.0693	1096.0682	0.00112	0.001
10	2	8	9	1	7	1096.0804	1096.0801	0.00032	0.001
10	2	9	9	1	8	1096.0916	1096.092	-0.00035	0.001
10	2	10	9	1	9	1096.1033	1096.1038	-0.00045	0.001
10	2	11	9	1	10	1096.1154	1096.1154	-0.00003	0.001
10	2	12	9	1	11	1096.1281	1096.1269	0.00116	0.001
10	2	13	9	1	12	1096.1389	1096.1382	0.00071	0.001
9	2	12	10	1	13	985.4176	985.41662	0.00098	0.001
9	2	11	10	1	12	985.436	985.43493	0.00107	0.001
9	2	10	10	1	11	985.4546	985.45359	0.00101	0.001
9	2	9	10	1	10	985.4743	985.47236	0.00194	0.001
9	2	8	10	1	9	985.4931	985.49101	0.00209	0.001
9	2	7	10	1	8	985.5092	985.50937	-0.00017	0.001
9	2	6	10	1	7	985.5288	985.52729	0.00151	0.001
12	2	9	11	1	8	1104.3666	1104.367	-0.00036	0.001
12	2	10	11	1	9	1104.3777	1104.378	-0.00029	0.001
12	2	11	11	1	10	1104.3877	1104.3889	-0.00123	0.001
12	2	12	11	1	11	1104.3981	1104.3998	-0.00167	0.001
12	2	13	11	1	12	1104.4091	1104.4105	-0.00136	0.001
12	2	14	11	1	13	1104.4204	1104.421	-0.00059	0.001
12	2	15	11	1	14	1104.4313	1104.4313	-0.00001	0.001
14	2	11	13	1	10	1112.1023	1112.1021	0.00016	0.001
14	2	12	13	1	11	1112.1121	1112.1122	-0.00014	0.001
14	2	13	13	1	12	1112.1215	1112.1222	-0.00071	0.001
14	2	14	13	1	13	1112.1312	1112.132	-0.00084	0.001
14	2	15	13	1	14	1112.1412	1112.1417	-0.00052	0.001
14	2	16	13	1	15	1112.1515	1112.1512	0.00026	0.001
14	2	17	13	1	16	1112.1611	1112.1606	0.00052	0.001
15	2	12	14	1	11	1115.7545	1115.7537	0.0008	0.001
15	2	13	14	1	12	1115.7635	1115.7633	0.00018	0.001

N'	v'	J'	N''	v''	J''	Observed	Calculated	Obs-Calc	Uncertainty
15	2	14	14	1	13	1115.7723	1115.7728	-0.00048	0.001
15	2	15	14	1	14	1115.7813	1115.7821	-0.0008	0.001
15	2	16	14	1	15	1115.7908	1115.7913	-0.00047	0.001
15	2	17	14	1	16	1115.8004	1115.8003	0.00013	0.001
15	2	18	14	1	17	1115.8097	1115.8091	0.00061	0.001
16	2	13	15	1	12	1119.2587	1119.2588	-0.00008	0.001
16	2	14	15	1	13	1119.2677	1119.2679	-0.00019	0.001
16	2	15	15	1	14	1119.2762	1119.2768	-0.00064	0.001
16	2	16	15	1	15	1119.2847	1119.2856	-0.00094	0.001
16	2	17	15	1	16	1119.2942	1119.2943	-0.00007	0.001
16	2	18	15	1	17	1119.3033	1119.3028	0.00055	0.001
16	2	19	15	1	18	1119.3124	1119.311	0.00136	0.001
17	2	14	16	1	13	1122.6156	1122.6155	0.00009	0.001
17	2	15	16	1	14	1122.624	1122.6241	-0.0001	0.001
17	2	16	16	1	15	1122.6324	1122.6325	-0.00013	0.001
17	2	17	16	1	16	1122.641	1122.6408	0.00021	0.001
17	2	18	16	1	17	1122.6505	1122.6489	0.00161	0.001
17	2	19	16	1	18	1122.6602	1122.6568	0.00338	0.001
17	2	20	16	1	19	1122.6678	1122.6646	0.00322	0.001
18	2	15	17	1	14	1125.8224	1125.822	0.00036	0.001
18	2	16	17	1	15	1125.8302	1125.8301	0.0001	0.001
18	2	17	17	1	16	1125.8376	1125.838	-0.00039	0.001
18	2	18	17	1	17	1125.8446	1125.8457	-0.00111	0.001
18	2	19	17	1	18	1125.8506	1125.8533	-0.00266	0.001
18	2	20	17	1	19	1125.8571	1125.8606	-0.00354	0.001
18	2	21	17	1	20	1125.8635	1125.8679	-0.00435	0.001
21	2	18	20	1	17	1134.5236	1134.5221	0.00154	0.001
21	2	19	20	1	18	1134.5287	1134.5285	0.00024	0.001
21	2	20	20	1	19	1134.5349	1134.5347	0.00023	0.001
21	2	21	20	1	20	1134.5406	1134.5407	-0.00009	0.001
21	2	22	20	1	21	1134.5468	1134.5465	0.00028	0.001
21	2	23	20	1	22	1134.5529	1134.5522	0.00072	0.001
21	2	24	20	1	23	1134.558	1134.5577	0.00033	0.001
2	3	5	3	2	6	1000.0382	1000.0416	-0.00339	0.001
2	3	4	3	2	5	1000.0589	1000.0569	0.00205	0.001
2	3	3	3	2	4	1000.0776	1000.0776	0.00001	0.001
2	3	2	3	2	3	1000.0961	1000.0992	-0.00311	0.001
2	3	1	3	2	2	1000.1134	1000.1186	-0.0052	0.001

N'	v'	J'	N''	v''	J''	Observed	Calculated	Obs-Calc	Uncertainty
4	3	7	5	2	8	988.2227	988.22351	-0.00081	0.001
4	3	6	5	2	7	988.2404	988.24001	0.00039	0.001
4	3	5	5	2	6	988.2596	988.25805	0.00155	0.001
5	3	3	6	2	4	982.2374	982.2358	0.0016	0.001
5	3	4	6	2	5	982.2194	982.21866	0.00074	0.001
5	3	5	6	2	6	982.2021	982.20076	0.00134	0.001
5	3	6	6	2	7	982.1829	982.18254	0.00036	0.001
5	3	8	6	2	9	982.1472	982.14767	-0.00047	0.001
5	3	7	6	2	8	982.16537	982.16459	0.00078	0.001
7	3	4	6	2	3	1051.9775	1051.9789	-0.0014	0.001
7	3	5	6	2	4	1051.9891	1051.9915	-0.00235	0.001
7	3	6	6	2	5	1052.0015	1052.0042	-0.00268	0.001
7	3	7	6	2	6	1052.0153	1052.017	-0.00172	0.001
7	3	8	6	2	7	1052.0283	1052.0298	-0.00151	0.001
7	3	9	6	2	8	1052.0421	1052.0423	-0.00023	0.001
7	3	10	6	2	9	1052.0546	1052.0543	0.00028	0.001
6	3	9	7	2	10	975.9629	975.96318	-0.00028	0.001
6	3	8	7	2	9	975.9805	975.98047	0.00003	0.001
6	3	7	7	2	8	975.9983	975.99849	-0.00019	0.001
6	3	6	7	2	7	976.0165	976.01672	-0.00022	0.001
6	3	5	7	2	6	976.0344	976.03471	-0.00031	0.001
6	3	4	7	2	5	976.0526	976.05212	0.00048	0.001
6	3	3	7	2	4	976.069	976.06872	0.00028	0.001
8	3	5	7	2	4	1056.4712	1056.4708	0.00042	0.001
8	3	6	7	2	5	1056.4832	1056.483	0.0002	0.001
8	3	7	7	2	6	1056.4948	1056.4953	-0.00049	0.001
8	3	8	7	2	7	1056.5079	1056.5076	0.00029	0.001
8	3	9	7	2	8	1056.5208	1056.5198	0.00097	0.001
8	3	10	7	2	9	1056.5326	1056.5318	0.00077	0.001
8	3	11	7	2	10	1056.5449	1056.5434	0.0015	0.001
9	3	6	8	2	5	1060.8289	1060.8273	0.00164	0.001
9	3	7	8	2	6	1060.8394	1060.8391	0.0003	0.001
9	3	8	8	2	7	1060.8514	1060.8509	0.00046	0.001
9	3	9	8	2	8	1060.8621	1060.8628	-0.00065	0.001
9	3	10	8	2	9	1060.8739	1060.8745	-0.00055	0.001
9	3	11	8	2	10	1060.8875	1060.8859	0.00156	0.001
9	3	12	8	2	11	1060.8986	1060.8971	0.00152	0.001
10	3	7	9	2	6	1065.0474	1065.0464	0.00098	0.001

N'	v'	J'	N''	v''	J''	Observed	Calculated	Obs-Calc	Uncertainty
10	3	8	9	2	7	1065.0582	1065.0578	0.00036	0.001
10	3	9	9	2	8	1065.0693	1065.0692	0.00007	0.001
10	3	10	9	2	9	1065.0802	1065.0805	-0.00033	0.001
10	3	12	9	2	11	1065.1045	1065.1027	0.0018	0.001
10	3	13	9	2	12	1065.1152	1065.1134	0.00182	0.001
10	3	11	9	2	10	1065.092	1065.0917	0.00028	0.001
11	3	8	10	2	7	1069.1285	1069.1263	0.00219	0.001
11	3	9	10	2	8	1069.1377	1069.1373	0.0004	0.001
11	3	12	10	2	11	1069.1693	1069.1697	-0.00038	0.001
11	3	13	10	2	12	1069.1816	1069.1802	0.00144	0.001
11	3	14	10	2	13	1069.1929	1069.1904	0.00253	0.001
15	3	12	14	2	11	1084.0146	1084.0143	0.00029	0.001
15	3	13	14	2	12	1084.0237	1084.0234	0.00034	0.001
15	3	14	14	2	13	1084.0319	1084.0323	-0.00036	0.001
15	3	15	14	2	14	1084.0396	1084.041	-0.0014	0.001
15	3	16	14	2	15	1084.0472	1084.0496	-0.00237	0.001
15	3	17	14	2	16	1084.0549	1084.058	-0.00306	0.001
15	3	18	14	2	17	1084.0623	1084.0661	-0.00384	0.001
16	3	13	15	2	12	1087.3688	1087.3687	0.00014	0.001
16	3	14	15	2	13	1087.3774	1087.3772	0.0002	0.001
16	3	15	15	2	14	1087.385	1087.3856	-0.00057	0.001
16	3	16	15	2	15	1087.3928	1087.3938	-0.00097	0.001
16	3	17	15	2	16	1087.4001	1087.4018	-0.00169	0.001
16	3	18	15	2	17	1087.4081	1087.4096	-0.00153	0.001
16	3	19	15	2	18	1087.4152	1087.4173	-0.00207	0.001
18	3	15	17	2	14	1093.6241	1093.6225	0.00157	0.001
18	3	16	17	2	15	1093.631	1093.63	0.00101	0.001
18	3	17	17	2	16	1093.6373	1093.6373	0.00003	0.001
18	3	18	17	2	17	1093.6438	1093.6444	-0.00055	0.001
18	3	19	17	2	18	1093.6495	1093.6513	-0.00176	0.001
18	3	20	17	2	19	1093.6552	1093.658	-0.00277	0.001
18	3	21	17	2	20	1093.6616	1093.6645	-0.00289	0.001
19	3	17	18	2	16	1096.5259	1096.525	0.00086	0.001
19	3	18	18	2	17	1096.5315	1096.5318	-0.00025	0.001
19	3	19	18	2	18	1096.5382	1096.5383	-0.00006	0.001
19	3	20	18	2	19	1096.5458	1096.5446	0.00121	0.001
19	3	21	18	2	20	1096.5537	1096.5507	0.00298	0.001

N'	v'	J'	N''	v''	J''	Observed	Calculated	Obs-Calc	Uncertainty
19	3	22	18	2	21	1096.5601	1096.5567	0.00343	0.001

Appendix B

Line lists for CoH and CoD

Line lists for CoH and CoD, together with uncertainties assigned to these lines and differences between calculated and observed wavenumbers. The calculated lines in these tables were obtained from the band constant fits, where we fitted the severely perturbed upper states to individual term values, while the ground state was fitted with Eq. 5.1. The data of Heimer (Ref. [1], Chapter 5), and Klynning and Kronekvist (Ref. [4,5], Chapter 5) are included.

B.1 Line list for CoH

Table B.1: Line list for CoH.

Lines from A. Heimer, Z. Physik 104, 448-457 (1937)

$A^3\Phi_4 - X^3\Phi_4$

v'	J'	parity$'$	v''	J''	parity$''$	Observed	Uncertainty	calc-obs
0	5	e	0	4	e	22305.84	0.04	-0.0189
0	6	e	0	5	e	22312.58	0.04	-0.0217
0	7	e	0	6	e	22318.02	0.04	-0.0314
0	8	e	0	7	e	22322.02	0.04	-0.0495
0	9	e	0	8	e	22324.43	0.04	0.0341
0	10	e	0	9	e	22325.53	0.04	-0.0297
0	11	e	0	10	e	22324.83	0.04	0.0123
0	12	e	0	11	e	22322.30	0.04	0.0090

υ'	J'	parity′	υ''	J''	parity″	Observed	Uncertainty	calc-obs
0	13	e	0	12	e	22325.58	0.04	-0.0100
0	14	e	0	13	e	22316.35	0.04	-0.0243
0	15	e	0	14	e	22308.44	0.04	-0.0665
0	16	e	0	15	e	22299.28	0.04	-0.0009
0	17	e	0	16	e	22288.24	0.04	-0.0243
0	18	e	0	17	e	22276.87	0.04	0.0145
0	19	e	0	18	e	22261.79	0.04	0.0863
0	20	e	0	19	e	22245.31	0.04	0.0073
0	21	e	0	20	e	22227.12	0.04	-0.0893
0	22	e	0	21	e	22206.78	0.04	-0.0630
0	23	e	0	22	e	22184.48	0.5	-0.2666
0	24	e	0	23	e	22260.07	0.04	0.0002
0	25	e	0	24	e	22133.93	0.04	0.0007
0	4	e	0	5	e	22169.45	0.04	-0.0217
0	5	e	0	6	e	22149.08	0.04	0.0006
0	6	e	0	7	e	22127.57	0.04	-0.0005
0	7	e	0	8	e	22104.89	0.04	-0.0139
0	8	e	0	9	e	22080.89	0.04	-0.0117
0	9	e	0	10	e	22055.55	0.04	0.0053
0	10	e	0	11	e	22028.95	0.04	0.0070
0	11	e	0	12	e	22000.89	0.04	-0.0240
0	12	e	0	13	e	21971.18	0.04	-0.0593
0	13	e	0	14	e	21947.40	0.04	0.0105
0	14	e	0	15	e	21911.46	0.04	-0.0039
0	15	e	0	16	e	21877.00	0.04	0.0757
0	16	e	0	17	e	21841.78	0.04	0.0765
0	17	e	0	18	e	21804.97	0.04	0.0243
0	18	e	0	19	e	21768.23	0.04	-0.0157
0	19	e	0	20	e	21728.22	0.04	-0.0873
0	20	e	0	21	e	21686.91	0.04	-0.0070
0	21	e	0	22	e	21644.29	0.04	0.0884
0	22	e	0	23	e	21600.23	0.04	0.0622
0	23	e	0	24	e	21554.25	0.5	0.2677
0	4	e	0	4	f	22240.70	0.04	0.0221
0	5	e	0	5	f	22234.51	0.04	0.0173
0	6	e	0	6	f	22227.09	0.04	0.0215
0	7	e	0	7	f	22218.40	0.04	0.0463
0	8	e	0	8	f	22208.34	0.04	0.0598

υ'	J'	parity′	υ''	J''	parity″	Observed	Uncertainty	calc-obs
0	9	e	0	9	f	22196.98	0.04	-0.0385
0	10	e	0	10	f	22184.09	0.04	0.0215
0	11	e	0	11	f	22169.67	0.04	0.0122
0	12	e	0	12	f	22153.43	0.04	0.0514
0	14	e	0	14	f	22120.48	0.04	0.0285
0	15	e	0	15	f	22099.26	0.04	-0.0101
0	16	e	0	16	f	22077.06	0.04	-0.0764
0	4	f	0	4	e	22240.70	0.04	0.0221
0	5	f	0	5	e	22234.51	0.04	0.0173
0	6	f	0	6	e	22227.09	0.04	0.0216
0	7	f	0	7	e	22218.40	0.04	0.0465
0	8	f	0	8	e	22208.34	0.04	0.0611
0	9	f	0	9	e	22196.98	0.04	-0.0377
0	10	f	0	10	e	22184.09	0.04	0.0243
0	11	f	0	11	e	22169.67	0.04	0.0030
0	14	f	0	14	e	22120.02	0.04	0.0325
0	15	f	0	15	e	22098.84	0.5	0.2311
0	16	f	0	16	e	22076.58	0.04	0.1207
0	5	f	0	4	f	22305.84	0.04	-0.0190
0	6	f	0	5	f	22312.58	0.04	-0.0217
0	7	f	0	6	f	22318.02	0.04	-0.0315
0	8	f	0	7	f	22322.02	0.04	-0.0487
0	9	f	0	8	f	22324.43	0.04	0.0338
0	10	f	0	9	f	22325.53	0.04	-0.0295
0	11	f	0	10	f	22324.83	0.04	-0.0025
0	12	f	0	11	f	22322.30	0.04	0.0002
0	13	f	0	12	f	22316.10	0.04	-0.0216
0	14	f	0	13	f	22315.84	0.04	-0.0107
0	15	f	0	14	f	22308.15	0.04	-0.0265
0	16	f	0	15	f	22298.89	0.04	-0.0151
0	17	f	0	16	f	22287.36	0.04	0.0666
0	4	f	0	5	f	22169.45	0.04	-0.0217
0	5	f	0	6	f	22149.08	0.04	0.0005
0	6	f	0	7	f	22127.57	0.04	-0.0007
0	7	f	0	8	f	22104.89	0.04	-0.0142
0	8	f	0	9	f	22080.89	0.04	-0.0115
0	9	f	0	10	f	22055.55	0.04	0.0035
0	10	f	0	11	f	22028.95	0.04	0.0042

υ'	J'	parity'	υ''	J''	parity''	Observed	Uncertainty	calc-obs
0	13	f	0	14	f	21937.88	0.04	0.0205
0	14	f	0	15	f	21910.95	0.04	-0.0211
0	15	f	0	16	f	21876.75	0.04	0.0256
0	16	f	0	17	f	21841.48	0.04	-0.1070
0	17	f	0	18	f	21804.15	0.04	-0.0671

This work

$A'^3\Phi_4 - X^3\Phi_4$

0	5	e	0	4	e	12406.6643	0.007	-0.0095
0	6	e	0	5	e	12401.3396	0.007	0.0029
0	7	e	0	6	e	12393.0810	0.007	0.0047
0	8	e	0	7	e	12382.0822	0.007	0.0065
0	9	e	0	8	e	12368.5191	0.007	0.0051
0	10	e	0	9	e	12352.6798	0.007	0.0074
0	11	e	0	10	e	12335.0318	0.007	-0.0009
0	12	e	0	11	e	12317.8105	0.007	-0.0055
0	13	e	0	12	e	12292.4629	0.007	-0.0090
0	14	e	0	13	e	12276.3352	0.007	0.0012
0	15	e	0	14	e	12263.4408	0.007	-0.0011
0	16	e	0	15	e	12166.0577	0.007	-0.0037
0	17	e	0	16	e	12135.7314	0.007	-0.0049
0	18	e	0	17	e	12102.0925	0.007	-0.0050
0	19	e	0	18	e	12066.6945	0.007	-0.0036
0	20	e	0	19	e	12024.8942	0.05	-0.0571
0	21	e	0	20	e	11986.1773	0.007	-0.0027
0	22	e	0	21	e	11949.8154	0.007	-0.0013
0	23	e	0	22	e	11907.5716	10	0.0155
0	24	e	0	23	e	11867.9272	10	0.0626
0	25	e	0	24	e	11832.0079	10	0.0988
0	4	e	0	5	e	12280.5272	0.007	-0.0025
0	5	e	0	6	e	12249.9227	0.007	-0.0085
0	6	e	0	7	e	12216.3597	0.007	-0.0060
0	7	e	0	8	e	12179.9710	0.007	0.0022
0	8	e	0	9	e	12140.9930	0.007	0.0036
0	9	e	0	10	e	12099.6120	0.007	0.0033

v'	J'	parity$'$	v''	J''	parity$''$	Observed	Uncertainty	calc-obs
0	10	e	0	11	e	12056.1356	0.007	0.0083
0	11	e	0	12	e	12011.0538	0.007	0.0008
0	12	e	0	13	e	11966.6183	0.007	-0.0016
0	13	e	0	14	e	11914.2849	0.007	0.0096
0	14	e	0	15	e	11871.4789	0.007	-0.0120
0	15	e	0	16	e	11832.1440	0.007	-0.0022
0	16	e	0	17	e	11708.6319	0.007	-0.0005
0	17	e	0	18	e	11652.5051	0.007	0.0000
0	18	e	0	19	e	11593.4173	0.007	0.0001
0	19	e	0	20	e	11532.9469	0.007	0.0004
0	20	e	0	21	e	11466.4710	0.05	-0.0482
0	21	e	0	22	e	11403.5184	0.007	0.0040
0	22	e	0	23	e	11343.3875	0.007	0.0018
0	23	e	0	24	e	11277.8945	0.007	-0.0031
0	24	e	0	25	e	11215.5628	0.007	0.0026
0	25	e	0	26	e	11157.6210	10	-0.0797
0	4	f	0	4	e	12351.8160	0.007	0.0025
0	5	f	0	5	e	12335.3550	0.007	0.0060
0	6	f	0	6	e	12315.8900	0.007	0.0058
0	7	f	0	7	e	12293.4460	0.007	0.0040
0	8	f	0	8	e	12268.2290	0.007	0.0027
0	9	f	0	9	e	12240.7420	0.007	0.0037
0	10	f	0	10	e	12211.0600	0.007	0.0047
0	4	e	0	4	f	12351.8160	0.007	0.0025
0	5	e	0	5	f	12335.3550	0.007	0.0060
0	6	e	0	6	f	12315.8900	0.007	0.0057
0	7	e	0	7	f	12293.5230	0.007	0.0204
0	8	e	0	8	f	12268.5110	0.007	0.0070
0	9	e	0	9	f	12240.9900	0.007	0.0115
0	10	e	0	10	f	12211.3020	0.007	-0.0036
0	5	f	0	4	f	12406.6643	0.007	-0.0095
0	6	f	0	5	f	12401.3396	0.007	0.0029
0	7	f	0	6	f	12392.9960	0.007	-0.0040
0	8	f	0	7	f	12381.7993	0.007	0.0026
0	9	f	0	8	f	12368.2658	0.007	0.0015
0	10	f	0	9	f	12352.4564	0.007	-0.0055
0	11	f	0	10	f	12334.9036	0.007	0.0026
0	12	f	0	11	f	12315.3381	0.007	0.0040

v'	J'	parity′	v''	J''	parity″	Observed	Uncertainty	calc-obs
0	13	f	0	12	f	12291.2482	0.007	0.0056
0	14	f	0	13	f	12261.7713	0.007	0.0034
0	15	f	0	14	f	12224.8669	0.007	-0.0022
0	16	f	0	15	f	12186.3966	0.007	0.0007
0	17	f	0	16	f	12148.0711	0.007	0.0031
0	18	f	0	17	f	12109.6290	0.007	0.0012
0	19	f	0	18	f	12050.2228	0.007	0.0013
0	20	f	0	19	f	12007.1657	0.007	0.0080
0	21	f	0	20	f	11962.5128	0.007	0.0083
0	22	f	0	21	f	11916.0772	0.007	0.0095
0	23	f	0	22	f	11867.1602	0.007	0.0064
0	24	f	0	23	f	11817.6957	0.007	-0.0081
0	25	f	0	24	f	11764.8521	0.007	-0.0003
0	26	f	0	25	f	11710.3209	0.007	-0.0089
0	27	f	0	26	f	11654.1484	0.007	-0.0135
0	28	f	0	27	f	11598.0765	0.007	-0.0027
0	29	f	0	28	f	11534.6100	0.007	-0.0034
0	30	f	0	29	f	11473.7459	0.03	0.0354
0	31	f	0	30	f	11411.1191	0.05	0.0941
0	32	f	0	31	f	11347.1088	0.007	-0.0031
0	4	f	0	5	f	12280.5272	0.007	-0.0025
0	5	f	0	6	f	12249.9227	0.007	-0.0085
0	6	f	0	7	f	12216.3597	0.007	-0.0061
0	7	f	0	8	f	12179.8820	0.007	-0.0027
0	8	f	0	9	f	12140.7110	0.007	-0.0019
0	9	f	0	10	f	12099.3573	0.007	-0.0004
0	10	f	0	11	f	12055.9083	0.007	-0.0038
0	11	f	0	12	f	12010.9184	0.007	0.0057
0	12	f	0	13	f	11964.1388	0.007	0.0045
0	13	f	0	14	f	11913.0861	0.007	-0.0102
0	14	f	0	15	f	11856.8670	0.007	0.0073
0	15	f	0	16	f	11793.5176	0.007	-0.0008
0	16	f	0	17	f	11728.8968	0.007	-0.0015
0	17	f	0	18	f	11664.7276	0.007	0.0029
0	18	f	0	19	f	11600.7749	0.007	0.0002
0	19	f	0	20	f	11516.2082	0.007	-0.0019
0	20	f	0	21	f	11448.3618	0.007	-0.0014
0	21	f	0	22	f	11379.3022	0.007	-0.0053

v'	J'	parity′	v''	J''	parity″	Observed	Uncertainty	calc-obs
0	22	f	0	23	f	11308.8494	0.007	0.0044
0	23	f	0	24	f	11236.3441	0.007	0.0004
0	24	f	0	25	f	11163.7200	0.007	-0.0080
0	25	f	0	26	f	11088.1730	0.007	0.0008
0	26	f	0	27	f	11011.3964	0.007	0.0007
0	27	f	0	28	f	10933.4577	0.007	0.0037
0	28	f	0	29	f	10856.1153	0.007	0.0158
0	29	f	0	30	f	10771.8858	0.007	0.0065
0	30	f	0	31	f	10690.7978	0.007	0.0010
0	31	f	0	32	f	10608.4685	0.007	-0.0010
0	32	f	0	33	f	10525.3015	10	-0.2022
0	5	e	1	4	e	10552.1272	0.007	0.0016
0	6	e	1	5	e	10548.9276	0.007	0.0047
0	7	e	1	6	e	10543.2180	0.007	-0.0024
0	8	e	1	7	e	10535.1854	0.007	-0.0020
0	9	e	1	8	e	10525.0139	0.007	-0.0055
0	10	e	1	9	e	10512.9882	0.007	-0.0025
0	11	e	1	10	e	10499.5716	0.007	-0.0043
0	12	e	1	11	e	10487.0002	0.007	0.0016
0	13	e	1	12	e	10466.7647	0.05	-0.0328
0	14	e	1	13	e	10456.0945	0.01	0.0189
0	15	e	1	14	e	10449.0747	0.05	0.0553
0	16	e	1	15	e	10357.9926	0.05	0.0753
0	17	e	1	16	e	10334.3702	0.05	0.0990
0	18	e	1	17	e	10307.8459	0.05	0.1133
0	19	e	1	18	e	10279.9657	0.05	0.1209
0	20	e	1	19	e	10246.0862	0.05	0.0614
0	21	e	1	20	e	10215.7026	0.07	0.0860
0	22	e	1	21	e	10188.0774	0.07	0.0434
0	23	e	1	22	e	10154.9759	0.007	0.0059
0	24	e	1	23	e	10124.8783	0.007	0.0029
0	25	e	1	24	e	10098.9314	0.007	-0.0038
0	4	e	1	5	e	10428.1144	0.007	0.0001
0	5	e	1	6	e	10400.0498	0.007	-0.0056
0	6	e	1	7	e	10369.4554	0.007	-0.0070
0	7	e	1	8	e	10336.4810	0.007	-0.0235
0	8	e	1	9	e	10301.3034	0.007	-0.0084
0	9	e	1	10	e	10264.1644	0.007	-0.0127

v'	J'	parity′	v''	J''	parity″	Observed	Uncertainty	calc-obs
0	10	e	1	11	e	10225.3502	0.007	-0.0094
0	11	e	1	12	e	10185.2968	0.02	0.0358
0	12	e	1	13	e	10146.3500	0.02	0.0437
0	13	e	1	14	e	10100.0314	0.15	-0.0466
0	14	e	1	15	e	10063.4122	0.05	0.0686
0	15	e	1	16	e	10030.7832	0.05	0.1013
0	16	e	1	17	e	9914.3846	0.05	0.1185
0	17	e	1	18	e	9865.7768	0.05	0.1240
0	18	e	1	19	e	9814.6122	0.05	0.1158
0	19	e	1	20	e	9762.4691	0.1	0.0921
0	20	e	1	21	e	9704.7283	0.007	0.0012
0	21	e	1	22	e	9650.9192	0.007	-0.0021
0	22	e	1	23	e	9600.3349	0.05	-0.0542
0	23	e	1	24	e	9544.8224	0.05	-0.1101
0	24	e	1	25	e	9492.8759	0.03	-0.0887
0	25	e	1	26	e	9445.6904	0.007	0.0031
0	5	f	1	4	f	10552.1272	0.007	0.0016
0	6	f	1	5	f	10548.9276	0.007	0.0047
0	7	f	1	6	f	10543.1180	0.007	0.0040
0	8	f	1	7	f	10534.8994	0.007	-0.0024
0	9	f	1	8	f	10524.7506	0.007	0.0018
0	10	f	1	9	f	10512.7571	0.007	-0.0056
0	11	f	1	10	f	10499.4561	0.007	-0.0090
0	12	f	1	11	f	10484.5569	0.007	-0.0086
0	13	f	1	12	f	10465.5023	0.03	0.0469
0	14	f	1	13	f	10441.5947	0.007	-0.0119
0	15	f	1	14	f	10410.6155	0.007	-0.0075
0	16	f	1	15	f	10378.4995	0.007	-0.0024
0	17	f	1	16	f	10346.9519	0.007	-0.0005
0	18	f	1	17	f	10315.6983	0.007	0.0064
0	19	f	1	18	f	10263.9016	0.007	0.0138
0	20	f	1	19	f	10228.8972	0.007	0.0043
0	21	f	1	20	f	10192.7087	0.007	-0.0034
0	22	f	1	21	f	10155.1534	0.007	-0.0061
0	23	f	1	22	f	10115.5253	0.007	-0.0009
0	24	f	1	23	f	10075.7516	0.007	0.0113
0	25	f	1	24	f	10033.0638	0.007	-0.0011
0	26	f	1	25	f	9989.0750	0.007	-0.0033

v'	J'	parity′	v''	J''	parity″	Observed	Uncertainty	calc-obs
0	27	f	1	26	f	9943.8460	0.007	0.0004
0	28	f	1	27	f	9899.1097	0.02	0.0133
0	29	f	1	28	f	9847.3446	0.007	0.0058
0	30	f	1	29	f	9798.5333	0.007	-0.0003
0	31	f	1	30	f	9748.1962	0.03	0.0240
0	32	f	1	31	f	9696.5162	0.007	0.0060
0	4	f	1	5	f	10428.1144	0.007	0.0001
0	5	f	1	6	f	10400.0498	0.007	-0.0055
0	6	f	1	7	f	10369.4554	0.007	-0.0068
0	7	f	1	8	f	10336.3630	0.007	0.0015
0	8	f	1	9	f	10301.0126	0.007	-0.0029
0	9	f	1	10	f	10263.9016	0.007	-0.0038
0	10	f	1	11	f	10225.1006	0.007	0.0101
0	11	f	1	12	f	10185.2187	0.007	0.0008
0	12	f	1	13	f	10143.9514	0.007	0.0000
0	13	f	1	14	f	10098.7223	0.05	0.0969
0	14	f	1	15	f	10048.9734	0.007	0.0008
0	15	f	1	16	f	9992.3842	0.007	0.0098
0	16	f	1	17	f	9934.9673	0.007	0.0026
0	17	f	1	18	f	9878.4279	0.007	-0.0061
0	18	f	1	19	f	9822.5116	0.007	-0.0087
0	19	f	1	20	f	9746.4042	0.007	-0.0138
0	20	f	1	21	f	9687.4327	0.007	-0.0117
0	21	f	1	22	f	9627.6682	0.07	-0.0135
0	22	f	1	23	f	9566.9377	0.007	-0.0086
0	23	f	1	24	f	9504.5619	0.007	-0.0065
0	24	f	1	25	f	9442.4677	0.007	0.0039
0	25	f	1	26	f	9377.8853	0.007	0.0000
0	26	f	1	27	f	9312.4351	0.007	0.0111
0	27	f	1	28	f	9246.1959	0.007	0.0093
0	28	f	1	29	f	9180.8967	0.007	-0.0140
0	29	f	1	30	f	9108.9599	0.02	-0.0605
0	30	f	1	31	f	9040.2626	0.05	-0.0472
0	4	f	1	4	e	10497.2641	0.07	0.0283
0	5	f	1	5	e	10482.9337	0.007	0.0171
0	6	f	1	6	e	10466.0252	0.007	0.0005
0	7	f	1	7	e	10446.5470	0.007	-0.0023
0	8	f	1	8	e	10424.7135	0.007	0.0025

υ'	J'	parity′	υ''	J''	parity″	Observed	Uncertainty	calc-obs
0	9	f	1	9	e	10401.0467	0.007	-0.0025
0	4	e	1	4	f	10497.2641	0.07	0.0283
0	5	e	1	5	f	10482.9337	0.007	0.0171
0	6	e	1	6	f	10466.0252	0.007	0.0006
0	7	e	1	7	f	10446.6390	0.007	-0.0005
0	8	e	1	8	f	10425.0096	0.007	-0.0064
0	9	e	1	9	f	10401.3036	0.007	-0.0015
1	5	e	2	4	e	10202.2810	0.007	-0.0062
1	6	e	2	5	e	10199.0070	0.007	-0.0031
1	7	e	2	6	e	10193.3484	0.007	-0.0048
1	8	e	2	7	e	10185.7312	0.007	0.0040
1	9	e	2	8	e	10178.5422	0.007	0.0009
1	10	e	2	9	e	10163.9680	0.007	-0.0027
1	11	e	2	10	e	10149.9973	0.007	0.0042
1	12	e	2	11	e	10138.5684	0.007	0.0009
1	13	e	2	12	e	10093.2007	0.07	-0.1186
1	14	e	2	13	e	10071.1249	0.007	-0.0057
1	15	e	2	14	e	10059.2072	0.007	-0.0057
1	16	e	2	15	e	10053.6818	0.007	0.0088
1	17	e	2	16	e	9990.3645	10	-0.3641
1	18	e	2	17	e	9947.5223	0.007	0.0107
1	19	e	2	18	e	9922.6187	0.007	0.0166
1	20	e	2	19	e	9896.7191	0.007	0.0012
1	21	e	2	20	e	9860.0746	0.007	-0.0071
1	22	e	2	21	e	9834.2850	0.007	0.0031
1	4	e	2	5	e	10082.2445	0.007	0.0051
1	5	e	2	6	e	10054.8811	0.007	-0.0037
1	6	e	2	7	e	10025.0438	0.007	0.0073
1	7	e	2	8	e	9992.9517	0.007	0.0044
1	8	e	2	9	e	9959.0513	0.007	0.0004
1	9	e	2	10	e	9925.7136	0.007	0.0062
1	10	e	2	11	e	9885.2380	0.07	-0.0612
1	11	e	2	12	e	9845.4401	0.007	0.0006
1	12	e	2	13	e	9808.4491	0.007	-0.0007
1	13	e	2	14	e	9737.9046	10	-0.2720
1	14	e	2	15	e	9690.5869	0.007	0.0061
1	15	e	2	16	e	9653.8621	0.007	0.0088
1	16	e	2	17	e	9623.8618	0.007	-0.0135

υ'	J'	parity′	υ''	J''	parity″	Observed	Uncertainty	calc-obs
1	18	e	2	19	e	9469.6304	0.007	-0.0099
1	19	e	2	20	e	9421.2051	0.007	-0.0109
1	20	e	2	21	e	9372.0946	0.007	0.0035
1	5	f	2	4	f	10202.2810	0.007	-0.0077
1	6	f	2	5	f	10199.0070	0.007	-0.0055
1	7	f	2	6	f	10193.3484	0.007	-0.0042
1	9	f	2	8	f	10175.5845	0.007	0.0083
1	10	f	2	9	f	10161.8427	0.007	0.0063
1	11	f	2	10	f	10147.9095	0.007	-0.0106
1	12	f	2	11	f	10146.3500	0.07	-0.0871
1	13	f	2	12	f	10131.8817	0.07	-0.0905
1	14	f	2	13	f	10072.6552	0.07	-0.1039
1	15	f	2	14	f	10057.2615	0.07	0.0485
1	16	f	2	15	f	10048.4962	0.07	-0.1034
1	17	f	2	16	f	10044.6286	0.007	-0.0012
1	4	f	2	5	f	10082.2445	0.007	0.0063
1	5	f	2	6	f	10054.8811	0.007	-0.0052
1	6	f	2	7	f	10025.0438	0.007	0.0052
1	7	f	2	8	f	9992.9517	0.007	0.0057
1	8	f	2	9	f	9958.8064	0.07	-0.0663
1	9	f	2	10	f	9922.7874	0.007	-0.0125
1	10	f	2	11	f	9883.0679	0.007	0.0051
1	11	f	2	12	f	9843.4390	0.07	-0.0736
1	12	f	2	13	f	9816.2988	0.07	-0.1011
1	13	f	2	14	f	9776.2907	10	0.1599
1	14	f	2	15	f	9692.3321	10	-0.1041
1	15	f	2	16	f	9652.3432	0.007	-0.0006
1	16	f	2	17	f	9618.9359	10	0.2431
1	17	f	2	18	f	9591.6380	0.007	0.0024
1	4	f	2	4	e	10149.2993	0.007	-0.0026
1	5	f	2	5	e	10135.2301	0.007	-0.0027
1	6	f	2	6	e	10118.6374	0.007	0.0126
1	7	f	2	7	e	10099.7786	0.05	-0.0358
1	5	e	0	4	e	13842.1714	0.007	0.0068
1	6	e	0	5	e	13834.6542	0.007	0.0053
1	7	e	0	6	e	13823.9007	0.007	0.0033
1	8	e	0	7	e	13810.3544	0.007	0.0003
1	9	e	0	8	e	13796.3799	0.007	-0.0014

υ'	J'	parity′	υ''	J''	parity″	Observed	Uncertainty	calc-obs
1	10	e	0	9	e	13774.1762	0.007	0.0002
1	11	e	0	10	e	13751.7532	0.007	-0.0018
1	12	e	0	11	e	13731.0239	0.007	0.0017
1	13	e	0	12	e	13675.4254	0.007	-0.0089
1	14	e	0	13	e	13642.5073	0.007	0.0008
1	15	e	0	14	e	13618.8286	0.007	-0.0027
1	16	e	0	15	e	13600.7327	0.007	0.0034
1	17	e	0	16	e	13523.6622	0.007	-0.0046
1	18	e	0	17	e	13466.9997	0.007	-0.0015
1	19	e	0	18	e	13427.1218	0.007	-0.0088
1	20	e	0	19	e	13385.4346	0.007	-0.0068
1	21	e	0	20	e	13332.2533	0.007	-0.0106
1	22	e	0	21	e	13289.2108	0.007	-0.0073
1	23	e	0	22	e	13196.8415	0.007	0.0102
1	24	e	0	23	e	13123.4806	0.007	0.0034
1	4	e	0	5	e	13717.9109	0.007	-0.0057
1	5	e	0	6	e	13685.4360	0.007	0.0018
1	6	e	0	7	e	13649.6807	0.007	-0.0100
1	7	e	0	8	e	13610.7945	0.007	-0.0030
1	8	e	0	9	e	13569.2664	0.007	-0.0038
1	9	e	0	10	e	13527.4741	0.007	-0.0044
1	10	e	0	11	e	13477.6290	0.007	0.0040
1	11	e	0	12	e	13427.7753	0.007	-0.0002
1	12	e	0	13	e	13379.8363	0.007	0.0010
1	13	e	0	14	e	13297.2471	0.007	0.0099
1	14	e	0	15	e	13237.6370	0.007	0.0015
1	15	e	0	16	e	13187.5263	0.007	0.0018
1	16	e	0	17	e	13143.3108	0.007	0.0027
1	17	e	0	18	e	13040.4319	0.007	0.0043
1	18	e	0	19	e	12958.3275	0.007	0.0005
1	19	e	0	20	e	12893.3678	0.007	0.0016
1	20	e	0	21	e	12827.0135	0.007	0.0000
1	21	e	0	22	e	12749.5739	0.007	0.0165
1	22	e	0	23	e	12682.7759	0.007	0.0027
1	23	e	0	24	e	12567.1661	0.007	-0.0101
1	24	e	0	25	e	12471.0626	0.007	-0.0029
1	4	f	0	4	e	13789.2009	0.007	-0.0007
1	5	f	0	5	e	13770.8746	0.007	0.0084

υ'	J'	parity′	υ''	J''	parity″	Observed	Uncertainty	calc-obs
1	6	f	0	6	e	13749.2141	0.007	-0.0037
1	7	f	0	7	e	13724.3639	0.007	-0.0016
1	5	f	0	4	f	13842.1714	0.007	0.0053
1	6	f	0	5	f	13834.6542	0.007	0.0029
1	7	f	0	6	f	13823.9007	0.007	0.0038
1	8	f	0	7	f	13810.0392	0.007	0.0016
1	9	f	0	8	f	13793.4222	0.007	0.0049
1	10	f	0	9	f	13772.0607	0.007	-0.0038
1	11	f	0	10	f	13749.6388	0.007	0.0021
1	12	f	0	11	f	13738.6998	0.007	0.0006
1	13	f	0	12	f	13714.0771	0.007	0.0075
1	14	f	0	13	f	13643.8548	0.007	0.0003
1	15	f	0	14	f	13616.7660	0.007	0.0001
1	16	f	0	15	f	13595.1189	0.007	0.0006
1	17	f	0	16	f	13577.7014	0.007	0.0016
1	4	f	0	5	f	13717.9109	0.007	-0.0046
1	5	f	0	6	f	13685.4360	0.007	0.0002
1	6	f	0	7	f	13649.6807	0.007	-0.0125
1	7	f	0	8	f	13610.7945	0.007	-0.0028
1	8	f	0	9	f	13568.9490	0.007	-0.0010
1	9	f	0	10	f	13524.5163	0.007	0.0004
1	10	f	0	11	f	13475.5164	0.007	-0.0058
1	11	f	0	12	f	13425.6488	0.007	0.0100
1	12	f	0	13	f	13387.5003	0.007	0.0013
1	13	f	0	14	f	13335.9135	0.007	-0.0068
1	14	f	0	15	f	13238.9542	0.007	0.0005
1	15	f	0	16	f	13185.4188	0.007	-0.0006
1	16	f	0	17	f	13137.6177	0.007	-0.0001
1	17	f	0	18	f	13094.3615	0.007	-0.0022
2	9	e	0	8	e	15117.0796	0.007	0.0016
2	10	e	0	9	e	15093.6455	0.007	0.0009
2	11	e	0	10	e	15065.3443	0.007	-0.0052
2	12	e	0	11	e	15036.0993	0.007	-0.0070
2	13	e	0	12	e	15005.8933	0.007	-0.0086
2	14	e	0	13	e	14977.3235	0.007	-0.0192
2	15	e	0	14	e	14947.5975	0.02	-0.0298
2	16	e	0	15	e	14917.8163	0.03	-0.0333
2	8	e	0	9	e	14897.2603	0.007	0.0000

v'	J'	parity′	v''	J''	parity″	Observed	Uncertainty	calc-obs
2	9	e	0	10	e	14848.1739	0.007	-0.0016
2	10	e	0	11	e	14797.1041	0.007	-0.0010
2	11	e	0	12	e	14741.3578	0.007	0.0050
2	12	e	0	13	e	14684.8972	0.007	0.0068
2	13	e	0	14	e	14627.7167	0.007	0.0085
2	14	e	0	15	e	14572.4156	0.007	0.0191
2	15	e	0	16	e	14516.2534	0.015	0.0165
2	16	e	0	17	e	14460.3275	0.03	0.0329
2	9	f	0	8	f	15117.0796	0.007	0.0023
2	10	f	0	9	f	15092.5806	0.007	-0.0030
2	11	f	0	10	f	15064.6088	0.007	-0.0028
2	12	f	0	11	f	15034.9730	0.007	0.0047
2	13	f	0	12	f	15004.2208	0.007	0.0112
2	14	f	0	13	f	14974.3107	0.007	0.0143
2	8	f	0	9	f	14897.2603	0.007	0.0000
2	9	f	0	10	f	14848.1739	0.007	-0.0023
2	10	f	0	11	f	14796.0284	0.007	0.0029
2	11	f	0	12	f	14740.6212	0.007	0.0027
2	12	f	0	13	f	14683.7835	0.007	-0.0047
2	13	f	0	14	f	14626.0656	0.007	-0.0114
2	14	f	0	15	f	14569.4392	0.007	-0.0146
				$A'^3\Phi_3 - X^3\Phi_4$				
0	5	f	0	4	f	12749.5739	0.1	0.0572
0	7	f	0	6	f	12756.6590	0.1	-0.0953
0	8	f	0	7	f	12757.1450	0.1	-0.0928
0	9	f	0	8	f	12755.5038	0.007	0.0079
0	10	f	0	9	f	12751.8543	0.007	-0.0013
0	11	f	0	10	f	12745.9934	0.007	0.0022
0	12	f	0	11	f	12737.8831	0.007	0.0043
0	13	f	0	12	f	12727.4799	0.007	-0.0078
0	14	f	0	13	f	12714.7307	0.007	0.0003
0	15	f	0	14	f	12699.6199	0.007	-0.0034
0	16	f	0	15	f	12682.0789	0.007	-0.0017
0	17	f	0	16	f	12661.4772	0.007	0.0007
0	18	f	0	17	f	12639.7991	0.007	-0.0042
0	19	f	0	18	f	12614.7708	0.007	0.0056

υ'	J'	parity$'$	υ''	J''	parity$''$	Observed	Uncertainty	calc-obs
0	20	f	0	19	f	12587.8996	0.007	0.0013
0	6	f	0	7	f	12569.0703	0.07	-0.0355
0	7	f	0	8	f	12543.4619	0.007	-0.0110
0	4	f	0	4	e	12686.0263	0.1	0.0870
0	5	f	0	5	e	12678.3331	0.1	0.0042
0	6	f	0	6	e	12668.7777	0.1	-0.2008
0	7	f	0	7	e	12657.0096	0.02	0.0120
0	8	f	0	8	e	12643.5724	0.1	-0.0905
0	9	f	0	9	e	12627.9945	0.007	-0.0042
0	10	f	0	10	e	12610.4735	0.007	-0.0067
0	11	f	0	11	e	12590.8461	0.007	-0.0050
0	12	f	0	12	e	12569.0703	0.007	0.0010
0	13	f	0	13	e	12545.0988	0.007	0.0127
0	14	f	0	14	e	12518.9520	0.007	0.0022
0	5	e	0	5	f	12678.2646	0.007	0.0090
0	6	e	0	6	f	12668.3296	0.007	0.0054
0	7	e	0	7	f	12657.1811	0.03	-0.0739
0	8	e	0	8	f	12643.5724	0.007	0.0044
0	9	e	0	9	f	12627.9945	0.02	-0.0093
0	10	e	0	10	f	12610.1200	0.007	0.0102
0	11	e	0	11	f	12589.8252	0.007	-0.0026
0	12	e	0	12	f	12568.1216	0.007	-0.0162
0	13	e	0	13	f	12543.5024	0.007	-0.0065
0	14	e	0	14	f	12516.8748	0.05	-0.0648
0	5	e	0	4	e	12749.5739	0.007	-0.0065
0	6	e	0	5	e	12753.7929	0.01	-0.0111
0	7	e	0	6	e	12756.6590	0.01	-0.0095
0	8	e	0	7	e	12757.1450	0.007	0.0025
0	9	e	0	8	e	12755.5038	0.007	0.0040
0	10	e	0	9	e	12751.5267	0.007	-0.0077
0	11	e	0	10	e	12744.9990	0.007	-0.0163
0	12	e	0	11	e	12736.9328	0.007	0.0003
0	13	e	0	12	e	12725.8853	0.007	-0.0067
0	14	e	0	13	e	12712.6289	0.007	-0.0017
0	15	e	0	14	e	12697.2013	0.007	0.0070
0	5	e	0	6	e	12592.8366	0.007	-0.0097
0	8	e	0	9	e	12516.0619	0.007	-0.0066
0	7	f	1	6	f	10906.7327	0.1	-0.0391

υ'	J'	parity$'$	υ''	J''	parity$''$	Observed	Uncertainty	calc-obs
0	8	f	1	7	f	10910.2271	0.1	-0.0799
0	9	f	1	8	f	10912.0786	0.1	-0.0817
0	10	f	1	9	f	10912.0786	0.1	0.0749
0	11	f	1	10	f	10910.5290	0.007	0.0075
0	12	f	1	11	f	10907.0933	0.007	0.0003
0	13	f	1	12	f	10901.7797	0.007	-0.0121
0	14	f	1	13	f	10894.5414	0.07	-0.0023
0	15	f	1	14	f	10885.3679	0.007	-0.0082
0	16	f	1	15	f	10874.1696	0.007	0.0075
0	17	f	1	16	f	10860.3496	0.007	0.0055
0	18	f	1	17	f	10845.8654	0.007	0.0039
0	19	f	1	18	f	10828.4721	0.007	-0.0042
0	20	f	1	19	f	10809.6317	0.007	-0.0030
0	10	f	1	11	f	10624.5279	0.007	-0.0151
0	5	f	1	5	e	10825.9258	0.007	0.0013
0	6	f	1	6	e	10818.7078	0.007	-0.0009
0	7	f	1	7	e	10810.1902	1	-0.0739
0	8	f	1	8	e	10800.1036	1	-0.1373
0	9	f	1	9	e	10788.2863	0.007	0.0023
0	10	f	1	10	e	10774.9907	0.007	0.0125
0	11	f	1	11	e	10760.0301	0.007	0.0079
0	12	f	1	12	e	10743.2873	0.07	0.0619
0	13	f	1	13	e	10724.8631	0.07	0.0254
0	14	f	1	14	e	10704.5925	0.07	0.0521
0	15	f	1	15	e	10682.5205	0.07	0.0575
0	7	e	1	7	f	10810.1902	0.007	0.0121
0	8	e	1	8	f	10800.1036	0.07	-0.0416
0	9	e	1	9	f	10788.2863	0.007	-0.0006
0	10	e	1	10	f	10774.6744	0.007	-0.0033
0	11	e	1	11	f	10759.0248	0.007	0.0039
0	12	e	1	12	f	10742.4330	0.07	-0.0321
0	13	e	1	13	f	10723.2994	0.007	0.0047
0	14	e	1	14	f	10702.5487	0.007	0.0046
0	15	e	1	15	f	10680.1926	0.007	-0.0080
0	5	e	1	4	e	10895.0331	0.007	0.0082
0	9	e	1	8	e	10912.0786	0.07	-0.0865
0	11	e	1	10	e	10909.5152	0.007	0.0038
0	12	e	1	11	e	10906.1160	0.007	0.0140

υ'	J'	parity′	υ''	J''	parity″	Observed	Uncertainty	calc-obs
0	13	e	1	12	e	10900.1483	0.007	0.0083
0	14	e	1	13	e	10892.3694	0.07	0.0348
0	15	e	1	14	e	10882.8273	0.07	0.0714
0	5	e	1	6	e	10743.0039	0.07	-0.0471
0	7	e	1	8	e	10700.0244	0.007	-0.0030
0	9	e	1	10	e	10651.2637	0.07	-0.1284
0	10	e	1	11	e	10624.0954	0.07	0.0772
0	11	e	1	12	e	10595.2732	0.007	0.0112
				$A'^3\Phi_4 - X^3\Phi_3$				
0	5	f	1	4	f	12022.6392	0.007	-0.0109
0	6	f	0	5	f	12025.6986	0.007	0.0158
0	7	f	0	6	f	12026.7225	0.007	-0.0068
0	8	f	0	7	f	12025.4484	0.007	0.0011
0	9	f	0	8	f	12021.9650	0.007	-0.0075
0	10	f	0	9	f	12016.1790	0.007	-0.0065
0	11	f	0	10	f	12008.0582	0.007	-0.0187
0	12	f	0	11	f	11997.5437	0.007	-0.0083
0	13	f	0	12	f	11984.6319	0.007	0.0038
0	14	f	0	13	f	11969.3208	0.07	0.0368
0	15	f	0	14	f	11951.6828	0.007	0.0107
0	16	f	0	15	f	11931.6385	0.007	-0.0031
0	17	f	0	16	f	11908.6010	0.007	-0.0053
0	18	f	0	17	f	11884.6155	0.007	-0.0123
0	19	f	0	18	f	11857.4260	0.07	0.0367
0	20	f	0	19	f	11828.7263	0.007	-0.0121
0	21	f	0	20	f	11797.3040	0.007	0.0054
0	22	f	0	21	f	11763.6648	0.007	0.0085
0	23	f	0	22	f	11726.8736	0.007	0.0125
0	24	f	0	23	f	11691.9993	0.007	-0.0094
0	3	f	0	4	f	11908.7414	0.007	-0.0004
0	4	f	0	5	f	11886.5126	0.007	-0.0023
0	5	f	0	6	f	11863.0353	0.007	0.0073
0	6	f	0	7	f	11837.4475	0.007	-0.0154
0	7	f	0	8	f	11809.8826	0.007	0.0141
0	8	f	0	9	f	11780.2807	0.007	-0.0019
0	9	f	0	10	f	11748.6450	0.007	0.0003

υ'	J'	parity′	υ''	J''	parity″	Observed	Uncertainty	calc-obs
0	10	f	0	11	f	11714.9394	0.007	0.0151
0	11	f	0	12	f	11679.1721	0.007	0.0048
0	12	f	0	13	f	11641.3145	0.007	0.0007
0	13	f	0	14	f	11601.3690	0.007	0.0023
0	14	f	0	15	f	11559.3924	0.007	-0.0037
0	15	f	0	16	f	11515.3868	0.007	-0.0003
0	16	f	0	17	f	11469.3866	0.007	-0.0030
0	17	f	0	18	f	11420.8216	0.007	-0.0012
0	18	f	0	19	f	11371.7400	0.007	0.0131
0	19	f	0	20	f	11320.0163	0.007	-0.0015
0	20	f	0	21	f	11267.1596	0.007	0.0147
0	21	f	0	22	f	11212.2162	0.007	-0.0040
0	22	f	0	23	f	11155.5904	0.007	-0.0069
0	23	f	0	24	f	11096.4089	0.007	-0.0105
0	24	f	0	25	f	11039.7181	0.007	0.0114
0	3	f	0	3	e	11966.8995	0.007	-0.0019
0	4	f	0	4	e	11959.0570	0.07	0.0671
0	5	f	0	5	e	11950.0609	0.07	0.0128
0	6	f	0	6	e	11938.8586	0.07	-0.0042
0	7	f	0	7	e	11925.5321	0.1	0.1841
0	8	f	0	8	e	11910.0915	0.5	0.4678
0	5	e	0	4	e	12022.6392	0.5	-0.0611
0	6	e	0	5	e	12025.6986	10	-0.1804
0	7	e	0	6	e	12026.7225	10	0.2044
0	8	e	0	7	e	12025.4484	10	0.3936
0	9	e	0	8	e	12021.9650	10	0.6203
0	10	e	0	9	e	12016.1790	10	0.8930
0	11	e	0	10	e	12008.0582	10	1.2203
0	14	e	0	13	e	11977.4499	0.007	-0.0029
0	16	e	0	15	e	11942.8805	0.007	-0.0009
0	17	e	0	16	e	11925.5321	0.007	-0.0011
0	3	e	0	4	e	11908.7414	10	-0.0012
0	4	e	0	5	e	11886.5126	10	-0.0011
0	5	e	0	6	e	11863.3069	10	-0.2025
0	6	e	0	7	e	11837.7463	10	-0.2587
0	7	e	0	8	e	11810.2829	10	0.3316
0	8	e	0	9	e	11780.9184	10	0.6900
0	9	e	0	10	e	11749.6956	10	1.1992

υ'	J'	parity′	υ''	J''	parity″	Observed	Uncertainty	calc-obs
0	10	e	0	11	e	11716.8787	10	1.6354
0	11	e	0	12	e	11682.9216	10	1.6687
0	12	e	0	13	e	11650.5633	0.007	0.0013

B.2 Line list for CoD

Table B.2: Line list for CoD.

Lines from Refs. [4,5] of Chapter 5								
$A^3\Phi_4 - X^3\Phi_4$								
υ'	J'	parity′	υ''	J''	parity″	Observed	Uncertainty	calc-obs
0	5	e	0	4	e	22299.23	0.03	0.074
0	6	e	0	5	e	22302.21	0.03	0.005
0	7	e	0	6	e	22304.29	0.03	0.002
0	8	e	0	7	e	22305.61	0.03	-0.030
0	9	e	0	8	e	22306.18	0.03	-0.065
0	10	e	0	9	e	22305.82	0.03	-0.001
0	11	e	0	10	e	22304.71	0.03	0.032
0	12	e	0	11	e	22302.81	0.03	-0.010
0	13	e	0	12	e	22300.27	0.03	-0.017
0	14	e	0	13	e	22297.04	0.03	0.033
0	15	e	0	14	e	22292.40	0.03	-0.005
0	16	e	0	15	e	22287.21	0.03	0.021
0	17	e	0	16	e	22281.17	0.03	0.007
0	18	e	0	17	e	22274.23	0.03	0.018
0	19	e	0	18	e	22266.45	0.03	-0.026
0	20	e	0	19	e	22257.75	0.03	0.015
0	21	e	0	20	e	22248.24	0.03	0.016
0	22	e	0	21	e	22237.66	0.03	0.064
0	23	e	0	22	e	22225.86	0.03	0.039
0	24	e	0	23	e	22211.96	0.03	-0.050
0	25	e	0	24	e	22204.58	0.03	0.012
0	26	e	0	25	e	22189.91	0.03	0.021

υ'	J'	parity′	υ''	J''	parity″	Observed	Uncertainty	calc-obs
0	27	e	0	26	e	22174.80	0.03	0.007
0	28	e	0	27	e	22158.91	0.03	0.009
0	29	e	0	28	e	22142.14	0.03	-0.006
0	30	e	0	29	e	22124.45	0.03	-0.016
0	31	e	0	30	e	22105.72	0.03	0.000
0	4	e	0	5	e	22228.79	0.03	-0.017
0	5	e	0	6	e	22217.59	0.03	-0.041
0	6	e	0	7	e	22205.63	0.03	0.035
0	7	e	0	8	e	22192.99	0.03	-0.009
0	8	e	0	9	e	22179.56	0.03	-0.011
0	9	e	0	10	e	22165.41	0.03	-0.001
0	10	e	0	11	e	22150.50	0.03	-0.012
0	11	e	0	12	e	22134.85	0.03	-0.009
0	12	e	0	13	e	22118.40	0.03	-0.009
0	13	e	0	14	e	22101.45	0.03	-0.048
0	14	e	0	15	e	22083.86	0.03	-0.009
0	15	e	0	16	e	22064.85	0.03	0.028
0	16	e	0	17	e	22045.46	0.03	0.041
0	17	e	0	18	e	22025.31	0.03	0.011
0	18	e	0	19	e	22004.34	0.03	0.016
0	19	e	0	20	e	21982.62	0.03	-0.027
0	20	e	0	21	e	21960.11	0.03	-0.013
0	21	e	0	22	e	21936.88	0.03	-0.023
0	22	e	0	23	e	21912.71	0.03	-0.005
0	23	e	0	24	e	21887.39	0.03	-0.014
0	24	e	0	25	e	21860.04	0.03	-0.036
0	25	e	0	26	e	21839.44	0.03	-0.011
0	26	e	0	27	e	21811.66	0.03	-0.020
0	27	e	0	28	e	21783.53	0.03	-0.007
0	28	e	0	29	e	21754.79	0.03	-0.009
0	29	e	0	30	e	21725.28	0.03	0.006
0	30	e	0	31	e	21695.01	0.03	0.015
0	4	f	0	4	e	22265.94	0.03	0.011
0	5	f	0	5	e	22262.17	0.03	-0.029
0	6	f	0	6	e	22257.64	0.03	0.001
0	7	f	0	7	e	22252.33	0.03	-0.009
0	8	f	0	8	e	22246.22	0.03	0.004
0	9	f	0	9	e	22239.45	0.03	-0.024

v'	J'	parity$'$	v''	J''	parity$''$	Observed	Uncertainty	calc-obs
0	10	f	0	10	e	22231.79	0.03	0.014
0	11	f	0	11	e	22223.40	0.03	0.027
0	12	f	0	12	e	22214.27	0.03	-0.027
0	13	f	0	13	e	22204.58	0.03	-0.065
0	14	f	0	14	e	22194.00	0.03	0.031
0	15	f	0	15	e	22182.20	0.03	0.001
0	16	f	0	16	e	22169.83	0.03	0.062
0	17	f	0	17	e	22156.79	0.03	-0.012
0	18	f	0	18	e	22142.86	0.03	0.012
0	4	f	0	4	e	22265.94	0.03	0.011
0	5	f	0	5	e	22262.17	0.03	-0.029
0	6	f	0	6	e	22257.64	0.03	0.001
0	7	f	0	7	e	22252.33	0.03	-0.009
0	8	f	0	8	e	22246.22	0.03	0.004
0	9	f	0	9	e	22239.45	0.03	-0.024
0	10	f	0	10	e	22231.79	0.03	0.014
0	11	f	0	11	e	22223.40	0.03	0.027
0	12	f	0	12	e	22214.27	0.03	-0.027
0	13	f	0	13	e	22204.58	0.03	-0.065
0	14	f	0	14	e	22194.00	0.03	0.031
0	15	f	0	15	e	22182.20	0.03	0.001
0	16	f	0	16	e	22169.83	0.03	0.062
0	17	f	0	17	e	22156.79	0.03	-0.012
0	18	f	0	18	e	22142.86	0.03	0.012
0	5	f	0	4	f	22299.23	0.03	0.086
0	6	f	0	5	f	22302.21	0.03	0.011
0	7	f	0	6	f	22304.29	0.03	0.001
0	8	f	0	7	f	22305.61	0.03	-0.045
0	9	f	0	8	f	22306.18	0.03	-0.064
0	10	f	0	9	f	22305.82	0.03	0.000
0	11	f	0	10	f	22304.71	0.03	0.032
0	12	f	0	11	f	22302.81	0.03	0.018
0	13	f	0	12	f	22300.27	0.03	0.068
0	14	f	0	13	f	22297.04	0.03	0.019
0	15	f	0	14	f	22292.40	0.03	-0.005
0	16	f	0	15	f	22287.21	0.03	0.004
0	17	f	0	16	f	22281.17	0.03	0.015
0	18	f	0	17	f	22274.32	0.03	0.000

v'	J'	parity′	v''	J''	parity″	Observed	Uncertainty	calc-obs
0	19	f	0	18	f	22266.61	0.03	0.003
0	20	f	0	19	f	22257.96	0.03	0.049
0	21	f	0	20	f	22248.49	0.03	-0.003
0	22	f	0	21	f	22238.05	0.03	0.054
0	23	f	0	22	f	22226.70	0.03	0.004
0	24	f	0	23	f	22214.27	0.03	0.030
0	25	f	0	24	f	22200.74	0.03	0.043
0	26	f	0	25	f	22185.53	0.03	0.046
0	27	f	0	26	f	22178.28	0.03	-0.009
0	28	f	0	27	f	22160.43	0.03	0.064
0	29	f	0	28	f	22142.86	0.03	0.022
0	30	f	0	29	f	22124.63	0.03	-0.024
0	4	f	0	5	f	22228.79	0.03	-0.014
0	5	f	0	6	f	22217.59	0.03	-0.029
0	6	f	0	7	f	22205.63	0.03	0.041
0	7	f	0	8	f	22192.99	0.03	-0.010
0	8	f	0	9	f	22179.56	0.03	-0.026
0	9	f	0	10	f	22165.41	0.03	0.000
0	10	f	0	11	f	22150.50	0.03	-0.012
0	11	f	0	12	f	22134.85	0.03	-0.009
0	12	f	0	13	f	22118.40	0.03	0.020
0	13	f	0	14	f	22101.45	0.03	0.037
0	14	f	0	15	f	22083.86	0.03	-0.024
0	15	f	0	16	f	22064.85	0.03	0.028
0	16	f	0	17	f	22045.46	0.03	0.024
0	17	f	0	18	f	22025.31	0.03	0.017
0	18	f	0	19	f	22004.45	0.03	-0.023
0	19	f	0	20	f	21982.78	0.03	0.001
0	20	f	0	21	f	21960.38	0.03	-0.042
0	21	f	0	22	f	21937.10	0.03	-0.015
0	22	f	0	23	f	21913.09	0.03	-0.009
0	23	f	0	24	f	21888.20	0.03	-0.025
0	24	f	0	25	f	21862.37	0.03	0.017
0	25	f	0	26	f	21835.58	0.03	0.030
0	26	f	0	27	f	21807.29	0.03	-0.019
0	27	f	0	28	f	21786.96	0.03	0.009
0	28	f	0	29	f	21756.40	0.03	-0.066
0	29	f	0	30	f	21726.03	0.03	-0.023

v'	J'	parity′	v''	J''	parity″	Observed	Uncertainty	calc-obs
0	30	f	0	31	f	21695.14	0.03	0.022
1	5	e	0	4	e	23413.63	0.03	0.031
1	6	e	0	5	e	23415.29	0.03	-0.003
1	7	e	0	6	e	23415.94	0.03	0.006
1	8	e	0	7	e	23415.61	0.03	0.001
1	9	e	0	8	e	23414.30	0.03	0.006
1	10	e	0	9	e	23411.98	0.03	-0.029
1	11	e	0	10	e	23408.64	0.03	-0.006
1	12	e	0	11	e	23404.33	0.03	-0.030
1	13	e	0	12	e	23399.85	0.03	-0.012
1	14	e	0	13	e	23392.84	0.03	0.014
1	15	e	0	14	e	23385.31	0.03	0.017
1	16	e	0	15	e	23376.79	0.03	0.024
1	17	e	0	16	e	23367.23	0.03	-0.034
1	18	e	0	17	e	23356.56	0.03	0.010
1	19	e	0	18	e	23344.80	0.03	0.024
1	20	e	0	19	e	23331.91	0.03	0.013
1	21	e	0	20	e	23317.87	0.03	0.051
1	22	e	0	21	e	23302.69	0.03	0.022
1	23	e	0	22	e	23286.30	0.03	0.000
1	24	e	0	23	e	23268.66	0.03	0.018
1	4	e	0	5	e	23343.97	0.03	0.017
1	5	e	0	6	e	23331.91	0.03	-0.004
1	6	e	0	7	e	23318.66	0.03	0.077
1	7	e	0	8	e	23304.60	0.03	0.035
1	8	e	0	9	e	23289.57	0.03	0.010
1	9	e	0	10	e	23273.55	0.03	0.050
1	10	e	0	11	e	23256.60	0.03	0.020
1	11	e	0	12	e	23238.72	0.03	0.013
1	12	e	0	13	e	23219.84	0.03	0.051
1	13	e	0	14	e	23200.96	0.03	0.027
1	14	e	0	15	e	23179.63	0.03	0.002
1	15	e	0	16	e	23157.78	0.03	0.030
1	16	e	0	17	e	23135.06	0.03	0.024
1	17	e	0	18	e	23111.33	0.03	0.010
1	18	e	0	19	e	23086.72	0.03	-0.042
1	19	e	0	20	e	23060.98	0.03	0.013
1	20	e	0	21	e	23034.28	0.03	-0.025

v'	J'	parity$'$	v''	J''	parity$''$	Observed	Uncertainty	calc-obs
1	21	e	0	22	e	23006.56	0.03	-0.038
1	22	e	0	23	e	22977.72	0.03	-0.027
1	23	e	0	24	e	22947.81	0.03	-0.033
1	24	e	0	25	e	22916.79	0.03	-0.018
1	4	f	0	4	e	23381.17	0.03	0.020
1	5	f	0	5	e	23376.50	0.03	-0.007
1	6	f	0	6	e	23370.70	0.03	0.006
1	7	f	0	7	e	23363.97	0.03	-0.006
1	8	f	0	8	e	23356.29	0.03	-0.011
1	9	f	0	9	e	23347.64	0.03	-0.016
1	10	f	0	10	e	23337.94	0.03	0.003
1	11	f	0	11	e	23327.33	0.03	-0.019
1	12	f	0	12	e	23315.68	0.03	0.001
1	5	f	0	4	f	23413.63	0.03	0.038
1	6	f	0	5	f	23415.29	0.03	-0.004
1	7	f	0	6	f	23415.94	0.03	-0.006
1	8	f	0	7	f	23415.61	0.03	0.010
1	9	f	0	8	f	23414.30	0.03	0.014
1	10	f	0	9	f	23411.98	0.03	-0.021
1	11	f	0	10	f	23408.64	0.03	-0.014
1	12	f	0	11	f	23404.33	0.03	-0.064
1	13	f	0	12	f	23398.91	0.03	-0.019
1	14	f	0	13	f	23392.48	0.03	0.007
1	15	f	0	14	f	23384.97	0.03	0.009
1	16	f	0	15	f	23376.37	0.03	-0.013
1	17	f	0	16	f	23366.51	0.03	0.032
1	18	f	0	17	f	23354.97	0.03	-0.017
1	20	f	0	19	f	23332.91	0.03	-0.003
1	21	f	0	20	f	23318.66	0.03	-0.026
1	22	f	0	21	f	23303.23	0.03	0.047
1	23	f	0	22	f	23286.80	0.03	0.020
1	4	f	0	5	f	23343.97	0.03	0.045
1	5	f	0	6	f	23331.91	0.03	0.003
1	6	f	0	7	f	23318.66	0.03	0.076
1	7	f	0	8	f	23304.60	0.03	0.023
1	8	f	0	9	f	23289.57	0.03	0.019
1	9	f	0	10	f	23273.55	0.03	0.058
1	10	f	0	11	f	23256.60	0.03	0.027

υ'	J'	parity′	υ''	J''	parity″	Observed	Uncertainty	calc-obs
1	11	f	0	12	f	23238.72	0.03	0.005
1	12	f	0	13	f	23219.84	0.03	0.018
1	13	f	0	14	f	23200.05	0.03	-0.010
1	14	f	0	15	f	23179.23	0.03	0.034
1	15	f	0	16	f	23157.47	0.03	-0.008
1	16	f	0	17	f	23134.61	0.03	0.017
1	17	f	0	18	f	23110.78	0.03	-0.096
1	18	f	0	19	f	23085.05	0.03	0.010
1	20	f	0	21	f	23035.28	0.03	-0.044
1	21	f	0	22	f	23007.26	0.03	-0.028
1	22	f	0	23	f	22978.29	0.03	-0.036
1	23	f	0	24	f	22948.32	0.03	-0.029
0	5	e	1	4	e	20961.53	0.03	-0.006
0	6	e	1	5	e	20965.29	0.03	-0.071
0	7	e	1	6	e	20968.21	0.03	0.027
0	8	e	1	7	e	20970.65	0.03	-0.027
0	9	e	1	8	e	20972.38	0.03	0.032
0	10	e	1	9	e	20973.50	0.03	0.027
0	11	e	1	10	e	20973.88	10	0.137
0	12	e	1	11	e	20973.78	0.03	0.018
0	13	e	1	12	e	20973.15	10	-0.019
0	14	e	1	13	e	20972.00	0.03	-0.015
0	15	e	1	14	e	20969.50	0.03	-0.001
0	16	e	1	15	e	20966.71	0.03	-0.029
0	17	e	1	16	e	20963.12	0.03	0.009
0	18	e	1	17	e	20958.89	0.03	-0.033
0	19	e	1	18	e	20953.79	0.03	0.055
0	20	e	1	19	e	20948.34	10	-0.188
0	21	e	1	20	e	20941.68	0.03	0.085
0	22	e	1	21	e	20934.53	0.03	-0.022
0	23	e	1	22	e	20926.07	0.03	0.043
0	24	e	1	23	e	20915.68	0.03	0.027
0	4	e	1	5	e	20891.59	0.1	0.187
0	5	e	1	6	e	20881.52	0.03	-0.026
0	6	e	1	7	e	20870.68	0.03	0.028
0	7	e	1	8	e	20859.30	0.03	-0.022
0	8	e	1	9	e	20847.19	0.03	0.067
0	9	e	1	10	e	20834.65	0.03	0.034

υ'	J'	parity′	υ''	J''	parity″	Observed	Uncertainty	calc-obs
0	10	e	1	11	e	20821.50	0.03	-0.014
0	11	e	1	12	e	20807.74	0.03	-0.021
0	12	e	1	13	e	20793.30	0.03	0.003
0	13	e	1	14	e	20778.44	0.03	0.066
0	14	e	1	15	e	20763.31	0.03	-0.009
0	15	e	1	16	e	20746.85	0.03	-0.020
0	16	e	1	17	e	20730.14	0.03	-0.030
0	17	e	1	18	e	20712.77	0.03	-0.028
0	18	e	1	19	e	20694.85	10	-0.107
0	19	e	1	20	e	20676.29	10	-0.188
0	20	e	1	21	e	20657.01	10	-0.129
0	21	e	1	22	e	20637.15	0.03	-0.079
0	22	e	1	23	e	20616.54	0.03	-0.038
0	23	e	1	24	e	20594.98	0.03	-0.069
0	24	e	1	25	e	20571.37	0.03	0.059
0	4	f	1	4	e	20928.18	0.03	-0.009
0	5	f	1	5	e	20925.14	0.03	0.005
0	6	f	1	6	e	20921.61	0.03	-0.024
0	7	f	1	7	e	20917.34	0.03	0.024
0	8	f	1	8	e	20912.47	0.03	0.051
0	9	f	1	9	e	20907.09	0.03	0.044
0	10	f	1	10	e	20901.11	0.03	-0.031
0	11	f	1	11	e	20894.48	0.03	-0.055
0	12	f	1	12	e	20887.18	0.03	-0.059
0	13	f	1	13	e	20879.47	0.03	-0.043
0	14	f	1	14	e	20871.27	10	-0.135
0	15	f	1	15	e	20861.50	10	0.151
0	16	f	1	16	e	20851.90	0.03	-0.056
0	5	f	1	4	f	20961.53	0.03	0.006
0	6	f	1	5	f	20965.29	0.03	-0.065
0	7	f	1	6	f	20968.21	0.03	0.026
0	8	f	1	7	f	20970.65	0.03	-0.042
0	9	f	1	8	f	20972.38	0.03	0.033
0	10	f	1	9	f	20973.50	0.03	0.028
0	11	f	1	10	f	20973.88	10	0.137
0	12	f	1	11	f	20973.78	0.03	0.047
0	13	f	1	12	f	20973.15	0.03	0.065
0	14	f	1	13	f	20972.00	0.03	-0.029

υ'	J'	parity′	υ''	J''	parity″	Observed	Uncertainty	calc-obs
0	15	f	1	14	f	20969.50	0.03	-0.002
0	16	f	1	15	f	20966.71	0.03	-0.046
0	17	f	1	16	f	20963.12	0.03	0.016
0	18	f	1	17	f	20958.89	0.03	0.038
0	19	f	1	18	f	20953.79	10	0.243
0	20	f	1	19	f	20948.34	0.03	0.055
0	21	f	1	20	f	20941.93	0.03	0.063
0	22	f	1	21	f	20934.87	0.03	0.015
0	23	f	1	22	f	20926.88	0.03	0.032
0	24	f	1	23	f	20918.11	0.03	-0.021
0	25	f	1	24	f	20908.38	0.03	-0.074
0	26	f	1	25	f	20897.01	0.03	-0.027
0	4	f	1	5	f	20891.59	10	0.190
0	5	f	1	6	f	20881.52	0.03	-0.014
0	6	f	1	7	f	20870.68	0.03	0.034
0	7	f	1	8	f	20859.30	0.03	-0.023
0	8	f	1	9	f	20847.19	0.03	0.052
0	9	f	1	10	f	20834.65	0.03	0.035
0	10	f	1	11	f	20821.50	0.03	-0.013
0	11	f	1	12	f	20807.74	0.03	-0.022
0	12	f	1	13	f	20793.30	0.03	0.032
0	13	f	1	14	f	20778.44	0.15	0.150
0	14	f	1	15	f	20763.31	0.03	-0.024
0	15	f	1	16	f	20746.85	0.03	-0.021
0	16	f	1	17	f	20730.14	0.03	-0.048
0	17	f	1	18	f	20712.77	0.03	-0.023
0	18	f	1	19	f	20694.85	0.03	-0.037
0	19	f	1	20	f	20676.29	0.03	-0.003
0	20	f	1	21	f	20657.18	0.03	-0.061
0	21	f	1	22	f	20637.34	0.03	-0.047
0	22	f	1	23	f	20616.93	0.03	-0.060
0	23	f	1	24	f	20595.81	0.1	-0.112
0	24	f	1	25	f	20573.82	0.03	-0.026
1	5	e	1	4	e	22075.92	0.03	-0.039
1	6	e	1	5	e	22078.31	0.03	-0.019
1	7	e	1	6	e	22079.86	0.03	0.031
1	8	e	1	7	e	22080.83	10	-0.176
1	9	e	1	8	e	22080.61	0.03	-0.007

υ'	J'	parity′	υ''	J''	parity″	Observed	Uncertainty	calc-obs
1	10	e	1	9	e	22079.64	0.03	0.019
1	11	e	1	10	e	22077.86	0.03	0.049
1	12	e	1	11	e	22075.17	10	0.128
1	13	e	1	12	e	22072.72	0.03	-0.004
1	14	e	1	13	e	22067.71	0.03	0.056
1	15	e	1	14	e	22062.38	0.03	0.051
1	16	e	1	15	e	22056.22	0.03	0.044
1	17	e	1	16	e	22049.10	0.03	0.048
1	18	e	1	17	e	22041.16	0.03	0.019
1	19	e	1	18	e	22032.24	0.03	0.005
1	20	e	1	19	e	22022.26	0.03	0.050
1	21	e	1	20	e	22011.41	0.03	0.020
1	22	e	1	21	e	21999.49	0.03	0.006
1	23	e	1	22	e	21986.48	0.03	0.034
1	4	e	1	5	e	22007.18	0.1	-0.189
1	5	e	1	6	e	21995.93	0.1	-0.079
1	6	e	1	7	e	21983.80	0.03	-0.020
1	7	e	1	8	e	21971.09	10	-0.158
1	8	e	1	9	e	21957.24	0.03	0.048
1	9	e	1	10	e	21942.87	0.03	0.005
1	10	e	1	11	e	21927.60	0.03	0.018
1	11	e	1	12	e	21911.60	0.03	0.011
1	12	e	1	13	e	21894.85	0.03	-0.047
1	13	e	1	14	e	21878.10	0.03	-0.009
1	14	e	1	15	e	21859.07	0.03	0.012
1	15	e	1	16	e	21839.75	0.03	0.012
1	16	e	1	17	e	21819.69	0.03	0.003
1	17	e	1	18	e	21798.70	0.03	0.061
1	18	e	1	19	e	21777.01	0.03	0.055
1	20	e	1	21	e	21731.04	0.03	-0.001
1	21	e	1	22	e	21706.72	0.03	0.016
1	4	f	1	4	e	22043.42	0.03	-0.010
1	5	f	1	5	e	22039.43	0.03	0.067
1	6	f	1	6	e	22034.62	0.03	0.031
1	7	f	1	7	e	22028.96	0.03	0.047
1	8	f	1	8	e	22022.57	0.03	0.006
1	9	f	1	9	e	22015.35	0.03	-0.018
1	10	f	1	10	e	22007.18	0.03	0.038

υ'	J'	parity′	υ''	J''	parity″	Observed	Uncertainty	calc-obs
1	11	f	1	11	e	21998.24	0.03	0.069
1	12	f	1	12	e	21988.49	0.03	0.069
1	5	f	1	4	f	22075.92	0.03	-0.032
1	6	f	1	5	f	22078.31	0.03	-0.020
1	7	f	1	6	f	22079.86	0.03	0.019
1	8	f	1	7	f	22080.83	10	-0.167
1	9	f	1	8	f	22080.61	0.03	0.001
1	10	f	1	9	f	22079.64	0.03	0.027
1	11	f	1	10	f	22077.86	0.03	0.041
1	12	f	1	11	f	22075.17	0.03	0.095
1	13	f	1	12	f	22071.72	0.03	0.048
1	14	f	1	13	f	22067.38	0.03	0.019
1	15	f	1	14	f	22062.04	0.03	0.042
1	16	f	1	15	f	22055.74	0.03	0.067
1	17	f	1	16	f	22048.44	0.03	0.053
1	18	f	1	17	f	22039.43	10	0.131
1	20	f	1	19	f	22023.28	0.03	0.013
1	21	f	1	20	f	22012.06	0.03	0.080
1	22	f	1	21	f	22000.07	0.03	-0.012
1	23	f	1	22	f	21987.02	0.03	0.008
1	4	f	1	5	f	22007.18	0.15	-0.161
1	5	f	1	6	f	21995.93	0.03	-0.072
1	6	f	1	7	f	21983.80	0.03	-0.021
1	7	f	1	8	f	21971.09	10	-0.170
1	8	f	1	9	f	21957.24	0.03	0.057
1	9	f	1	10	f	21942.87	0.03	0.013
1	10	f	1	11	f	21927.60	0.03	0.026
1	11	f	1	12	f	21911.60	0.03	0.002
1	12	f	1	13	f	21894.85	0.03	-0.080
1	13	f	1	14	f	21877.11	0.03	0.033
1	14	f	1	15	f	21858.65	0.03	0.064
1	15	f	1	16	f	21839.44	0.03	-0.027
1	16	f	1	17	f	21819.23	0.03	0.005
1	17	f	1	18	f	21798.07	0.03	0.034
1	18	f	1	19	f	21775.34	0.1	0.106
1	20	f	1	21	f	21732.13	0.1	-0.113
1	21	f	1	22	f	21707.26	10	0.180
2	5	e	1	4	e	23124.56	0.03	-0.060

υ'	J'	parity$'$	υ''	J''	parity$''$	Observed	Uncertainty	calc-obs
2	6	e	1	5	e	23125.43	0.03	-0.005
2	7	e	1	6	e	23125.43	0.03	0.004
2	8	e	1	7	e	23124.25	0.03	-0.007
2	9	e	1	8	e	23121.88	0.03	-0.011
2	10	e	1	9	e	23118.57	0.03	-0.024
2	11	e	1	10	e	23114.14	0.03	-0.016
2	12	e	1	11	e	23108.37	0.03	0.047
2	13	e	1	12	e	23101.19	0.03	-0.062
2	4	e	1	5	e	23056.75	0.03	-0.001
2	5	e	1	6	e	23044.41	0.03	0.060
2	6	e	1	7	e	23030.91	0.03	0.004
2	7	e	1	8	e	23016.48	0.03	-0.005
2	8	e	1	9	e	23000.87	0.03	0.007
2	9	e	1	10	e	22984.13	0.03	0.011
2	10	e	1	11	e	22966.48	0.03	0.025
2	11	e	1	12	e	22947.81	0.03	0.016
2	12	e	1	13	e	22927.97	0.03	-0.048
2	13	e	1	14	e	22906.44	0.03	0.063
2	4	f	1	4	e	23093.38	0.03	0.000
2	5	f	1	5	e	23088.02	0.03	-0.001
2	6	f	1	6	e	23081.82	0.03	0.000
2	7	f	1	7	e	23074.57	0.03	0.000
2	8	f	1	8	e	23066.10	0.03	-0.001
1	5	e	2	4	e	20773.34	0.03	0.022
1	6	e	2	5	e	20776.56	0.03	-0.003
1	7	e	2	6	e	20779.12	0.03	-0.021
1	8	e	2	7	e	20780.99	0.03	-0.031
1	9	e	2	8	e	20782.13	0.03	0.032
1	10	e	2	9	e	20782.59	0.03	0.035
1	11	e	2	10	e	20782.59	10	-0.151
1	12	e	2	11	e	20781.50	0.03	0.046
1	13	e	2	12	e	20780.99	10	-0.153
1	14	e	2	13	e	20777.92	0.03	-0.006
1	15	e	2	14	e	20774.78	0.03	-0.022
1	16	e	2	15	e	20770.99	0.03	-0.065
1	17	e	2	16	e	20766.36	0.03	-0.063
1	18	e	2	17	e	20760.94	0.03	0.029
1	19	e	2	18	e	20754.87	0.03	-0.040

υ'	J'	parity′	υ''	J''	parity″	Observed	Uncertainty	calc-obs
1	20	e	2	19	e	20747.88	0.03	-0.034
1	21	e	2	20	e	20740.12	0.03	-0.049
1	6	e	2	7	e	20684.12	0.03	-0.035
1	7	e	2	8	e	20672.54	0.03	-0.049
1	8	e	2	9	e	20660.28	0.03	-0.026
1	9	e	2	10	e	20647.49	0.03	-0.085
1	10	e	2	11	e	20633.93	0.03	-0.064
1	11	e	2	12	e	20619.80	0.03	-0.068
1	12	e	2	13	e	20604.97	0.03	-0.019
1	14	e	2	15	e	20573.82	0.03	-0.077
1	15	e	2	16	e	20557.00	0.03	-0.089
1	16	e	2	17	e	20539.51	0.03	-0.027
1	17	e	2	18	e	20521.37	0.03	-0.024
1	18	e	2	19	e	20502.67	0.03	-0.069
1	19	e	2	20	e	20483.35	10	-0.207
1	4	f	2	4	e	20740.94	0.03	-0.049
1	5	f	2	5	e	20737.79	0.03	-0.027
1	6	f	2	6	e	20733.89	0.03	-0.031
1	7	f	2	7	e	20729.29	0.03	0.022
1	8	f	2	8	e	20724.18	0.03	-0.045
1	9	f	2	9	e	20718.31	0.03	-0.012
1	10	f	2	10	e	20711.79	0.03	-0.042
1	11	f	2	11	e	20704.56	0.03	-0.003
1	5	f	2	4	f	20773.34	0.03	0.029
1	6	f	2	5	f	20776.56	0.03	-0.004
1	7	f	2	6	f	20779.12	0.03	-0.033
1	8	f	2	7	f	20780.99	0.03	-0.022
1	9	f	2	8	f	20782.13	0.03	0.039
1	10	f	2	9	f	20782.59	10	0.043
1	11	f	2	10	f	20782.59	10	-0.159
1	12	f	2	11	f	20781.50	0.03	0.013
1	13	f	2	12	f	20779.94	0.03	-0.051
1	14	f	2	13	f	20777.61	0.03	-0.065
1	15	f	2	14	f	20774.40	0.03	0.007
1	16	f	2	15	f	20770.50	0.03	-0.037
1	17	f	2	16	f	20765.62	0.03	0.014
1	18	f	2	17	f	20759.34	0.03	-0.002
1	20	f	2	19	f	20748.75	0.03	0.046

υ'	J'	parity′	υ''	J''	parity″	Observed	Uncertainty	calc-obs
1	21	f	2	20	f	20740.76	0.03	-0.026
1	6	f	2	7	f	20684.12	0.03	-0.036
1	7	f	2	8	f	20672.54	0.03	-0.062
1	8	f	2	9	f	20660.28	0.03	-0.017
1	9	f	2	10	f	20647.49	0.03	-0.077
1	10	f	2	11	f	20633.93	0.03	-0.056
1	11	f	2	12	f	20619.80	0.03	-0.077
1	12	f	2	13	f	20604.97	0.03	-0.054
1	13	f	2	14	f	20589.66	10	-0.192
1	14	f	2	15	f	20573.43	0.03	-0.060
1	15	f	2	16	f	20556.58	0.03	-0.026
1	16	f	2	17	f	20539.05	0.03	-0.038
1	17	f	2	18	f	20520.71	0.03	-0.041
1	18	f	2	19	f	20501.07	10	-0.121
					$A^3\Phi_3 - X^3\Phi_3$			
0	4	f	1	3	f	21955.15	0.03	-0.0600
0	5	f	1	4	f	21958.77	0.03	0.0013
0	6	f	1	5	f	21961.73	0.03	-0.0025
0	7	f	1	6	f	21963.89	0.03	0.0058
0	8	f	1	7	f	21965.30	0.03	-0.0105
0	9	f	1	8	f	21965.90	0.03	-0.0160
0	10	f	1	9	f	21965.72	0.03	-0.0079
0	11	f	1	10	f	21964.72	0.03	0.0110
0	12	f	1	11	f	21962.96	0.03	0.0392
0	13	f	1	12	f	21960.38	0.03	-0.0195
0	14	f	1	13	f	21957.06	0.03	0.0353
0	15	f	1	14	f	21952.92	0.03	0.0311
0	16	f	1	15	f	21948.03	0.03	0.0116
0	17	f	1	16	f	21942.34	0.03	0.0168
0	18	f	1	17	f	21935.94	0.03	-0.0271
0	19	f	1	18	f	21928.75	0.03	-0.0086
0	20	f	1	19	f	21920.93	0.03	-0.0063
0	21	f	1	20	f	21912.49	0.3	0.1391
0	23	f	1	22	f	21894.39	0.03	0.0031
0	24	f	1	23	f	21885.45	0.03	0.0059
0	3	f	1	4	f	21898.02	0.03	-0.0167
0	4	f	1	5	f	21887.50	0.03	0.0445

υ'	J'	parity$'$	υ''	J''	parity$''$	Observed	Uncertainty	calc-obs
0	5	f	1	6	f	21876.25	0.03	0.0178
0	6	f	1	7	f	21864.28	0.03	0.0175
0	7	f	1	8	f	21851.61	0.03	-0.0330
0	8	f	1	9	f	21838.15	0.03	-0.0239
0	9	f	1	10	f	21823.92	0.03	0.0070
0	10	f	1	11	f	21809.02	0.03	0.0002
0	11	f	1	12	f	21793.39	0.03	-0.0185
0	12	f	1	13	f	21777.01	0.03	0.0393
0	13	f	1	14	f	21759.89	0.03	0.0191
0	14	f	1	15	f	21742.28	0.03	-0.0354
0	15	f	1	16	f	21723.85	0.03	-0.0302
0	16	f	1	17	f	21704.78	0.03	-0.0121
0	17	f	1	18	f	21685.12	0.03	-0.0176
0	18	f	1	19	f	21664.84	0.03	0.0277
0	19	f	1	20	f	21644.12	0.03	0.0091
0	20	f	1	21	f	21623.00	0.03	0.0087
0	21	f	1	22	f	21601.86	0.3	-0.1359
0	3	e	1	3	f	21928.02	0.03	0.0130
0	4	e	1	4	f	21925.05	0.03	0.0103
0	5	e	1	5	f	21921.28	0.03	-0.0245
0	6	e	1	6	f	21916.76	0.03	-0.0202
0	7	e	1	7	f	21911.43	0.03	0.0235
0	8	e	1	8	f	21905.38	0.03	0.0330
0	9	e	1	9	f	21898.59	0.03	0.0091
0	10	e	1	10	f	21891.03	0.03	0.0150
0	11	e	1	11	f	21882.69	0.03	0.0262
0	12	e	1	12	f	21873.71	0.03	-0.0345
0	3	f	1	3	e	21928.02	0.03	0.0130
0	4	f	1	4	e	21925.05	0.03	0.0103
0	5	f	1	5	e	21921.28	0.03	-0.0244
0	6	f	1	6	e	21916.76	0.03	-0.0201
0	7	f	1	7	e	21911.43	0.03	0.0236
0	8	f	1	8	e	21905.38	0.03	0.0327
0	9	f	1	9	e	21898.59	0.03	0.0054
0	10	f	1	10	e	21891.03	0.03	0.0068
0	11	f	1	11	e	21882.69	0.03	0.0060
0	12	f	1	12	e	21873.71	0.03	-0.0777
0	4	e	1	3	e	21955.15	0.03	-0.0600

υ'	J'	parity′	υ''	J''	parity″	Observed	Uncertainty	calc-obs
0	5	e	1	4	e	21958.77	0.03	0.0013
0	6	e	1	5	e	21961.73	0.03	-0.0024
0	7	e	1	6	e	21963.89	0.03	0.0059
0	8	e	1	7	e	21965.30	0.03	-0.0104
0	9	e	1	8	e	21965.90	0.03	-0.0143
0	10	e	1	9	e	21965.72	0.03	-0.0066
0	11	e	1	10	e	21964.72	0.03	0.0128
0	12	e	1	11	e	21962.96	0.03	0.0400
0	13	e	1	12	e	21960.38	0.03	0.0223
0	14	e	1	13	e	21957.06	0.03	0.0122
0	15	e	1	14	e	21952.92	0.03	-0.0171
0	16	e	1	15	e	21947.94	0.03	-0.0168
0	17	e	1	16	e	21942.12	0.03	-0.0163
0	18	e	1	17	e	21935.50	0.03	-0.0026
0	19	e	1	18	e	21928.02	0.03	0.0099
0	20	e	1	19	e	21919.80	0.03	-0.0108
0	21	e	1	20	e	21910.70	0.03	-0.0711
0	22	e	1	21	e	21900.76	0.03	-0.0204
0	23	e	1	22	e	21889.99	0.03	0.0044
0	24	e	1	23	e	21878.38	0.03	-0.0082
0	25	e	1	24	e	21865.98	0.03	0.0104
0	26	e	1	25	e	21852.65	0.03	-0.0013
0	27	e	1	26	e	21838.52	0.03	-0.0151
0	28	e	1	27	e	21823.46	0.03	-0.0349
0	30	e	1	29	e	21790.88	0.03	0.0272
0	3	e	1	4	e	21898.02	0.03	-0.0167
0	4	e	1	5	e	21887.50	0.03	0.0446
0	5	e	1	6	e	21876.25	0.03	0.0179
0	6	e	1	7	e	21864.28	0.03	0.0176
0	7	e	1	8	e	21851.61	0.03	-0.0333
0	8	e	1	9	e	21838.15	0.03	-0.0256
0	9	e	1	10	e	21823.92	0.03	0.0038
0	10	e	1	11	e	21809.02	0.03	-0.0100
0	11	e	1	12	e	21793.39	0.03	-0.0407
0	12	e	1	13	e	21777.01	0.03	-0.0058
0	13	e	1	14	e	21759.89	0.03	-0.0221
0	14	e	1	15	e	21742.09	0.03	-0.0108
0	15	e	1	16	e	21723.52	0.03	0.0177

υ'	J'	parity′	υ''	J''	parity″	Observed	Uncertainty	calc-obs
0	16	e	1	17	e	21704.26	0.03	0.0184
0	17	e	1	18	e	21684.26	0.03	0.0179
0	18	e	1	19	e	21663.59	0.03	0.0052
0	19	e	1	20	e	21642.17	0.03	-0.0081
0	20	e	1	21	e	21620.06	0.03	0.0117
0	21	e	1	22	e	21597.11	0.03	0.0734
0	22	e	1	23	e	21573.67	0.03	0.0228
0	23	e	1	24	e	21549.48	0.03	-0.0026
0	24	e	1	25	e	21524.51	0.03	0.0097
0	25	e	1	26	e	21498.95	0.03	-0.0081
0	26	e	1	27	e	21472.54	0.03	0.0051
0	27	e	1	28	e	21445.47	0.03	0.0193
0	28	e	1	29	e	21417.60	0.03	0.0412
0	30	e	1	31	e	21360.03	0.03	-0.0144
1	4	e	1	3	e	23064.19	0.03	0.0770
1	5	e	1	4	e	23066.93	0.03	0.0143
1	6	e	1	5	e	23068.60	0.03	0.0016
1	7	e	1	6	e	23069.26	0.03	0.0229
1	8	e	1	7	e	23068.97	0.03	-0.0134
1	9	e	1	8	e	23067.66	0.03	-0.0013
1	10	e	1	9	e	23065.34	0.03	-0.0036
1	11	e	1	10	e	23062.00	0.03	0.0028
1	12	e	1	11	e	23057.67	0.03	0.0270
1	13	e	1	12	e	23052.33	0.03	-0.0177
1	14	e	1	13	e	23045.93	0.03	0.0412
1	15	e	1	14	e	23038.56	0.03	-0.0121
1	16	e	1	15	e	23030.04	0.03	0.0132
1	17	e	1	16	e	23020.55	0.03	0.0187
1	18	e	1	17	e	23010.01	0.03	-0.0026
1	19	e	1	18	e	22998.42	0.03	-0.0001
1	20	e	1	19	e	22985.70	0.03	0.0142
1	21	e	1	20	e	22972.00	0.1	-0.0561
1	3	e	1	4	e	23008.15	0.03	-0.0417
1	4	e	1	5	e	22996.76	0.03	-0.0384
1	5	e	1	6	e	22984.44	0.03	0.0009
1	6	e	1	7	e	22971.20	0.03	-0.0284
1	7	e	1	8	e	22956.98	0.03	-0.0163
1	8	e	1	9	e	22941.80	0.03	-0.0086

v'	J'	parity′	v''	J''	parity″	Observed	Uncertainty	calc-obs
1	9	e	1	10	e	22925.69	0.03	0.0068
1	10	e	1	11	e	22908.65	0.03	-0.0170
1	11	e	1	12	e	22890.69	0.03	-0.0707
1	12	e	1	13	e	22871.73	0.03	-0.0288
1	13	e	1	14	e	22851.83	0.03	-0.0521
1	14	e	1	15	e	22830.96	0.03	0.0182
1	15	e	1	16	e	22809.17	0.03	0.0127
1	16	e	1	17	e	22786.42	0.03	-0.0116
1	17	e	1	18	e	22762.76	0.03	-0.0171
1	18	e	1	19	e	22738.10	0.03	0.0052
1	19	e	1	20	e	22712.55	0.03	0.0019
1	20	e	1	21	e	22686.01	0.03	-0.0134
1	21	e	1	22	e	22658.44	0.1	0.0584
1	3	e	1	3	f	23038.10	0.03	0.0380
1	4	e	1	4	f	23034.28	0.03	-0.0427
1	5	e	1	5	f	23029.45	0.03	-0.0215
1	6	e	1	6	f	23023.59	0.03	0.0238
1	7	e	1	7	f	23016.85	0.03	-0.0095
1	8	e	1	8	f	23009.06	0.03	0.0200
1	9	e	1	9	f	23000.38	0.03	-0.0079
1	10	e	1	10	f	22990.65	0.03	0.0180
1	11	e	1	11	f	22979.92	0.03	0.0662
1	12	e	1	12	f	22968.37	0.03	0.0025
1	13	e	1	13	f	22955.66	0.03	0.0693
1	14	e	1	14	f	22942.25	0.03	-0.0589
1	4	f	1	3	f	23064.19	0.03	0.0560
1	5	f	1	4	f	23066.93	0.03	0.0053
1	6	f	1	5	f	23068.60	0.03	0.0135
1	7	f	1	6	f	23069.26	0.03	0.0178
1	8	f	1	7	f	23068.97	0.03	-0.0045
1	9	f	1	8	f	23067.66	0.03	-0.0070
1	10	f	1	9	f	23065.34	0.03	0.0001
1	11	f	1	10	f	23062.00	0.03	0.0240
1	12	f	1	11	f	23057.67	0.03	0.0052
1	13	f	1	12	f	23052.33	0.03	-0.0245
1	14	f	1	13	f	23045.93	0.03	0.0503
1	15	f	1	14	f	23038.56	0.03	0.0361
1	16	f	1	15	f	23030.21	0.03	0.0066

υ'	J'	parity′	υ''	J''	parity″	Observed	Uncertainty	calc-obs
1	17	f	1	16	f	23020.81	0.03	-0.0182
1	18	f	1	17	f	23010.47	0.03	-0.0421
1	19	f	1	18	f	22999.09	0.03	-0.0286
1	20	f	1	19	f	22986.86	0.03	0.0137
1	21	f	1	20	f	22973.75	0.1	0.1341
1	3	f	1	4	f	23008.15	0.03	-0.0017
1	4	f	1	5	f	22996.76	0.03	-0.0595
1	5	f	1	6	f	22984.44	0.03	-0.0082
1	6	f	1	7	f	22971.20	0.03	-0.0165
1	7	f	1	8	f	22956.98	0.03	-0.0210
1	8	f	1	9	f	22941.80	0.03	0.0021
1	9	f	1	10	f	22925.69	0.03	0.0060
1	10	f	1	11	f	22908.65	0.03	-0.0018
1	11	f	1	12	f	22890.69	0.03	-0.0255
1	12	f	1	13	f	22871.73	0.03	-0.0047
1	13	f	1	14	f	22851.83	0.03	0.0241
1	14	f	1	15	f	22831.18	0.03	-0.0504
1	15	f	1	16	f	22809.50	0.03	-0.0352
1	16	f	1	17	f	22786.95	0.03	-0.0071
1	17	f	1	18	f	22763.52	0.03	0.0174
1	18	f	1	19	f	22739.34	0.03	0.0427
1	19	f	1	20	f	22714.42	0.03	0.0291
1	20	f	1	21	f	22688.97	0.03	-0.0113
1	21	f	1	22	f	22663.11	0.1	-0.1309

This work

				$A'^3\Phi_4 - X^3\Phi_4$				
0	5	e	0	4	e	12441.8781	0.007	0.0007
0	6	e	0	5	e	12439.9182	0.007	-0.0039
0	7	e	0	6	e	12436.4031	0.007	-0.0024
0	8	e	0	7	e	12431.3429	0.007	-0.0015
0	9	e	0	8	e	12424.7522	0.007	0.0012
0	10	e	0	9	e	12416.6451	0.007	-0.0028
0	11	e	0	10	e	12407.0289	0.007	-0.0003
0	12	e	0	11	e	12395.8563	0.007	0.0017
0	13	e	0	12	e	12383.2904	0.007	-0.0040
0	14	e	0	13	e	12369.2242	0.007	0.0003

v'	J'	parity′	v''	J''	parity″	Observed	Uncertainty	calc-obs
0	15	e	0	14	e	12353.7110	0.007	0.0008
0	16	e	0	15	e	12337.0895	0.007	0.0056
0	17	e	0	16	e	12318.3053	0.007	0.0022
0	18	e	0	17	e	12298.5293	0.007	-0.0024
0	19	e	0	18	e	12277.3528	0.007	0.0033
0	20	e	0	19	e	12254.9036	0.007	0.0034
0	21	e	0	20	e	12230.8069	0.007	-0.0044
0	22	e	0	21	e	12205.5396	0.007	-0.0059
0	23	e	0	22	e	12179.0098	0.007	-0.0058
0	24	e	0	23	e	12151.1560	0.05	0.0642
0	25	e	0	24	e	12122.1046	0.007	0.0078
0	26	e	0	25	e	12091.7580	0.007	0.0042
0	27	e	0	26	e	12060.1948	0.007	0.0058
0	28	e	0	27	e	12027.4486	0.007	0.0015
0	29	e	0	28	e	11993.7157	0.007	-0.0006
0	30	e	0	29	e	11958.6446	0.007	0.0097
0	31	e	0	30	e	11922.6286	0.007	0.0021
0	32	e	0	31	e	11885.6612	0.007	0.0009
0	33	e	0	32	e	11847.8318	0.007	0.0017
0	34	e	0	33	e	11809.2692	0.007	0.0022
0	35	e	0	34	e	11770.0096	0.007	0.0023
0	4	e	0	5	e	12375.3616	0.007	0.0116
0	5	e	0	6	e	12360.1163	0.007	0.0076
0	6	e	0	7	e	12343.3622	0.007	0.0021
0	7	e	0	8	e	12325.0885	0.007	0.0015
0	8	e	0	9	e	12305.3122	0.007	-0.0020
0	9	e	0	10	e	12284.0461	0.007	0.0008
0	10	e	0	11	e	12261.3140	0.007	-0.0030
0	11	e	0	12	e	12237.1257	0.007	0.0023
0	12	e	0	13	e	12211.4479	0.007	0.0012
0	13	e	0	14	e	12184.4384	0.007	-0.0031
0	14	e	0	15	e	12156.0046	0.007	-0.0023
0	15	e	0	16	e	12126.1957	0.007	-0.0006
0	16	e	0	17	e	12095.3601	0.007	0.0050
0	17	e	0	18	e	12062.4502	0.007	0.0007
0	18	e	0	19	e	12028.6377	0.007	-0.0028
0	19	e	0	20	e	11993.5110	0.007	0.0145
0	20	e	0	21	e	11957.2372	0.007	0.0017

v'	J'	parity′	v''	J''	parity″	Observed	Uncertainty	calc-obs
0	21	e	0	22	e	11919.4073	0.007	-0.0038
0	22	e	0	23	e	11880.5197	0.007	-0.0049
0	23	e	0	24	e	11840.4822	0.007	-0.0010
0	24	e	0	25	e	11799.3230	0.007	-0.0087
0	25	e	0	26	e	11756.9430	0.007	0.0058
0	26	e	0	27	e	11713.4640	0.007	0.0071
0	27	e	0	28	e	11668.9117	0.007	0.0049
0	28	e	0	29	e	11623.3045	0.007	0.0080
0	29	e	0	30	e	11576.8653	0.007	0.0024
0	30	e	0	31	e	11529.2693	0.02	-0.0238
0	31	e	0	32	e	11480.8081	0.007	0.0049
0	32	e	0	33	e	11431.5864	0.007	0.0062
0	33	e	0	34	e	11381.6705	0.007	0.0028
0	34	e	0	35	e	11331.1879	0.007	-0.0016
0	35	e	0	36	e	11280.1791	0.007	-0.0077
0	4	f	0	4	e	12412.5613	0.007	-0.0125
0	5	f	0	5	e	12404.6982	0.007	-0.0002
0	6	f	0	6	e	12395.3340	0.007	-0.0011
0	7	f	0	7	e	12384.4285	0.007	0.0026
0	8	f	0	8	e	12371.9974	0.007	0.0041
0	9	f	0	9	e	12358.0600	0.007	0.0019
0	10	f	0	10	e	12342.6248	0.007	0.0035
0	11	f	0	11	e	12325.7086	0.007	0.0048
0	12	f	0	12	e	12307.2713	0.007	0.0005
0	13	f	0	13	e	12287.4454	0.1	0.0212
0	14	f	0	14	e	12266.1897	0.007	0.0061
0	5	f	0	4	f	12441.8781	0.007	-0.0054
0	6	f	0	5	f	12439.9182	0.007	-0.0051
0	7	f	0	6	f	12436.4031	0.007	-0.0020
0	8	f	0	7	f	12431.3429	0.007	-0.0006
0	9	f	0	8	f	12424.7522	0.007	0.0001
0	10	f	0	9	f	12416.6451	0.007	-0.0007
0	11	f	0	10	f	12407.0289	0.007	-0.0002
0	12	f	0	11	f	12395.8563	0.007	0.0008
0	13	f	0	12	f	12383.2904	0.007	-0.0002
0	14	f	0	13	f	12369.2242	0.007	-0.0009
0	15	f	0	14	f	12353.7110	0.007	0.0022
0	16	f	0	15	f	12336.7099	0.007	-0.0007

v'	J'	parity′	v''	J''	parity″	Observed	Uncertainty	calc-obs
0	17	f	0	16	f	12318.3053	0.007	0.0023
0	18	f	0	17	f	12298.5293	0.007	0.0016
0	19	f	0	18	f	12277.3528	0.007	0.0021
0	20	f	0	19	f	12254.7591	0.007	-0.0076
0	21	f	0	20	f	12230.8069	0.007	0.0007
0	22	f	0	21	f	12205.5396	0.007	-0.0003
0	23	f	0	22	f	12179.0098	0.007	0.0018
0	24	f	0	23	f	12151.1570	0.02	-0.0269
0	25	f	0	24	f	12121.9471	0.007	-0.0049
0	26	f	0	25	f	12091.5286	0.007	-0.0043
0	27	f	0	26	f	12059.8732	0.007	-0.0046
0	28	f	0	27	f	12026.9448	0.007	-0.0050
0	29	f	0	28	f	11993.6098	1	-0.1904
0	30	f	0	29	f	11958.6446	0.1	0.0744
0	31	f	0	30	f	11923.0570	0.007	-0.0121
0	32	f	0	31	f	11885.4860	0.007	-0.0111
0	33	f	0	32	f	11847.1602	0.007	0.0071
0	34	f	0	33	f	11808.2386	0.007	-0.0034
0	35	f	0	34	f	11768.7792	0.007	0.0005
0	4	f	0	5	f	12375.3616	0.007	0.0125
0	5	f	0	6	f	12360.1163	0.007	0.0015
0	6	f	0	7	f	12343.3622	0.007	0.0009
0	7	f	0	8	f	12325.0885	0.007	0.0019
0	8	f	0	9	f	12305.3122	0.007	-0.0011
0	9	f	0	10	f	12284.0461	0.007	-0.0003
0	10	f	0	11	f	12261.3140	0.007	-0.0010
0	11	f	0	12	f	12237.1257	0.007	0.0023
0	12	f	0	13	f	12211.4479	0.007	0.0002
0	13	f	0	14	f	12184.4384	0.007	0.0006
0	14	f	0	15	f	12156.0046	0.007	-0.0037
0	15	f	0	16	f	12126.1957	0.007	0.0005
0	16	f	0	17	f	12094.9803	0.007	-0.0017
0	17	f	0	18	f	12062.4502	0.007	0.0000
0	18	f	0	19	f	12028.6377	0.007	0.0002
0	19	f	0	20	f	11993.5110	0.007	0.0117
0	20	f	0	21	f	11957.1286	0.05	-0.0473
0	21	f	0	22	f	11919.4073	0.007	-0.0018
0	22	f	0	23	f	11880.5197	0.007	-0.0036

v'	J'	parity′	v''	J''	parity″	Observed	Uncertainty	calc-obs
0	23	f	0	24	f	11840.4822	0.007	0.0008
0	24	f	0	25	f	11799.2243	0.007	-0.0078
0	25	f	0	26	f	11756.7691	0.007	-0.0006
0	26	f	0	27	f	11713.2219	0.007	-0.0022
0	27	f	0	28	f	11668.5695	0.007	-0.0022
0	28	f	0	29	f	11622.7825	0.007	-0.0025
0	29	f	0	30	f	11576.5860	0.1	-0.0422
0	30	f	0	31	f	11529.2693	0.007	0.0052
0	31	f	0	32	f	11481.1896	0.007	-0.0070
0	32	f	0	33	f	11431.3587	0.007	-0.0089
0	33	f	0	34	f	11380.9421	0.007	-0.0035
0	34	f	0	35	f	11330.0623	0.007	0.0036
0	35	f	0	36	f	11278.8356	0.007	0.0007
0	36	f	0	37	f	11227.4269	0.007	0.0106
0	5	e	1	4	e	11104.1082	0.007	-0.0097
0	6	e	1	5	e	11102.9232	0.007	-0.0048
0	7	e	1	6	e	11100.3464	0.007	-0.0007
0	8	e	1	7	e	11096.3866	0.007	-0.0024
0	9	e	1	8	e	11091.0500	0.007	0.0005
0	10	e	1	9	e	11084.3523	0.007	-0.0022
0	11	e	1	10	e	11076.3079	0.007	-0.0045
0	12	e	1	11	e	11066.8530	0.007	0.0031
0	13	e	1	12	e	11056.1664	0.007	-0.0026
0	14	e	1	13	e	11044.1386	0.007	-0.0016
0	15	e	1	14	e	11030.8153	0.007	0.0000
0	16	e	1	15	e	11016.5405	0.007	0.0046
0	17	e	1	16	e	11000.2580	0.007	0.0015
0	18	e	1	17	e	10983.1409	0.007	-0.0050
0	19	e	1	18	e	10964.7795	0.007	-0.0022
0	20	e	1	19	e	10945.3004	0.007	-0.0055
0	21	e	1	20	e	10924.3114	0.007	0.0001
0	22	e	1	21	e	10902.3167	0.007	0.0017
0	23	e	1	22	e	10879.2175	0.007	0.0008
0	24	e	1	23	e	10855.0112	0.007	0.0066
0	25	e	1	24	e	10829.6591	0.007	-0.0121
0	26	e	1	25	e	10803.1942	0.007	-0.0070
0	27	e	1	26	e	10775.6754	0.007	-0.0063
0	28	e	1	27	e	10747.1214	0.007	-0.0065

v'	J'	parity$'$	v''	J''	parity$''$	Observed	Uncertainty	calc-obs
0	29	e	1	28	e	10717.7267	0.007	0.0025
0	30	e	1	29	e	10687.1812	0.007	-0.0110
0	31	e	1	30	e	10655.8086	0.007	-0.0078
0	32	e	1	31	e	10623.6482	0.007	-0.0094
0	33	e	1	32	e	10590.7736	0.007	-0.0044
0	34	e	1	33	e	10557.3210	0.007	-0.0024
0	35	e	1	34	e	10523.3236	0.007	-0.0008
0	36	e	1	35	e	10491.2224	0.007	-0.0007
0	37	e	1	36	e	10457.6534	0.007	-0.0003
0	5	e	1	6	e	11024.0248	0.07	0.0441
0	6	e	1	7	e	11008.3955	0.007	0.0116
0	7	e	1	8	e	10991.3902	0.007	-0.0032
0	8	e	1	9	e	10973.0203	0.007	-0.0023
0	9	e	1	10	e	10953.3216	0.007	0.0001
0	10	e	1	11	e	10932.3127	0.007	-0.0037
0	11	e	1	12	e	10910.0075	0.007	-0.0022
0	12	e	1	13	e	10886.3641	0.007	-0.0024
0	13	e	1	14	e	10861.5436	0.007	-0.0047
0	14	e	1	15	e	10835.4486	0.007	0.0039
0	15	e	1	16	e	10808.1510	0.007	-0.0039
0	16	e	1	17	e	10779.9765	0.007	-0.0024
0	17	e	1	18	e	10749.8727	0.007	-0.0008
0	18	e	1	19	e	10719.0232	0.007	-0.0004
0	19	e	1	20	e	10687.0373	0.007	-0.0028
0	20	e	1	21	e	10654.0280	0.007	-0.0044
0	21	e	1	22	e	10619.6140	0.007	0.0036
0	22	e	1	23	e	10584.3040	0.007	0.0085
0	23	e	1	24	e	10548.0101	0.007	0.0058
0	24	e	1	25	e	10510.7389	0.007	0.0004
0	25	e	1	26	e	10472.4192	0.007	-0.0019
0	26	e	1	27	e	10433.1413	0.007	-0.0053
0	27	e	1	28	e	10392.9360	0.007	-0.0053
0	28	e	1	29	e	10351.8327	0.007	-0.0044
0	29	e	1	30	e	10310.0433	0.007	-0.0055
0	30	e	1	31	e	10267.1950	0.02	0.0272
0	31	e	1	32	e	10223.7494	0.007	-0.0006
0	32	e	1	33	e	10179.6384	0.007	0.0013
0	33	e	1	34	e	10134.9851	0.007	-0.0007

v'	J'	parity′	v''	J''	parity″	Observed	Uncertainty	calc-obs
0	34	e	1	35	e	10089.9115	0.007	0.0023
0	35	e	1	36	e	10044.4607	0.007	0.0075
0	36	e	1	37	e	10001.0915	0.007	0.0003
0	5	f	1	4	f	11104.1082	0.05	-0.0158
0	6	f	1	5	f	11102.9232	0.007	-0.0060
0	7	f	1	6	f	11100.3464	0.007	-0.0003
0	8	f	1	7	f	11096.3866	0.007	-0.0015
0	9	f	1	8	f	11091.0500	0.007	-0.0006
0	10	f	1	9	f	11084.3523	0.007	-0.0001
0	11	f	1	10	f	11076.3079	0.007	-0.0045
0	12	f	1	11	f	11066.8530	0.007	0.0022
0	13	f	1	12	f	11056.1664	0.007	0.0011
0	14	f	1	13	f	11044.1386	0.007	-0.0029
0	15	f	1	14	f	11030.8153	0.007	0.0013
0	16	f	1	15	f	11016.1591	0.007	-0.0002
0	17	f	1	16	f	11000.2580	0.007	0.0011
0	18	f	1	17	f	10983.1409	0.007	-0.0018
0	19	f	1	18	f	10964.7795	0.007	-0.0048
0	20	f	1	19	f	10945.1326	0.007	0.0048
0	21	f	1	20	f	10924.3114	0.007	0.0022
0	22	f	1	21	f	10902.3167	0.007	0.0028
0	23	f	1	22	f	10879.2175	0.007	0.0020
0	24	f	1	23	f	10854.8777	0.02	0.0411
0	25	f	1	24	f	10829.4456	0.02	0.0187
0	26	f	1	25	f	10802.9094	0.02	0.0225
0	27	f	1	26	f	10775.2907	0.02	0.0229
0	28	f	1	27	f	10746.5458	0.02	0.0271
0	29	f	1	28	f	10717.3911	0.007	0.0002
0	30	f	1	29	f	10687.1812	0.007	-0.0020
0	31	f	1	30	f	10656.1248	0.02	0.0177
0	32	f	1	31	f	10623.3451	0.007	0.0126
0	33	f	1	32	f	10589.9820	0.007	0.0004
0	34	f	1	33	f	10556.1196	0.007	0.0090
0	35	f	1	34	f	10521.8968	0.007	-0.0006
0	36	f	1	35	f	10487.4763	0.007	-0.0090
0	37	f	1	36	f	10442.0488	0.007	-0.0001
0	5	f	1	6	f	11024.0248	0.02	0.0380
0	6	f	1	7	f	11008.3955	0.007	0.0104

υ'	J'	parity′	υ''	J''	parity″	Observed	Uncertainty	calc-obs
0	7	f	1	8	f	10991.3902	0.007	-0.0028
0	8	f	1	9	f	10973.0203	0.007	-0.0014
0	9	f	1	10	f	10953.3216	0.007	-0.0010
0	10	f	1	11	f	10932.3127	0.007	-0.0017
0	11	f	1	12	f	10910.0075	0.007	-0.0022
0	12	f	1	13	f	10886.3641	0.007	-0.0035
0	13	f	1	14	f	10861.5436	0.007	-0.0013
0	14	f	1	15	f	10835.4486	0.007	0.0021
0	15	f	1	16	f	10808.1510	0.007	-0.0033
0	16	f	1	17	f	10779.5836	0.007	0.0032
0	17	f	1	18	f	10749.8727	0.007	-0.0028
0	18	f	1	19	f	10719.0232	0.007	0.0005
0	19	f	1	20	f	10687.0373	0.007	-0.0086
0	20	f	1	21	f	10653.8576	0.007	0.0040
0	21	f	1	22	f	10619.6140	0.007	-0.0007
0	22	f	1	23	f	10584.3040	0.007	0.0008
0	23	f	1	24	f	10548.0101	0.007	-0.0049
0	24	f	1	25	f	10510.5764	0.02	0.0478
0	25	f	1	26	f	10472.1900	0.02	0.0234
0	26	f	1	27	f	10432.8252	0.02	0.0277
0	27	f	1	28	f	10392.5102	0.02	0.0290
0	28	f	1	29	f	10351.2104	0.02	0.0298
0	29	f	1	30	f	10309.6473	0.02	-0.0059
0	30	f	1	31	f	10267.1950	0.02	-0.0377
0	31	f	1	32	f	10223.9821	0.007	0.0157
0	32	f	1	33	f	10179.2377	0.007	0.0056
0	33	f	1	34	f	10134.0609	0.007	-0.0058
0	34	f	1	35	f	10088.5592	0.007	-0.0103
0	35	f	1	36	f	10042.8667	0.05	-0.0389
0	36	f	1	37	f	9997.1382	0.05	-0.0603
0	4	e	1	4	f	11074.7801	0.007	-0.0125
0	5	e	1	5	f	11067.7133	0.007	-0.0051
0	6	e	1	6	f	11059.2825	0.007	-0.0032
0	7	e	1	7	f	11049.4742	0.007	-0.0006
0	8	e	1	8	f	11038.3027	0.007	-0.0051
0	9	e	1	9	f	11025.7787	0.007	-0.0079
0	10	e	1	10	f	11011.9059	0.007	-0.0049
0	11	e	1	11	f	10996.7070	0.007	0.0044

υ'	J'	parity′	υ''	J''	parity″	Observed	Uncertainty	calc-obs
0	12	e	1	12	f	10980.1603	0.007	-0.0103
1	5	e	2	4	e	10846.0822	0.007	-0.0010
1	6	e	2	5	e	10845.3315	0.007	-0.0043
1	7	e	2	6	e	10843.3074	0.007	-0.0092
1	8	e	2	7	e	10839.9849	0.007	0.0043
1	9	e	2	8	e	10835.4486	0.007	-0.0113
1	10	e	2	9	e	10829.6591	0.007	0.0101
1	11	e	2	10	e	10822.7321	0.007	0.0031
1	12	e	2	11	e	10814.6796	0.007	0.0065
1	13	e	2	12	e	10805.6926	0.007	0.0028
1	14	e	2	13	e	10795.9246	0.007	0.0068
1	15	e	2	14	e	10786.4225	0.007	0.0031
1	16	e	2	15	e	10766.5840	0.007	0.0035
1	17	e	2	16	e	10756.8221	0.007	-0.0036
1	18	e	2	17	e	10744.3775	0.007	-0.0090
1	19	e	2	18	e	10731.2049	0.007	-0.0160
1	20	e	2	19	e	10717.7267	0.02	-0.0243
1	5	e	2	6	e	10767.7808	0.007	-0.0028
1	6	e	2	7	e	10752.8534	0.007	0.0013
1	7	e	2	8	e	10736.6826	0.007	0.0076
1	8	e	2	9	e	10719.2965	0.007	-0.0118
1	9	e	2	10	e	10700.6766	0.007	0.0040
1	10	e	2	11	e	10680.9072	0.007	0.0027
1	11	e	2	12	e	10660.0252	0.007	0.0026
1	12	e	2	13	e	10638.0886	0.007	0.0021
1	13	e	2	14	e	10615.2787	0.007	-0.0016
1	14	e	2	15	e	10591.7544	0.007	0.0065
1	15	e	2	16	e	10568.5772	0.007	0.0013
1	16	e	2	17	e	10535.1544	0.007	-0.0092
1	17	e	2	18	e	10511.8769	0.007	-0.0096
1	18	e	2	19	e	10486.0038	0.007	-0.0032
1	19	e	2	20	e	10459.4779	0.007	0.0239
1	20	e	2	21	e	10432.6135	10	0.1856
1	4	f	2	4	e	10817.0173	0.007	0.0051
1	5	f	2	5	e	10810.4745	0.007	0.0005
1	6	f	2	6	e	10802.6340	0.007	-0.0041
1	7	f	2	7	e	10793.5275	0.007	-0.0040
1	8	f	2	8	e	10783.1488	0.007	0.0062

υ'	J'	parity′	υ''	J''	parity″	Observed	Uncertainty	calc-obs
1	9	f	2	9	e	10771.5658	0.007	0.0007
1	10	f	2	10	e	10758.7773	0.007	0.0063
1	11	f	2	11	e	10744.8535	0.007	0.0081
1	12	f	2	12	e	10729.8598	0.007	-0.0056
1	13	f	2	13	e	10713.9334	0.007	0.0018
1	5	f	2	4	f	10846.0822	0.007	-0.0018
1	6	f	2	5	f	10845.3315	0.007	-0.0038
1	7	f	2	6	f	10843.3074	0.007	-0.0093
1	8	f	2	7	f	10839.9849	0.007	0.0034
1	9	f	2	8	f	10835.4486	0.007	-0.0110
1	10	f	2	9	f	10829.6591	0.007	0.0099
1	11	f	2	10	f	10822.7321	0.007	0.0032
1	12	f	2	11	f	10814.6796	0.007	0.0076
1	13	f	2	12	f	10805.6926	0.007	0.0035
1	14	f	2	13	f	10795.8423	0.007	0.0044
1	15	f	2	14	f	10786.1172	0.007	0.0015
1	16	f	2	15	f	10766.1283	0.007	0.0044
1	17	f	2	16	f	10756.5434	0.007	0.0030
1	18	f	2	17	f	10744.1203	0.007	-0.0019
1	19	f	2	18	f	10730.9264	0.007	-0.0024
1	20	f	2	19	f	10717.3911	0.007	-0.0042
1	5	f	2	6	f	10767.7808	0.007	-0.0036
1	6	f	2	7	f	10752.8534	0.007	0.0018
1	7	f	2	8	f	10736.6826	0.007	0.0074
1	8	f	2	9	f	10719.2965	0.007	-0.0128
1	9	f	2	10	f	10700.6766	0.007	0.0041
1	10	f	2	11	f	10680.9072	0.007	0.0020
1	11	f	2	12	f	10660.0252	0.007	0.0019
1	12	f	2	13	f	10638.0886	0.007	0.0018
1	13	f	2	14	f	10615.2787	0.007	-0.0032
1	14	f	2	15	f	10591.6783	0.007	-0.0059
1	15	f	2	16	f	10568.2802	0.007	-0.0146
1	16	f	2	17	f	10534.6826	0.007	-0.0016
1	17	f	2	18	f	10511.5839	0.007	-0.0026
1	18	f	2	19	f	10485.7277	0.007	0.0023
1	19	f	2	20	f	10459.1917	0.007	0.0155
1	20	f	2	21	f	10432.5077	0.1	-0.0660
0	5	e	2	4	e	9801.6141	0.1	-0.0344

υ'	J'	parity′	υ''	J''	parity″	Observed	Uncertainty	calc-obs
0	6	e	2	5	e	9801.1905	0.007	-0.0059
0	7	e	2	6	e	9799.5602	0.007	-0.0069
0	8	e	2	7	e	9796.6804	0.007	0.0087
0	9	e	2	8	e	9792.6088	0.007	-0.0002
0	10	e	2	9	e	9787.3089	0.007	0.0079
0	11	e	2	10	e	9780.8374	0.007	-0.0037
0	12	e	2	11	e	9773.1001	0.007	0.0044
0	13	e	2	12	e	9764.2776	0.007	0.0072
0	14	e	2	13	e	9754.2846	0.007	-0.0001
0	15	e	2	14	e	9743.1402	0.007	0.0028
0	16	e	2	15	e	9731.2102	0.007	-0.0036
0	17	e	2	16	e	9717.4437	0.02	-0.0352
0	18	e	2	17	e	9702.9317	0.007	-0.0056
0	19	e	2	18	e	9687.3760	0.007	-0.0133
0	20	e	2	19	e	9670.8249	0.007	0.0054
0	21	e	2	20	e	9652.9132	0.02	0.0394
0	22	e	2	21	e	9634.0636	0.1	0.1581
0	23	e	2	22	e	9614.1311	10	0.4115
0	5	e	2	6	e	9723.3544	0.1	-0.0779
0	6	e	2	7	e	9708.7062	0.007	0.0059
0	7	e	2	8	e	9692.9335	0.007	0.0118
0	8	e	2	9	e	9675.9811	0.007	0.0036
0	9	e	2	10	e	9657.8473	0.007	0.0047
0	10	e	2	11	e	9638.5499	0.007	0.0075
0	11	e	2	12	e	9618.1232	0.007	0.0031
0	12	e	2	13	e	9596.5086	0.007	0.0005
0	13	e	2	14	e	9573.8607	0.007	0.0059
0	14	e	2	15	e	9550.1152	0.007	-0.0013
0	15	e	2	16	e	9525.2963	0.007	-0.0003
0	16	e	2	17	e	9499.7744	0.007	-0.0101
0	17	e	2	18	e	9472.4568	0.007	0.0006
0	18	e	2	19	e	9444.5418	0.007	0.0164
0	19	e	2	20	e	9415.6337	0.05	0.0419
0	20	e	2	21	e	9385.6958	10	0.2313
0	21	e	2	22	e	9354.5544	10	0.3876
0	4	e	2	4	f	9772.1705	0.1	0.0783
0	5	e	2	5	f	9765.9677	0.007	0.0066
0	6	e	2	6	f	9758.4877	0.007	-0.0010

v'	J'	parity$'$	v''	J''	parity$''$	Observed	Uncertainty	calc-obs
0	7	e	2	7	f	9749.7514	0.05	0.0271
0	8	e	2	8	f	9739.8194	0.05	0.0364
1	5	e	0	4	e	13486.3790	0.007	0.0012
1	6	e	0	5	e	13484.0574	0.007	-0.0004
1	7	e	0	6	e	13480.1440	0.007	0.0016
1	8	e	0	7	e	13474.6390	0.007	0.0023
1	9	e	0	8	e	13467.5809	0.007	0.0011
1	10	e	0	9	e	13458.9999	0.007	-0.0052
1	11	e	0	10	e	13448.9305	0.007	-0.0004
1	12	e	0	11	e	13437.4454	0.007	-0.0059
1	13	e	0	12	e	13424.7025	0.007	-0.0055
1	14	e	0	13	e	13410.8803	0.007	-0.0089
1	15	e	0	14	e	13397.0034	0.007	-0.0091
1	16	e	0	15	e	13372.4702	0.007	0.0057
1	17	e	0	16	e	13357.7112	0.007	0.0063
1	18	e	0	17	e	13339.9614	0.007	0.0079
1	19	e	0	18	e	13321.1862	0.007	-0.0038
1	4	e	0	5	e	13420.1150	0.007	0.0000
1	5	e	0	6	e	13404.6238	0.007	0.0015
1	6	e	0	7	e	13387.5018	0.007	0.0051
1	7	e	0	8	e	13368.8293	0.007	0.0057
1	8	e	0	9	e	13348.6074	0.007	0.0028
1	9	e	0	10	e	13326.8774	0.007	-0.0019
1	10	e	0	11	e	13303.6684	0.007	-0.0050
1	11	e	0	12	e	13279.0359	0.007	-0.0064
1	12	e	0	13	e	13253.0344	0.007	-0.0038
1	13	e	0	14	e	13225.8375	0.007	0.0084
1	14	e	0	15	e	13197.6584	0.007	-0.0091
1	15	e	0	16	e	13169.4878	0.007	-0.0103
1	16	e	0	17	e	13130.7362	0.007	0.0097
1	17	e	0	18	e	13101.8533	0.007	0.0074
1	18	e	0	19	e	13070.0728	0.007	0.0045
1	19	e	0	20	e	13037.3548	0.007	-0.0031
1	20	e	0	21	e	13004.1077	0.007	0.0033
1	5	f	0	4	f	13486.3790	0.007	0.0004
1	6	f	0	5	f	13484.0574	0.007	0.0001
1	7	f	0	6	f	13480.1440	0.007	0.0015
1	8	f	0	7	f	13474.6390	0.007	0.0015

υ'	J'	parity′	υ''	J''	parity″	Observed	Uncertainty	calc-obs
1	9	f	0	8	f	13467.5809	0.007	0.0015
1	10	f	0	9	f	13458.9999	0.007	-0.0053
1	11	f	0	10	f	13448.9305	0.007	-0.0001
1	12	f	0	11	f	13437.4454	0.007	-0.0043
1	13	f	0	12	f	13424.7025	0.007	-0.0038
1	14	f	0	13	f	13410.7863	0.007	0.0021
1	15	f	0	14	f	13396.6818	0.007	0.0087
1	16	f	0	15	f	13372.0287	0.007	-0.0023
1	17	f	0	16	f	13357.4559	0.007	-0.0017
1	18	f	0	17	f	13339.7339	0.007	-0.0006
1	19	f	0	18	f	13320.9453	0.007	-0.0059
1	4	f	0	5	f	13420.1150	0.05	0.0318
1	5	f	0	6	f	13404.6238	0.007	0.0007
1	6	f	0	7	f	13387.5018	0.007	0.0056
1	7	f	0	8	f	13368.8293	0.007	0.0056
1	8	f	0	9	f	13348.6074	0.007	0.0020
1	9	f	0	10	f	13326.8774	0.007	-0.0016
1	10	f	0	11	f	13303.6684	0.007	-0.0052
1	11	f	0	12	f	13279.0359	0.007	-0.0061
1	12	f	0	13	f	13253.0344	0.007	-0.0023
1	13	f	0	14	f	13225.8375	0.007	0.0099
1	14	f	0	15	f	13197.5660	0.007	0.0001
1	15	f	0	16	f	13169.1693	0.007	0.0042
1	16	f	0	17	f	13130.2993	0.007	-0.0033
1	17	f	0	18	f	13101.6026	0.007	-0.0058
1	19	f	0	20	f	13037.1132	0.007	-0.0060
1	20	f	0	21	f	13003.8219	0.007	0.0050
1	4	f	0	4	e	13457.3263	0.007	-0.0048
1	5	f	0	5	e	13449.1996	0.007	0.0052
1	6	f	0	6	e	13439.4748	0.007	0.0024
1	7	f	0	7	e	13428.1704	0.007	0.0053
1	8	f	0	8	e	13415.3007	0.007	-0.0009
1	9	f	0	9	e	13400.8936	0.007	-0.0016
1	10	f	0	10	e	13384.9825	0.007	-0.0040
1	11	f	0	11	e	13367.6220	0.007	-0.0069
1	12	f	0	12	e	13348.8535	0.007	0.0023
1	7	e	3	6	e	9577.6638	0.007	-0.0056
1	8	e	3	7	e	9575.4406	0.007	0.0023

υ'	J'	parity$'$	υ''	J''	parity$''$	Observed	Uncertainty	calc-obs
1	9	e	3	8	e	9572.1423	0.007	-0.0019
1	10	e	3	9	e	9567.7811	0.007	-0.0041
1	11	e	3	10	e	9562.4000	0.007	0.0027
1	12	e	3	11	e	9556.0641	0.007	0.0037
1	13	e	3	12	e	9548.9451	0.007	0.0005
1	14	e	3	13	e	9541.1651	0.03	0.0389
1	15	e	3	14	e	9533.8686	0.007	0.0054
1	16	e	3	15	e	9516.3766	0.007	-0.0117
1	17	e	3	16	e	9509.0997	0.03	-0.0221
1	5	e	3	6	e	9502.0895	0.03	0.0484
1	6	e	3	7	e	9488.3084	0.007	0.0001
1	7	e	3	8	e	9473.3917	0.007	0.0017
1	8	e	3	9	e	9457.3910	0.007	0.0016
1	9	e	3	10	e	9440.3373	0.007	0.0108
1	10	e	3	11	e	9422.2897	0.007	0.0018
1	11	e	3	12	e	9403.2798	0.007	-0.0017
1	12	e	3	13	e	9383.3664	0.007	-0.0032
1	13	e	3	14	e	9362.7316	0.007	-0.0060
1	14	e	3	15	e	9341.5004	0.04	0.0380
1	15	e	3	16	e	9320.8306	0.007	0.0070
1	7	f	3	6	f	9577.6638	0.007	-0.0057
1	8	f	3	7	f	9575.4406	0.007	0.0015
1	9	f	3	8	f	9572.1423	0.007	-0.0016
1	10	f	3	9	f	9567.7811	0.007	-0.0044
1	11	f	3	10	f	9562.4000	0.007	0.0025
1	12	f	3	11	f	9556.0641	0.007	0.0043
1	13	f	3	12	f	9548.9451	0.007	0.0004
1	14	f	3	13	f	9541.1651	0.05	-0.0473
1	15	f	3	14	f	9533.5772	0.05	-0.0126
1	16	f	3	15	f	9515.9039	0.007	0.0019
1	17	f	3	16	f	9508.7920	0.007	0.0065
1	5	f	3	6	f	9502.0895	0.05	0.0476
1	6	f	3	7	f	9488.3084	0.007	0.0005
1	7	f	3	8	f	9473.3917	0.007	0.0015
1	8	f	3	9	f	9457.3910	0.007	0.0006
1	9	f	3	10	f	9440.3373	0.007	0.0107
1	10	f	3	11	f	9422.2897	0.007	0.0008
1	11	f	3	12	f	9403.2798	0.007	-0.0032

υ'	J'	parity′	υ''	J''	parity″	Observed	Uncertainty	calc-obs
1	12	f	3	13	f	9383.3664	0.007	-0.0049
1	13	f	3	14	f	9362.7316	0.007	-0.0101
1	14	f	3	15	f	9341.5004	0.05	-0.0549
1	15	f	3	16	f	9320.5568	0.05	-0.0392
2	5	e	0	4	e	14484.5800	0.007	0.0017
2	6	e	0	5	e	14481.9514	0.007	-0.0236
2	7	e	0	6	e	14477.6506	0.007	-0.0066
2	8	e	0	7	e	14471.7577	0.007	0.0018
2	9	e	0	8	e	14464.3192	0.007	0.0050
2	10	e	0	9	e	14455.3629	0.007	0.0039
2	11	e	0	10	e	14444.9601	0.007	0.0068
2	12	e	0	11	e	14433.1781	0.007	-0.0037
2	13	e	0	12	e	14420.0601	0.007	0.0112
2	14	e	0	13	e	14405.8225	0.007	-0.0075
2	15	e	0	14	e	14390.4582	0.05	-0.0601
2	4	e	0	5	e	14418.3674	10	0.1415
2	5	e	0	6	e	14402.8285	0.007	-0.0018
2	6	e	0	7	e	14385.3813	0.007	-0.0036
2	7	e	0	8	e	14366.3419	0.007	-0.0085
2	8	e	0	9	e	14345.7313	0.007	-0.0030
2	9	e	0	10	e	14323.6224	0.007	-0.0047
2	10	e	0	11	e	14300.0350	0.007	0.0004
2	11	e	0	12	e	14275.0734	0.007	-0.0071
2	12	e	0	13	e	14248.7664	0.007	-0.0010
2	13	e	0	14	e	14221.2147	0.007	0.0054
2	14	e	0	15	e	14192.5973	0.007	-0.0044
2	15	e	0	16	e	14162.8686	0.05	0.0127
2	5	f	0	4	f	14484.5800	0.007	0.0037
2	6	f	0	5	f	14481.9514	0.007	-0.0219
2	7	f	0	6	f	14477.6506	0.007	-0.0038
2	8	f	0	7	f	14471.7577	0.007	0.0055
2	9	f	0	8	f	14464.3192	0.007	0.0076
2	10	f	0	9	f	14455.3629	0.007	0.0021
2	11	f	0	10	f	14444.9601	0.007	0.0051
2	12	f	0	11	f	14433.1781	0.007	-0.0030
2	13	f	0	12	f	14420.0601	0.007	0.0165
2	14	f	0	13	f	14405.8225	0.007	-0.0073
2	15	f	0	14	f	14390.4582	0.05	-0.0637

υ'	J'	parity′	υ''	J''	parity″	Observed	Uncertainty	calc-obs
2	5	f	0	6	f	14402.8285	0.007	0.0002
2	6	f	0	7	f	14385.3813	0.007	-0.0019
2	7	f	0	8	f	14366.3419	0.007	-0.0057
2	8	f	0	9	f	14345.7313	0.007	0.0007
2	9	f	0	10	f	14323.6224	0.007	-0.0021
2	10	f	0	11	f	14300.0350	0.007	-0.0014
2	11	f	0	12	f	14275.0734	0.007	-0.0088
2	12	f	0	13	f	14248.7664	0.007	-0.0003
2	13	f	0	14	f	14221.2147	0.007	0.0106
2	14	f	0	15	f	14192.5973	0.007	-0.0044
2	15	f	0	16	f	14162.8686	0.007	0.0088
2	4	e	0	4	f	14455.8250	10	-0.1414
2	5	e	0	5	f	14447.4004	0.007	0.0066
2	6	e	0	6	f	14437.3396	0.007	0.0079
2	7	e	0	7	f	14425.6562	0.007	0.0179
2	8	e	0	8	f	14412.3835	0.1	0.0352
2	6	e	1	5	e	13144.9384	0.007	-0.0065
2	7	e	1	6	e	13141.5859	0.007	0.0032
2	8	e	1	7	e	13136.8012	0.007	0.0011
2	9	e	1	8	e	13130.6169	0.007	0.0044
2	10	e	1	9	e	13123.0746	0.007	0.0000
2	11	e	1	10	e	13114.2419	0.007	-0.0002
2	12	e	1	11	e	13104.1701	0.007	0.0023
2	13	e	1	12	e	13092.9566	0.007	-0.0080
2	14	e	1	13	e	13080.7187	0.007	0.0089
2	15	e	1	14	e	13067.4881	0.007	0.0135
2	16	e	1	15	e	13053.3417	0.007	-0.0001
2	17	e	1	16	e	13039.0326	0.007	-0.0001
2	5	e	1	6	e	13066.7788	0.007	-0.0070
2	6	e	1	7	e	13050.3953	0.007	0.0252
2	7	e	1	8	e	13032.6372	0.007	-0.0067
2	8	e	1	9	e	13013.4367	0.007	-0.0006
2	9	e	1	10	e	12992.8973	0.007	-0.0048
2	10	e	1	11	e	12971.0379	0.007	-0.0044
2	11	e	1	12	e	12947.9431	0.007	0.0005
2	12	e	1	13	e	12923.6753	0.007	0.0027
2	13	e	1	14	e	12898.3320	0.007	-0.0084
2	14	e	1	15	e	12872.0397	0.007	0.0033

υ'	J'	parity$'$	υ''	J''	parity$''$	Observed	Uncertainty	calc-obs
2	15	e	1	16	e	12844.8460	0.007	-0.0126
2	6	f	1	5	f	13144.9384	0.007	-0.0048
2	7	f	1	6	f	13141.5859	0.007	0.0060
2	8	f	1	7	f	13136.8012	0.007	0.0048
2	9	f	1	8	f	13130.6169	0.007	0.0070
2	10	f	1	9	f	13123.0746	0.007	-0.0019
2	11	f	1	10	f	13114.2419	0.007	-0.0019
2	12	f	1	11	f	13104.1701	0.007	0.0030
2	13	f	1	12	f	13092.9566	0.007	-0.0027
2	14	f	1	13	f	13080.7187	0.007	0.0090
2	15	f	1	14	f	13067.4881	0.007	0.0098
2	16	f	1	15	f	13053.3417	0.007	-0.0001
2	17	f	1	16	f	13039.0326	0.007	0.0000
2	5	f	1	6	f	13066.7788	0.007	-0.0050
2	6	f	1	7	f	13050.3953	0.007	0.0269
2	7	f	1	8	f	13032.6372	0.007	-0.0039
2	8	f	1	9	f	13013.4367	0.007	0.0031
2	9	f	1	10	f	12992.8973	0.007	-0.0022
2	10	f	1	11	f	12971.0379	0.007	-0.0062
2	11	f	1	12	f	12947.9431	0.007	-0.0013
2	12	f	1	13	f	12923.6753	0.007	0.0033
2	13	f	1	14	f	12898.3320	0.007	-0.0033
2	14	f	1	15	f	12872.0397	0.007	0.0030
2	15	f	1	16	f	12844.8460	0.007	-0.0171
2	5	f	1	5	e	13110.4128	0.007	0.0003
2	6	f	1	6	e	13101.2413	0.05	0.0531
2	7	f	1	7	e	13090.7134	0.007	0.0064
2	8	f	1	8	e	13078.7344	0.007	-0.0149
2	9	f	1	9	e	13065.3549	0.007	-0.0107
2	10	f	1	10	e	13050.6165	0.007	0.0072
2	11	f	1	11	e	13034.6412	0.007	0.0068
2	12	f	1	12	e	13017.4702	0.007	-0.0030
2	13	f	1	13	e	12999.1863	0.007	-0.0206
				$A'^3\Phi_3 - X^3\Phi_3$				
0	9	f	0	8	f	12038.5857	0.007	-0.0067
0	10	f	0	9	f	12033.6369	0.007	-0.0068

υ'	J'	parity′	υ''	J''	parity″	Observed	Uncertainty	calc-obs
0	11	f	0	10	f	12027.4486	10	0.1844
0	12	f	0	11	f	12020.1671	0.007	0.0101
0	13	f	0	12	f	12010.8493	0.07	0.0632
0	14	f	0	13	f	12000.0652	0.007	0.0091
0	15	f	0	14	f	11988.4073	0.007	-0.0102
0	16	f	0	15	f	11975.9427	0.007	-0.0040
0	17	f	0	16	f	11962.5110	0.007	-0.0153
0	18	f	0	17	f	11947.9947	0.015	-0.0527
0	19	f	0	18	f	11932.2117	0.015	-0.0344
0	20	f	0	19	f	11917.3223	0.007	0.0234
0	9	f	0	10	f	11896.6167	0.007	0.0053
0	10	f	0	11	f	11876.9321	0.007	0.0060
0	11	f	0	12	f	11856.2741	0.007	-0.0005
0	12	f	0	13	f	11834.2152	0.007	0.0121
0	13	f	0	14	f	11810.4490	0.007	0.0120
0	14	f	0	15	f	11785.2327	0.007	-0.0091
0	15	f	0	16	f	11759.2554	0.007	0.0104
0	16	f	0	17	f	11732.6613	0.007	0.0037
0	17	f	0	18	f	11705.2265	0.007	0.0149
0	18	f	0	19	f	11676.8848	0.007	0.0119
0	19	f	0	20	f	11647.5564	0.007	0.0087
0	20	f	0	21	f	11619.4517	0.007	-0.0210
0	12	e	0	11	e	12013.2217	0.007	-0.0047
0	13	e	0	12	e	12004.4712	0.007	0.0021
0	14	e	0	13	e	11997.5885	0.007	-0.0004
0	15	e	0	14	e	11985.9062	0.007	-0.0013
0	16	e	0	15	e	11979.8797	0.007	0.0095
0	17	e	0	16	e	11964.2326	0.007	0.0041
0	18	e	0	17	e	11947.7437	0.007	0.0027
0	19	e	0	18	e	11930.8335	0.02	0.0494
0	20	e	0	19	e	11914.2535	0.02	0.0007
0	12	e	0	13	e	11827.2160	0.007	0.0052
0	13	e	0	14	e	11803.9400	0.007	-0.0011
0	14	e	0	15	e	11782.5947	0.007	0.0005
0	15	e	0	16	e	11756.5363	0.007	0.0034
0	16	e	0	17	e	11736.2523	0.007	-0.0079
0	17	e	0	18	e	11706.4145	0.007	-0.0036
0	18	e	0	19	e	11675.8452	0.007	-0.0010

υ'	J'	parity$'$	υ''	J''	parity$''$	Observed	Uncertainty	calc-obs
0	19	e	0	20	e	11645.0200	0.007	-0.0050
0	20	e	0	21	e	11614.6160	10	-0.0793
0	12	f	0	12	e	11930.8335	0.007	-0.0231
0	13	f	0	13	e	11914.2535	0.007	-0.0123
0	14	f	0	14	e	11895.9149	10	0.2080
0	16	f	0	16	e	11858.1006	10	-0.6279
				$[13.3]4 - X^3\Phi_4$				
0	14	e	0	13	e	13332.6685	0.01	-0.0219
0	15	e	0	14	e	13325.5972	0.007	-0.0111
0	16	e	0	15	e	13315.1554	0.007	-0.0108
0	17	e	0	16	e	13302.0365	0.007	0.0029
0	18	e	0	17	e	13286.5101	0.007	0.0024
0	19	e	0	18	e	13268.6273	0.007	-0.0036
0	20	e	0	19	e	13248.3690	0.007	0.0016
0	21	e	0	20	e	13225.8375	0.05	-0.0545
0	22	e	0	21	e	13201.1174	0.007	-0.0008
0	23	e	0	22	e	13174.2910	0.007	-0.0031
0	24	e	0	23	e	13145.6175	0.007	-0.0018
0	25	e	0	24	e	13115.2558	0.007	-0.0066
0	26	e	0	25	e	13083.3183	0.007	-0.0035
0	27	e	0	26	e	13048.4269	0.007	-0.0014
0	28	e	0	27	e	13012.3167	0.007	-0.0010
0	29	e	0	28	e	12976.3927	0.007	-0.0011
0	30	e	0	29	e	12938.8007	0.007	-0.0027
0	31	e	0	30	e	12899.9828	0.007	0.0044
0	32	e	0	31	e	12860.0772	0.007	0.0020
0	33	e	0	32	e	12819.1898	0.007	-0.0023
0	34	e	0	33	e	12777.4329	0.007	0.0067
0	35	e	0	34	e	12734.9819	0.007	0.0045
0	36	e	0	35	e	12691.9910	0.007	0.0015
0	37	e	0	36	e	12648.6592	0.007	0.0016
0	38	e	0	37	e	12605.1349	0.007	0.0025
0	39	e	0	38	e	12561.4992	0.007	0.0029
0	17	e	0	18	e	13046.2000	0.007	-0.0174
0	18	e	0	19	e	13016.6177	0.007	0.0029
0	20	e	0	21	e	12950.7038	0.007	-0.0012

υ'	J'	parity′	υ''	J''	parity″	Observed	Uncertainty	calc-obs
0	21	e	0	22	e	12914.3794	0.007	0.0045
0	22	e	0	23	e	12876.0955	0.007	0.0022
0	23	e	0	24	e	12835.7607	0.007	0.0044
0	24	e	0	25	e	12793.7069	0.007	0.0029
0	25	e	0	26	e	12750.0787	0.007	0.0069
0	26	e	0	27	e	12705.0193	0.007	0.0043
0	27	e	0	28	e	12657.1402	0.007	0.0014
0	28	e	0	29	e	12608.1764	0.007	0.0017
0	29	e	0	30	e	12559.5423	0.007	0.0019
0	30	e	0	31	e	12509.3867	0.007	0.0025
0	31	e	0	32	e	12458.1730	0.007	-0.0035
0	32	e	0	33	e	12406.0107	0.007	-0.0010
0	33	e	0	34	e	12353.0251	0.007	0.0022
0	34	e	0	35	e	12299.3602	0.007	-0.0057
0	35	e	0	36	e	12245.1483	0.007	-0.0025
0	15	f	0	14	f	13327.0826	0.01	-0.0116
0	16	f	0	15	f	13316.4531	0.007	0.0061
0	17	f	0	16	f	13303.2497	0.007	0.0102
0	18	f	0	17	f	13287.8031	0.007	0.0076
0	19	f	0	18	f	13270.2620	0.007	0.0025
0	20	f	0	19	f	13250.9065	0.007	-0.0028
0	21	f	0	20	f	13230.5498	0.007	-0.0037
0	22	f	0	21	f	13195.9787	0.007	0.0018
0	23	f	0	22	f	13170.2520	0.007	0.0040
0	24	f	0	23	f	13141.5859	0.007	0.0004
0	25	f	0	24	f	13114.9985	0.007	0.0049
0	26	f	0	25	f	13083.3183	0.007	0.0025
0	16	f	0	17	f	13074.7096	0.007	0.0192
0	17	f	0	18	f	13047.3870	0.007	0.0154
0	18	f	0	19	f	13017.9140	0.007	0.0037
0	19	f	0	20	f	12986.4274	0.007	0.0047
0	20	f	0	21	f	12953.2377	0.007	-0.0042
0	21	f	0	22	f	12919.1498	0.007	-0.0058
0	22	f	0	23	f	12870.9586	0.007	-0.0013
0	23	f	0	24	f	12831.7310	0.007	-0.0036
0	24	f	0	25	f	12789.6722	0.007	0.0005
0	25	f	0	26	f	12749.8351	0.007	-0.0054
0	26	f	0	27	f	12705.0193	0.007	-0.0031

υ'	J'	parity$'$	υ''	J''	parity$''$	Observed	Uncertainty	calc-obs
					$[13.3]4 - X^3\Phi_3$			
0	14	e	1	13	e	12631.8731	0.007	-0.0039
0	15	e	0	14	e	12623.9293	0.007	0.0146
0	16	e	0	15	e	12612.5904	0.007	0.0058
0	17	e	0	16	e	12598.5378	0.007	0.0109
0	18	e	0	17	e	12582.0403	0.007	0.0090
0	19	e	0	18	e	12563.1597	0.007	0.0042
0	20	e	0	19	e	12541.8969	0.007	0.0003
0	21	e	0	20	e	12518.2881	0.007	-0.0022
0	22	e	0	21	e	12492.6012	0.03	-0.0076
0	23	e	0	22	e	12464.7558	0.03	-0.0113
0	24	e	0	23	e	12435.0722	0.03	-0.0074
0	25	e	0	24	e	12403.7160	0.03	-0.0047
0	13	e	0	14	e	12436.8010	0.007	0.0009
0	14	e	0	15	e	12416.8593	0.007	0.0169
0	15	e	0	16	e	12394.5804	0.007	-0.0016
0	16	e	0	17	e	12368.9438	0.007	0.0076
0	17	e	0	18	e	12340.7158	0.007	0.0071
0	18	e	0	19	e	12310.1596	0.007	-0.0124
0	13	f	0	12	f	12639.4308	0.05	-0.0643
0	14	f	0	13	f	12633.4083	0.007	0.0020
0	15	f	0	14	f	12625.5341	0.007	0.0070
0	16	f	0	15	f	12614.1355	0.007	-0.0228
0	17	f	0	16	f	12600.1411	0.007	-0.0253
0	18	f	0	17	f	12583.9331	0.007	-0.0121
0	19	f	0	18	f	12565.7292	0.007	-0.0058
0	20	f	0	19	f	12545.8270	0.015	0.0347
0	21	f	0	20	f	12525.2057	0.01	0.0194
0	13	f	0	14	f	12438.9141	0.007	0.0010
0	14	f	0	15	f	12418.5615	0.007	-0.0019
0	15	f	0	16	f	12396.4110	0.007	-0.0012
0	16	f	0	17	f	12370.8416	0.007	-0.0026
0	17	f	0	18	f	12342.7718	0.05	0.0896
0	18	f	0	19	f	12312.8245	0.05	0.0512

Appendix C

Line list for YbO

Output from least-square fits for Systems 1, 2 and 3. All values are in cm^{-1} .

C.1 Line list for YbO. System 1

Table C.1: Line list for System 1.

J'	Parity	J''	Observed	Obs.-Calc.	Uncertainty
8	e	9	10249.502	0.00071	0.005
9	e	10	10248.723	0.00172	0.005
10	e	11	10247.924	-0.00843	0.005
11	e	12	10247.137	0.00228	0.005
12	e	13	10246.304	-0.02415	0.005
13	e	14	10245.499	-0.0137	0.005
14	e	15	10244.679	-0.00934	0.005
15	e	16	10243.838	-0.01705	0.005
16	e	17	10243.015	0.00219	0.005
17	e	18	10242.148	-0.01357	0.005
18	e	19	10241.317	0.01568	0.005
19	e	20	10240.448	0.016	0.005
20	e	21	10239.56	0.00642	0.005
21	e	22	10238.674	0.00798	0.005
22	e	23	10237.745	-0.02426	0.005
23	e	24	10236.872	0.00875	0.005

J'	Parity	J''	Observed	Obs.-Calc.	Uncertainty
24	e	25	10235.946	-0.00192	0.005
25	e	26	10234.999	-0.02422	0.005
26	e	27	10234.074	-0.01507	0.005
27	e	28	10233.149	0.0036	0.005
28	e	29	10232.208	0.01587	0.005
29	e	30	10231.235	0.00583	0.005
30	e	31	10230.268	0.01158	0.005
31	e	32	10229.291	0.01722	0.005
32	e	33	10228.289	0.00785	0.005
33	e	34	10227.299	0.0206	0.005
34	e	35	10226.278	0.01258	0.005
35	e	36	10225.254	0.01192	0.005
36	e	37	10224.215	0.00677	0.005
37	e	38	10223.177	0.01328	0.005
38	e	39	10222.121	0.0126	0.005
39	e	40	10221.056	0.01391	0.005
40	e	41	10219.983	0.01838	0.005
41	e	42	10218.887	0.0112	0.005
42	e	43	10217.771	-0.00443	0.005
43	e	44	10216.663	-0.00029	0.005
44	e	45	10215.549	0.00983	0.005
45	e	46	10214.38	-0.02281	0.005
46	e	47	10213.266	0.01201	0.005
47	e	48	10212.081	-0.01143	0.005
48	e	49	10210.928	0.01015	0.005
2	e	1	10257.504	0.00463	0.005
3	e	2	10258.179	0.00553	0.005
4	e	3	10258.83	-0.0087	0.005
5	e	4	10259.511	0.01598	0.005
6	e	5	10260.148	0.00556	0.005
7	e	6	10260.781	0.00009	0.005
8	e	7	10261.409	-0.00143	0.005
9	e	8	10262.037	0.00605	0.005
10	e	9	10262.632	-0.01046	0.005
11	e	10	10263.244	-0.00092	0.005
12	e	11	10263.843	0.0047	0.005
13	e	12	10264.423	0.00044	0.005

J'	Parity	J''	Observed	Obs.-Calc.	Uncertainty
14	e	13	10264.997	-0.00066	0.005
15	e	14	10265.563	-0.00056	0.005
16	e	15	10266.116	-0.00421	0.005
17	e	16	10266.666	-0.00156	0.005
18	e	17	10267.205	-0.00057	0.005
19	e	18	10267.731	-0.00316	0.005
20	e	19	10268.254	0.00071	0.005
21	e	20	10268.763	0.00011	0.005
22	e	21	10269.259	-0.00388	0.005
23	e	22	10269.75	-0.0032	0.005
24	e	23	10270.23	-0.00377	0.005
25	e	24	10270.703	-0.0015	0.005
26	e	25	10271.158	-0.00731	0.005
27	e	26	10271.613	-0.00309	0.005
28	e	27	10272.056	-0.00076	0.005
29	e	28	10272.484	-0.0032	0.005
30	e	29	10272.906	-0.0013	0.005
31	e	30	10273.315	-0.00194	0.005
32	e	31	10273.709	-0.00699	0.005
33	e	32	10274.096	-0.00832	0.005
34	e	33	10274.474	-0.00779	0.005
35	e	34	10274.845	-0.00325	0.005
36	e	35	10275.197	-0.00653	0.005
37	e	36	10275.542	-0.00547	0.005
38	e	37	10275.883	0.00311	0.005
39	e	38	10276.185	-0.0156	0.005
40	e	39	10276.501	-0.00841	0.005
41	e	40	10276.794	-0.01211	0.005
42	e	41	10277.085	-0.00548	0.005
43	e	42	10277.364	0.00172	0.005
44	e	43	10277.616	-0.00528	0.005
45	e	44	10277.861	-0.00621	0.005
46	e	45	10278.087	-0.01282	0.005
47	e	46	10278.321	0.00218	0.005
48	e	47	10278.501	-0.02291	0.005
49	e	48	10278.718	0.00322	0.005
50	e	49	10278.895	0.00389	0.005
51	e	50	10279.051	-0.00156	0.005

J'	Parity	J''	Observed	Obs.-Calc.	Uncertainty
52	e	51	10279.199	0.00023	0.005
53	e	52	10279.329	-0.00037	0.005
54	e	53	10279.456	0.01204	0.005
5	f	5	10256.037	0.01653	0.005
6	f	6	10255.996	0.01725	0.005
7	f	7	10255.936	0.00597	0.005
8	f	8	10255.885	0.01071	0.005
9	f	9	10255.817	0.0055	0.005
10	f	10	10255.746	0.00437	0.005
11	f	11	10255.668	0.00335	0.005
12	f	12	10255.579	-0.00152	0.005
13	f	13	10255.484	-0.0052	0.005
14	f	14	10255.384	-0.00664	0.005
15	f	15	10255.278	-0.00681	0.005
16	f	16	10255.168	-0.00363	0.005
17	f	17	10255.049	-0.00206	0.005
18	f	18	10254.925	0.00196	0.005
19	f	19	10254.783	-0.00449	0.005
20	f	20	10254.639	-0.00535	0.005
21	f	21	10254.493	-0.00053	0.005
22	f	22	10254.334	-0.00096	0.005
23	f	23	10254.17	0.00145	0.005
24	f	24	10253.997	0.00281	0.005
25	f	25	10253.814	0.0022	0.005
26	f	26	10253.618	-0.00326	0.005
27	f	27	10253.417	-0.00547	0.005
28	f	28	10253.217	0.00171	0.005
29	f	29	10252.991	-0.00861	0.005
30	f	30	10252.776	0.00072	0.005
31	f	31	10252.544	0.00184	0.005
32	f	32	10252.306	0.00589	0.005
33	f	33	10252.059	0.01004	0.005
34	f	34	10251.785	-0.00354	0.005
35	f	35	10251.524	0.00533	0.005
36	f	36	10251.235	-0.00416	0.005
37	f	37	10250.951	0.00118	0.005
38	f	38	10250.653	0.00256	0.005

J'	Parity	J''	Observed	Obs.-Calc.	Uncertainty
39	f	39	10250.331	-0.00979	0.005
40	f	40	10250.031	0.01035	0.005
41	f	41	10249.683	-0.00678	0.005
42	f	42	10249.354	0.00609	0.005
43	f	43	10248.985	-0.00978	0.005
44	f	44	10248.632	0.00189	0.005
45	f	45	10248.261	0.0074	0.005
47	f	47	10247.474	0.01016	0.005
49	f	49	10246.603	-0.01984	0.005
50	f	50	10246.179	-0.00323	0.005
51	f	51	10245.737	0.00929	0.005

C.2 Line list for YbO. System 2

Table C.2: Line list for the System 2.

J'	J''	Observed	Obs.-Calc.	Uncertainty
0	1	10942.334	-0.00672	0.005
1	2	10941.638	-0.00169	0.005
2	3	10940.937	-0.00128	0.005
3	4	10940.234	-0.00251	0.005
4	5	10939.531	-0.00337	0.005
5	6	10938.832	0.00011	0.005
6	7	10938.127	-0.00205	0.005
7	8	10937.426	0.00014	0.005
8	9	10936.722	-0.00033	0.005
9	10	10936.017	-0.00144	0.005
10	11	10935.316	0.00179	0.005
11	12	10934.611	0.00139	0.005
12	13	10933.907	0.00236	0.005
13	14	10933.202	0.00272	0.005
14	15	10932.496	0.00249	0.005
15	16	10931.793	0.00568	0.005
16	17	10931.084	0.00334	0.005
17	18	10930.377	0.0035	0.005
18	19	10929.672	0.00621	0.005

J'	J''	Observed	Obs.-Calc.	Uncertainty
19	20	10928.961	0.00351	0.005
20	21	10928.254	0.00547	0.005
21	22	10927.542	0.00317	0.005
22	23	10926.83	0.00169	0.005
23	24	10926.119	0.00212	0.005
24	25	10925.406	0.00157	0.005
25	26	10924.689	-0.00184	0.005
26	27	10923.976	0.00004	0.005
27	28	10923.257	-0.00265	0.005
28	29	10922.538	-0.00372	0.005
29	30	10921.814	-0.00799	0.005
30	31	10921.092	-0.00825	0.005
31	32	10920.369	-0.00725	0.005
32	33	10919.64	-0.00975	0.005
33	34	10918.907	-0.01346	0.005
34	35	10918.175	-0.01307	0.005
35	36	10917.441	-0.01125	0.005
36	37	10916.699	-0.01362	0.005
37	38	10915.962	-0.00679	0.005
38	39	10915.209	-0.01133	0.005
39	40	10914.452	-0.01477	0.005
40	41	10913.696	-0.01161	0.005
41	42	10912.949	0.00669	0.005
42	43	10912.173	0.00271	0.005
43	44	10911.395	0.00408	0.005
44	45	10910.592	-0.01153	0.005
45	46	10909.811	0.00359	0.005
46	47	10908.987	-0.0148	0.005
47	48	10908.16	-0.02587	100
48	49	10907.302	-0.05676	100
49	50	10906.467	-0.05255	100
50	51	10905.475	-0.19226	100
51	52	10904.447	-0.35384	100
52	53	10903.235	-0.68419	100
53	54	10901.826	-1.19514	100
54	55	10899.896	-2.20946	100
55	56	10896.939	-4.23183	100
56	57	10892.851	-7.36489	100

J'	J''	Observed	Obs.-Calc.	Uncertainty
57	58	10911.557	12.31784	100
1	0	10943.728	-0.01363	0.005
2	1	10944.435	-0.00648	0.005
3	2	10945.131	-0.00993	0.005
4	3	10945.837	-0.00294	0.005
5	4	10946.535	-0.00352	0.005
6	5	10947.237	0.00036	0.005
7	6	10947.933	-0.0013	0.005
8	7	10948.631	-0.00046	0.005
9	8	10949.328	-0.00012	0.005
10	9	10950.026	0.00176	0.005
11	10	10950.723	0.00319	0.005
12	11	10951.417	0.00221	0.005
13	12	10952.111	0.00186	0.005
14	13	10952.808	0.00516	0.005
15	14	10953.5	0.00417	0.005
16	15	10954.193	0.00493	0.005
17	16	10954.885	0.00551	0.005
18	17	10955.576	0.00595	0.005
19	18	10956.266	0.00635	0.005
20	19	10956.954	0.00577	0.005
21	20	10957.641	0.0053	0.005
22	21	10958.326	0.00406	0.005
23	22	10959.01	0.00316	0.005
24	23	10959.693	0.00272	0.005
25	24	10960.375	0.00288	0.005
26	25	10961.056	0.0038	0.005
27	26	10961.733	0.00266	0.005
28	27	10962.408	0.00165	0.005
29	28	10963.078	-0.00202	0.005
30	29	10963.75	-0.00113	0.005
31	30	10964.418	-0.00141	0.005
32	31	10965.083	-0.0016	0.005
33	32	10965.744	-0.00238	0.005
34	33	10966.402	-0.00244	0.005
35	34	10967.058	-0.00042	0.005
36	35	10967.707	-0.00092	0.005

J'	J''	Observed	Obs.-Calc.	Uncertainty
37	36	10968.354	0.00146	0.005
38	37	10968.997	0.00518	0.005
39	38	10969.632	0.00672	0.005
40	39	10970.262	0.0096	0.005
41	40	10970.887	0.01438	0.005
42	41	10971.503	0.01767	0.005
43	42	10972.113	0.0231	0.005
44	43	10972.707	0.02136	0.005
45	44	10973.292	0.02019	0.005
46	45	10973.86	0.01237	0.005
47	46	10974.409	-0.00326	0.005
48	47	10974.932	-0.03282	0.005
49	48	10975.436	-0.06837	100
50	49	10975.866	-0.16391	100
51	50	10976.229	-0.31137	100
52	51	10976.421	-0.61363	100
53	52	10976.421	-1.09051	100
54	53	10975.778	-2.19175	100
55	54	10974.182	-4.22602	100
56	55	10971.503	-7.32193	100

C.3 Line list for YbO. System 3

Table C.3: Line list for the System 3.

J'	J''	Observed	Obs.-Calc.	Uncertainty
5	6	11191.679	-0.02778	0.05
6	7	11190.589	-0.00189	0.005
7	8	11189.400	-0.00449	0.005
8	9	11188.158	0.01037	0.005
9	10	11186.824	0.00367	0.005
11	12	11183.962	0.00741	0.005
12	13	11182.409	-0.00721	0.005
13	14	11180.803	-0.00452	0.005
14	15	11179.133	0.00445	0.005
15	16	11177.392	0.01271	0.005

J'	J''	Observed	Obs.-Calc.	Weight
16	17	11175.550	-0.00975	0.005
17	18	11173.676	0.0061	0.005
18	19	11171.719	0.00929	0.005
19	20	11169.695	0.01588	0.05
20	21	11167.586	0.00795	0.005
21	22	11165.403	-0.00339	0.005
22	23	11163.164	-0.00001	0.005
23	24	11160.849	-0.00174	0.005
24	25	11158.452	-0.01437	0.005
25	26	11156.021	0.01034	0.05
26	27	11153.478	-0.00532	0.005
27	28	11150.885	0.001	0.005
28	29	11148.196	-0.01633	0.05
29	30	11145.447	-0.02084	0.05
30	31	11142.633	-0.01704	0.05
31	32	11139.755	-0.00334	0.005
32	33	11136.782	-0.0101	0.005
33	34	11133.749	-0.00159	0.005
34	35	11130.630	-0.00301	0.005
35	36	11127.433	-0.00547	0.005
36	37	11124.176	0.01003	0.005
37	38	11120.819	0.00456	0.005
38	39	11117.396	0.01331	0.005
39	40	11113.888	0.01859	0.05
40	41	11110.279	0.0058	0.005
41	42	11106.614	0.02149	0.05
42	43	11102.853	0.02733	0.05
43	44	11098.961	-0.00988	0.005
44	45	11094.968	-0.05819	0.05
5	4	11199.311	-0.00974	0.005
7	6	11199.775	-0.01147	0.005
11	10	11199.874	0.0035	0.005
13	12	11199.476	-0.01302	0.005
14	13	11199.193	0.00058	0.005
15	14	11198.828	0.00277	0.005
16	15	11198.393	0.00558	0.005
17	16	11197.866	-0.01295	0.005

J'	J''	Observed	Obs.-Calc.	Weight
18	17	11197.309	0.00924	0.005
19	18	11196.660	0.01022	0.005
20	19	11195.937	0.0081	0.005
21	20	11195.136	-0.001	0.005
22	21	11194.286	0.01208	0.005
23	22	11193.347	0.00754	0.005
24	23	11192.334	0.00059	0.005
25	24	11191.253	-0.00249	0.005
26	25	11190.102	-0.00339	0.005
27	26	11188.866	-0.01676	0.05
28	27	11187.579	-0.00818	0.005
29	28	11186.206	-0.01218	0.005
30	29	11184.768	-0.00723	0.005
31	30	11183.262	0.00426	0.005
32	31	11181.634	-0.03103	0.05
33	32	11179.961	-0.03536	0.05
34	33	11178.259	0.00809	0.005
35	34	11176.445	0.01725	0.05
36	35	11174.524	-0.00189	0.005
37	36	11172.547	0.00279	0.005
38	37	11170.48	-0.0015	0.005
39	38	11168.358	0.02154	0.05